ABSTRACT

Title of Dissertation: ENERGY ABSORPTION AND DIFFUSION IN CHAOTIC SYSTEMS UNDER RAPID PERIODIC DRIVING

Wade Hodson
Doctor of Philosophy, 2022

Dissertation Directed by: Professor Christopher Jarzynski
Department of Physics

In this thesis, we study energy absorption in classical chaotic, ergodic systems subject to rapid periodic driving, and in related systems. Under a rapid periodic drive, we find that the energy evolution of chaotic systems appears as a random walk in energy space, which can be described as a process of *energy diffusion*. We characterize this process, and show that it generally predicts three stages of energy evolution: Initial relaxation to a prethermal state, followed by slow evolution of the system's energy probability distribution in accordance with a Fokker-Planck equation, followed by either unbounded energy absorption or relaxation to an infinite temperature state. We then study the energy diffusion model in detail in driven billiard systems specifically; in particular, we obtain numerical results which corroborate the energy diffusion description for a specific choice of billiard. This is followed by an analysis of energy diffusion in one-dimensional oscillator systems subject to weak, correlated noise. Finally, we begin to investigate energy absorption in periodically driven quantum chaotic systems, i.e., quantum systems with a classical chaotic analogue. We invoke tools from Floquet theory and random matrix theory to investigate whether the classical energy diffusion framework can be applied to quantum systems, and under

what conditions. We conclude with a discussion of potential models for energy absorption in quantum chaotic systems, and with an overview of open questions and directions for future work.

ENERGY ABSORPTION AND DIFFUSION IN CHAOTIC SYSTEMS UNDER RAPID PERIODIC DRIVING

by

Wade Hodson

Dissertation submitted to the Faculty of the Graduate School of the
University of Maryland, College Park in partial fulfillment
of the requirements for the degree of
Doctor of Philosophy
2022

Advisory Committee:
Professor Christopher Jarzynski, Chair/Advisor
Professor Charles Levermore, Dean's Representative
Professor Victor Galitski
Professor Ed Ott
Professor Rajarshi Roy

Dedication

To Mom and Dad, of course.

Acknowledgments

A PhD can take a lot out of someone. These people have made my journey over the past six years a bit easier.

I'd first like to thank everyone in my research group, past and present, and everyone else who I discussed physics with over the years. Special thanks to Andrew, Kanu, and Debankur, whose mentorship and friendship I didn't know I needed. And thanks of course to Chris, my kind and thoughtful advisor.

I'd also like to thank all the friends that supported me. Thanks to Laura, Jimena, and Aislinn, some of my oldest and dearest friends, who I've always been able to count on. Thanks to Hugh, Luke, and Eamonn. Thanks to Christina. Thanks to Eve. Thanks to Stavros. Thanks to Kat and Brandon. Thanks to Prathum. Thanks to Sophie, my cousin but more importantly my friend. Thanks to Landry. And thanks to Jalyn, a wonderful friend that I still can't believe I found.

Finally, I'd like to thank my family. Thanks to all my aunts, uncles, cousins, and grandparents who have cheered me on. Thanks to my brothers, Shane and Christian, and thanks to Mom and Dad. I love you all so much.

Table of Contents

List of Figures

List of Symbols

Chapter 2:

z	phase space point
z_t	phase space trajectory
$H(z,t)$	classical Hamiltonian
$H_0(z)$	time-averaged classical Hamiltonian
T	driving period
ω	driving frequency
$V(z,t/T)$	driving term in classical Hamiltonian
$\{\cdot,\cdot\}$	Poisson bracket
E	energy
$\rho(z,t)$	phase space distribution
$\eta(E,t)$	energy probability distribution
$\rho_E(z)$	microcanonical distribution at energy E
$\Sigma(E)$	classical density of states
τ_C	correlation timescale
$g_1(E,\omega)$	energy drift coefficient
$g_2(E,\omega)$	energy diffusion coefficient
$\tau_E(\omega,E)$	energy absorption timescale
$\mathcal{R}(\omega)$	range of energies for which the energy diffusion model is valid
$\dot{V}(z)$	time derivative of $V(z)$
$\langle ... \rangle$	ensemble average
$\mathrm{Var}(E)$	ensemble variance of the energy distribution
$C(t;E)$	microcanonical autocorrelation function for $\dot{V}(z)$
$S(\omega;E)$	microcanonical power spectrum for $\dot{V}(z)$

k_B	Boltzmann's constant
$T_\mu(E)$	microcanonical temperature
T_c	canonical temperature
$\overline{\Sigma}(E)$	infinite temperature energy distribution
$\mathfrak{S}(t)$	coarse-grained Gibbs entropy
$\mathfrak{s}(E_t, t)$	trajectory entropy
z_t^R	time-reversed phase space trajectory
$T(E\|E';\tau)$	transition kernel from energy E' to E over a time τ
$\{E_i\}$	sequence of energies $E_0 \to E_1 \to ... \to E_K$
$\{E_i\}^*$	time-reversed energy sequence
$P_F(\{E_i\})$	probability distribution over energy sequences
$P_R(\{E_i\}^*)$	distribution over reversed energy sequences

Chapter 3:

m	particle mass
$\mathbf{x}$	position vector
$\mathbf{v}$	velocity vector
$U(\mathbf{x})$	static potential in the billiard
$U_F(\mathbf{x})\cos(\omega t)$	driving potential in the billiard
$\mathbf{F}(\mathbf{x})\cos(\omega t)$	driving force in the billiard
$\hat{\mathbf{n}}(\mathbf{x})$	outward-facing unit vector normal to the billiard wall
$\mathcal{E}$	billiard particle energy
F	typical magnitude of $\mathbf{F}(\mathbf{x})$
v	typical speed of a billiard particle
l	shortest length scale in the billiard system
$v_E(\mathbf{x})$	speed of a billiard particle
$\gamma_E(\mathbf{x})$	collision rate per unit hyper-area of the billiard wall
B_n	hyper-volume of the unit ball in n-dimensional space
V	d-dimensional hyper-volume enclosed by the billiard
S	$(d-1)$-dimensional hyper-area of the billiard wall

λ	mean free path in the billiard
N	number of particles
$\mathbf{X}$	collection of N particle positions
$\mathbf{V}$	collection of N particle velocities
m_i	mass of the i^{th} particle
μ_{ij}	reduced mass of the i^{th} and j^{th} particles
$\mathbf{r}_{ij}$	relative position of the i^{th} and j^{th} particles
$\mathbf{u}_{ij}$	relative velocity of the i^{th} and j^{th} particles
R_i	radius of the i^{th} sphere
R_{ij}	sum of the radii of the i^{th} and j^{th} spheres

Chapter 4:

$U(x)$	potential well
$f(t)$	noise force
$C_f(t)$	noise force autocorrelation function
$a_k(E)$	Fourier coefficient for the unperturbed particle velocity
$S_f(\omega)$	noise force power spectrum
$T(E)$	period of oscillation
$\gamma(t)$	damping kernel
T_b	temperature of the thermal bath
λ	eigenvalue of the Fokker-Planck operator for the harmonic oscillator
$\phi_\lambda(E)$	eigenfunction of the Fokker-Planck operator for the harmonic oscillator
$\mathbf{S}(t)$	spin vector
$\mathbf{B}(t)$	magnetic field vector
ϕ	spin azimuthal angle
S_z	z-component of $\mathbf{S}$
$\mathbf{B}_0$	static magnetic field
B_0	magnitude of $\mathbf{B}_0$
$\mathbf{b}(t)$	magnetic field noise
$C_b(t)$	autocorrelation function of $b_i(t)$

$S_b(\omega)$	power spectrum of $b_i(t)$
λ_n	eigenvalue of the Fokker-Planck operator for the Heisenberg spin
$\phi_n(E)$	eigenfunction of the Fokker-Planck operator for the Heisenberg spin

Chapter 5:

$\|\psi(t)\rangle$	state vector
$\hat{H}(t)$	quantum Hamiltonian
$\hat{H}_0$	quantum time-averaged Hamiltonian
$\hat{V}(t/T)$	driving term in quantum Hamiltonian
E_n	eigenvalue of $\hat{H}_0$
$\|n\rangle$	eigenvector of $\hat{H}_0$
$c_n(t)$	expansion coefficient of $\|\psi(t)\rangle$ in the eigenbasis of $\hat{H}_0$
$\langle ... \rangle_t$	expectation value
$\eta^Q(E,t)$	quantum energy distribution
$\hat{\rho}(t)$	density operator
$[\cdot,\cdot]$	commutator
h	Planck's constant
$\hbar$	reduced Planck's constant
$\hat{U}(t,t_0)$	evolution operator from t_0 to t
$\hat{U}_F$	Floquet operator
$\hat{H}_F$	Floquet Hamiltonian
ε_α	quasi-energies of $\hat{H}_F$
$\|\alpha\rangle$	eigenvector of $\hat{U}_F$ and $\hat{H}_F$
$\hat{P}(t)$	fast-motion operator
$\|\alpha,t\rangle$	Floquet mode
$\|\psi_\alpha(t)\rangle$	Floquet state
$\hat{\mathcal{L}}$	Liouvillian operator
$\hat{\mathcal{L}}_F$	Floquet Liouvillian operator
$H_F(z)$	classical Floquet Hamiltonian
$\hat{H}_F^{(n)}$	n^{th}-order coefficient in the Floquet-Magnus expansion

$\hat{H}_{F,M}$	M^{th}-order truncation of the Floquet-Magnus expansion
$\hat{U}_{F,M}$	M^{th}-order approximation of $\hat{U}_F$
$\rho(E)$	smoothed quantum density of states
$f(\varepsilon)$	distribution of normalized nearest-neighbor level spacings
$f_{WD}(\varepsilon)$	Wigner-Dyson level spacing distribution
A_{mn}	(m, n) matrix element of $\hat{A}$ in the eigenbasis of $\hat{H}_0$
$\langle ... \rangle_E$	microcanonical average
$\overline{...}$	average over m, n such that $\frac{1}{2}(E_m + E_n) \approx \overline{E}$ and $E_n - E_m \approx \Delta$
$C_A(t; E)$	microcanonical autocorrelation function for $A(z)$
$S_A(\omega; E)$	microcanonical power spectrum for $A(z)$
$\Gamma_{k,k\pm1}$	transition rate from state k to state $k \pm 1$

Chapter 1: Introduction

1.1 Chapter summary

In this chapter, we give an introduction to the key topics discussed in this thesis, the main results obtained, and the essential tools used to obtain them. We begin by providing some motivation for the thesis in Section 1.2, where we explain our focus on energy absorption in periodically driven systems. In Section 1.3, we present an overview of our analysis of energy absorption and diffusion in classical systems. We introduce our primary systems of interest, classical chaotic systems under rapid periodic driving, and outline how energy absorption in these and other classical systems can be described with the energy diffusion model. Then, in Section 1.4, we turn to quantum systems. We discuss the various tools that we use in the thesis to understand energy absorption in quantum systems, including Floquet theory and random matrix theory. Finally, in Section 1.5, we summarize the structure of the thesis, chapter by chapter.

1.2 Motivation

Periodic driving, defined as the time-periodic application of an external force or influence on a system, is a ubiquitous phenomenon in the natural world. It can be observed across physical scales, from the planetary scale, where bodies in the Solar system are periodically

perturbed by the gravitational influence of orbiting planets, to the microscopic level, where the oscillations of the electromagnetic field drive transitions between atomic energy levels. Across these various systems, the consequences of periodic driving range from regulatory effects, including synchronization, stabilization, and localization [1–10], to the potentially destabilizing processes of energy absorption [11, 12] and the onset of chaos [1, 13]. These effects are important to understand in a range of scientific disciplines, beyond just physics: Ecological and meteorological systems are organized around the regular influence of the seasonal and day-night cycles, biochemical processes in living systems are shaped by periodic processes like breathing, hormone regulation, and sleep cycles, and long- and short-term business cycles influence the decisions of individual economic actors and drive macroeconomic trends.

Of course, periodic driving is not only a natural process to be understood, but a tool to be applied to meet technological and engineering challenges. There are examples everywhere. The operation of many engines and motors is fundamentally cyclical, whether they are driven by the periodic control of electromagnetic fields, gas combustion, or heat flow. All computer processes are ultimately organized by a clock cycle, which ensures that computations occur synchronously and in the proper order. The Paul trap or radio-frequency (RF) trap [14, 15], which uses high-frequency oscillating electric fields to dynamically confine charged particles (see Figure 1.1), earned its inventors a Nobel prize, and has found applications in spectroscopy [16], metrology [17, 18], and quantum computing [19]. In solid state nuclear magnetic resonance (NMR) spectroscopy, rapidly spinning a sample introduces a periodically oscillating magnetic field in the reference frame of the sample, producing an averaging effect which ensures high-resolution spectra (see Figure 1.2) [20, 21]. Finally, laser fields constitute an especially precise, controllable means of periodic driving, which can be used for heating or cooling [22, 23], for

high-resolution microscopy [24], and for the excitation of atoms and molecules in spectroscopy and photochemistry [25, 26].

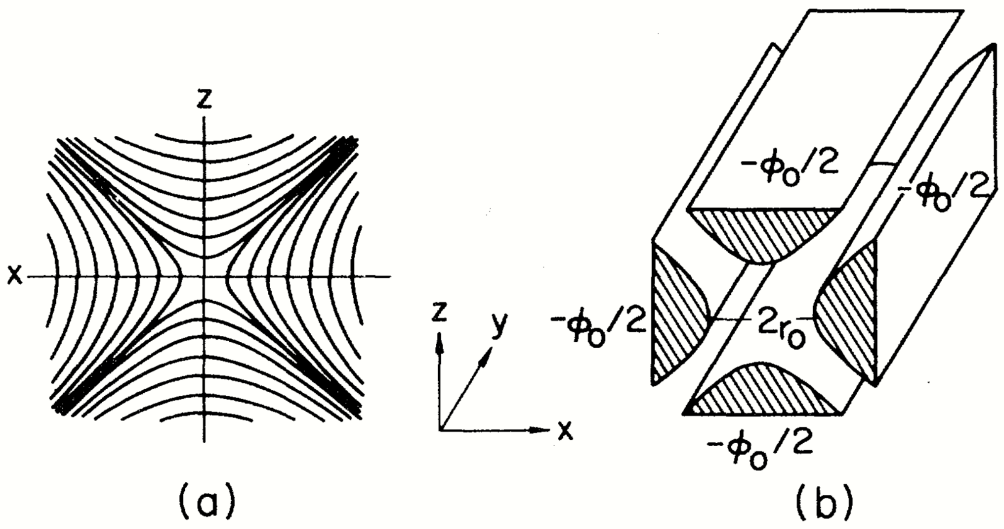

Figure 1.1: Schematic of a quadrapole Paul trap, taken from [14]. (a) displays the equipotential lines of the quadrupole electrode configuration illustrated in (b). The left and right electrodes are set to the same voltage, and the upper and lower electrodes are set to the opposite voltage. When these voltages are made to oscillate rapidly in time, an effective field is generated which traps charged particles at the center of the configuration (along the y-axis). The mathematical explanation for this dynamical stabilization effect is similar to the explanation for the stability of the Kapitza pendulum, which we discuss in Chapter 6, Section 6.2.

Given this range of applications, it is not surprising that in today's research on quantum systems, periodic driving has emerged as an essential tool for the design and manipulation of these systems. The profound developments of quantum technology in the late twentieth and early twenty-first centuries are sometimes referred to as the "second quantum revolution" [27–29]:[1] This is the stage of technological advancement which has allowed us to observe, design, and control systems at the level of individual atoms and molecules, while preserving quantum properties like coherence and entanglement. During this time, great strides have been made

[1]The "first quantum revolution" is associated with the initial development of quantum mechanics, and with technologies like lasers and transistors: Technologies which are built on irreducibly quantum mechanical principles, but which do not necessarily require a fine-grained control over quantum phenomena for their operation.

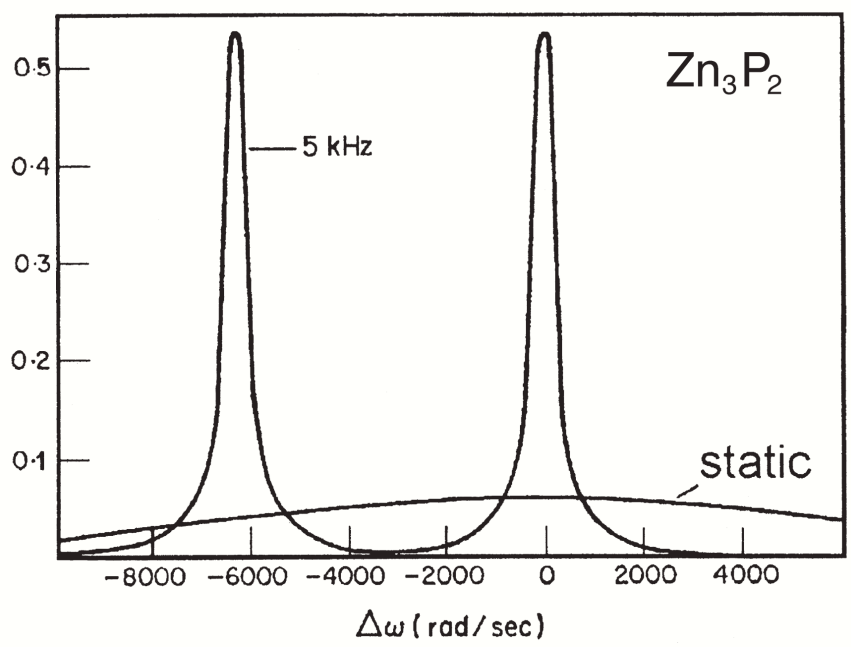

Figure 1.2: NMR spectrum for Zn_3P_2, taken from [21]. Without spinning the sample, the observed spectrum is very broad (curve labelled "static"), while with sample spinning, the two peaks in the spectrum can be clearly resolved (curve labelled "5 kHz"). This technique is also referred to as "magic angle spinnning," since the sample must be rotated around an axis tilted at a special angle relative to the applied magnetic field [20, 21].

in the fields of quantum optics, quantum computing, and quantum metrology, on experimental platforms including ion traps, NMR systems, superconducting circuits, quantum dots, and correlated electron systems like graphene. The use of periodic driving protocols in the context of quantum technology has been termed "Floquet engineering," after Floquet theory, the standard formalism used to analyze periodically driven systems (see Chapter 5, Section 5.3) [12, 30, 31]. Such protocols have been exploited to design effective Floquet Hamiltonians [12, 30, 32, 33], effective magnetic fields [34, 35], and tunable interactions between subsystems [36–38]. Using these and other Floquet engineering tools, researchers have theorized and engineered novel quantum states, including Floquet prethermal phases [33, 39–49], discrete time crystal states [50–56], dynamically stabilized states [5, 57, 58], and Floquet topological insulator phases [59–

61]. The precise control of quantum systems has also allowed for the reproduction of classical thermodynamic cycles at the microscale, even at the level of individual atoms [62–64]. Also, in the context of quantum computation, Floquet engineering has been proposed as a technique for realizing quantum gates [65–67].

In many Floquet quantum systems, controlling the absorption of energy from the periodic drive is a task of prime importance. In some cases, energy absorption is the goal: For example, in a system acting as a quantum refrigerator or heat pump, the energy absorbed from a periodic drive in the form of work facilitates the cooling of another body. However, in other settings, energy absorption appears as a potential obstacle to the stabilization of quantum states. Generally speaking, a driven system in a nonequilibrium steady state attains a balance in which energy absorbed from the drive is dissipated into an environment, such as a thermal bath. Therefore, if a system is instead *isolated*, save its interaction with the drive, then maintaining a stable state requires the suppression of energy absorption from the drive. For many quantum technologies, careful isolation from uncontrolled thermal influence is necessary to preserve delicate superpositions or entanglement relationships [68, 69]. It follows that to successfully apply the techniques of Floquet engineering to quantum systems, an understanding of energy absorption and the conditions under which it might be suppressed is essential. Indeed, this is a research topic which has generated much theoretical interest and experimental work in the past ten years [11, 33, 41, 44–47, 49, 70–81].

This question of energy absorption in periodically driven systems is the central motivation for this thesis. We approach this problem from a primarily classical perspective, focusing on the energy dynamics of chaotic, ergodic classical Hamiltonian systems under rapid periodic driving. In short, we find that the periodic drive in such systems induces an effectively stochastic

evolution of the system's energy, describable as a process of diffusion in energy space. The energy dynamics of these systems are interesting in their own right, but they also offer a potential approximate description of *quantum* energy absorption, in terms of purely classical mechanisms. We begin to probe this possible quantum-classical correspondence with the help of semiclassical theory, Floquet theory, and ideas from quantum chaos. To get a better sense of how these various threads tie together, we now provide an overview of the main contents of the thesis. We first summarize our analysis of classical systems as found in Chapters 2, 3, and 4, and then outline the discussion of quantum systems given in Chapter 5.

1.3 Classical energy diffusion

The starting point of our analysis is classical chaotic, ergodic Hamiltonian systems, subject to a rapid periodic drive. As an example for visualization purposes, one may have in mind a system of interacting charged particles, subject to an oscillating electric field. As described in more detail in Chapter 2, Section 2.2, the dynamics of such systems are fully characterized by a Hamiltonian phase space function $H(z,t) = H(z,t+T)$ which is periodic in time, with period T. The state of a Hamiltonian system is specified by a set of evolving positions $\mathbf{q}_t \equiv \mathbf{q}$ and momenta $\mathbf{p}_t \equiv \mathbf{p}$, which trace out a phase space trajectory $z_t \equiv z \equiv (\mathbf{q}, \mathbf{p})$ according to Hamilton's equations of motion

$$\frac{d\mathbf{q}}{dt} = \frac{\partial H}{\partial \mathbf{p}}, \quad \frac{d\mathbf{p}}{dt} = -\frac{\partial H}{\partial \mathbf{q}}. \tag{1.1}$$

Here, the periodic drive is modelled by the explicit periodic time-dependence of the system's Hamiltonian $H(z,t)$. We identify the energy of the system as $E(t) \equiv H_0(z_t)$, the time-averaged

Hamiltonian $H_0(z) \equiv T^{-1} \int_0^T dt\, H(z,t)$ evaluated along the trajectory z_t. The central question of Chapter 2 is, how does this energy evolve for a chaotic, ergodic system, in the limit of high-frequency driving?

Our focus on systems with chaotic, ergodic dynamics stems from the central importance of these concepts in the foundations of thermodynamics and statistical physics. Over the course of its evolution, a chaotic, ergodic Hamiltonian system fully explores the phase space available to it at a given energy, and does so in a complex, effectively random manner [82–84]. The statistical properties of these pseudorandom dynamics coincide with the probabilistic description furnished by equilibrium statistical mechanics, providing the basis of a first-principles justification for the validity of statistical mechanics. Given the great success of statistical mechanics as a tool for predicting equilibrium and near-equilibrium thermodynamic properties, studying systems with chaotic and ergodic dynamics was a natural choice. Meanwhile, the reasoning behind studying *rapidly* driven systems specifically is twofold. First, many phenomena which are useful for tuning and controlling systems manifest at high driving frequencies, including prethermalization and dynamical stabilization. Second, for sufficiently rapid driving, the drive can be treated as a weak perturbation away from the undriven dynamics, making the energy dynamics more tractable to describe.

Given these two assumptions on our system, (a) rapid periodic driving and (b) chaotic, ergodic dynamics, we find that the system's energy evolves diffusively. In other words, the influence of the drive causes the system to perform an effectively random walk in energy space. If we consider a statistical ensemble of such systems, the time-dependent distribution of energies in the ensemble satisfies a Fokker-Planck equation

$$\frac{\partial \eta}{\partial t} = -\frac{\partial}{\partial E}\left(g_1 \eta\right) + \frac{1}{2}\frac{\partial^2}{\partial E^2}\left(g_2 \eta\right), \tag{1.2}$$

where $\eta(E,t) \equiv \eta$ is the energy distribution, and where the drift and diffusion coefficients $g_1(E,\omega) \equiv g_1$ and $g_2(E,\omega) = g_2$ determine the rate at which this distribution shifts and spreads in energy space. We develop this diffusive description in Chapter 2, starting with Section 2.3. In particular, we obtain explicit expressions for the rates g_1 and g_2 in Section 2.4, and in Section 2.5, we show that evolution under the energy diffusion description may generally be divided into three stages: Initial relaxation to a prethermal state, followed by slow evolution of the system's energy probability distribution in accordance with the Fokker-Planck equation, followed by either unbounded energy absorption or relaxation to an infinite temperature state. Also, in Section 2.7, we compare our model to other systems described by an energy diffusion description, including slowly driven chaotic systems, and systems weakly coupled to a thermal bath.

After this general analysis, we turn to a discussion of specific systems which can be treated within the energy diffusion framework. First, we apply this framework to rapidly driven dynamical billiard systems. That is, we consider systems consisting of a single particle in a cavity, subject to a rapidly oscillating force. Billiards are an ideal testing ground for the energy diffusion model, since certain billiards have been rigorously proven to exhibit chaotic, ergodic dynamics [85, 86]. In Chapter 3, we calculate the rates g_1 and g_2 for billiard systems in Section 3.4, and we perform numerical simulations on a driven billiard particle to corroborate the energy diffusion model in Section 3.5. Also, in Section 3.6, we generalize our results to systems of multiple interacting particles in a billiard. This explicitly demonstrates the applicability of the energy diffusion description to many-body interacting systems. Then, in Chapter 4, we consider energy

diffusion in a slightly different setting: In one-dimensional oscillator systems driven by weak, correlated noise. For these systems, the Fokker-Planck equation (1.2) may be solved exactly in certain special cases.

1.4 Energy absorption and diffusion in quantum systems

The energy diffusion models just discussed are descriptions of classical systems. How are these models connected to energy absorption in periodically driven quantum mechanical systems? In Chapter 5, we probe this question, focusing primarily on quantum chaotic systems, or quantum systems with a classical chaotic counterpart. We first approach this issue from the standpoint of Floquet theory, and then from the perspective of the field of quantum chaos. Let us discuss each of these ideas in turn.

First, Floquet theory is the general formalism for studying quantum systems subject to periodic driving [12]. As reviewed in Chapter 5, Section 5.2, the state of a quantum system is described by a time-dependent state vector $|\psi(t)\rangle \equiv |\psi\rangle$, which evolves according to the Schrodinger equation

$$i\hbar\frac{d|\psi\rangle}{dt} = \hat{H}|\psi\rangle, \tag{1.3}$$

where $\hbar$ is the reduced Planck's constant. For a periodically driven quantum system, the system's Hamiltonian operator $\hat{H} \equiv \hat{H}(t) = \hat{H}(t+T)$ is time-periodic with period T. As in the classical setup just discussed, our key concern is with the evolution of the system's energy, which is associated with the time-averaged Hamiltonian $\hat{H}_0 \equiv T^{-1}\int_0^T dt\, \hat{H}(t)$.

A central object in Floquet theory is the Floquet operator $\hat{U}_F$, which evolves the state

vector for the system over a single period, from $t = NT$ to $t = (N+1)T$: $\hat{U}_F|\psi(NT)\rangle = |\psi((N+1)T)\rangle$. However, in general, this operator is difficult to obtain exactly, and approximation schemes are necessary. For rapid driving, one method to approximate the action of $\hat{U}_F$ is with the Floquet-Magnus (FM) expansion, a perturbative expansion in powers of the driving period T. In Chapter 5, Section 5.3, we introduce Floquet theory and the FM expansion, and explore how these tools have been used to understand the energy evolution of quantum systems. In particular, we show how bounds on energy absorption in quantum systems, derived with the help of the FM expansion and other techniques, are consistent with the predictions of the classical energy diffusion description. This quantum-classical connection is closely tied to the phenomenon of Floquet prethermalization, in which a periodically driven system initially comes to equilibrium with an effective Hamiltonian, before ultimately gaining energy at long times.

Second, in Chapter 5, Section 5.4, we continue to explore the possibility of quantum-classical correspondence by looking at quantum chaotic systems, or quantum systems with a classical chaotic counterpart. In the semiclassical limit (the limit of small $\hbar$), the properties of a quantum chaotic system can be related to the properties of the corresponding classical system. We primarily focus on two tools commonly used to understand this correspondence: Random matrix theory (RMT) and the Eigenstate Thermalization Hypothesis (ETH) [87, 88]. RMT is the study of statistical ensembles of matrices with randomly sampled entries. This theory is applied to quantum chaotic systems via the famous Bohigas-Giannoni-Schmit conjecture, which connects the statistical properties of random matrices to the energy spectra of quantum chaotic systems in the semiclassical limit [89]. Meanwhile, the ETH provides a description of the operators of a quantum chaotic system in the system's energy eigenbasis. Both RMT and the ETH reveal how classical chaotic dynamics can leave "imprints" on the properties of quantum systems. This

makes these ideas an ideal starting ground for thinking about the possible application of the classical energy diffusion description to the quantum regime.

Based on this discussion, we conclude Chapter 5 with a discussion of several models which may provide insight into the possibility of energy diffusion in periodically driven quantum systems. First, in Section 5.4.4, we present a review of the literature on energy diffusion in *slowly* driven quantum chaotic systems. This body of research includes studies of both "real" quantum chaotic models, and systems where the Hamiltonian has been modelled by an appropriate random matrix. Second, in Section 5.5.1, we construct a random matrix model of a periodically driven quantum chaotic system, which could be used to test the energy diffusion description in a quantum setting. Finally, in Section 5.5.2, we describe a heuristic model of energy absorption in quantum chaotic systems, based on Fermi's golden rule. Although this model has significant limitations, it does reduce to the classical energy diffusion model in the semiclassical limit, suggesting that the classical mechanisms leading to energy diffusion may be relevant to understanding energy absorption in quantum systems as well.

1.5 Organization of thesis

In summary, the thesis is organized as follows. In Chapter 2, we develop the energy diffusion description as it applies to chaotic, ergodic classical systems under rapid periodic driving. We discuss the key assumptions in our analysis, derive expressions for the drift and diffusion coefficients g_1 and g_2, and describe the three-stage energy evolution predicted by the energy diffusion model. We also study entropy production in the context of the energy diffusion framework, and we compare our energy diffusion description to other work on energy diffusion

models. Then, in Chapter 3, we apply the energy diffusion model to periodically driven billiard systems. We obtain expressions for g_1 and g_2 for billiards in the high-frequency driving limit, present numerical simulations which validate the energy diffusion description for a particular billiard shape, and generalize our results to billiards with many interacting particles. In Chapter 4, we use the energy diffusion description to study one-dimensional oscillator systems, subject to weak, correlated noise. We find that the Fokker-Planck equation in these systems can be solved exactly in some cases, and that energy diffusion in these models is closely related to energy diffusion in systems weakly coupled to a stochastic thermal bath. In Chapter 5, we shift our focus to energy absorption in periodically driven quantum systems. We explore connections between the Floquet-Magnus expansion, bounds on quantum energy absorption, and the energy diffusion description. We also discuss random matrix theory, along with related ideas from quantum chaos and semiclassical physics, to probe the conditions under which the classical energy diffusion model may approximately describe quantum systems. Finally, we conclude the main body of the thesis in Chapter 6, where we provide some last thoughts about future directions for research.

After Chapter 6, there are five appendices which provide extra details concerning calculations from Chapters 2 and 3. In Appendix A, we generalize the calculation of the drift coefficient g_2 in Chapter 2 to systems with non-monochromatic drives. In Appendix B, we clarify a technical point in the derivation of the fluctuation-dissipation relation (Equation (2.22) in Chapter 2). In Appendix C, we fill in details in the calculation of the diffusion coefficient for billiards in Chapter 3. Then, in Appendix D, we present an alternative calculation of this same diffusion coefficient, which confirms the correspondence between the general energy diffusion description in Chapter 2, and the billiard-specific results in Chapter 3. Last, in Appendix E, we describe the details of the numerical simulations given in Chapter 3, of a driven particle confined

to a clover-shaped billiard.

Chapter 2: Energy diffusion in chaotic Hamiltonian systems under rapid periodic driving

2.1 Chapter summary

In this chapter, we describe the energy dynamics of classical chaotic, ergodic Hamiltonian systems subject to a rapid periodic drive. In such systems, energy absorption proceeds via a process of energy diffusion, wherein small energy changes induced by the drive cause the system to perform an effectively random walk in energy space. This stochastic evolution is described by a Fokker-Planck equation on energy space, which determines the evolution of the system's energy probability distribution $\eta(E, t)$. Overall, we find that systems described by the diffusion model absorb energy in a predictable series of stages. First, a prethermalization phase occurs, in which the system reaches a statistical equilibrium state at nearly constant energy. This is followed by slow energy absorption and diffusion according to the Fokker-Planck equation. Finally, if the diffusive description remains valid at long times, then the system will either continue to absorb energy indefinitely, or relax to an infinite temperature steady state. Alternatively, when the system has reached sufficiently high energies, the diffusion model may begin to fail, leading to the possibility of especially rapid energy absorption at these energies.

The chapter is organized as follows. In Section 2.2, we mathematically define the class of

systems treated by our analysis, explain our assumptions, and introduce some key concepts. Next, in Section 2.3 we argue that the energy of such systems evolves diffusively, and we introduce the Fokker-Planck equation (given by (2.11)). In Section 2.4, we obtain explicit expressions for the coefficients g_1 and g_2 in this equation ((2.22) and (2.20)), which specify the rates at which $\eta(E,t)$ shifts and spreads in energy space. Then, we develop the implications of the energy diffusion description in Section 2.5. In particular, we describe the initial prethermalization stage, we investigate the long-time dynamics of the energy distribution, and we discuss the scaling of the energy absorption rate with respect to driving frequency. In Section 2.6, we derive a fluctuation theorem for the diffusive energy dynamics, which relates the probabilities of different trajectories in energy space. Finally, in Section 2.7, we place our results in the context of other systems which exhibit energy diffusion, including adiabatically driven chaotic systems, and systems weakly coupled to a thermal bath. The results presented in this chapter, excluding those in Section 2.6, were previously published in [90].

2.2 Preliminaries and assumptions

2.2.1 Setup

We now define the class of systems studied in this chapter. We consider a classical Hamiltonian system with $N \geq 2$ degrees of freedom, subject to a rapid periodic driving force. At any instant of time t, the state of the system is specified by a point $z_t \equiv z \equiv (\mathbf{q}, \mathbf{p})$ in its $2N$-dimensional phase space, where the N-dimensional vectors $\mathbf{q}$ and $\mathbf{p}$ define a set of canonical coordinates and momenta. We assume that the Hamiltonian for the system, which governs the evolution of z_t, is a periodic function of time at constant z: $H(z,t) = H(z,t+T)$, for

some driving period T. We decompose this Hamiltonian into its time average $H_0(z) \equiv H_0 \equiv T^{-1}\int_0^T dt\, H(z,t)$, and a remainder $V(z,t/T) \equiv V$ with vanishing average:

$$H(z,t) = H_0(z) + V(z,t/T), \quad V(z,s) = V(z,s+1). \tag{2.1}$$

We will refer to H_0 as the"undriven" or "bare" Hamiltonian and V as the "drive." As an example, the bare Hamiltonian may correspond to the kinetic and potential energy of a collection of interacting point particles, and the drive may induce a oscillating force on these particles. However, we will allow the form of H_0 and V to be quite general, provided that two key assumptions (given later in this section) are satisfied.

Given this Hamiltonian (and an initial phase space point z_0), the system's phase space trajectory z_t is obtained by time-integrating Hamilton's equations of motion:

$$\frac{d\mathbf{q}}{dt} = \frac{\partial H}{\partial \mathbf{p}}, \quad \frac{d\mathbf{p}}{dt} = -\frac{\partial H}{\partial \mathbf{q}}. \tag{2.2}$$

We will also consider statistical ensembles of trajectories, wherein initial conditions are sampled according to an initial phase space distribution $\rho(z_0,0)$, and then evolved via Hamilton's equations. In this case, the phase space distribution that describes the evolving ensemble, denoted by $\rho(z,t) \equiv \rho$ at time t, satisfies the Liouville equation

$$\frac{\partial \rho}{\partial t} = \{H,\rho\} = \frac{\partial H}{\partial \mathbf{q}} \cdot \frac{\partial \rho}{\partial \mathbf{p}} - \frac{\partial H}{\partial \mathbf{p}} \cdot \frac{\partial \rho}{\partial \mathbf{q}}, \tag{2.3}$$

where $\{\cdot,\cdot\}$ denotes the Poisson bracket, and $\partial/\partial\mathbf{q}$ ($\partial/\partial\mathbf{p}$) is the gradient operator with respect to the coordinate (momentum) variables [91].

Our main object of study is the time evolution of the system's energy E, which we define as the bare Hamiltonian of the system, evaluated along a trajectory: $E \equiv E(t) \equiv H_0(z_t)$. In the absence of a drive ($V = 0$), E is a constant of the motion. Meanwhile, for nonzero V, Hamilton's equations imply

$$\frac{dE}{dt} \equiv \frac{d}{dt} H_0(z_t) = -\{H_0, V\}(z_t, t/T), \tag{2.4}$$

In particular, we will be concerned with the evolution of E in the limit of large driving frequencies $\omega \equiv 2\pi/T$. In Section 2.3, we establish our main result: For sufficiently rapid driving, the system's energy evolution can be described as a random walk in energy space, leading to a process of diffusion in energy space. To characterize this diffusion process, it will be useful to introduce $\eta(E, t) \equiv \eta$, the time-dependent probability distribution for the system's energy:

$$\eta(E, t) \equiv \int dz\, \delta(H_0(z) - E)\rho(z, t), \tag{2.5}$$

η is obtained by marginalizing the full phase space distribution ρ with respect to energy. The integral defining η, and similar integrals elsewhere in this text, are over all of phase space.

2.2.2 Key assumptions

We will make two essential assumptions in our analysis. First, we assume that in the absence of driving, the dynamics of the system are chaotic and ergodic on each energy shell (surface of constant $H_0(z)$) in phase space. By chaos, we mean that the dynamics of the system are exponentially sensitive to initial conditions: Two trajectories with infinitesimally different initial conditions will, in the long time limit, diverge from one another exponentially in time

[13, 84]. The rate of this divergence is quantified by the system's maximal Lyapunov exponent, which will be positive for a chaotic system. By ergodicity, we mean that for almost all initial conditions z_0 with energy E, the corresponding trajectory z_t eventually comes arbitrarily close to any point in phase space with the same energy [83, 84]. Essentially, given enough time, each trajectory fully explores the energy shell associated with E.

For an ergodic system, the exploration of each energy shell is necessarily "uniform," in the sense that each trajectory spends equal amounts of time in equal volumes of phase space. This can be shown as a consequence of Liouville's theorem, which expresses the incompressibility of phase space volume under Hamiltonian dynamics [84]. The distribution on phase space which captures this uniformity is the microcanonical distribution $\rho_E(z) \equiv \rho_E$:

$$\rho_E(z) \equiv \frac{1}{\Sigma(E)}\delta(H_0(z) - E), \tag{2.6}$$

where $\Sigma(E) \equiv \Sigma$ is the classical density of states, given by

$$\Sigma(E) = \frac{\partial \Omega}{\partial E} = \int dz\, \delta(H_0(z) - E), \tag{2.7}$$

and where $\Omega(E)$ is the phase space volume enclosed by the energy shell E, expressible in terms of the Heaviside step function $\Theta(x)$:

$$\Omega(E) = \int dz\, \Theta(E - H_0(z)). \tag{2.8}$$

That is, in the long-time limit, ρ_E specifies the relative frequency at which a trajectory visits different regions of the energy shell [83, 84]. Going forward, the term "uniform" will be used to

mean uniformity with respect to this distribution. As a side note, we assume that $\Omega(E)$ is finite for all E.

Taken together, the properties of chaos and ergodicity imply that the system exhibits *chaotic mixing* at each energy. That is, given any finite-measure set of initial conditions with energy E, the resulting trajectories will spread or "mix" across the energy shell, repelled from one another by the chaotic nature of the dynamics. In particular, because the evolution is ergodic, this spreading must extend to every region of the energy shell, ultimately resulting in a uniform distribution of trajectories across the shell (up to some coarse-graining of phase space, see Figure 2.1) [83, 84]. In other words, chaotic mixing results in a process of "self-thermalization": Regardless of the system's initial distribution in phase space, chaotic mixing implies that the ensemble of trajectories will eventually attain an effectively microcanonical, or thermal, distribution.

Figure 2.1: Schematic drawing of the evolution of a set of phase space points (blue) evolving on an energy shell of H_0 (shaded shape). As time moves forward from left to right, the set shifts and stretches while maintaining a constant phase space volume, as required by Liouville's theorem. After enough time, the set is fibrillated across the entire energy shell, and is uniformly distributed across the shell at a coarse-grained level.

One way to characterize this thermalization process is to study statistical correlations between the state of the system at different times. Consider a function $A(z)$ on phase space,

corresponding to some physical observable. For example, $A(z)$ might give the momentum of a particular particle in the system, when the system is in the state z. Given an ensemble of trajectories with energy E at some initial time $t = 0$, the probability distribution $\rho(z_0, 0)$ gives us some statistical information about $A(z_0)$, the value of the observable at this time. However, regardless of this initial distribution, chaotic mixing leads to an effectively uniform distribution on the energy shell after a certain time $t = \tau$. Therefore, our statistical knowledge of $A(z_0)$ gives us no information about $A(z_\tau)$, the value of the observable at this later time. That is, $A(z_0)$ and $A(z_\tau)$ are uncorrelated or statistically independent random variables. This *decay of correlations* is characteristic of chaotic systems, and is one way to quantify the (un)predictability of their dynamics.

The second key assumption in our analysis is that the driving frequency ω is sufficiently large. For large ω, the effect of the drive nearly averages to zero over a single period, since the system cannot appreciably respond to the drive in such a short time. More precisely, consider an initial condition z_0, and two trajectories evolved from it: One generated by evolution under the bare Hamiltonian H_0, and another generated under the full Hamiltonian $H = H_0 + V$. Denote these trajectories as z_t^0 and z_t, respectively. For any fixed time t, the value of z_t converges to that of z_t^0 in the limit $\omega \to \infty$ (see Figure 2.2). This limit can be established rigorously for time-periodic Hamiltonians $H(z, t)$ which are smooth functions of z and t, using mathematical tools such as the method of averaging or multi-scale perturbation theory [32, 92]. However, it is also a physically reasonable result. For example, suppose that the system of interest is a collection of interacting point particles, and that the effect of the drive is to impose a force field $\mathbf{F}(\mathbf{x})\cos(\omega t)$, where $\mathbf{x}$ denotes position. Over the course of a very short period, the particles move within the force field by a negligible amount, owing to their finite speed. Therefore, $\mathbf{F}(\mathbf{x})$

is essentially constant for each particle, and the effect of the force $\mathbf{F}(\mathbf{x})\cos(\omega t)$ nearly integrates to zero over the period. This averaging effect becomes better and better as $\omega \to \infty$. Note that is conclusion is valid independent of the magnitude of the force $\mathbf{F}(\mathbf{x})\cos(\omega t)$ (or more generally, of the magnitude of the drive V).

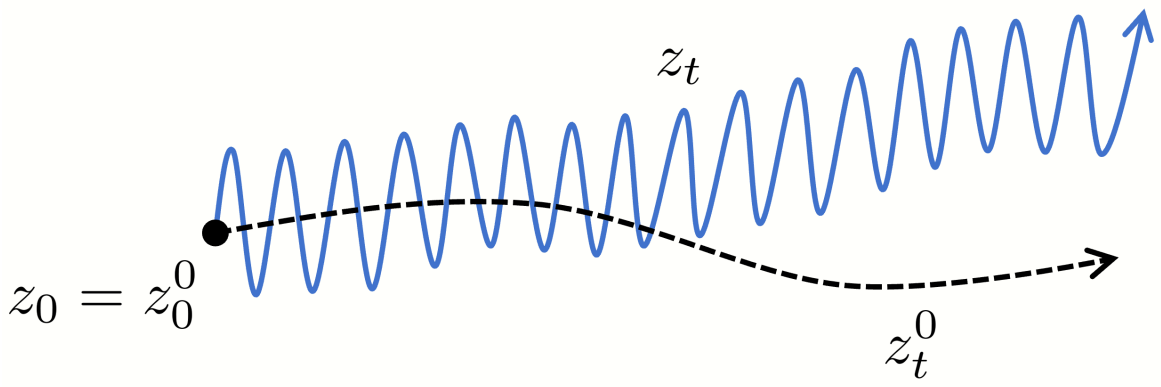

Figure 2.2: Evolution of a driven trajectory z_t (solid blue curve) and its undriven counterpart z_t^0 (dashed black curve), which both start from the same initial condition $z_0 = z_0^0$. In the rapid driving limit, a driven trajectory will generally perform small oscillations about the corresponding undriven trajectory, while also slow drifting away from the undriven evolution over the course of many driving periods. This figure is adapted from a similar image in [92].

How large must ω be for our analysis to be approximately valid? We answer this question in detail in Section 2.3, but we briefly state our conclusions here. Consider a time interval of duration τ_C, the timescale over which chaotic mixing generates a decay of correlations in the undriven system. We choose ω large enough so that over this interval, the trajectories z_t^0 and z_t closely resemble one another, and so that even after *many* such intervals, the total change in the system's energy is small. As we will see, both of these conditions can generically be satisfied for a large enough choice of ω.

2.3 Argument for energy diffusion

We now argue that when a chaotic, ergodic Hamiltonian system is subject to a rapid periodic drive, its energy $E = H_0(z_t)$ evolves diffusively. We first sketch the broad strokes of our reasoning, highlighting the key assumptions of rapid driving and chaotic dynamics discussed in Section 2.2. We then go through the argument in detail, describing how the chaotic motion of the system in phase space induces an effectively random, diffusive evolution in energy space. To conclude this section, we discuss how large the driving frequency ω must be for our result to hold, and we identify the coarse-grained timescale on which the diffusive description is approximately valid.

The essence of our argument is as follows. Consider an ensemble of trajectories in phase space, evolving according to Hamilton's equations (2.2) with the Hamiltonian $H = H_0 + V$ given by 2.1. Given our assumption of rapid driving, the drive term V exerts a weak influence on the evolution of the system, and therefore only produces small changes in the energy (at least over short times). Because the chaotic dynamics induce a decay of correlations on the timescale τ_C, successive energy changes separated by times of order τ_C will be effectively statistically independent. Therefore, on a coarse-grained timescale much longer than this correlation time, the energy evolution of the system appears as a series of many small, statistically independent steps in energy space. This random walk constitutes a process of diffusion in energy space, just like how a colloidal particle undergoes diffusive motion in *real* space due to random, uncorrelated collisions with molecules of the surrounding medium [93]. These dynamics are described by a Fokker-Planck equation (see (2.11)), which governs the evolution of the energy distribution $\eta(E, t)$.

To make the above argument more precise (though still not mathematically rigorous), consider the evolution of our system of interest (as defined in Section 2.2) over the time interval $[0, \Delta t]$, as it evolves under the driven Hamiltonian $H_0 + V$. Specifically, we look at the dynamics of a statistical ensemble of initial conditions z_0 at $t = 0$, all with a common energy $H_0(z_0) = E_0$. For simplicity, we sample z_0 from a microcanonical distribution, as defined previously in 2.6:

$$\rho(z_0, 0) = \rho_{E_0}(z_0) \equiv \frac{1}{\Sigma(E_0)} \delta(E_0 - H_0(z_0)). \tag{2.9}$$

For each trajectory z_t in this ensemble, there is a net change $\Delta E \equiv H_0(z_{\Delta t}) - H_0(z_0)$ in the system's energy from $t = 0$ to $t = \Delta t$. Since the trajectory is fully determined by the initial condition z_0, the value of ΔE is fixed by z_0 as well. Thus, the quantity ΔE is a random variable, whose value is set by the random initial condition z_0. Understanding the statistics of ΔE in the high-frequency driving regime, for an appropriate choice of Δt (to be clarified below), will be the key to establishing diffusion in energy space.

To investigate the properties of ΔE, let us divide the time interval $[0, \Delta t]$ into $M \gg 1$ subintervals of equal duration $\delta t = \Delta t / M$, defining $t_i = (i - 1)\delta t$ as the beginning of the i^{th} subinterval. We then consider ΔE as a sum of energy changes

$$\Delta E = \sum_{i=1}^{M} \delta E_i, \tag{2.10}$$

where δE_i denotes the change in the system's energy between t_i and t_{i+1}. Each increment δE_i is itself a random variable, which may be determined by integrating the power (2.4) along the trajectory z_t over the subinterval. We can view δE_i as a function of $z^{(i)} \equiv z_{t_i}$ alone, since this phase space point at the beginning of the subinterval determines the rest of the trajectory.

Now, as discussed in Section 2.2, for sufficiently large ω the driven trajectories z_t closely resemble their undriven counterparts z_t^0. This means that we can choose Δt and ω so that over the interval $[0, \Delta t]$, the driven trajectories in our ensemble remain close to the initial energy shell E_0. Moreover, the similarity of this evolution to the undriven motion tells us that the chaotic mixing property of the dynamics is approximately preserved. As a result, continual mixing of the trajectories ensures that an effectively uniform distribution is maintained throughout the time interval. In particular, each $z^{(i)}$ will have the same microcanonical distribution. Since δE_i is a function of $z^{(i)}$, it follows that each δE_i will have nearly identical statistics, provided that we choose δt (and therefore also Δt) to be an integer multiple of the driving period T: This ensures that each subinterval begins at the same phase of the drive. For rapid driving, we generically expect $T \ll \delta t (\ll \Delta t)$.

Moreover, for an appropriate choice of δt, the energy increments δE_i will also be statistically independent of one another. Recall that chaotic mixing on the energy shell E_0 produces a decay of correlations over a characteristic correlation time $\tau_C(E_0) \equiv \tau_C$. Let us choose δt to be longer than $\tau_C(E_0)$, so that each δE_i is approximately statistically uncorrelated with the others. The energy change ΔE is then a sum of $M \gg 1$ independent, identically distributed increments δE_i: The system effectively performs a random walk on the energy axis. By the central limit theorem ΔE is a normally-distributed random variable, whose mean and variance grow in proportion to the number of increments M, equivalently (for fixed δt) the time elapsed Δt.

The statistical behavior just described is characteristic of a diffusive process in energy space,[1] motivating us to model it by a Fokker-Planck equation [94]. That is, we postulate that the

[1]We will refer to this as "energy diffusion," though to be precise, it is not energy that is diffusing, but rather

energy distribution $\eta(E,t) = \int dz\, \delta(H_0(z) - E)\rho(z,t)$ evolves according to:

$$\frac{\partial \eta}{\partial t} = -\frac{\partial}{\partial E}\left(g_1 \eta\right) + \frac{1}{2}\frac{\partial^2}{\partial E^2}\left(g_2 \eta\right). \tag{2.11}$$

The drift and diffusion coefficients $g_1(E,\omega)$ and $g_2(E,\omega)$ characterize, respectively, the rate at which the distribution η shifts and spreads on the energy axis. These coefficients generally depend on the system energy E and the driving frequency ω, and are obtained in Section 2.4 in the limit of large ω. Energy diffusion and its description in terms of the Fokker-Planck equation have been studied in a variety of physical and mathematical contexts, including in externally driven Hamiltonian systems, in systems weakly coupled to a thermal bath, and in other models [72, 95–123]. In Section 2.7 of this chapter, we discuss some of these other systems in more detail, and compare them to our results.

To conclude this section, is worth emphasizing the central role that a separation of timescales plays in our analysis. First, we have assumed that Δt is much smaller than the timescale $\tau_E(\omega, E_0)$ over which the energy of the system changes significantly, to ensure that the energy increments δE_i have approximately identical microcanonical statistics. We have also assumed that the interval Δt contains many subintervals of duration δt, and that $\delta t > \tau_C(E_0)$, guaranteeing approximate statistical independence among the increments δE_i. Thus our analysis requires the hierarchy of timescales:

$$T \ll \tau_C(E_0) \ll \Delta t \ll \tau_E(\omega, E_0). \tag{2.12}$$

Since $\tau_E(\omega, E_0) \to \infty$ as $\omega \to \infty$, this hierarchy can be satisfied for any particular energy shell

probability which is diffusing across energy space.

E_0 by setting ω sufficiently large. We conclude that Eq. (2.11) is valid over an interval of the energy axis whose extent is determined by, and increases with, the value of ω.

The above arguments suggest that the energy diffusion description is valid on a coarse-grained timescale of order Δt. On shorter timescales, computing the fine details of the system's energy evolution requires the full Hamiltonian equations of motion (2.2). These details vary greatly from system to system. However, as we will see, the characteristics of the energy diffusion process ultimately only depend on a few key details of these system-specific dynamics, as captured in the coefficients g_1 and g_2.

In the same vein, we can now see that our assumption of an initial microcanonical distribution at $t = 0$ is ultimately unnecessary. If the initial distribution is non-microcanonical (but still confined to the energy shell with energy E_0), then the short-time evolution of the energy distribution η may be non-diffusive, and poorly described by the Fokker-Planck equation (2.11). However, on timescales of order τ_C, chaotic mixing will establish an effectively microcanonical distribution on the energy shell. After this time, our previous arguments ensure that diffusive evolution will proceed on the longer timescale Δt. Since $\Delta t \gg \tau_C$, energy changes accumulated during this diffusive evolution will typically dominate over changes during the short pre-diffusive regime. Thus, if we are only concerned with dynamics on the coarse-grained timescale set by Δt, then the energy changes accrued at short times only constitute a small correction to the diffusive description.

2.4 Calculation of g_1 and g_2

In this section, we calculate the drift and diffusion coefficients g_1 and g_2, in the limit of large driving frequencies ω. Given these coefficients, the Fokker-Planck equation (2.11) fully characterizes the evolution of the energy distribution η, at least on a coarse-grained timescale. We begin by computing g_2, by considering the variance in energy acquired by an ensemble of trajectories evolving under the driven Hamiltonian. We then derive the fluctuation-dissipation relation (2.22), which allows us to obtain g_1 in terms of g_2. Ultimately, we find that both coefficients may be expressed in terms of a power spectrum $S(\omega; E)$ (given by (2.19)) associated with the chaotic dynamics of the undriven system, and in terms of the classical density of states Σ.

In what follows, we will restrict our attention to monochromatic driving protocols of the form $V(z, t/T) = V(z)\cos(\omega t)$, where $V(z) \equiv V$ is time-independent. Under this simplifying assumption, the power (2.4) takes the form

$$\frac{dE}{dt} = -\dot{V}(z_t)\cos(\omega t), \tag{2.13}$$

where $\dot{V}(z) \equiv \{V, H_0\}$. While the generalization to arbitrary periodic drives is straightforward, for simplicity of presentation we leave this generalization to Appendix A.

2.4.1 Calculation of the diffusion coefficient g_2

To obtain the diffusion coefficient g_2, consider an ensemble of initial conditions z_0 with energy $H_0(z_0) = E_0$, sampled from a microcanonical distribution $\rho_{E_0}(z_0)$ at time $t = 0$. If

we allow this ensemble to evolve for a time Δt under the driven Hamiltonian $H_0 + V\cos(\omega t)$, the resulting ensemble of trajectories will generally acquire some variance in energy $\mathrm{Var}(E) \equiv \langle E^2\rangle - \langle E\rangle^2$. For a particular choice of Δt, this variance may be calculated in two independent ways. We can then extract g_2 by comparing the two resulting expressions.

First, if Δt is much longer than the correlation time τ_C, then we can use the energy diffusion description. The microcanonical distribution $\rho_{E_0}(z_0)$ in phase space corresponds to an initial distribution $\eta(E,0) = \delta(E - E_0)$ in energy space, which may then be evolved under the Fokker-Planck equation (2.11) to a distribution $\eta(E, \Delta t)$. In particular, if Δt is also chosen to be much less than τ_E, the timescale over which significant energy changes occur, then it is straightforward to show that the final distribution $\eta(E, \Delta t)$ is a normal distribution, with mean and variance [94]:

$$\mathrm{Mean}(E) \approx E_0 + g_1(E_0,\omega)\Delta t \tag{2.14}$$

$$\mathrm{Var}(E) \approx g_2(E_0,\omega)\Delta t. \tag{2.15}$$

This result is consistent with the terminology "drift coefficient" and "diffusion coefficient": g_1 specifies the rate at which the mean of the energy distribution shifts in energy space, while g_2 characterizes the rate of spreading or diffusion.

Second, we can compute $\mathrm{Var}(E)$ directly from knowledge of the phase space trajectories z_t. For each trajectory, the change in energy ΔE over the time interval is obtained by integrating the power (2.13) from $t = 0$ to $t = \Delta t$. Noting that $\mathrm{Var}(E) = \langle(\Delta E)^2\rangle - \langle\Delta E\rangle^2$ (since E_0 is the same for all trajectories), this allows us to write

$$\mathrm{Var}(E) = \int_0^{\Delta t} dt \int_0^{\Delta t} dt' \, \cos(\omega t)\cos(\omega t') C_{neq}(t, t'; E_0), \tag{2.16}$$

where $C_{neq}(t, t'; E_0) \equiv \langle \dot{V}(z_t)\dot{V}(z_{t'})\rangle - \langle \dot{V}(z_t)\rangle\langle \dot{V}(z_{t'})\rangle$ is a nonequilibrium correlation function and angular brackets $\langle ...\rangle$ denote an ensemble average.

So far, no approximations have been made. Now, recall that in the high-frequency limit $\omega \to \infty$, the driven trajectories z_t approach their undriven counterparts z_t^0. In this regime, we are justified in replacing $C_{neq}(t, t'; E_0)$ by the corresponding *equilibrium* correlation function $C(t' - t; E_0)$, defined by

$$C(s; E_0) \equiv \langle \dot{V}(z_0^0)\dot{V}(z_s^0)\rangle - \langle \dot{V}(z_0^0)\rangle\langle \dot{V}(z_s^0)\rangle, \tag{2.17}$$

which depends only on the difference $s \equiv t' - t$, due to the time-translation symmetry of the microcanonical distribution under the undriven dynamics. Upon making this replacement, and using standard manipulations to approximate the resulting double integral (see, e.g. [124]), we arrive at

$$\mathrm{Var}(E) \approx \frac{1}{2} S(\omega; E_0)\Delta t, \tag{2.18}$$

where

$$S(\omega; E_0) = \int_{-\infty}^{\infty} dt \, e^{-i\omega t} C(t; E_0) \tag{2.19}$$

is the power spectrum of $\dot{V}(z_t^0)$, which is equal to the Fourier transform of $C(t; E_0)$ by the Wiener-Khinchin theorem [125]. The approximation in (2.18) contains correction terms that are sublinear in Δt. Comparing (2.18) with (2.15) and relabeling E_0 as E, we obtain our final expression for g_2:

$$g_2(E,\omega) \approx \frac{1}{2}S(\omega;E) \geq 0. \tag{2.20}$$

Note that (2.20) gives g_2 entirely in terms of properties of the *undriven* system, as $C(t;E)$ and thus $S(\omega;E)$ are defined in terms of the undriven trajectories z_t^0.

2.4.2 The fluctuation-dissipation relation and the drift coefficient g_1

We now move to the calculation of the drift coefficient g_1. We obtain g_1 by deriving the fluctuation-dissipation relation (2.22), which expresses g_1 in terms of g_2, and also the classical density of states Σ. This result emerges as a consequence of Liouville's theorem, which expresses the incompressibility of phase space volume under Hamiltonian dynamics [84]. Some technical details in the following calculation are omitted; these details are provided in Appendix B.

To begin, we return again to the phase space description of the system, where the distribution ρ for an ensemble of trajectories evolves according to the Liouville equation (2.3). The constant function $\rho(z) = 1$ is a stationary solution to this equation; this reflects the incompressibility of phase space volume under Hamiltonian dynamics (Liouville's theorem) [84]. Since $\rho = 1$ is stationary under the dynamics in *phase space*, the corresponding (unnormalized) distribution in *energy space* should be stationary under the Fokker-Planck equation. This energy distribution, obtained by marginalizing over the constant solution $\rho = 1$, is the density of states $\Sigma(E)$ – see (2.7). Setting $\eta(E,t) = \Sigma(E)$ as a stationary solution of the Fokker-Planck equation (2.11), we have

$$0 = -\frac{\partial}{\partial E}\left[g_1\Sigma - \frac{1}{2}\frac{\partial}{\partial E}\left(g_2\Sigma\right)\right]. \tag{2.21}$$

Thus the quantity in square brackets is constant as a function of E. In Appendix B, we show that this constant is in fact zero. Solving for g_1 then yields:

$$g_1(E,\omega) = \frac{1}{2\Sigma}\frac{\partial}{\partial E}\Big(g_2\Sigma\Big). \tag{2.22}$$

This result is a fluctuation-dissipation relation, which relates the average rate of energy change (given by g_1) to the fluctuations in energy characterized by g_2. Similar relations have been previously established for various driven Hamiltonian systems [103–105, 108, 110, 114, 119].

Using (2.20) and (2.22), the Fokker-Planck equation (2.11) takes the compact form

$$\frac{\partial \eta}{\partial t} = \frac{1}{4}\frac{\partial}{\partial E}\left[S\Sigma\frac{\partial}{\partial E}\left(\frac{\eta}{\Sigma}\right)\right]. \tag{2.23}$$

Eq. (2.23) is our main result in this chapter. It describes the stochastic evolution of the system's energy, under rapid driving, in terms of quantities $S(\omega;E)$ and $\Sigma(E)$ that characterize the undriven system.

As discussed in Section 2.3, we expect (2.23) to be valid over a region of the energy axis $\mathcal{R}(\omega)$, whose extent depends on ω. If $H_0(z)$ has a finite range, then ω can be chosen so that (2.11) is valid over all allowable energies. If the range of $H_0(z)$ is unbounded then the extent of validity of (2.11) can be made arbitrarily large, though not necessarily infinite, by appropriate choice of ω.

2.5 Implications of the energy diffusion description

With the expressions for g_1 and g_2 obtained in the previous section ((2.20) and (2.22)), the Fokker-Planck equation ((2.11) or (2.23)) now fully characterizes the diffusive evolution of the system's energy. In this section, we investigate the consequences of the energy diffusion description. We find that energy absorption generally proceeds in a predictable series of stages. First, we have an initial prethermalization phase at nearly constant energy, as the chaotic mixing of trajectories establishes a microcanonical distribution at the initial energy. Then, energy absorption and diffusion proceed as dictated by the Fokker-Planck equation. For systems with many degrees of freedom, the diffusion model typically predicts one of two outcomes: An indefinite increase in the system's mean energy, or a relaxation to an infinite temperature steady state. Alternatively, in either case, the energy diffusion description may potentially fail at sufficiently high energies, leading to the possibility of especially rapid energy absorption at long times. We will discuss each of these stages in turn, beginning with the process of prethermalization.

2.5.1 Stage 1: Floquet prethermalization

For purposes of illustration, we consider an initial ensemble of trajectories in phase space with a common energy E_0, distributed on the E_0 energy shell in a potentially nonuniform (non-microcanonical) way. Let us recall how these trajectories evolve for short times. As argued in Section 2.3, the diffusive description at energy E_0 is only valid on a coarse-grained timescale much longer than $\tau_C(E_0)$, the intrinsic correlation time associated with the chaotic motion of the system in phase space. For times of order $\tau_C(E_0)$ or shorter, the trajectories will remain

quite close to their undriven counterparts, and consequently their energy will remain nearly constant. Moreover, the process of chaotic mixing will spread these trajectories uniformly across the E_0 energy shell and nearby shells, resulting in an effectively microcanonical distribution at this energy. That is, the system thermalizes with respect to the undriven Hamiltonian H_0, on a timescale of order $\tau_C(E_0)$.

This short-time behavior is an example of the phenomenon of *Floquet prethermalization*. A driven system is said to prethermalize if it reaches thermal equilibrium with respect to an effective Hamiltonian on short to intermediate timescales, before ultimately gaining energy at far longer times [33, 39–49]. Here, the effective Hamiltonian is just the bare Hamiltonian H_0. The adjective "Floquet" specifies that the prethermalization process is governed by a time-periodic Hamiltonian. As detailed in the references above, Floquet prethermalization has been observed in a range of classical and quantum model systems.

When does the prethermalization stage come to an end? For times much longer than $\tau_C(E_0)$, the energy evolution becomes diffusive. Under the dynamics generated by the Fokker-Planck equation, the ensemble begins to spread away from the E_0 energy shell, while remaining uniformly distributed at each energy. Eventually, a significant fraction of the ensemble will have energies for which the associated microcanonical distribution is appreciably different from the microcanonical distribution for E_0. At this point, the statistics of the ensemble are no longer well-described by the microcanonical distribution for E_0, and we say that the prethermalization phase is over. Clearly, the timescale over which this process occurs will scale inversely with the rates of energy drift and diffusion, given by the coefficients g_1 and g_2 of the Fokker-Planck equation. As given in equations (2.20) and (2.22), these coefficients are determined by the power spectrum $S(\omega; E)$, which may be exceedingly small for large ω, leading to a very slow absorption

of energy. In particular, if the autocorrelation function $C(t;E)$ is a smooth function of time, then its Fourier transform $S(\omega;E)$ will decay faster than any power of ω^{-1} for large ω [126]. $C(t;E)$ will be smooth whenever $H_0(z)$ is a smooth function on phase space, since this implies that the trajectories z_t^0 will be smooth as well (conversely, see the analysis of billiard systems in Chapter 3 for an example of a non-smooth system). This rapid decay of $S(\omega;E)$ is consistent with observed exponential-in-frequency suppression of energy absorption in a range of classical and quantum model systems [33, 39, 41, 44, 45, 48, 49, 71, 75, 76, 80]. Prethermalization thus occurs when ω lies deep within the tail of the power spectrum.

2.5.2 Stage 2: Energy absorption under the Fokker-Planck equation

Once prethermalization is over, energy diffusion continues in accordance with the Fokker-Planck equation. To get an idea of how this evolution proceeds, let us compute the average rate of energy absorption predicted by the energy diffusion model. Multiplying the Fokker-Planck equation (2.11) by E and integrating over energy, we obtain

$$\frac{d\langle E\rangle}{dt} = \langle g_1(E,\omega)\rangle, \tag{2.24}$$

where $\langle f\rangle \equiv \int dE\, \eta f$ for any $f(E)$. Defining a microcanonical temperature $T_\mu(E) \equiv T_\mu$ via

$$\frac{1}{T_\mu} = \frac{\partial s}{\partial E}\,, \tag{2.25}$$

where $s(E) \equiv k_B \log \Sigma(E)$ is the microcanonical entropy and k_B is Boltzmann's constant, (2.22) becomes:

$$g_1(E,\omega) = \frac{1}{2k_B T_\mu}\left[g_2(E,\omega) + k_B T_\mu \frac{\partial g_2(E,\omega)}{\partial E}\right]. \tag{2.26}$$

The expression in square brackets is an expansion of $g_2(E + k_B T_\mu, \omega)$ for small $k_B T_\mu$, truncated after first order. For a system with N degrees of freedom, the difference between E and $E + k_B T_\mu$ corresponds to an energy change of $k_B T_\mu / N$ per degree of freedom. For a many-body system, with $N \gg 1$, this change is negligible, and we obtain the simplified fluctuation-dissipation relation

$$g_1(E,\omega) = \frac{g_2(E,\omega)}{2k_B T_\mu(E)}. \tag{2.27}$$

Substituting this result into (2.24), and remembering that $g_2(E,\omega) = \frac{1}{2}S(\omega;E)$, we have

$$\frac{d\langle E\rangle}{dt} = \left\langle \frac{S(\omega;E)}{4k_B T_\mu(E)} \right\rangle. \tag{2.28}$$

Recall that the power spectrum $S(\omega;E)$ is necessarily nonnegative. Thus, the sign of the average energy absorption rate is determined by the microcanonical temperature T_μ.

Given this expression for $d\langle E\rangle/dt$, we can classify a range of many-body systems into one of two broad categories. First, for a system of particles such as a gas or a liquid, the density of states $\Sigma(E)$ increases with energy, hence $T_\mu(E) > 0$ for any E. Thus, the average energy of the system continually increases with time, as expected intuitively. In fact, we can show that this result is encouragingly consistent with the Second Law of Thermodynamics, if we can identify the system's periodic drive with the variation of some macroscopic thermodynamic parameter,

like the position of a piston or the strength of an external magnetic field. From this perspective, we might consider a protocol as follows: Begin the system in a state of equilibrium at a fixed value of the thermodynamic parameter, then rapidly oscillate the parameter over an interval of time, and finally allow the system to relax to a new equilibrium state, with the parameter fixed back at its initial value. If the system is thermally isolated during this procedure, then the Second Law states that the entropy of the system cannot decrease in this process [83]. But for a system with positive thermodynamic temperature, this implies that the internal energy of the system also cannot decrease, since the temperature is the derivative of internal energy with respect to entropy (with other parameters held fixed). Thus, if we identify the average energy $\langle E \rangle$ with the thermodynamic internal energy, and the microcanonical temperature T_μ with the thermodynamic temperature, then (2.28) is just an expression of the Second Law.

Alternatively, there are some systems for which $T_\mu(E)$ is negative at some energies. This is typical in systems with a bounded phase space, with finite total volume $\int dz = \int dE\, \Sigma(E)$. For example, for N classical spin degrees of freedom described by the Hamiltonian $H_0 = \mathbf{B} \cdot \sum_n \mathbf{S}_n$, $T_\mu(E)$ is positive for $E > 0$ and negative for $E > 0$. Thus $d\langle E \rangle / dt$ can be negative, provided that the distribution η has sufficient weight on regions of energy space with $T_\mu(E) < 0$. For this class of systems, energy diffusion comes to an end when the ensemble has spread uniformly across the entire phase space, according to the following reasoning. The finite volume of phase space allows us to define a normalized constant distribution $\rho(z) \propto 1$; the corresponding distribution in energy space is the normalized density of states as $\overline{\Sigma}(E) \equiv \Sigma(E) / \int dE'\, \Sigma(E')$. This "infinite temperature" energy distribution, obtained by considering the canonical energy distribution $\eta_{T_c}(E) \propto \Sigma(E) e^{-E/k_B T_c}$ in the limit $T_c \to \infty$, is a stationary distribution under the Fokker-Planck equation (2.23). Moreover, if $g_2(E, \omega)$ is strictly positive for all E, ensuring

that there are no insurmountable barriers along the energy axis, then the Fokker-Planck equation describes an *ergodic* Markov process, and $\overline{\Sigma}(E)$ is the *unique* stationary distribution to which any initial distribution evolves as $t \to \infty$ [127, 128]. In this asymptoptic limit, although individual trajectories in the ensemble may gain or lose energy, evolution of the distribution η ceases.

2.5.3 Stage 3: Breakdown of the energy diffusion description?

Up until now, the discussion in this section has assumed that the energy diffusion description remains valid throughout the system's evolution. But this need not be the case: In general, the diffusion model is only accurate over a certain region $\mathcal{R}(\omega)$ of energy space. Beyond this range of energies, our rapid driving assumption is not valid, and the assumed separation of timescales (2.12) breaks down. As the diffusion process proceeds, the distribution η will slowly leak out of $\mathcal{R}(\omega)$, and a significant fraction of trajectories in the ensemble will eventually reach energies outside of this region. At this point, diffusive evolution is no longer guaranteed, and the possibility of especially rapid energy absorption arises, for example via resonances between the system and the drive.

For an illustrative example of this breakdown, we can look to particle systems, such as gases or liquids. For such systems, particle speeds will typically increase as η spreads to higher and higher energies. Larger speeds entail a shorter intrinsic correlation time $\tau_C(E)$, and a consequent broadening of the power spectrum $S(\omega; E)$ as a function of ω. As a result, the rate of energy absorption and diffusion may begin to speed up, since the driving frequency might no longer be located in the far tail of the broadened power spectrum. Eventually, at sufficiently large E, $\tau_C(E)$ may become comparable to the driving period T: The drive is no longer rapid relative to the

motion of the system, and the hierarchy of timescales (2.12) is no longer satisfied. At this point, while the diffusive description may no longer be applicable, the thermodynamic arguments earlier in this section plausibly suggest that the mean energy will continue to increase. As the system's phase space and energy are unbounded, this energy absorption may continue indefinitely.

For systems with a bounded phase space, the diffusive description may similarly fail at certain energies. However, such systems will typically have a finite range of possible energies. This means that if we increase ω, the region $\mathcal{R}(\omega)$ will eventually expand to include to the whole range of allowed energies, and the energy diffusion model will be valid everywhere in energy space. In this case, energy diffusion will simply continue unabated until the infinite temperature distribution $\overline{\Sigma}(E)$ is reached.

In summary, the energy of a chaotic system under rapid periodic driving generally proceeds as follows. First, chaotic mixing establishes a statistical prethermal state at the system's initial energy E_0, on a timescale of order $\tau_C(E_0)$. Then, slow energy evolution proceeds in accordance with the diffusive description; for many macroscopic systems, this entails either indefinite energy absorption or relaxation to the infinite temperature state. However, at long times, the energy diffusion model may ultimately break down, if the system reaches energies where the rapid driving assumption is no longer valid.

2.6 Entropy, detailed balance, and fluctuation theorems

In this section, we study the evolution of entropy in systems described by our energy diffusion model. We define a coarse-grained Gibbs entropy for the system, which may be expressed in terms of the system's energy distribution η. This motivates us to define an entropy

at the level of individual trajectories, which yields the coarse-grained Gibbs entropy when averaged over an ensemble. We are then able to establish a detailed fluctuation theorem for such trajectories, which relates the probability of transition from one energy to another to the probability of the reverse transition. This fluctuation theorem implies that the system obeys the Second Law for thermally isolated systems.

2.6.1 Entropy and the Second Law in the energy diffusion model

We begin by defining an appropriate entropy for statistical ensembles evolving according to the energy diffusion description. In standard statistical mechanics, the *fine-grained* Gibbs entropy $\mathfrak{S}_G(t) \equiv \mathfrak{S}_G$ is given by an average with respect to the system's phase space distribution ρ:

$$\mathfrak{S}_G(t) \equiv -k_B \int dz\, \rho(z,t) \ln \rho(z,t). \tag{2.29}$$

When a macroscopic system is in thermal equilibrium, this quantity can be identified with the thermodynamic entropy. However, for nonequilibrium systems, this straightforward identification is not always possible. In particular, for Hamiltonian systems, $\mathfrak{S}_G$ is conserved under the dynamics, which tells us that it cannot capture the increase in thermodynamic entropy suggested by the Second Law.

To see this, consider the quantity $dz\, \rho(z,t)$, which gives the probability that the system at time t will be found in the infinitesimal volume element dz surrounding the point z. For a deterministic system, $dz\, \rho(z,t) = dz_0\, \rho(z_0, 0)$, where z_0 is the initial condition that maps to z under the evolution between times 0 and t, and dz_0 is the volume element which maps to dz. By Liouville's theorem, which expresses conservation of phase space volume under Hamiltonian

evolution, $dz = dz_0$, and therefore $\rho(z,t) = \rho(z_0,0)$. Upon substituting these relations into (2.29), and treating z_0 as the new variable of integration, we find that $\mathfrak{S}_G(t) = \mathfrak{S}_G(0)$.

Instead, we can define a more suitable entropy by considering a *coarse-grained* version of the Gibbs entropy. Recall that in the energy diffusion description, our information about the system is characterized by the energy probability distribution η. Moreover, continual chaotic mixing ensures that the ensemble is effectively microcanonically distributed on each energy shell. Therefore, instead of needing the full distribution ρ, we can describe the ensemble (for all practical purposes) with a coarse-grained density $\bar{\rho}(z,t) \equiv \bar{\rho}$, that (a) is *uniform* on each energy shell, and (b) has an energy distribution which matches η. This motivates us to define the Gibbs entropy associated with $\bar{\rho}$ as a coarse-grained entropy $\mathfrak{S}(t) \equiv \mathfrak{S} \equiv -k_B \int dz\, \bar{\rho}(z,t) \ln \bar{\rho}(z,t)$.

We can then express this coarse-grained entropy in terms of η. To do so, first note that by condition (a) above, $\bar{\rho}$ is a function of only $H_0(z)$ and t. Then, if we marginalize $\bar{\rho}$ with respect to energy, condition (b) requires that this function is $\bar{\rho}(z,t) = \eta(H_0(z),t)/\Sigma(H_0(z))$. Finally, if we substitute this expression for $\bar{\rho}$ into the definition $\mathfrak{S} \equiv -k_B \int dz\, \bar{\rho} \ln \bar{\rho}$, then introducing the resolution of the identity $1 = \int dE\, \delta(H_0(z) - E)$ allows us to integrate over z and obtain:

$$\mathfrak{S}(t) = -k_B \int dE\, \eta(E,t) \ln \left[\frac{\eta(E,t)}{\Sigma(E)} \right]. \tag{2.30}$$

That is, $\mathfrak{S}/k_B$ is just the Kullback-Leibler divergence [129, 130] of η with respect to the (unnormalized) distribution Σ.

For macroscopic systems, it is reasonable to identify this entropy with the thermodynamic entropy, for at least two reasons. First, when the system is in a thermal equilibrium state at temperature T, the canonical distribution $\rho_T(z) \propto e^{-H_0(z)/k_B T}$ is unchanged by coarse-graining,

so the coarse-grained entropy and the Gibbs entropy coincide. Second, the coarse-grained entropy $\mathfrak{S}$ obeys a Second Law inequality appropriate for thermally isolated systems. In classical thermodynamics, if a system moves between two equilibrium states without exchanging heat with its environment (a thermodynamically adiabatic, but not necessarily quasistatic, process[2]), then the Second Law implies that this process cannot decrease the thermodynamic entropy of the system [83]. Correspondingly, we can show that under the dynamics generated by the Fokker-Planck equation 2.23, the entropy production rate $d\mathfrak{S}/dt$ is always nonnegative:

$$\begin{aligned}
\frac{d\mathfrak{S}}{dt} &= -k_B \frac{d}{dt} \int dE\, \eta \ln\left(\frac{\eta}{\Sigma}\right) \\
&= -k_B \int dE\, \frac{\partial \eta}{\partial t} \ln\left(\frac{\eta}{\Sigma}\right) \\
&= -\frac{k_B}{4} \int dE\, \frac{\partial}{\partial E}\left[S\Sigma \frac{\partial}{\partial E}\left(\frac{\eta}{\Sigma}\right)\right] \ln\left(\frac{\eta}{\Sigma}\right) \\
&= \frac{k_B}{4} \int dE\, S\Sigma \frac{\partial}{\partial E}\left(\frac{\eta}{\Sigma}\right) \frac{\partial}{\partial E}\left[\ln\left(\frac{\eta}{\Sigma}\right)\right] \\
\frac{d\mathfrak{S}}{dt} &= \frac{k_B}{4} \int dE\, \eta S \left\{\frac{\partial}{\partial E}\left[\ln\left(\frac{\eta}{\Sigma}\right)\right]\right\}^2 \geq 0
\end{aligned} \tag{2.31}$$

Here, in moving from the first line to the second line, we apply the product rule and invoke conservation of probability ($\int dE\, \eta = 1 = \text{const.}$), and to obtain the third line, we use the expression for $\partial\eta/\partial t$ furnished by the Fokker-Planck equation (2.23). Recall that S is the power spectrum defined in (2.19). In moving from the third line to the fourth line, we perform an integration by parts and assume that the boundary terms vanish.

Thus, we see that $\mathfrak{S}$ indeed possesses properties consistent with the thermodynamic

[2]Note that the term "adiabatic" has more than one meaning. Here, "adiabatic" refers to an absence of heat flow. Elsewhere, like in the quantum adiabatic theorem [131], "adiabatic" means slow.

entropy. The inequality $d\mathfrak{S}/dt \geq 0$ also gives us insight into the asymptotic evolution of the system at long times. Assume for simplicity that η and the power spectrum are nonzero for all energies E. Then, the final line of (2.31) tells us that the *equality* $d\mathfrak{S}/dt = 0$ is only achieved when the quantity in curly brackets vanishes for all E. This is only possible for $\eta \propto \Sigma$. This means that $\mathfrak{S}$ (and therefore η) will continue to evolve unless the distribution $\eta \propto \Sigma$ is reached. For systems with an unbounded phase space, such a distribution does not exist, since Σ is not a normalizable probability distribution, so we generally expect $\mathfrak{S}$ to grow without bound. Alternatively, for spin systems and other systems with a bounded phase space, this final distribution is simply the infinite temperature distribution $\overline{\Sigma}(E) \equiv \Sigma(E)/\int dE' \, \Sigma(E')$, defined in Section 2.5 (for an example of such a system, see Chapter 4, Section 4.3). Once this distribution is attained, the entropy $\mathfrak{S}$ stabilizes at the final value $\mathfrak{S}_{\max} = k_B \ln(\int dE \, \Sigma)$, proportional to the logarithm of the total phase space volume $\int dE \, \Sigma$.

The coarse-grained entropy $\mathfrak{S}$ is defined at the ensemble level. We can also define an entropy $\mathfrak{s}(E_t, t) \equiv \mathfrak{s}$ for individual trajectories, which yields $\mathfrak{S}$ upon averaging over the ensemble. Consider a phase space trajectory z_t, with energy $E_t \equiv H_0(z_t)$. We define the corresponding trajectory entropy as

$$\mathfrak{s}(E_t, t) \equiv -k_B \ln \left[\frac{\eta(E_t, t)}{\Sigma(E_t)} \right]. \tag{2.32}$$

The physical interpretation of this entropy is somewhat unclear. While a trajectory-specific quantity, the value of $\mathfrak{s}$ is still a property of the entire ensemble, since it depends on the distribution η. Nevertheless, it is worth investigating the properties of $\mathfrak{s}$, since entropies of this type have been frequently studied in the field of stochastic thermodynamics (see for instance

[132, 133]).

First, we immediately see that averaging $\mathfrak{s}$ with respect to η at the time t yields $\mathfrak{S}$:

$$\langle \mathfrak{s}(E_t, t) \rangle = -k_B \int dE_t \, \eta(E_t, t) \ln \left[\frac{\eta(E_t, t)}{\Sigma(E_t)} \right] = \mathfrak{S}(t), \tag{2.33}$$

which tells us that the Second Law inequality $d\mathfrak{S}/dt \geq 0$ is a statement about the on-average increase of $\mathfrak{s}$. Later, we will see that $d\langle \mathfrak{s} \rangle/dt \geq 0$ is a corollary of a fluctuation theorem involving $\mathfrak{s}$, which relates the probability of the system performing a given evolution in energy space to the probability of the time-reversed evolution. In preparation for the proof of this result, we now turn to a discussion of time-reversal symmetry in the energy diffusion model.

2.6.2 Time-reversal symmetry and detailed balance

Consider a phase space trajectory z_t for a system described by the energy diffusion model, for $t \in \mathbb{R}$. We can define a corresponding "time-reversed" trajectory by $z_t^R \equiv z_{-t}$: A system following this reversed trajectory moves through the same sequence of phase space points as the original trajectory, but in the opposite order (see Figure 2.3). Such an evolution can be understood as being generated by the Hamiltonian $-H_0 - V(-t/T)$. Let us refer to a system governed by these dynamics as the reversed system, and the original system as the forward system. Note that this time reversal with respect to *phase space* should be distinguished from the more common notion of time reversal, in which the particles in a system reverse their motion in *real space*, while the signs of particle velocities are flipped.

With a little thought, we can see that the reversed system satisfies the assumptions necessary for energy diffusion. First, the evolution of the reversed system will be ergodic. Since a typical

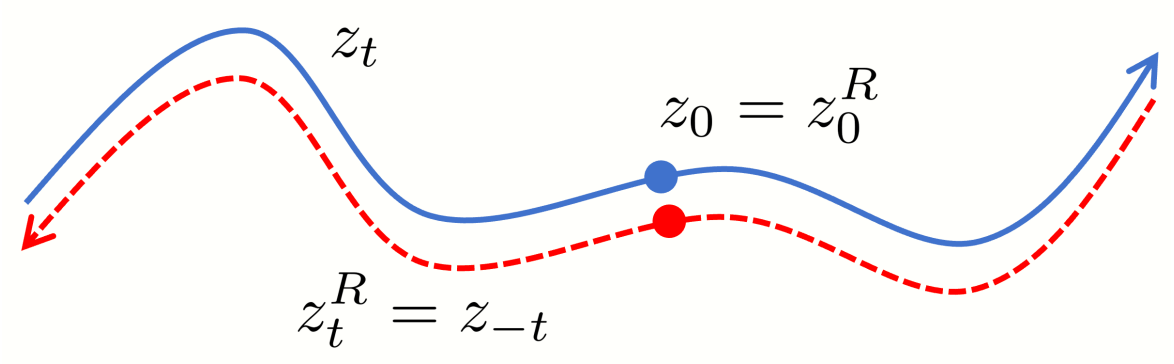

Figure 2.3: A pair of counterpart forward and reverse trajectories z_t and $z_t^R = z_{-t}$ (the blue solid curve and red dashed curve, respectively), with the common initial condition $z_0 = z_0^R$. Here, the trajectories are slightly displaced relative to one another for visualization purposes, but in reality they trace out the exact same curve in phase space, but in the opposite time order as denoted by the arrows.

trajectory of the forward system ergodically explores the corresponding H_0 energy shell, a typical time-reversed trajectory will as well, since any pair of forward and reversed trajectories explore the same region of phase space, just in the opposite order. Second, the reversed dynamics will be chaotic. In the forward system, although a set of nearby evolving trajectories will stretch out along some directions in phase space (in order to achieve the exponential divergence of trajectories characteristic of chaos), the set must contract in other directions, since Liouville's theorem requires that the volume of the set remain constant. This means that a set of reversed trajectories will also diverge exponentially, since it will stretch out along the same directions that a counterpart forward set would contract along. Finally, for finite V, the same arguments as Section 2.3 tell us that for large ω, the driven trajectories will be weakly perturbed from their undriven counterparts. Thus, just like in the original system, the energy H_0 will evolve via a series of small, random changes, manifesting as a process of diffusion in energy space. The evolution of the energy probability distribution will then be described by a Fokker-Planck equation akin to (2.11).

In fact, the energy diffusion process for the reversed system is governed by the *same* Fokker-Planck equation as the original system, with identical expressions for the coefficients g_1 and g_2. To see this, consider the diffusion coefficient g_2 for the reversed system. We can calculate g_2 via the same steps that we followed to obtain g_2 for the original system, as given in Section 2.3. In this way, we find that g_2 for the time-reversed system is one-half the Fourier transform of an autocorrelation function $C_R(s; E_0) \equiv \langle \dot{V}(z_0^{R,0}) \dot{V}(z_s^{R,0}) \rangle - \langle \dot{V}(z_0^{R,0}) \rangle \langle \dot{V}(z_s^{R,0}) \rangle$, defined in terms of the *time-reversed* undriven trajectories $z_t^{R,0} \equiv z_{-t}^0$. However, as is easy to show, this correlation function is identical to the correlation function for the original system, defined in (2.17):

$$\begin{aligned} C_R(s; E_0) &= \langle \dot{V}(z_0^0) \dot{V}(z_{-s}^0) \rangle - \langle \dot{V}(z_0^0) \rangle \langle \dot{V}(z_{-s}^0) \rangle \\ &= \langle \dot{V}(z_s^0) \dot{V}(z_0^0) \rangle - \langle \dot{V}(z_s^0) \rangle \langle \dot{V}(z_0^0) \rangle \\ &= C(s; E_0). \end{aligned} \tag{2.34}$$

Here, in moving from the first line to the second line, we have used the time-translation symmetry of the microcanonical distribution under the undriven dynamics. Thus, we see that the diffusion coefficient for the reversed system is given by $g_2(E, \omega) = \frac{1}{2} S(\omega; E)$, just as in the original system.

Moreover, the energy diffusion process for the time-reversed system will satisfy the fluctuation-dissipation relation (2.22), by the same arguments used to justify this relation for the original system. This implies that the drift coefficient g_1 for the two systems will also be the same. Since the Fokker-Planck dynamics are fully characterized by the quantities g_1 and g_2, we

see that the energy dynamics of the original system and the reversed system are governed by the same Fokker-Planck equation. In this sense, we say that the energy diffusion model possesses time-reversal symmetry. Notably, this symmetry obtains whether or not the system of interest has any fundamental time-reversal symmetry at the level of the microscopic dynamics, e.g., in systems of interacting particles in the absence of external magnetic fields.

The time-reversal symmetry property of the diffusive description allows us to derive a relation of *detailed balance*, analogous to similar relations valid for systems in contact with a thermal bath. In such systems, the condition of detailed balance relates the probability of a transition $A \to B$ between some states A and B, to the probability of the reverse transition $B \to A$ [93]. In the same vein, the detailed balance condition in the context of energy diffusion connects the probability of an energy transition $E' \to E$ to the probability of the reverse $E \to E'$. More precisely, suppose that an ensemble of systems described by the energy diffusion model is allowed to evolve from $t = 0$ to some time $t = \tau$. We define the transition kernel $T(E|E';\tau)$ as the probability distribution for the system's energy E at $t = \tau$, given that the system's energy was E' at $t = 0$. Our aim is to establish a relation between $T(E|E';\tau)$ and the transition probability for the reverse transition, $T(E'|E;\tau)$.

In terms of the Fokker-Planck equation, $T(E|E';\tau)$ may be obtained in principle by solving the Fokker-Planck equation with the initial condition $\eta(E,0) = \delta(E-E')$. However, to establish the detailed balance condition, it is best to compute $T(E|E';\tau)$ in terms of the underlying Hamiltonian description in phase space. To do so, consider an ensemble of initial conditions z_0 with energy E' at $t = 0$; for simplicity, we sample them according to a microcanonical distribution $\rho_{E'}(z_0)$ (see (2.6)). Each initial condition evolves according to Hamilton's equations (2.2), and reaches the phase space point z_τ at $t = \tau$. Then, $T(E|E';\tau)$ is given by the resulting

distribution of energies at $t = \tau$, obtained by integrating $\rho_{E'}(z_0)$ over all initial conditions which attain the energy E at $t = \tau$:

$$\begin{aligned} T(E|E';\tau) &= \int dz_0\, \rho_{E'}(z_0)\delta\left(H_0(z_\tau) - E\right) \\ &= \frac{1}{\Sigma(E')} \int dz_0\, \delta\left(H_0(z_0) - E'\right) \delta\left(H_0(z_\tau) - E\right). \end{aligned} \tag{2.35}$$

Note that our choice of the initial microcanonical distribution is for convenience; any distribution confined to the E' energy shell would do. As long as τ is large enough that the energy diffusion description is valid, any non-microcanonical distribution will become effectively microcanonical on timescales $\ll \tau$, and the resulting kernel $T(E|E';\tau)$ will be approximately the same. Moreover, the choice of initial time $t = 0$ is arbitrary. The periodic nature of the drive means that that the transition kernel must have discrete time-translation symmetry: The conditional probability of a transition $E' \to E$ between $t = 0$ and $t = \tau$ is the same as the probability of that same transition between $t = nT$ and $t = nT + \tau$, where n is an integer. So as long as we restrict our attention to times which are an integer multiple of the driving period, $T(E|E';\tau)$ simply characterizes the probability of transitions from E' and E over *any* interval of duration τ, irrespective of the initial time.

On the other hand, we just established that the reversed system undergoes the same energy diffusion process, with the same transition probabilities. Therefore, we can also compute $T(E|E';\tau)$ in terms of the trajectories of the reversed system $z_t^R = z_{-t}$:

$$
\begin{aligned}
T(E|E';\tau) &= \int dz_0^R\, \rho_{E'}(z_0^R)\delta\left(H_0(z_\tau^R) - E\right) \\
&= \frac{1}{\Sigma(E')}\int dz_0^R\, \delta\left(H_0(z_0^R) - E'\right)\delta\left(H_0(z_\tau^R) - E\right) \\
&= \frac{1}{\Sigma(E')}\int dz_0\, \delta\left(H_0(z_0) - E'\right)\delta\left(H_0(z_{-\tau}) - E\right) \\
&= \frac{\Sigma(E)}{\Sigma(E')}T(E'|E;\tau).
\end{aligned}
\tag{2.36}
$$

In moving from the third line to the fourth line above, we have noted that the integral on the third line is $\Sigma(E)$ times the transition kernel for transitions $E \to E'$ between $t = -\tau$ and $t = 0$. But by the discrete time translation symmetry of the dynamics, this kernel is just $T(E'|E)$. Rearranging the final equality, we arrive at the desired detailed balance condition:

$$
\Sigma(E')T(E|E';\tau) = \Sigma(E)T(E'|E;\tau). \tag{2.37}
$$

2.6.3 A detailed fluctuation theorem

We are now in a position to prove a fluctuation theorem for the energy diffusion model, which emerges as a straightforward corollary of the detailed balance condition (2.37). We begin by laying out a few preliminary definitions, which allow us to state the theorem, and then we proceed to the proof.

To proceed, consider an ensemble of systems described by the energy diffusion model, with associated energy distribution $\eta(E,t)$. Let us observe the system at $K+1$ discrete times $t_i = i\tau$, where $i = 0, 1, 2 \ldots K$. As before, assume that the time τ is long enough that the diffusive description is valid. For each trajectory in the ensemble, the energy of the system at

these discrete times will be given by some definite sequence $\{E_i\} \equiv E_0 \to E_1 \to ... \to E_K$, where E_i is the energy of the system at $t = t_i$. Therefore, given a particular ensemble, we can then consider the corresponding probability distribution over possible energy sequences $\{E_i\}$, denoted by $P(\{E_i\})$.

The fluctuation theorem connects the distribution of sequences for two related ensembles, a "forward" ensemble and a "backward" ensemble. The forward ensemble is described by an arbitrary initial energy distribution $\eta_F(E, t_0)$, which evolves according to the Fokker-Planck equation to some final distribution $\eta_F(E, t_K)$. Let $P_F(\{E_i\})$ denote the probability distribution over possible sequences $\{E_i\}$ for this ensemble; speaking loosely, we say that $P_F(\{E_i\})$ is the probability of observing the sequence $\{E_i\}$ in the forward ensemble. Conversely, the reverse ensemble is defined as the ensemble with an *initial* distribution $\eta_R(E, t_0) \equiv \eta_F(E, t_K)$ which matches the *final* distribution of the forward ensemble, which is then allowed to evolve under the Fokker-Planck dynamics from $t = t_0$ to $t = t_K$ (see Figure 2.4). This ensemble has its own distribution of sequences $P_R(\{E_i\})$. For a given sequence $\{E_i\} \equiv E_0 \to E_1 \to ... \to E_K$, the fluctuation theorem relates its probability in the forward ensemble, to the probability of the corresponding *time-reversed* sequence $\{E_i\}^* \equiv E_K \to E_{K-1} \to ... \to E_0$ in the reverse ensemble:

$$\frac{P_F(\{E_i\})}{P_R(\{E_i\}^*)} = \exp\left(\frac{\Delta\mathfrak{s}(\{E_i\})}{k_B}\right), \tag{2.38}$$

Here, $\Delta\mathfrak{s}(\{E_i\}) = \mathfrak{s}(E_K, t_K) - \mathfrak{s}(E_0, t_0) \equiv \Delta\mathfrak{s}$ is the net change in the trajectory entropy (2.32) when the system evolves through the sequence $\{E_i\}$.

To prove this result, we reason as follows. The forward sequence distribution $P_F(\{E_i\})$ is

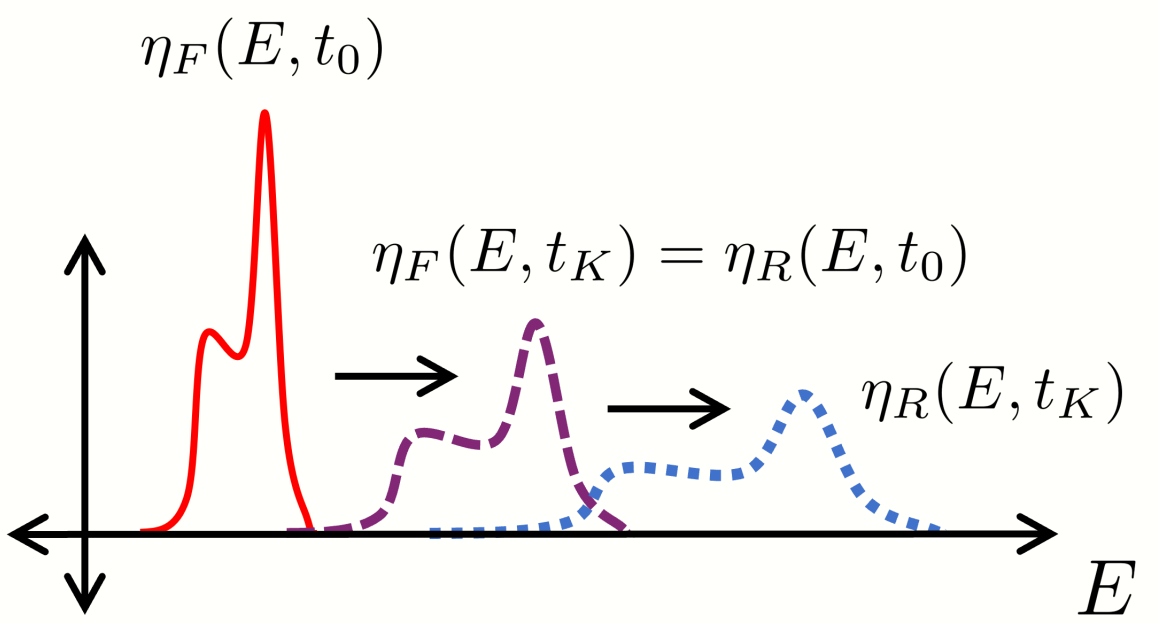

Figure 2.4: Plot displaying the relationship between the forward and reverse distributions $\eta_F(E,t)$ and $\eta_R(E,t)$. The initial forward distribution $\eta_F(E,t_0)$ (solid red curve) evolves between $t = t_0$ and $t = t_K$ to the final forward distribution $\eta_F(E,t_K)$ (dashed purple curve). This evolved distribution is also equal to the *initial* reverse distribution $\eta_R(E,t_0)$, which evolves from $t = t_0$ to $t = t_K$ into the final reverse distribution $\eta_R(E,t_K)$ (dotted blue curve).

simply the joint distribution for the $K+1$ random variables $E_0, E_1 \ldots E_K$, given the ensemble with distribution $\eta_F(E,t)$. Now, note that energy diffusion (and diffusion more generally) is a type of *Markov* process: Given the system's energy E' at some time t, the probability for the system to transition to a new energy at $t + \Delta t$ is independent of the past history of the system, including the value of the energy at previous times [93]. As a result, the joint distribution may be factorized into a product of transition probabilities $T(E_{i+1}|E_i;\tau)$

$$P_F(\{E_i\}) = \eta_F(E_0,t_0)T(E_1|E_0;\tau)T(E_2|E_1;\tau)\ldots T(E_K|E_{K-1};\tau). \tag{2.39}$$

By identical reasoning, the sequence distribution for the reverse ensemble, evaluated for the reverse sequence $\{E_i\}^*$, is given by

$$P_R(\{E_i\}^*) = \eta_R(E_K, t_0)T(E_{K-1}|E_K;\tau)T(E_{K-2}|E_{K-1};\tau)\ldots T(E_0|E_1;\tau). \tag{2.40}$$

We can now take the ratio of these expressions for $P_F(\{E_i\})$ and $P_R(\{E_i\}^*)$. The result depends on a series of ratios $T(E_{i+1}|E_i;\tau)/T(E_i|E_{i+1};\tau)$, which by the detailed balance condition (2.37) are equal to $\Sigma(E_{i+1})/\Sigma(E_i)$. All the factors of Σ cancel except for two, and we are left with

$$\frac{P_F(\{E_i\})}{P_R(\{E_i\}^*)} = \frac{\eta_F(E_0, t_0)}{\eta_R(E_K, t_0)}\frac{\Sigma(E_K)}{\Sigma(E_0)}. \tag{2.41}$$

Finally, if we recall the definition of the trajectory entropy (2.32), and that $\eta_R(E_K, t_0) = \eta_F(E_K, t_K)$ by definition, then we obtain the fluctuation theorem (2.38).

This relation is a so-called "detailed" fluctuation theorem, which concerns the probabilities of individual sequences in energy space. As with fluctuation theorems for other systems, an immediate corollary of this result is the corresponding integral fluctuation theorem. To see this, multiply both sides of (2.41) by $P_R(\{E_i\}^*)\exp(-\Delta\mathfrak{s}/k_B)$, and then integrate over $E_0, E_1 \ldots E_K$. Then, on the right-hand side, we have an average of $\exp(-\Delta\mathfrak{s}/k_B)$ over all possible sequences, and on the left-hand side, we have the integral of the normalized probability distribution $P_R(\{E_i\}^*)$, which must be 1:

$$\left\langle \exp\left(-\frac{\Delta\mathfrak{s}(\{E_i\})}{k_B}\right)\right\rangle = 1. \tag{2.42}$$

We can use this integral fluctuation theorem to corroborate the previously established

Second Law inequality (2.31), which states that the coarse-grained entropy $\mathfrak{S}$ cannot decrease. To do so, we invoke Jensen's inequality applied to the exponential function, which states that for a random variable X, $e^{\langle X \rangle} \leq \langle e^X \rangle$ [128]. Setting $X = -\Delta\mathfrak{s}/k_B$, the integral fluctuation theorem then implies that $\exp(-\langle \Delta\mathfrak{s} \rangle / k_B) \leq 1$, or $\langle \Delta\mathfrak{s} \rangle \geq 0$. Since $\mathfrak{S} = \langle \mathfrak{s} \rangle$, this is just the Second Law for the coarse-grained entropy $\mathfrak{S}$.

The detailed and integral fluctuation theorems derived above are both closely related to results previously obtained by other authors. The literature on fluctuation theorems is enormous (for reviews of this topic see [134, 135]), so it is difficult to exhaustively catalogue all the possible connections, but we highlight three important points of comparison here. First, the general structure of the above proof is very similar to the original derivation of the Crooks fluctuation theorem [136]. In both proofs, the probability of a discrete sequence of system states is expressed as a chain of transition probabilities, and these transition probabilities are related to their reverse counterparts via a detailed balance relation. Second, the integral fluctuation theorem (2.42) is closely analogous to the result $\langle e^{-\Delta s_{\mathrm{tot}}/k_B} \rangle = 1$ derived by Seifert in [133] for a diffusing colloidal particle. Beyond the obviously distinct physical settings, there are two key differences between our result and Seifert's: (a) the diffusion coefficient in Seifert's model is a constant in the Fokker-Planck equation, while in our model it varies with energy, and (b) while the entropy change Δs_{tot} in Seifert's work corresponds mathematically to $\Delta\mathfrak{s}$ in our result, physically Δs_{tot} represents the total entropy change of the colloidal particle and the surround medium, while $\Delta\mathfrak{s}$ corresponds to the entropy change of the system alone. Third and finally, if the Fokker-Planck equation admits a normalized stationary distribution (the infinite temperature distribution $\overline{\Sigma}(E)$), then it is possible to obtain the fluctuation theorems (2.41) and (2.42) by applying the formalism presented in [137], which establishes fluctuation theorems for a broad class of diffusive processes.

2.7 Overview of other energy diffusion models

To conclude this chapter, we present a brief review of work by other authors on the topic of energy diffusion. The diffusive evolution of energies have been studied in a diverse range of physical and mathematical settings, from the escape of a Brownian particle over a potential barrier [95, 96, 106], to atoms excited by an oscillating electromagnetic field [101, 102], to the adiabatic driving of chaotic systems [98, 103–105, 108, 110, 111]. In this section, we provide an overview of this body of work, describe the typical conditions under which an energy diffusion description is appropriate, and point out which results from other authors are most closely related to our own. Broadly speaking, the systems discussed here fall into one of two related categories: Systems subject to a coherent external drive, modelled by a time-dependent Hamiltonian, and systems which exchange energy with a weakly coupled thermal bath. Note that in this section, we primarily consider classical systems; a review of energy diffusion models in quantum systems is postponed to Chapter 5.

First, let us sketch out some qualitative conditions under which we expect an energy diffusion description of a system to be potentially valid. We can use our chaotic system under rapid periodic driving as a guiding example. Recall from our arguments in Section 2.3 that the diffusion of energies emerged as a consequence of two key properties of the dynamics: The decay of correlations characteristic of the chaotic evolution, with associated correlation timescale τ_C, and the effective weakness of the drive. This first property implies that on a coarse-grained timescale much longer than τ_C, the system gains and loses energy from the drive in a series of effectively random, uncorrelated energy changes (the quantities δE_i in Section 2.3). Meanwhile, the second property tells us that the system's energy and statistical properties will change very

slowly, implying that many successive energy changes in a row will have essentially identical statistics. The result is a random walk or diffusion in energy space.

Extrapolating from this example, we can see that an energy diffusion model might be more generally applicable to systems with two features: (a) a source of randomness or effective randomness, resulting in a decay of correlations on a timescale τ_C, and (b) an external perturbation which has a sufficiently small effect, at least on a timescale much longer than τ_C. The property (a) could emerge from a variety of sources: In our work, effective stochasticity follows from the chaotic nature of the system's internal dynamics, but randomness might also appear in an interaction with a thermal bath, or from chaotic motion induced by the external perturbation itself. On the other hand, systems with property (b) could include certain adiabatically (slowly) driven systems, rapidly driven systems, or systems where the magnitude of the perturbation is small. Indeed, for the great majority of systems cited in this section, both of these general features are present in the systems studied in one way or another.

Within this general characterization, many classical systems which have been analyzed with an energy diffusion model fall into two loose, somewhat overlapping categories. The first category, which is most directly connected to our work, consists of Hamiltonian systems which are isolated except for a prescribed external drive, modelled by an explicit time dependence of the system's Hamiltonian. In the language of thermodynamics, these systems gain or lose energy via *work* done by an external drive, whose dynamics are unaffected by any "back-action" from the system. A range of classical systems under this heading have been studied. For example, driven oscillator systems with a single degree of freedom may exhibit energy diffusion, provided that the drive is strong enough to induce chaos [138]. This effect appears in models such as the kicked rotor [13, 139], and in semiclassical models of hydrogen-like atoms driven by an electromagnetic

field [101, 102]. Another class of relevant systems is adiabatically driven systems, in which a time-dependent parameter in the system's Hamiltonian is varied very slowly; a paradigmatic example of this is a gas of particles in a cavity, where one of the walls (a "piston") is moved at a slow speed relative to the particle speeds. Specifically, beginning with studies by Ott and coworkers [98, 103, 104], much work has been done with adiabatically driven systems which are chaotic and ergodic in the absence of driving [105, 108, 110, 111]. In these systems, the slow rate of driving implies that the system's adiabatic invariant [91, 98] is nearly conserved, and the energy diffusion description can be used to quantify the deviation from perfect conservation. Last, a comparatively recent use of an energy diffusion model can be found in [119], in which the fluctuations in energy of a periodically driven system are calculated in an energy diffusion description, under the assumption that the energy change per driving cycle is small, and that successive cycles are uncorrelated.

Our work on periodically driven chaotic systems is most closely related to energy diffusion in adiabatically driven chaotic systems. In both types of systems, an effectively random energy evolution emerges the chaotic mixing property of the underlying Hamiltonian dynamics. The result is an energy diffusion process, with drift and diffusion rates that coincide with the predictions of linear response theory. These rates are connected via the fluctuation-dissipation relation (2.22) [108]. Of course, there are some key differences in the analysis of these two types of systems. One distinction is that for adiabatically driven systems, the energy is often identified with the *full* Hamiltonian of the system, whereas in our analysis the energy is given by the bare Hamiltonian H_0. Another difference is that energy diffusion in adiabatically driven systems can be derived in terms of an expansion in a small "slowness" parameter that specifies the rate of driving, via techniques such as multiscale perturbation theory. On the other hand, we are not

aware of a way to obtain our results via an analogous expansion in the obvious small parameter ω^{-1}, except in the case of driven billiard systems (see Chapter 3, Section 3.4).

A second class of models which have been found to exhibit energy diffusion are systems which exchange energy with a weakly coupled thermal bath (additional discussion of these systems can also be found in Chapter 4). In these models, thermal noise provides the random element necessary for diffusive evolution. Much analysis of these systems descends from early work by Kramers, who considered a Brownian particle in a potential well as a model for chemical and nuclear reactions [95]. In this model, the escape of the particle from the potential well (facilitated by thermal fluctuations) corresponds to the surmounting of an energetic barrier necessary for a reaction to take place. Kramers obtained a diffusive description of the particle's energy evolution by marginalizing over a Fokker-Planck equation for the particle's motion in phase space, and then used this description to calculate the rate of escape from the potential well. This model has since been generalized mathematically, to include the effects of external driving forces and and non-Markovian thermal noise [96, 99, 100, 106], and similar models have been derived for classical spin degrees of freedom coupled to a thermal bath [97]. Moreover, versions of this model have been used to analyze other systems and models which "switch" between two or more states, including Josephson junctions [107, 109] and a semiclassical version of the Duffing oscillator [118]. Now, in addition to these models following the work of Kramers, in which the stochastic nature of thermal noise is mostly assumed *a priori*, energy diffusion and related phenomena have also been studied starting from a purely deterministic description of the system and bath. Systems analyzed in this way include systems of particles interacting with hard or soft scatterers [120, 123], a pair of weakly interacting chaotic degrees of freedom in a classical Bose-Hubbard model [122], and a model of a Brownian particle as a heavy particle coupled to a

rapidly evolving chaotic system [112]. Such analyses have provided insights into how statistical phenomena like thermalization can emerge from an underlying deterministic dynamics, even in systems with relatively few degrees of freedom.

Although we have divided the systems mentioned in this section in two categories, these categories are clearly not mutually exclusive. For one thing, in many energy diffusion models, the effects of both coherent external driving and thermal noise have been included simultaneously [106, 107, 109, 116, 118]. But more interestingly, for many physical scenarios, these two types of external perturbation are simply two ways of viewing the same phenomenon. This point, which has been emphasized in works such as [105] and [114], can be most easily illustrated by considering a slow, heavy hard sphere, confined to a chaotic cavity and immersed in a gas of small, fast-moving particles (see Figure 2.5). On one hand, before the sphere's speed is significantly altered due to collisions with the particles, the motion of the sphere appears as a fixed external influence imposed on the system of particles, which is unresponsive to the particle dynamics. In this approximation, we can think of the particles as an example of our first class of systems, with the sphere playing the role of the external drive. However, on longer timescales, the effect of many sphere-particle collisions will accumulate, and the particles emerge as a source of friction and noise acting on the sphere. From this perspective, it is natural to instead focus on the *sphere* as our system of interest, and to view the slow dissipation of the sphere's energy as an example of the energy diffusion processes in our second class of systems.

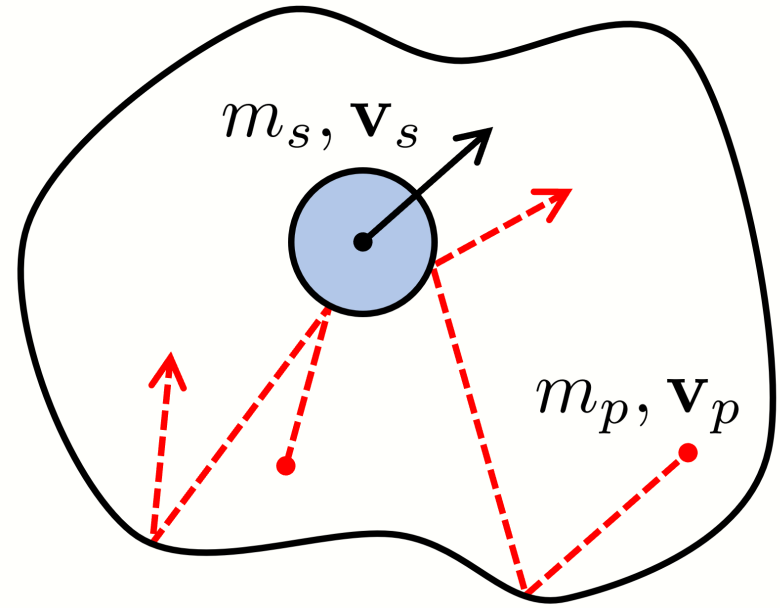

Figure 2.5: A hard sphere of mass m_s with velocity $\mathbf{v}_s$ (blue circle), confined to a chaotic cavity. The sphere is immersed in a bath of point particles (red dashed lines), each with some mass m_p and velocity $\mathbf{v}_p$. We assume that for all the particles, $m_p \ll m_s$ and $|\mathbf{v}_p| \gg |\mathbf{v}_s|$.

Chapter 3: Energy diffusion in billiard systems under rapid periodic driving

3.1 Chapter summary

Dynamical billiard systems, in which a particle confined to a cavity collides elastically with the cavity walls, are a paradigmatic model in the study of Hamiltonian chaos. In this chapter, we apply the energy diffusion framework established in Chapter 2 to billiard systems subject to a rapid periodic driving force. As we will see, energy diffusion in billiards results in *Fermi acceleration*, or a systematic increase in the average energy. The relative simplicity of billiard dynamics allows us to study this process in detail, with both analytical methods and numerical techniques.

We begin this chapter with Section 3.2, where we precisely define the billiard systems under consideration. Then, in Section 3.3, we discuss the conditions under which the energy diffusion description is valid for driven billiards. This is followed by a calculation of the energy drift and diffusion coefficients g_1 and g_2 for billiard systems, given in Section 3.4 (see (3.19) and (3.18)). In Section 3.5, we present simulations which corroborate our theoretical results. Then, in Section 3.6, we extend our theoretical results to many-body systems, by considering systems of interacting particles confined to a billiard cavity. Finally, we conclude with Section 3.7, where we compare our results to existing work on driven billiards and Fermi acceleration. Except for the results for many-particle billiards presented in Section 3.6, the results in this chapter were

previously published in [140].

3.2 Setup

In this section, we introduce the class of driven billiard systems under consideration, and establish some important definitions and notation. In these systems, a particle is subject to a rapid time-periodic driving force as it moves chaotically within a cavity. These systems constitute a special case of the Hamiltonian systems studied in Chapter 2.

We begin by defining our system of interest. We consider a point particle of mass m, with position $\mathbf{x} \equiv \mathbf{x}_t$ and velocity $\mathbf{v} \equiv \mathbf{v}_t$, confined to the inside of a cavity or "billiard" (see Figure 3.1). Precisely, the billiard is a bounded, connected subset of d-dimensional Euclidean space ($d \geq 2$), with a boundary or "wall" consisting of one or more $(d-1)$-dimensional surfaces. When strictly inside the billiard, the particle evolves smoothly according to Newton's laws. Whenever the particle reaches the billiard boundary, it undergoes an instantaneous elastic collision with the wall.

Specifically, we assume that between collisions, the particle is subject to two forces. First, the particles experiences a conservative force $-\nabla U(\mathbf{x})$, generated by a static potential $U(\mathbf{x})$. Second, we apply a time-periodic driving force $\mathbf{F}(\mathbf{x})\cos(\omega t) = -\nabla U_F(\mathbf{x})\cos(\omega t)$, with period $T = 2\pi/\omega$, where $U_F(\mathbf{x})$ is some potential. Therefore, the equations of motion for $\mathbf{x}$ and $\mathbf{v}$ are given by:

$$\frac{d\mathbf{x}}{dt} = \mathbf{v}, \quad m\frac{d\mathbf{v}}{dt} = -\nabla U(\mathbf{x}) + \mathbf{F}(\mathbf{x})\cos(\omega t). \tag{3.1}$$

When the particle reaches the billiard boundary, an instantaneous elastic collision occurs.

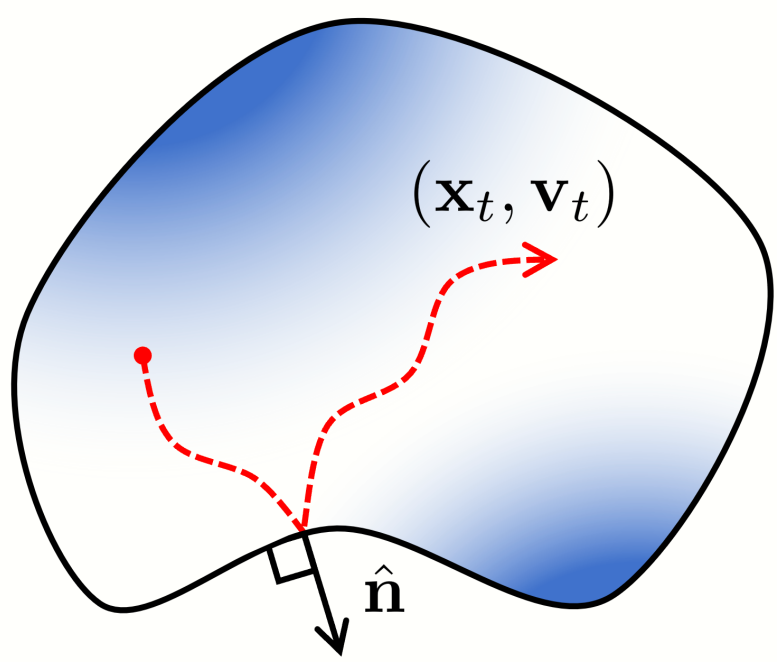

Figure 3.1: A sample trajectory $(\mathbf{x}, \mathbf{v}_t)$ (red dashed line) in a $d = 2$ dimensional billiard cavity. The particle collides with the wall at a point with unit normal $\hat{\mathbf{n}}$. The blue shading within the billiard represents variations in the potential fields $U(\mathbf{x})$ and $U_F(\mathbf{x})\cos(\omega t)$.

This collision leaves the position of the particle unchanged, but the component of the velocity perpendicular to the wall is instantly reversed. That is, the velocity of the particle is updated from $\mathbf{v}$ to $\mathbf{v}'$ according to the reflection law

$$\mathbf{v}' = \mathbf{v} - 2(\mathbf{v} \cdot \hat{\mathbf{n}}(\mathbf{x}))\hat{\mathbf{n}}(\mathbf{x}), \tag{3.2}$$

where $\hat{\mathbf{n}}(\mathbf{x})$ is the outward-facing unit vector normal to the billiard boundary at $\mathbf{x}$, the point of collision.

The equations (3.1) and (3.2) fully define the dynamics of the driven particle. We note here that our use of the term "billiard" is more general than the typical usage: The word "billiard" often simply refers to a free particle in a cavity, corresponding to the case of vanishing $U(\mathbf{x})$ and $\mathbf{F}(\mathbf{x})$. In light of this, we will use the term "standard billiard" to refer to the special case of $U(\mathbf{x}) = 0$.

For a driven standard billiard, the associated *undriven* billiard (obtained by additionally setting $\mathbf{F}(\mathbf{x}) = \mathbf{0}$) corresponds to a billiard in the more common sense of the word.

In our analysis, we are most interested in the evolution of the particle's energy, defined as $\mathcal{E} \equiv \mathcal{E}(\mathbf{x}, \mathbf{v}) \equiv \frac{1}{2}m|\mathbf{v}|^2 + U(\mathbf{x})$. In the absence of driving, $\mathcal{E}$ is a constant of the motion: $\mathcal{E}$ is conserved under the equations of motion (3.1) for $\mathbf{F}(\mathbf{x}) = \mathbf{0}$, and is also unchanged under the reflection law (3.2). For nonzero $\mathbf{F}(\mathbf{x})$, the collisions are still energy-conserving, but (3.1) implies that the particle's energy between collisions changes according to:

$$\frac{d\mathcal{E}}{dt} = \mathbf{F}(\mathbf{x}) \cdot \mathbf{v} \cos(\omega t). \tag{3.3}$$

In particular, we will consider the energy dynamics for large ω, in the rapid driving regime.

We note here that the billiard systems we study are one example of a Hamiltonian system like those described in Chapter 2. That is, $\mathbf{x}$ and $\mathbf{p} \equiv m\mathbf{v}$ correspond to a set of canonical coordinates and momenta, the energy $\mathcal{E}$ corresponds to an undriven Hamiltonian $H_0(\mathbf{x}, \mathbf{p}) = |\mathbf{p}|^2/2m + U(\mathbf{x})$, and the driving potential $U_F(\mathbf{x}) \cos(\omega t)$ acts as the drive $V(t)$. Thus, provided that the two key assumptions of chaotic dynamics and rapid driving are satisfied, the energy of the billiard particle will evolve diffusively, and all of the conclusions of Chapter 2 will apply. We discuss the validity of these assumptions for billiard systems in Section 3.3.

As in Chapter 2, our analysis will concern statistical ensembles of particle trajectories, and the energy distributions of such ensembles. Each trajectory in an ensemble is determined by an initial condition $(\mathbf{x}_0, \mathbf{v}_0)$ at $t = 0$, which is sampled according to some probability distribution $\rho_0(\mathbf{x}_0, \mathbf{v}_0)$ on phase space (that is, the $2d$-dimensional space of particle positions and velocities). The ensemble is then evolved in time by evolving each initial condition according to (3.1) and

(3.2), yielding $\mathbf{x}_t$ and $\mathbf{v}_t$. The system's time-dependent energy distribution $\eta(E,t)$ is then given by

$$\eta(E,t) = \int d^d\mathbf{x}_0 d^d\mathbf{v}_0\, \rho_0(\mathbf{x}_0,\mathbf{v}_0)\, \delta\Big(\mathcal{E}(\mathbf{x}_t,\mathbf{v}_t) - E\Big). \tag{3.4}$$

Here, $d^d\mathbf{x}_0 d^d\mathbf{v}_0$ is a $2d$-dimensional infinitesimal "hyper-volume" element in phase space, and $(\mathbf{x}_t,\mathbf{v}_t)$ is the phase space location, at time t, of the trajectory with initial conditions $(\mathbf{x}_0,\mathbf{v}_0)$. For this integral, and for similar integrals in this chapter unless otherwise stated, the integration over $\mathbf{x}_0$ is performed over the interior of the billiard, and the integration over $\mathbf{v}_0$ runs over all $\mathbf{v}_0 \in \mathbb{R}^d$.

Finally, we note that if the driving force is generated by a more general time-periodic potential $U_F(\mathbf{x},t)$, then it is straightforward to extend our analysis by decomposing this potential as a Fourier series with fundamental frequency ω. However, in order to keep the calculations in this chapter relatively simple, we restrict our attention to the monochromatic driving force $\mathbf{F}(\mathbf{x})\cos(\omega t)$.

3.3 Conditions for energy diffusion in billiard systems

In this section, we describe the conditions under with the energy diffusion description is a good model for the energy evolution of periodically driven billiards. As for the general Hamiltonian systems described in Chapter 2, the validity of the energy diffusion model for billiards depends on two key assumptions: The chaotic and ergodic nature of the undriven dynamics, and the high speed of the periodic drive. On one hand, whether the dynamics are chaotic and ergodic is contingent upon the shape of the billiard cavity, and the forces that the particle is subjected to. On the other hand, we find that the rapid driving assumption can be

encapsulated by the two conditions (3.5) and (3.6), which may be satisfied for sufficiently large driving frequencies ω.

3.3.1 Chaos and ergodicity in billiard systems

We begin by discussing the assumptions of chaos and ergodicity. In Chapter 2, we required that in the absence of driving, our system of interest explore phase space chaotically and ergodically at each energy E. When do billiard systems exhibit such dynamics? This question has been most frequently studied for standard billiards ($U(\mathbf{x}) = 0$), where the billiard particle moves inertially between collisions with the wall. Recall that chaotic dynamics are characterized by an exponential divergence of similar trajectories over time. Speaking loosely, chaotic motion in a standard billiard tends to arise when nearby parallel trajectories diverge or "defocus" from one another after a collision, due to curvature of the billiard wall. Clearly, this will occur if a segment of the wall is convex, in which case the trajectories begin to diverge immediately (see Figure 3.2). But it may also occur if the wall is concave, in which case the trajectories will initially converge, but may begin to diverge if there is enough time before the next collision. Although this is only an intuitive plausibility argument, the existence of chaotic and ergodic motion has been rigorously demonstrated for certain classes of billiard shapes [85, 86]. Classic examples are the Sinai billiard [141], defined by a square cavity with a circular scattering center inside, and the Bunimovich stadium [142], which consists of two semicircular walls connected by parallel lines (see Figure 3.3).

For the $U(\mathbf{x}) \neq 0$ case, less is known in general. In this case, the nature of the undriven dynamics depends on both the shape of the billiard and the characteristics of the static potential

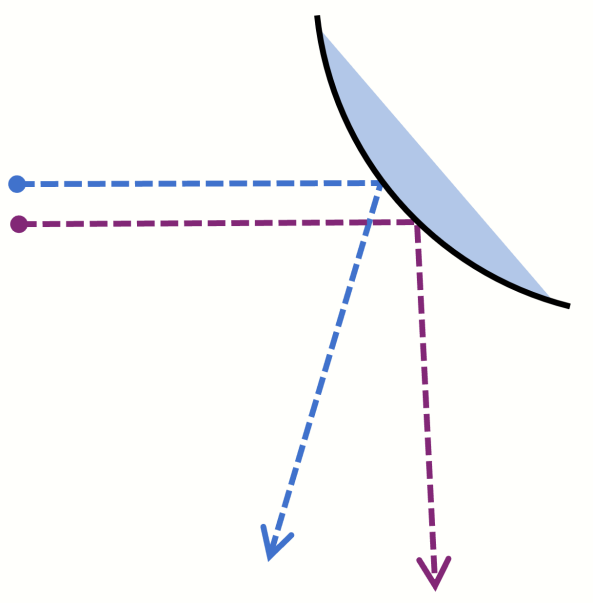

Figure 3.2: Nearby parallel trajectories diverging after a collision with a convex wall.

$U(\mathbf{x})$. However, some of the rigorous results for standard billiards may be extended, at least approximately, to establish chaotic and ergodic motion for non-standard billiards. For example, suppose we have a standard billiard for which chaos and ergodicity has been proven. Then, if we introduce a sufficiently weak potential $U(\mathbf{x})$, then it can be shown that this non-standard billiard inherits the chaotic and ergodic properties of its standard counterpart [143]. Alternatively, we note that motion in a potential is mathematically equivalent to *free* motion in some non-Euclidean space. Therefore, if chaotic and ergodic dynamics can be established for such non-Euclidean motion in a standard billiard, then the corresponding motion in a potential field will also be chaotic and ergodic [144].

Regardless of the particular method of proof, we now assume that all billiards studied in this chapter satisfy this assumption of chaos and ergodicity. We now move to a discussion of our second key assumption, the assumption of rapid driving.

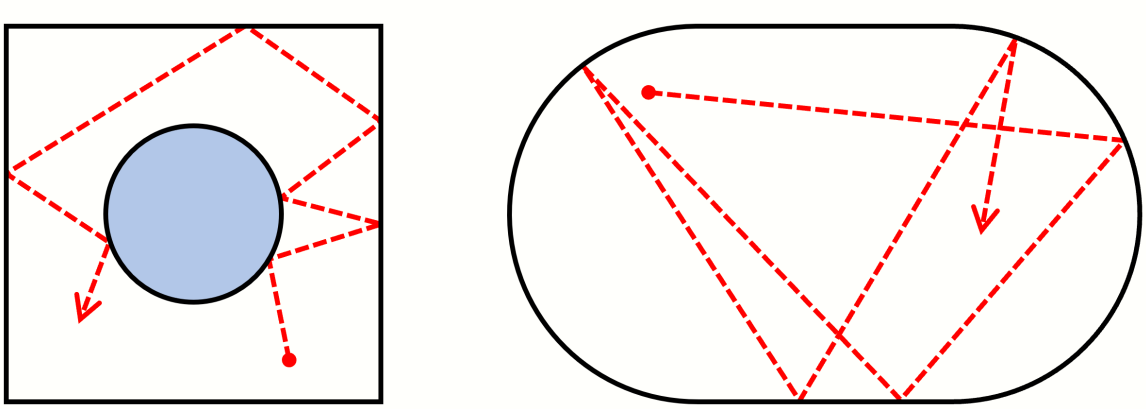

Figure 3.3: The Sinai billiard (left) and the Bunimovich stadium billiard (right), each with a sample trajectory given by the red dashed line.

3.3.2 Rapid periodic driving in billiard systems

As in the general case, described in Chapter 2, sufficiently rapid periodic driving of a billiard system results in an averaging effect, in which the net impulse imparted by the driving force $\mathbf{F}(\mathbf{x})\cos(\omega t)$ nearly integrates to zero over a period. Because of the weak effect of the drive, there exists a separation of timescales (see (2.12)) between the typical correlation time of the chaotic motion τ_C, and the typical timescale τ_E over which the system gains a significant amount of energy. The result is a process of energy diffusion, described by the Fokker-Planck equation (2.11), which occurs on timescales $\gg \tau_C$.

However, for the specific case of billiard systems, we can go further than this general picture. How large must ω be for the energy diffusion description, and the associated Fokker-Planck equation, to be approximately valid? The requirement that the drive act as a weak perturbation on the undriven dynamics suggests two conditions. First, we assume that over the course of a single period, the forces $-\nabla U(\mathbf{x})$ and $\mathbf{F}(\mathbf{x})\cos(\omega t)$ produce a very small change in the particle's velocity. If the typical magnitude of these forces is denoted by F, then from (3.1)

we can estimate that the velocity will change by an amount of order $F/(m\omega)$ during a period (provided a collision does not occur). We assume that this change is much smaller than v, the typical speed of the particle:

$$\frac{F}{m\omega} \ll v. \tag{3.5}$$

This is our first condition. Importantly, this ensures that when a collision occurs, the outgoing trajectory of the particle will only be slightly altered relative to the undriven motion. If (3.5) is not satisfied, then the particle's direction of motion will oscillate wildly back and forth due to the force $\mathbf{F}(\mathbf{x})\cos(\omega t)$. As a result, the drive may cause the particle to collide with the wall at a substantially different angle relative to a corresponding undriven particle. The associated driven and undriven trajectories would then rapidly diverge, contrary to our requirement that the drive act as a small perturbation.

Second, we assume that the distance travelled by the particle over a typical period is very small, much smaller than any other relevant length scale associated with the system. Since (3.5) ensures that the particle's velocity changes little during a period, this distance travelled will be of order $vT \sim v/\omega$. So we may write our second condition as

$$\frac{v}{\omega} \ll l, \tag{3.6}$$

where l is the shortest length scale in the system. l may be the mean free path for the particle, or a length scale characterizing the roughness of the billiard wall, or the typical distance over which the forces $-\nabla U(\mathbf{x})$ and $\mathbf{F}(\mathbf{x})$ vary by a significant amount.

With the condition (3.6) satisfied, a large number of periods will occur between successive

collisions with the billiard wall. Moreover, over a single period, the quantity $\mathbf{F}(\mathbf{x})$ will be nearly constant, since the particle will hardly move during this short time interval. As a result, during any period without a collision (the great majority of periods), integrating (3.1) reveals that the driving force perturbs the particle's velocity by an amount $\approx \mathbf{F}(\mathbf{x})\sin(\omega t)/(m\omega)$, and its position by $\approx -\mathbf{F}(\mathbf{x})\left[\cos(\omega t) - 1\right]/(m\omega^2)$. Thus, the cumulative effect of the force essentially integrates to zero as $\omega \to \infty$. Taken together, we see that if the conditions (3.5) and (3.6) are satisfied, the drive acts as a weak perturbation during periods both with and without collisions. When subject to such a drive, the particle will typically experience several collisions with the wall before its trajectory is significantly altered relative to the undriven motion.

As a result, when the conditions (3.5) and (3.6) are both satisfied for a chaotic, ergodic billiard, we expect that the billiard particle's energy will evolve diffusively. As with the more general class of systems discussed in Chapter 2, this evolution will proceed in accordance with the Fokker-Planck equation (2.11). In Section 3.4, we derive expressions for the drift and diffusion coefficients g_1 and g_2 for billiard systems, which are valid for large ω (see (3.19) and (3.18)).

3.3.3 Violation of the rapid driving assumption at high energies

Now, for any given energy E, which determines the typical particle speed v, the conditions (3.5) and (3.6) may always be satisfied for sufficiently large ω. However, at fixed driving frequency ω, there will generally be some energies for which at least one of these conditions does not hold. This leads to the follow picture. Let $\mathcal{R}(\omega)$ denote the range of energies for which conditions (3.5) and (3.6) are satisfied. For a statistical ensemble with particle energies in $\mathcal{R}(\omega)$, the energy distribution η will evolve according to the Fokker-Planck equation (2.11). Of

course, under the Fokker-Planck dynamics, this distribution will shift and spread in energy space, ultimately spreading outside of the interval $\mathcal{R}(\omega)$. At this point, the conditions (3.5) and (3.6) are not satisfied for all particles in the ensemble. In particular, we expect condition (3.6) to generally break down for sufficiently high energy particles, which are fast enough to travel a significant distance over a single period.

What happens in this high energy regime, when particle speeds have increased so that $v/\omega \sim l$? As before, condition (3.5) (which remains valid at high energies) tells us that the forces $-\nabla U(\mathbf{x})$ and $\mathbf{F}(\mathbf{x})\cos(\omega t)$ only weakly perturb the particle's velocity over a given period. However, the increased speed of the particle now means that the particle travels a distance of order $v/\omega \sim l$ during this period. Assuming for simplicity that l is comparable to the particle's mean free path, we see that the velocity is only slightly altered between successive collisions: Many collisions with the wall must occur before the drive significantly perturbs the particle's velocity relative to the undriven motion. Similarly, the drive will only weakly affect the particle's position: We can estimate from (3.1) that the drive will perturb the particle's position by an amount of order $F/(m\omega^2)$ during a period, which by (3.5) and $v/\omega \sim l$ is much smaller than l. Therefore, the energy diffusion description may still be valid at high energies, even when (3.6) is not satisfied, since we can potentially treat the drive as a small perturbation on the undriven dynamics. With that said, our main focus in this chapter is rapidly driven particles, for which the conditions (3.5) and (3.6) are *both* satisfied. In particular, the expressions for g_1 and g_2 obtained in Section 3.4 are only valid in this regime.

3.4 g_1 and g_2 for billiard systems

We now derive expressions for the drift and diffusion coefficients g_1 and g_2 for billiard systems, in the limit of large ω. We calculate these quantities in terms of powers of the small parameter ω^{-1}, and ultimately only retain terms of order $O(\omega^{-2})$, the lowest non-zero order. The structure of this calculation is similar to the derivation of g_2 in Chapter 2. First, we compute g_2 in terms of the variance in energy acquired by an ensemble of particles, initialized in a microcanonical ensemble at $t = 0$ and then subject to the rapid drive. Then, we use the fluctuation-dissipation relation (2.22), established in Chapter 2, Section 2.4, which allows us to calculate g_1 from our knowledge of g_2.

3.4.1 Calculation of g_1 and g_2

We begin as in Chapter 2, Section 2.4, in which the general form of g_2 was obtained. Recall that for systems described by the energy diffusion model, the diffusion coefficient g_2 may be related to the variance $\mathrm{Var}(\mathcal{E})$ of an ensemble of driven trajectories. Specifically, if a microcanonical ensemble of trajectories with initial energy E_0 is allowed to evolve for a time Δt, we have (see also (2.15)):

$$\mathrm{Var}(\mathcal{E}) \approx g_2(E_0, \omega)\Delta t. \tag{3.7}$$

Here, Δt should satisfy the hierarchy of timescales (2.12): It should be long enough that the energy diffusion description is valid, yet short enough that the change in energy of the system is small. The microcanonical distribution of initial conditions is defined in the usual way:

$$\rho_{E_0}(\mathbf{x}_0, \mathbf{v}_0) \equiv \frac{1}{\Sigma(E_0)} \delta(\mathcal{E}(\mathbf{x}_0, \mathbf{v}_0) - E), \tag{3.8}$$

where the density of states $\Sigma(E)$ is given by

$$\Sigma(E) = \int d^d\mathbf{x} d^d\mathbf{v}\, \delta(\mathcal{E}(\mathbf{x}_0, \mathbf{v}_0) - E), \tag{3.9}$$

To determine $g_2(E_0, \omega)$ for any particular E_0, it is sufficient to calculate $\mathrm{Var}(\mathcal{E})$, with trajectories sampled according to the appropriate microcanonical distribution $\rho_{E_0}(\mathbf{x}_0, \mathbf{v}_0)$.

This calculation may be summarized as follows, with details given below and in Appendix C. First, for a given trajectory in the ensemble over the time Δt, we evaluate the associated energy change $\Delta\mathcal{E}$. From the fact that the drive acts as a small perturbation for large ω, it follows that the dominant contribution to $\Delta\mathcal{E}$ is associated with driving periods during which a collision occurs. These $O(\omega^{-1})$ contributions are given by (3.12). We then average over the ensemble to obtain $\mathrm{Var}(\mathcal{E})$. Since the energy changes associated with different collisions become uncorrelated in the rapid driving limit, this average simplifies to (3.14), as shown in Appendix C. Finally, we express this result in terms of an integral over the billiard boundary, leading to the expression (3.18) for g_2.

It may be surprising that we do not simply derive g_2 for billiard systems from the previously established general result $g_2(E, \omega) = \frac{1}{2} S(\omega; E)$, valid for general chaotic systems subject to a rapid periodic drive (see (2.19) and (2.20)). Taking this approach is certainly possible, and we pursue it in Appendix D, to ensure consistency between our analysis of billiards and the general theory described in Chapter 2. However, while this alternative derivation is shorter, the present approach provides more physical insight into the result. In particular, the derivation given below

shows how the largest energy changes occur during periods with a collision, and shows how the rapid oscillations of the drive destroy correlations between these energy changes.

To begin, let us consider $\Delta\mathcal{E}$ for a particular particle in the ensemble. We may view this energy change as a sum of the $M = \Delta t/T$ small energy changes that occur over each period of the drive (assuming, for simplicity, that Δt is an integer multiple of the period T). For sufficiently small T, *at most* one collision will occur over each driving period. This property is guaranteed for a typical trajectory by condition (3.6). Therefore, in this regime, $\Delta\mathcal{E}$ is a sum of two contributions: Energy changes from periods with no collisions, and energy changes from periods with a single collision. We will examine these two possibilities in turn.

First, suppose that no collision occurs during the i^{th} period, from $t = (i-1)T$ to $t = iT$, with associated energy change $\Delta\mathcal{E}_i$. If we integrate (2.4) over this period and perform an integration by parts, we find that the boundary terms vanish, and the resulting expression for $\Delta\mathcal{E}_i$ is:

$$\begin{aligned}\Delta\mathcal{E}_i &= -\omega^{-1}\int_{(i-1)T}^{iT} dt\,\frac{d}{dt}\left[\mathbf{F}(\mathbf{x}_t)\cdot\mathbf{v}_t\right]\sin(\omega t)\\ &= -\omega^{-1}\int_{(i-1)T}^{iT} dt\left[\mathbf{v}_t\cdot D\mathbf{F}(\mathbf{x}_t)\mathbf{v}_t - \frac{\nabla U(\mathbf{x}_t)\cdot\mathbf{F}(\mathbf{x}_t)}{m} + \frac{|\mathbf{F}(\mathbf{x}_t)|^2}{m}\cos(\omega t)\right]\sin(\omega t).\end{aligned} \tag{3.10}$$

In moving from the first line to the second line, we have used the equations of motion (3.1) to evaluate the derivative $d\left[\mathbf{F}(\mathbf{x}_t)\cdot\mathbf{v}_t\right]/dt$. The symbol $D\mathbf{F}(\mathbf{x})$ denotes the Jacobian matrix for the function $\mathbf{F}(\mathbf{x})$, with matrix elements $[D\mathbf{F}(\mathbf{x})]_{ij} \equiv \partial F_i/\partial x_j$, where x_i and F_i are the i^{th} components of $\mathbf{x}$ and $\mathbf{F}(\mathbf{x})$.

So far, this is exact. Let us estimate the size of this quantity, in terms of orders of the small

parameter ω^{-1}. Since there is a factor of ω^{-1} outside the second integral in (3.10), and since we are integrating over a single period of duration $T = O(\omega^{-1})$, $\Delta\mathcal{E}_i$ is at most an $O(\omega^{-2})$ quantity. To approximate $\Delta\mathcal{E}_i$, we may replace $\mathbf{x}_t$ and $\mathbf{v}_t$ in the integrand by their values at the beginning of the period. Since $\mathbf{x}_t$ and $\mathbf{v}_t$ change over a period by an amount of order $O(\omega^{-1})$, the resulting expression for $\Delta\mathcal{E}_i$ is valid up to corrections of order $O(\omega^{-3})$. After this replacement, we are simply integrating the functions $\sin(\omega t)$ and $\cos(\omega t)\sin(\omega t)$ over a single period, which both vanish. Thus, $\Delta\mathcal{E}_i$ is a $O(\omega^{-3})$ quantity. Of course, the number of periods in which no collision occurs will scale like ω; thus, the total energy change associated with collisionless periods is of order $O(\omega^{-2})$.

The periods during which a collision takes place are more interesting. Suppose that the particle experiences N collisions between $t = 0$ and $t = \Delta t$, at times $t_1, t_2 \ldots t_N$. If the k^{th} collision occurs during the i^{th} period, then integrating (2.4) over this period yields the associated energy change $\Delta\mathcal{E}_i$:

$$\Delta\mathcal{E}_i = \int_{(i-1)T}^{t_k} dt\, \mathbf{F}(\mathbf{x}_t) \cdot \mathbf{v}_t \cos(\omega t) + \int_{t_k}^{iT} dt\, \mathbf{F}(\mathbf{x}_t) \cdot \mathbf{v}_t \cos(\omega t). \tag{3.11}$$

Each integral above is over a fraction of the period, and is therefore of order $O(\omega^{-1})$. By the same logic that we used for the collisionless case, we may approximate $\mathbf{F}(\mathbf{x}_t)$ and $\mathbf{v}_t$ in the first integral by $\mathbf{F}_k$ and $\mathbf{v}_k$, their values instantaneously prior to the k^{th} collision. Similarly, $\mathbf{F}(\mathbf{x}_t)$ and $\mathbf{v}_t$ in the second integral can be approximated by $\mathbf{F}_k$ and $\mathbf{v}_k^+$, where $\mathbf{v}_k^+$ is the particle's velocity immediately after the collision. The reflection law (3.2) tells us that $\mathbf{v}_k^+ = \mathbf{v}_k - 2\,(\mathbf{v}_k \cdot \hat{\mathbf{n}}_k)\,\hat{\mathbf{n}}_k$, where $\hat{\mathbf{n}}_k$ is the normal to the wall at the point of collision.

Upon making these substitutions, the resulting approximation for $\Delta\mathcal{E}_i$ is valid up to

corrections of order $O(\omega^{-2})$. The integrals over $\cos(\omega t)$ are easily evaluated, and we obtain:

$$\Delta\mathcal{E}_i = 2\omega^{-1}\left(\mathbf{F}_k \cdot \hat{\mathbf{n}}_k\right)\left(\mathbf{v}_k \cdot \hat{\mathbf{n}}_k\right)\sin(\omega t_k) + O(\omega^{-2}). \tag{3.12}$$

Therefore, each collision that occurs is accompanied by a corresponding energy change of order $O(\omega^{-1})$ over the associated period, given by the above expression. Moreover, since the total energy change associated with *collisionless* periods is of order $O(\omega^{-2})$, the energy changes corresponding to collisions are the dominant contribution to $\Delta\mathcal{E}$ for large ω. After summing over all N collisions to obtain $\Delta\mathcal{E}$, we can substitute this result into $\mathrm{Var}(\mathcal{E}) = \langle(\Delta\mathcal{E})^2\rangle - \langle\Delta\mathcal{E}\rangle^2$:

$$\begin{aligned}\mathrm{Var}(\mathcal{E}) = {} & 4\omega^{-2}\left\langle\left[\sum_{k=1}^{N}\left(\mathbf{F}_k \cdot \hat{\mathbf{n}}_k\right)\left(\mathbf{v}_k \cdot \hat{\mathbf{n}}_k\right)\sin(\omega t_k)\right]^2\right\rangle \\ & - 4\omega^{-2}\left\langle\sum_{k=1}^{N}\left(\mathbf{F}_k \cdot \hat{\mathbf{n}}_k\right)\left(\mathbf{v}_k \cdot \hat{\mathbf{n}}_k\right)\sin(\omega t_k)\right\rangle^2 + O(\omega^{-3}).\end{aligned} \tag{3.13}$$

This expression is computed in Appendix C. In this calculation, we find that the oscillating factors $\sin(\omega t_k)$ are uncorrelated with one another, and with the quantities $\left(\mathbf{F}_k \cdot \hat{\mathbf{n}}_k\right)\left(\mathbf{v}_k \cdot \hat{\mathbf{n}}_k\right)$, for large ω. The phases $\omega t_k \bmod 2\pi$ may be thought of as effectively independent random variables, uniformly distributed on $[0, 2\pi)$. Intuitively, this lack of correlation arises because otherwise similar trajectories in the ensemble may have totally different values of $\sin(\omega t_k)$: Two nearby trajectories with even a small difference between the associated collision times t_k will have a huge $O(\omega)$ difference in the value of ωt_k, for large ω.

As a result, averages over the oscillating factors $\sin(\omega t_k)$ are found to vanish. The only non-vanishing terms in (3.13) are the "diagonal" terms in $\langle(\Delta\mathcal{E})^2\rangle$, which include a factor of

$\sin^2(\omega t_k)$ that averages to $1/2$. We are left with:

$$\mathrm{Var}(\mathcal{E}) = 2\omega^{-2}\left\langle \sum_{k=1}^{N} \left(\mathbf{F}_k \cdot \hat{\mathbf{n}}_k\right)^2 \left(\mathbf{v}_k \cdot \hat{\mathbf{n}}_k\right)^2 \right\rangle_0 + O(\omega^{-3}). \tag{3.14}$$

Here, the subscript 0 denotes that the average is now taken over an ensemble of *undriven* trajectories, evolved with $\mathbf{F}(\mathbf{x}) = \mathbf{0}$. The error accrued by replacing the true driven trajectories with their undriven counterparts is of order $O(\omega^{-3})$, so we neglect it.

Then, using standard techniques for evaluating ensemble averages in billiard systems, we may express this average as an integral over the billiard boundary. We simply present the results here; the details of this calculation are also found in Appendix C. Let dS denote an infinitesimal $(d-1)$-dimensional patch of "surface" or "hyper-area" of the billiard wall, surrounding a location $\mathbf{x}$ on the wall. Such a patch has an associated outward-facing normal vector $\hat{\mathbf{n}} \equiv \hat{\mathbf{n}}(\mathbf{x})$, defined as in (3.2), and an associated value of $\mathbf{F} \equiv \mathbf{F}(\mathbf{x})$. We may express $\mathrm{Var}(\mathcal{E})$ as an integral over all such patches:

$$\mathrm{Var}(\mathcal{E}) = \frac{4\omega^{-2}\Delta t}{d+1} \int dS\, \gamma_{E_0} v_{E_0}^2 \left(\mathbf{F} \cdot \hat{\mathbf{n}}\right)^2 + O(\omega^{-3}). \tag{3.15}$$

Here, we define $v_E \equiv v_E(\mathbf{x})$ as

$$v_E(\mathbf{x}) \equiv \begin{cases} \left[2\left(E - U(\mathbf{x})\right)/m\right]^{1/2} & \text{if } U(\mathbf{x}) \leq E \\ 0 & \text{otherwise} \end{cases} \tag{3.16}$$

which for $U(\mathbf{x}) \leq E$ is the speed of an undriven particle at position $\mathbf{x}$ with energy E. $\gamma_E \equiv \gamma_E(\mathbf{x})$ is the average collision rate per unit hyper-area of the billiard boundary for particles at position

$\mathbf{x}$, averaged over undriven particles in the microcanonical ensemble at energy E. As explained in Appendix C, an explicit expression for $\gamma_E(\mathbf{x})$ is given by

$$\gamma_E(\mathbf{x}) = \frac{B_{d-1}}{m} \frac{v_E(\mathbf{x})^{d-1}}{\Sigma(E)}, \tag{3.17}$$

where $B_n = \pi^{n/2}/\Gamma\left(\frac{n}{2}+1\right)$ is the hyper-volume of the unit ball in n-dimensional space [145], and where $\Sigma(E)$ is the density of states defined in (3.9). $\Gamma(s)$ is the gamma function, which coincides with the factorial $(s-1)!$ for positive integers s.

Upon comparing (3.15) with (3.7), and relabelling E_0 as E, we obtain our final expression for g_2:

$$g_2(E,\omega) = \frac{4\omega^{-2}}{d+1} \int dS\, \gamma_E v_E^2 \left(\mathbf{F}\cdot\hat{\mathbf{n}}\right)^2. \tag{3.18}$$

In this equation and in the remainder of this section, we suppress the $O(\omega^{-3})$ corrections. Notably, the above expression can be computed without any knowledge of the particle trajectories, and depends on $\mathbf{F}(\mathbf{x})$ only via the value of this force at the boundary of the billiard. This special dependence on $\mathbf{F}(\mathbf{x})$ is sensible, since we know that the dominant changes in the particle's energy are associated with collisions with the wall. Also, we emphasize that while the potential $U(\mathbf{x})$ does not appear explicitly in (3.18), g_2 does depend on $U(\mathbf{x})$ via the quantities $v_E(\mathbf{x})$ and $\gamma_E(\mathbf{x})$.

It is worth noting that the ω^{-2} scaling of the diffusion coefficient is somewhat peculiar to billiard systems. As discussed in Chapter 2, Section 2.5, whenever time evolution under the bare Hamiltonian H_0 is smooth, the power spectrum $S(\omega;E)$ (and therefore $g_2(E,\omega) = \frac{1}{2}S(\omega;E)$) goes to zero faster than any power of ω^{-1} for large ω. In contrast, the dynamics in a billiard are

discontinuous whenever a collision with the wall occurs. In Appendix D, in which we provide an alternative derivation of the above expression for g_2, we show that these discontinuities manifest as a cusp at $t = 0$ in the correlation function $C(t; E)$. This cusp then implies that the Fourier transform $S(\omega; E)$ will decay like ω^{-2} for large ω.

To calculate the drift coefficient g_1, we use fluctuation-dissipation relation (2.22), established in Chapter 2 for general chaotic systems under a rapid periodic drive. If we substitute (3.9) and (3.16) - (3.18) into the fluctuation-dissipation relation, then after some differentiation we arrive at our final expression for the drift coefficient:

$$g_1(E, \omega) = \frac{2\omega^{-2}}{m} \int dS \, \gamma_E \left(\mathbf{F} \cdot \hat{\mathbf{n}}\right)^2 . \tag{3.19}$$

This result implies that g_1 is always nonnegative (up to the $O(\omega^{-3})$ corrections), since $\gamma_E(\mathbf{x}) \geq 0$ for all $\mathbf{x}$ on the billiard boundary. From the Fokker-Planck equation (2.11), we know that $d\langle \mathcal{E} \rangle / dt = \langle g_1(\mathcal{E}, \omega) \rangle$ (see (2.24)), where the ensemble average $\langle ... \rangle$ is given by $\langle f(\mathcal{E}) \rangle = \int dE \, \eta(E, t) f(E)$ for any function $f(\mathcal{E})$. Therefore, (3.19) implies that the average energy of particles in the ensemble never decreases; that is, the system exhibits *Fermi acceleration* on average.

Combined with the expressions (3.19) and (3.18) for g_1 and g_2, the Fokker-Planck equation (2.11) now fully characterizes the diffusive dynamics of the particle's energy under high frequency driving. Note that these expressions are only valid for energies in the range $\mathcal{R}(\omega)$, for which conditions (3.5) and (3.6) both hold. For energies above this range, the condition (3.6) breaks down, and the $O(\omega^{-3})$ corrections can no longer be ignored. Also, as mentioned previously, all of the above arguments and calculations may also be generalized to

non-monochromatic driving forces.

3.4.2 Simplified expressions for g_1 and g_2 for $U(\mathbf{x}) = 0$

We now set $U(\mathbf{x}) = 0$, in order to evaluate g_1 and g_2 for a standard billiard. In this case, the undriven particle maintains a constant speed $v_E = \sqrt{2E/m}$, independent of position. This greatly simplifies the calculation of both the density of states $\Sigma(E)$ and the collision rate $\gamma_E(\mathbf{x})$ – note that (3.8) factorizes into two d-dimensional integrals, over position and velocity. We obtain

$$\Sigma(E) = dB_d \frac{V v_E^{d-2}}{m}, \quad \gamma_E = \frac{1}{S}\frac{v_E}{\lambda}, \tag{3.20}$$

where V is the d-dimensional hyper-volume of space enclosed by the billiard, S denotes the $(d-1)$-dimensional hyper-area of the billiard boundary, and $\lambda \equiv d\dfrac{B_d}{B_{d-1}}\dfrac{V}{S}$ is the mean free path (the average distance between collisions) of the undriven billiard particle [145]. Our expressions for the drift and diffusion coefficients now become

$$g_1(E,\omega) = \frac{2\omega^{-2} v_E}{m\lambda}\,\frac{1}{S}\int dS\ (\mathbf{F}\cdot\hat{\mathbf{n}})^2 \qquad (U=0) \tag{3.21}$$

$$g_2(E,\omega) = \frac{4\omega^{-2} v_E^3}{(d+1)\lambda}\,\frac{1}{S}\int dS\ (\mathbf{F}\cdot\hat{\mathbf{n}})^2 \qquad (U=0) \tag{3.22}$$

In these expressions, the dependence of g_1 and g_2 on the particle energy E enters only through the quantity $v_E = \sqrt{2E/m}$. This means that g_1 scales like $E^{1/2}$, and g_2 scales like $E^{3/2}$. As in discussed in Appendix E, for this simple dependence on energy, the Fokker-Planck equation may be solved exactly. This facilitates the numerical calculations described later in Section 3.5. It is also worth noting that both g_1 and g_2 are inversely proportional to the mean free path λ.

At first glance, this suggests that as we decrease the size of the billiard, the rates of energy drift and diffusion approach infinity. However, recall that our expressions for g_1 and g_2 are only valid for $v/\omega \ll l \lesssim \lambda$ (this is condition (3.6)). As the billiard shrinks and λ approaches zero, this condition is inevitably violated. In this limit, the $O(\omega^{-3})$ corrections to the expressions (3.21) and (3.22) become relevant, and the diffusive description may even break down altogether.

We now focus specifically on average energy absorption. Using the relation $d\langle\mathcal{E}\rangle/dt = \langle g_1(\mathcal{E},\omega)\rangle$, we obtain

$$\frac{d\langle\mathcal{E}\rangle}{dt} = \frac{2\bar{v}(t)}{m\lambda\omega^2}\frac{1}{S}\int dS\ (\mathbf{F}\cdot\hat{\mathbf{n}})^2 \qquad (U=0) \tag{3.23}$$

where $\bar{v}(t) \equiv \int dE\,\eta(E,t)\,v_E(E)$ is the mean particle speed at time t. Thus the average rate of energy absorption is proportional to the mean particle speed and inversely proportional to the square of the driving frequency, with a constant of proportionality determined by the particle mass, the shape and dimensionality of the billiard, and the driving field $\mathbf{F}(\mathbf{x})$. For a three-dimensional billiard this result becomes

$$\frac{d\langle\mathcal{E}\rangle}{dt} = \frac{\bar{v}(t)}{2m\omega^2 V}\int dS\ (\mathbf{F}\cdot\hat{\mathbf{n}})^2 \qquad (U=0, d=3) \tag{3.24}$$

This expression resembles the *wall formula*, a semiclassical estimate of dissipation in low-energy nuclear processes, which gives a dissipation rate proportional to mean particle speed, with a constant of proportionality that includes a surface integral over the boundary of the nucleus; see Eq. (1.2) of Ref. [146]. This resemblance is not surprising, since in both cases the system's energy evolves via an accumulation of small changes, sometimes positive, sometimes negative,

occurring at collisions between the particle and the billiard boundary. In fact, the wall formula can be derived within an energy diffusion approach analogous to the one developed above [110].

3.5 Numerical results

We now present numerical simulation results that corroborate our calculations. We consider the special case of a particle in a two-dimensional "clover" billiard, (see Figure 3.4), subject only to a time-periodic, spatially uniform force. Since a *free* particle in the clover billiard is known [110] to exhibit chaotic and ergodic motion, this system satisfies all the assumptions of our paper, as long as the drive is sufficiently rapid. Specifically, in the equations of motion (3.1), we set $U(\mathbf{x}) = 0$, and take $\mathbf{F}(\mathbf{x}) = \mathbf{F}$ to be independent of position. This special case is particularly amenable to simulation, since the motion of the particle between collisions may be computed exactly. Moreover, as described in Appendix E, the Fokker-Planck equation admits an explicit analytical solution for this choice of $U(\mathbf{x})$ and $\mathbf{F}(\mathbf{x})$.

For this system, we calculate the evolution of the energy distribution $\eta(E, t)$ in two ways: By directly evolving an ensemble of particle trajectories according to (3.1) and (3.2), and by solving the Fokker-Planck equation (2.11). If the energy diffusion description is accurate, then the energy distributions obtained in both cases will coincide. We present the results of these computations here, and leave the details of our calculations to Appendix E.

To test our model, we evolve an ensemble of driven particles with mass $m = 1$ in the clover billiard, with $R_1 = 1$ and $R_2 = 2$ (see Figure 3.4). The mean free path for particles in this billiard is $\lambda \approx 2.610$, as shown in Appendix E. The particles are initialized at $t = 0$ with speed $v_0 = 1$, in a microcanonical ensemble at energy $E_0 = mv_0^2/2 = 1/2$. We set $\mathbf{F} = F(\hat{\mathbf{x}} + \hat{\mathbf{y}})/\sqrt{2}$, where $\hat{\mathbf{x}}$

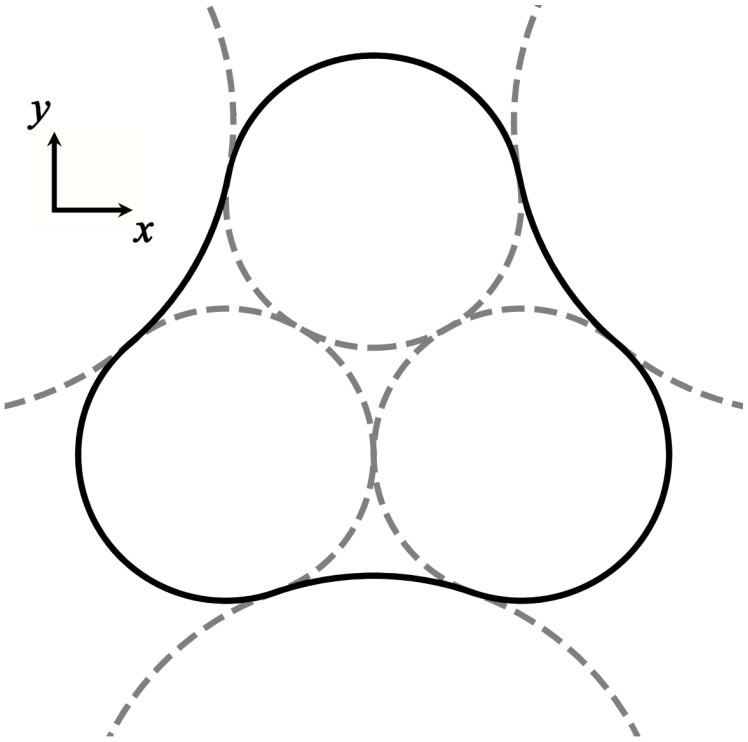

Figure 3.4: Diagram of the clover billiard, constructed from six mutually tangent circles. The billiard boundary is given by the solid line. The inner circles have radius $R_1 = 1$, and the outer circles have radius $R_2 = 2$.

and $\hat{\mathbf{y}}$ are the unit vectors for the coordinate system in Figure 3.4, and choose $F = |\mathbf{F}| = 10$. We run simulations for a range of driving frequencies ω, with a focus on the high-frequency driving regime.

First, we verify the validity of the Fokker-Planck equation. For various values of ω, we evolve an ensemble of $N = 10^5$ driven particles, and then compare the energy distribution of this ensemble with the energy distribution obtained by solving the Fokker-Planck equation. The plots in Figures 3.5 and 3.6 illustrate this comparison at times $t = 10$, 100, and 1000, for driving frequencies $\omega = 40\pi$ and $\omega = 320\pi$ (note that the conditions (3.5) and (3.6) are satisfied for these parameter choices). We find close agreement between the true energy distribution (represented by the histograms) and the Fokker-Planck energy distribution (the solid lines).

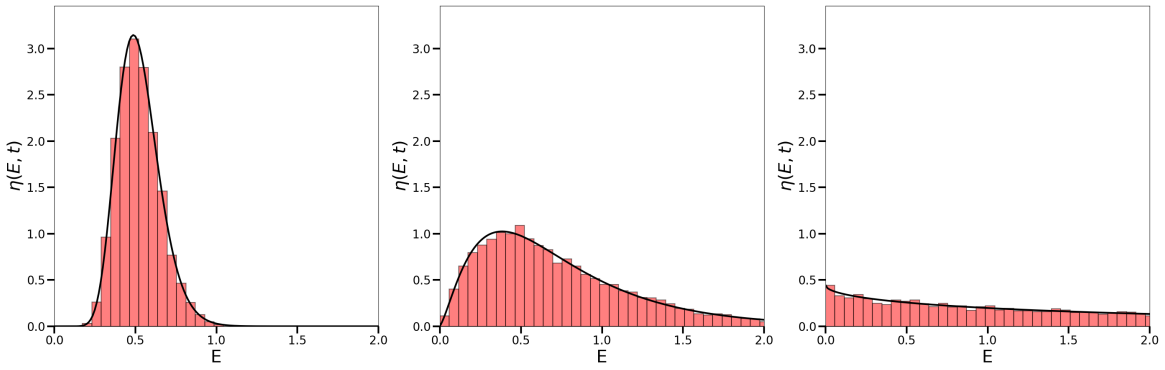

Figure 3.5: Evolution of an ensemble starting with energy $E_0 = 1/2$, with $F = 10$ and $\omega = 40\pi$. The three snapshots are captured at $t = 10$, $t = 100$, and $t = 1000$. The histograms are populated from the numerical simulations, and the solid lines are the solution to the Fokker-Planck equation.

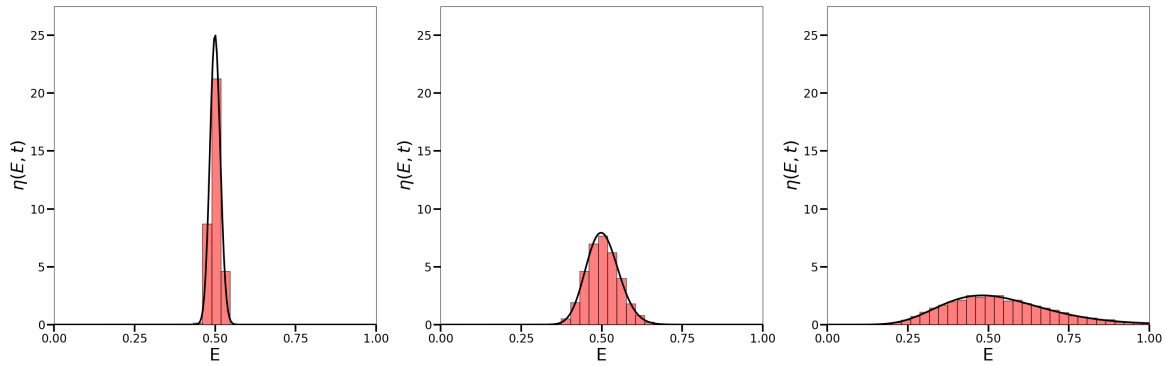

Figure 3.6: Same as Fig. 3.5, but with $\omega = 320\pi$, and with a different scaling of the axes.

Second, we look specifically at the ensemble mean $\langle \Delta\mathcal{E} \rangle$ and variance $\mathrm{Var}(\Delta\mathcal{E})$ of the energy change $\Delta\mathcal{E}$. Recall that if a microcanonical ensemble of initial conditions at energy E_0 is evolved for a short time Δt, then the Fokker-Planck equation predicts that $\langle \Delta\mathcal{E} \rangle \approx g_1(E_0, \omega)\Delta t$ and $\mathrm{Var}(\Delta\mathcal{E}) \approx g_2(E_0, \omega)\Delta t$ (see (2.14) and (2.15)). Here, Δt must satisfy the separation of timescales (2.12): It should be longer than the correlation timescale associated with the particle's undriven motion, but short enough that the relative change in the energy of any particle in the ensemble is still very small. To test this theoretical result, we evolve an ensemble of $N = 10^6$ driven particles for a time $\Delta t = 20$, and then compute the resulting values of $\langle \Delta\mathcal{E} \rangle$ and $\mathrm{Var}(\Delta\mathcal{E})$.

We repeat this for a range of driving frequencies from $\omega = 10\pi$ to $\omega = 2560\pi$, and then plot $\langle \Delta\mathcal{E} \rangle$ and $\mathrm{Var}(\Delta\mathcal{E})$ versus ω in Figure 3.7. For sufficiently large ω, the true values of $\langle \Delta\mathcal{E} \rangle$ and $\mathrm{Var}(\Delta\mathcal{E})$ are in good agreement with the theoretical predictions $\langle \Delta\mathcal{E} \rangle \approx g_1(E_0, \omega)\Delta t$ and $\mathrm{Var}(\Delta\mathcal{E}) \approx g_2(E_0, \omega)\Delta t$, where g_1 and g_2 are given by the formulas (3.21) and (3.22). Note that for large ω, the error bars in Figure 3.7 associated with $\langle \Delta\mathcal{E} \rangle$ become very large. This is because the fluctuations in $\Delta\mathcal{E}$ about its average are on the order of $\sqrt{\mathrm{Var}(\Delta\mathcal{E})} = O(\omega^{-1})$, while $\langle \Delta\mathcal{E} \rangle = O(\omega^{-2})$ itself is much smaller.

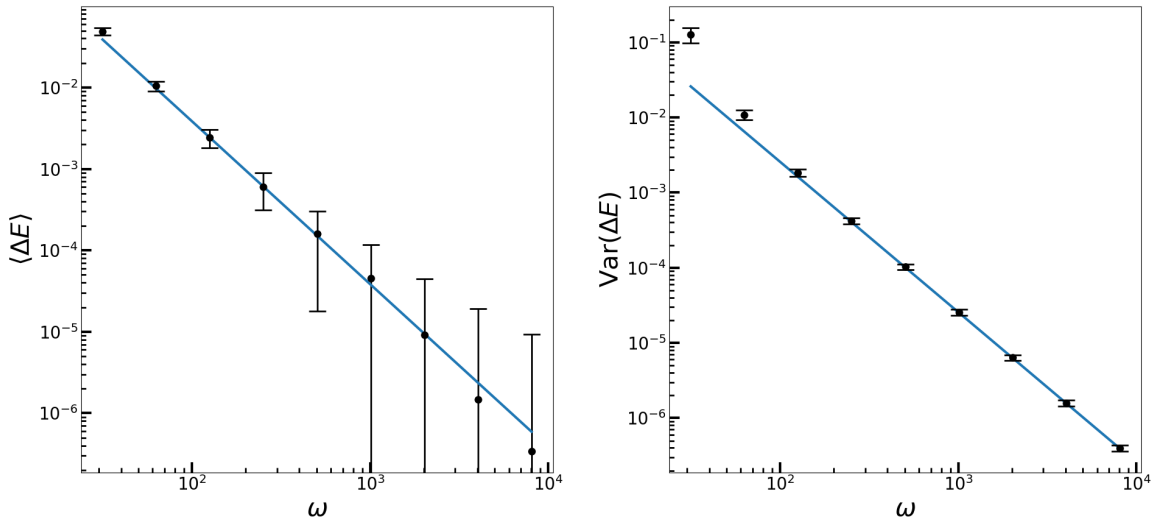

Figure 3.7: $\langle \Delta\mathcal{E} \rangle$ and $\mathrm{Var}(\Delta\mathcal{E})$ versus ω, for an initial ensemble with energy $E_0 = 1/2$, with $F = 10$ and $\Delta t = 20$. The points denote results of the numerical simulations, and the solid line corresponds to the theoretical predictions given by (3.21) and (3.22).

We note that the value of $F = 10$ corresponds to a "strong" driving force, in the following sense. Suppose that we set $\omega = 0$, so that the driving force is time-*independent*, and then estimate the change in a particle's energy as it moves across the billiard. In the $\omega = 0$ case, the particle simply experiences free-fall within the billiard, with a uniform gravitational field pointing in the direction of $\mathbf{F} = F(\hat{\mathbf{x}} + \hat{\mathbf{y}})/\sqrt{2}$. If we initialize the particle on one side of the billiard and let

it "fall" to the other side, then the (kinetic) energy gained by the particle during its descent will be given by $\Delta E = F\Delta x$, where Δx is the distance that the particle moves in the direction of $\mathbf{F}$. Δx will be on the order of the mean free path $\lambda \approx 2.610$, and so we find $\Delta E \sim 26$. This energy change is an order of magnitude larger than the particle's initial energy $E_0 = 1/2$. Clearly, when $\omega = 0$ (or generally, if ω is small), the driving force has a very large effect on the particle trajectories, and therefore we should not expect an energy diffusion description to apply. For $F = 10$, we should only expect energy diffusion for sufficiently large values of ω. Testing our model with this value of F thus insures that energy diffusion is really a consequence of rapid driving, and not simply the result of a weak driving force.

3.6 Application to many-particle billiards

We now apply the results on billiard systems in this chapter to systems of many particles. We consider N hard sphere particles confined to a billiard cavity, where the potentials U and $U_F \cos(\omega t)$ may now generate both external forces and interactions between the particles. For this system, the derivation of the energy drift and diffusion coefficients proceeds along the same general lines as in the single-particle case. We therefore provide a relatively condensed version of this calculation, and then present the results. We find that the expressions for g_1 and g_2 contain two sets of terms: contributions associated with sphere-wall collisions, and contributions associated with sphere-sphere collisions. Although these expressions are generally difficult to evaluate, significant simplifications occur in the thermodynamic limit, where we take N to infinity at fixed particle density and energy density. Moreover, for large enough N, we find that stochastic fluctuations in energy can be neglected, and that the process of energy diffusion limits

to a deterministic evolution of the system's energy. In this limit, the evolution of the system's energy is entirely determined by the drift coefficient g_1, which gives the instantaneous rate of energy absorption. To conclude this section, we further evaluate g_1 for the special case of a low density system, in which the particles interact only via elastic collisions.

3.6.1 Setup

Our system of interest is a collection of N particles confined to a d-dimensional cavity, each labelled by a different value of the index $i = 1, 2 \ldots N$. The i^{th} particle is a d-dimensional sphere of radius R_i and mass m_i. The instantaneous state of this particle is specified by the position and velocity of its center, denoted by $\mathbf{x}_i$ and $\mathbf{v}_i$ respectively. For convenience, we collect these positions and velocities into two $(d \times N)$-dimensional vectors $\mathbf{X} \equiv (\mathbf{x}_1, \mathbf{x}_2 \ldots \mathbf{x}_N)$ and $\mathbf{V} \equiv (\mathbf{v}_1, \mathbf{v}_2 \ldots \mathbf{v}_N)$. In between collisions with the wall or with each other, the particles are subject to a static potential $U(\mathbf{X}) \equiv U$ and a periodic drive $U_F(\mathbf{X}) \cos(\omega t) \equiv U_F \cos(\omega t)$, which generate forces which act on the centers of the particles. Each center evolves in accordance with Newton's equations of motion:

$$\frac{d\mathbf{x}_i}{dt} = \mathbf{v}_i, \quad m\frac{d\mathbf{v}_i}{dt} = -\nabla_i U(\mathbf{X}) + \mathbf{F}_i(\mathbf{X}) \cos(\omega t). \tag{3.25}$$

Here, ∇_i is the gradient with respect to the position variable $\mathbf{x}_i$, and $\mathbf{F}_i \equiv \mathbf{F}_i(\mathbf{X}) \equiv -\nabla_i U_F(\mathbf{X})$. Note that for many physical systems of interest, the nature of the potentials U and U_F may be significantly restricted: U might be expressible as a sum of two-particle interaction potentials, or the force $\mathbf{F}_i$ might be solely determined by the position of the i^{th} particle. We will consider some of these special cases later, but for the moment, we take the form of U and U_F to be quite general.

In this system, two types of collisions can occur, both of which are assumed to be elastic: sphere-wall collisions, and sphere-sphere collisions. In a sphere-wall collision, the velocity of the colliding particle is instantaneously updated via the same reflection law as in the single-particle case (see (3.2)). In a sphere-sphere collision between particles i and j, the two particles exchange energy and momentum, while the total energy $\frac{1}{2}m_i|\mathbf{v}_i|^2+\frac{1}{2}m_j|\mathbf{v}_j|^2$ and total momentum $m_i\mathbf{v}_i + m_j\mathbf{v}_j$ remain constant. Assuming that the contact force between the spheres acts radially (i.e., parallel to the line connecting the centers of the two spheres), then a standard analysis of elastic collisions tells us that the particle velocities $\mathbf{v}_i$ and $\mathbf{v}_j$ are updated to $\mathbf{v}_i'$ and $\mathbf{v}_j'$ according to the rules:

$$\mathbf{v}_i' = \mathbf{v}_i + \frac{2\mu_{ij}}{m_i}(\mathbf{u}_{ij}\cdot\hat{\mathbf{r}}_{ij})\hat{\mathbf{r}}_{ij}, \quad \mathbf{v}_j' = \mathbf{v}_j - \frac{2\mu_{ij}}{m_j}(\mathbf{u}_{ij}\cdot\hat{\mathbf{r}}_{ij})\hat{\mathbf{r}}_{ij}. \tag{3.26}$$

In these expressions, $\mu_{ij} \equiv m_i m_j/(m_i+m_j)$ is the reduced mass of the two particles, $\mathbf{u}_{ij} = \mathbf{v}_j - \mathbf{v}_i$ is their relative velocity, and $\hat{\mathbf{r}}_{ij}$ is the unit vector parallel to the line connecting the centers of the two spheres (equivalently, it is the unit vector normal to the surfaces of the spheres at their point of contact). See the diagram in Figure 3.8.

In both types of collisions, the energy of the system is $\mathcal{E} \equiv \mathcal{E}(\mathbf{X},\mathbf{V}) = \sum_{i=1}^N \frac{1}{2}m_i|\mathbf{v}_i|^2 + U(\mathbf{X})$ is conserved. Meanwhile, in between collisions, Newton's Law (3.25) implies that the instantaneous rate of change of $\mathcal{E}$ is

$$\frac{d\mathcal{E}}{dt} = \sum_{i=1}^N \mathbf{F}_i(\mathbf{X})\cdot\mathbf{v}_i\cos(\omega t). \tag{3.27}$$

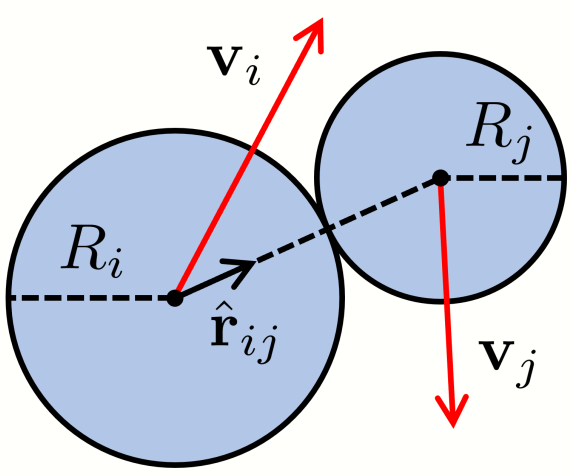

Figure 3.8: Anatomy of a collision between two spheres with radii R_i and R_j, and velocities $\mathbf{v}_i$ and $\mathbf{v}_j$.

3.6.2 Calculation of g_1 and g_2 for many-particle billiards

Given the dynamics described above, we can now begin to calculate the energy drift and diffusion coefficients for this many-particle system. Despite the complications introduced by interactions between the particles, g_1 and g_2 may be evaluated by the same general procedure as in the single-particle case, as given in Section 3.4. Let us take a moment to recall the single-particle analysis. First, we evaluated the energy change $\Delta\mathcal{E}$ for a single trajectory of the particle, by integrating the power (3.3). We found that the dominant changes in the particle's energy are associated with periods during which a collision occurs: The energy change over each such period is given by (3.12). Upon using this result to compute the variance in energy $\mathrm{Var}(\mathcal{E})$ of an ensemble of trajectories, we found that energy changes during different periods are effectively uncorrelated, due to the high driving frequency ω. Our expression for $\mathrm{Var}(\mathcal{E})$ then simplifies to the average (3.14). In Appendix C, we evaluated this average in terms of an integral over the billiard boundary, resulting in our final expression (2.20) for g_2.

We now summarize the many-particle generalization of this procedure. For our system of N particles, consider the energy change of the system during a single period, which we denote by $\Delta\mathcal{E}$. We obtain $\Delta\mathcal{E}$ by integrating the power (3.27) over the period; $\Delta\mathcal{E}$ is then a sum of N terms $\Delta\mathcal{E}^{(1)}, \Delta\mathcal{E}^{(2)} \ldots \Delta\mathcal{E}^{(N)}$, one for each term in (3.27). For each term, there are three possibilities. First, if the i^{th} particle does not experience a collision in this period, we may neglect the corresponding term $\Delta\mathcal{E}^{(i)}$, by the same reasoning that we used to ignore periods without a collision in the single-particle case (see (3.10) and the subsequent paragraph). Second, if the i^{th} particle collides with the wall during the period at the time $t = t_c$, the corresponding term in $\Delta\mathcal{E}$ is

$$\Delta\mathcal{E}^{(i)} = 2\omega^{-1} \left(\mathbf{F}_i \cdot \hat{\mathbf{n}}_i\right) \left(\mathbf{v}_i \cdot \hat{\mathbf{n}}_i\right) \sin(\omega t_c) + O(\omega^{-2}), \tag{3.28}$$

where $\mathbf{v}_i$ and $\mathbf{F}_i$ are evaluated at the instant prior to the collision, and $\hat{\mathbf{n}}_i$ is the unit normal vector to the wall at the point of collision. This follows from the same calculation that leads to (3.12) in the single-particle case, which uses the reflection law (3.2). Third and finally, by a similar calculation with the two-particle reflection rule (3.26), if the i^{th} and j^{th} particles collide with each other during the period at $t = t_c$, the associated pair of terms $\Delta\mathcal{E}^{(i)} + \Delta\mathcal{E}^{(j)}$ is

$$\Delta\mathcal{E}^{(i)} + \Delta\mathcal{E}^{(j)} = 2\omega^{-1} \left(\mathbf{f}_{ij} \cdot \hat{\mathbf{r}}_{ij}\right) \left(\mathbf{u}_{ij} \cdot \hat{\mathbf{r}}_{ij}\right) \sin(\omega t_c) + O(\omega^{-2}), \tag{3.29}$$

where $\mathbf{f}_{ij} \equiv \mu_{ij} \left(\mathbf{F}_j/m_j - \mathbf{F}_i/m_i\right)$ is proportional to the relative acceleration of the particles, and where all quantities are again evaluated at the instant prior to the collision.

Thus, to obtain the energy change $\Delta\mathcal{E}$ over a longer time $t = 0$ to $t = \Delta t$, we can sum all of these contributions together for each period, and then sum over all periods in the time interval.

Equivalently, for the sphere-wall contributions (3.28), we must sum over all sphere-wall collisions for each particle, and then sum over all particles, while for the sphere-sphere contributions (3.29), we sum over all sphere-sphere collisions for each particle pair, and then sum over all pairs. The result may be written as:

$$\begin{aligned}\Delta\mathcal{E} = 2\omega^{-1} &\sum_{i=1}^{N}\sum_{k=1}^{N_i} (\mathbf{F}_i \cdot \hat{\mathbf{n}}_i)\,(\mathbf{v}_i \cdot \hat{\mathbf{n}}_i) \sin\left(\omega t_i^{(k)}\right) \\ + 2\omega^{-1} &\sum_{i=1}^{N}\sum_{j=i+1}^{N}\sum_{k=1}^{N_{ij}} (\mathbf{f}_{ij} \cdot \hat{\mathbf{r}}_{ij})\,(\mathbf{u}_{ij} \cdot \hat{\mathbf{r}}_{ij}) \sin\left(\omega t_{ij}^{(k)}\right) + O(\omega^{-2}).\end{aligned} \tag{3.30}$$

Here, the first line gives the sphere-wall contributions. We use the index i to sum over all N particles, and for each particle i, we use the index k to sum over all N_i collisions between this particle and the wall during the time interval. $t_i^{(k)}$ denotes the time of the k^{th} such collision for the i^{th} particle; each quantity in the (i,k) term of the double sum is evaluated at this time. The second line gives the sphere-sphere contributions. We use the indices i and j to sum over all pairs of particles, and for each pair (i,j), we use the index k to sum over all N_{ij} collisions between this pair during the time interval. $t_{ij}^{(k)}$ denotes the time of the k^{th} such collision for the (i,j) pair; each quantity in the (i,j,k) term of the triple sum is evaluated at this time. This expression is the many-particle generalization of summing over the contributions (3.12) in the single-particle case.

If we now consider an ensemble of systems with initial energy E_0, we can use the above expression to calculate the variance in energies $\mathrm{Var}(\mathcal{E}) = g_2(E_0,\omega)\Delta t = \langle(\Delta\mathcal{E})^2\rangle - \langle\Delta\mathcal{E}\rangle^2$ acquired by the ensemble over the time interval. Just as in the single-particle case, the resulting expression for $\mathrm{Var}(\mathcal{E})$ then simplifies due to the high frequency of the drive, which causes each term in (3.30) to become effectively uncorrelated with the others (see the argument in Appendix

C). The result is the many-particle generalization of (3.14):

$$\begin{aligned}\mathrm{Var}(\mathcal{E}) = 2\omega^{-2}\sum_{i=1}^{N}\left\langle\sum_{k=1}^{N_i}\left(\mathbf{F}_i\cdot\hat{\mathbf{n}}_i\right)^2\left(\mathbf{v}_i\cdot\hat{\mathbf{n}}_i\right)^2\right\rangle_0 \\ + 2\omega^{-2}\sum_{i=1}^{N}\sum_{j=i+1}^{N}\left\langle\sum_{k=1}^{N_{ij}}\left(\mathbf{f}_{ij}\cdot\hat{\mathbf{r}}_{ij}\right)^2\left(\mathbf{u}_{ij}\cdot\hat{\mathbf{r}}_{ij}\right)^2\right\rangle_0 + O(\omega^{-3}).\end{aligned} \tag{3.31}$$

In this expression, the brackets $\langle ...\rangle_0$ denote an average over an ensemble of undriven systems, initialized in a microcanonical ensemble at $t = 0$.

Finally, we can re-evaluate the above averages as integrals. For the sphere-wall contributions, we follow the same procedure that we used to evaluate (3.14) in Appendix C in the single-particle calculation. That is, for each particle and for each infinitesimal patch of the wall, we sum over all collisions occurring on that patch, integrate over all wall patches, and then integrate out the velocity variables in the resulting average. For the sphere-sphere contributions, the method is similar, except that for a given particle pair, we sum over all collisions where the spheres make contact on a given infinitesimal patch of their surfaces (see Figure 3.9). We then integrate over all such patches, and integrate out the velocity variables.

The result of these calculations yields the desired expression for g_2 (we now drop the $O(\omega^{-3})$ corrections):

$$\begin{aligned}g_2(E,\omega) = \frac{4C_{dN}}{dN+1}\omega^{-2}\left[\sum_{i=1}^{N}\int dS_i\int d\mathbf{X}_i^*\,\rho_E v_i^3\left(\mathbf{F}_i\cdot\hat{\mathbf{n}}_i\right)^2\right. \\ \left. + \sum_{i=1}^{N}\sum_{j=i+1}^{N}R_{ij}^{d-1}\int d\Omega_{ij}d\mathbf{X}_{ij}^*\,\rho_E v_{ij}^3\left(\mathbf{f}_{ij}\cdot\hat{\mathbf{r}}_{ij}\right)^2\right].\end{aligned} \tag{3.32}$$

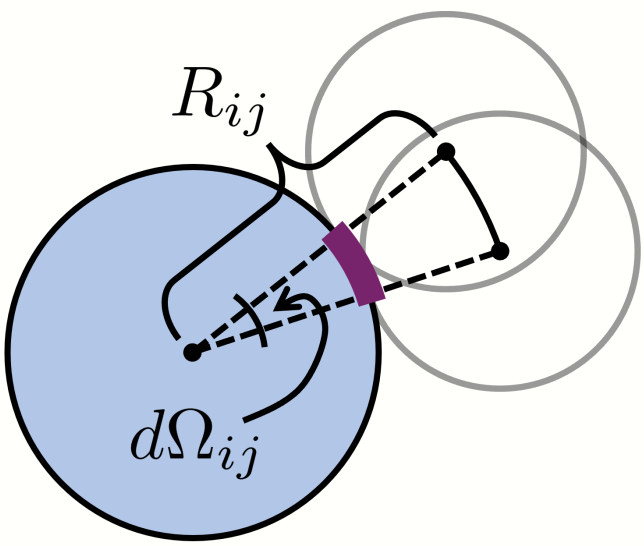

Figure 3.9: Diagram for integration over possible collisions between spheres i and j, in the $d = 2$ dimensional case. Holding sphere i fixed (the circle on the left), we can imagining sliding sphere j (represented by the circles on the right) along a small patch of sphere i's surface (thick purple curve). This corresponds to integrating over a small range of orientations of the relative position vector $\mathbf{r}_{ij}$, or an associated range of solid angles $d\Omega_{ij}$. While sweeping through these orientations, the spheres remain in constant contact, so the magnitude of $\mathbf{r}_{ij}$ is fixed at $|\mathbf{r}_{ij}| = R_{ij} = R_i + R_j$.

In this expression, we have introduced a number of new pieces of notation. In the first line, which gives the sphere-wall contribution, we have defined the constant $C_{dN} \equiv B_{dN-1}/(dNB_{dN})$, where $B_n = \pi^{n/2}/\Gamma\left(\frac{n}{2}+1\right)$. For each particle i, we integrate over all allowed configurations $\mathbf{X}$ of the N particles such that particle i is in contact with the wall (here, allowed means that there are no overlaps between particles, or between any particle and the wall). This means an integral over all patches of the wall that the i^{th} particle touches, denoted by $\int dS_i \ldots$, and an integral over all $\mathbf{X}_i^*$, the vector of all particle positions excluding $\mathbf{x}_i$. In the integrand, $\rho_E(\mathbf{X}) \equiv \rho_E$ is the marginal distribution over particle configurations $\mathbf{X}$, given that the system is described by a microcanonical ensemble at energy E. This is obtained by integrating the full microcanonical distribution $\rho_E(\mathbf{X}, \mathbf{V}) \equiv \delta(\mathcal{E}(\mathbf{X}, \mathbf{V}) - E)/\Sigma(E)$ over the particle velocities $\mathbf{V}$. Finally, we define a speed v_i by $v_i \equiv v_i(\mathbf{X}) \equiv \sqrt{2[E - U(\mathbf{X})]/m_i}$ for $E > U(\mathbf{X})$, and $v_i = 0$ otherwise.

In the second line, which corresponds to the sphere-sphere contribution, we define the sum of radii $R_{ij} \equiv R_i + R_j$ for each pair of spheres. For each pair i and j, we integrate over all allowed configurations of the N particles such that these two particles are touching. In such configurations, the relative position of these particles $\mathbf{r}_{ij} \equiv \mathbf{r}_j - \mathbf{r}_i$ is given by $\mathbf{r}_{ij} = R_{ij}\hat{\mathbf{r}}_{ij}$. To perform this integration, we first integrate over all orientations of $\hat{\mathbf{r}}_{ij}$ with the solid angle integral $\int d\Omega_{ij} \ldots$ (see Figure 3.9), and then integrate over all $\mathbf{X}^*_{ij}$, a vector encoding the configuration $\mathbf{X}$ modulo the value of $\mathbf{r}_{ij}$. In the integrand, we define the speed v_{ij} by $v_{ij} \equiv v_{ij}(\mathbf{X}) \equiv \sqrt{2[E - U(\mathbf{X})]/\mu_{ij}}$ for $E > U(\mathbf{X})$, and $v_{ij} = 0$ otherwise.

We can then invoke the fluctuation-dissipation relation (2.22) to compute the drift coefficient g_1. After some differentiation, we find

$$\begin{aligned} g_1(E,\omega) = 2C_{dN}\omega^{-2} \Bigg[&\sum_{i=1}^{N} \frac{1}{m_i} \int dS_i \int d\mathbf{X}_i^* \, \rho_E v_i \left(\mathbf{F}_i \cdot \hat{\mathbf{n}}_i\right)^2 \\ &+ \sum_{i=1}^{N} \sum_{j=i+1}^{N} \frac{R_{ij}^{d-1}}{\mu_{ij}} \int d\Omega_{ij} \int d\mathbf{X}_{ij}^* \, \rho_E v_{ij} \left(\mathbf{f}_{ij} \cdot \hat{\mathbf{r}}_{ij}\right)^2 \Bigg] . \end{aligned} \tag{3.33}$$

With this expression for g_1 and the expression (3.32) for g_2, we have now fully specified the diffusive energy evolution of our many particle system.

3.6.3 The thermodynamic limit of many-particle billiard systems

For certain special choices of particle interaction, we may continue to develop the expressions (3.33) and (3.32). For example, for weakly interacting particles or low-density systems, the integrals may be evaluated by assuming that the positions of different particles are approximately statistically independent. We will examine such a special case shortly, in Section

3.6.4. However, before doing so, we now turn to a discussion of the thermodynamic limit. For a large number of particles, we obtain simplified expressions for g_1 and g_2, by invoking the equivalence between the canonical and microcanonical ensembles. Moreover, we will see for large enough N, statistical fluctuations in the system's energy will become negligible relative to the mean rate of energy absorption, given by the drift coefficient g_1.

To take the thermodynamic limit, we consider the limit in which the particle number N, the volume of the cavity V, and the energy E are all taken to infinity, while the number density N/V and energy per particle E/N are held fixed. In this limiting process, we assume that the relative shape of the billiard is held fixed as the volume is increased, and that the potentials U and U_F are varied in an appropriate way. For example, if U and U_F only encode two-particle interactions, then as N is increased, the strength and functional form of these interactions is held fixed. Moreover, as more particles are added, the typical radius and mass of new particles should not grow with N. Going forward, we assume that this limit is well-defined. One way to ensure this is to require that the interactions between particles be sufficiently weak at long distances, and sufficiently repulsive at short distances (precise conditions for the existence of the thermodynamic limit can be found in [147–151]).

Let us consider our expression for g_1 in this limit. A common property of systems with a thermodynamic limit is the the equivalence of statistical ensembles [149–153]. That is, for large enough N, the equivalence of ensembles allows us to replace a microcanonical average at energy E with a canonical average at temperature $T(E) \equiv T$, where T is the microcanonical temperature as defined in (2.25) in Chapter 2. The integrals in (3.33) are proportional to microcanonical averages. Therefore, assuming the equivalence of ensembles, we may replace the microcanonical distribution ρ_E with the canonical distribution $\rho_T \equiv \rho_T(\mathbf{X}) \propto e^{-U(\mathbf{X})/k_B T}$.

Furthermore, in the thermodynamic limit, fluctuations of macroscopic quantities are generally suppressed: For almost all samples from the canonical ensemble, the value of such a quantity will be very close to its mean value [151]. We may thus treat these quantities as essentially constant and equal to their canonical averages. One such quantity is the total kinetic energy of the system, $K \equiv \sum_{i=1}^{N} \frac{1}{2} m_i |\mathbf{v}_i|^2 = E - U(\mathbf{X})$. The suppression of fluctuations means that over almost the entire range of integration in (3.33), K will be very close to its canonical average $\frac{d}{2} N k_B T$. As a result, we incur little error by taking $v_i = \sqrt{2K/m_i}$ and $v_{ij} = \sqrt{2K/\mu_{ij}}$ out of the integrals in (3.33), and setting these quantities equal to $v_i = \sqrt{dNk_BT/m_i}$ and $v_{ij} = \sqrt{dNk_BT/\mu_{ij}}$.

Finally, we note that for large N, $C_{dN} = B_{dN-1}/(dNB_{dN})$ is approximately $1/\sqrt{2\pi dN}$, which follows from the fact that $B_n = \pi^{n/2}/\Gamma\left(\frac{n}{2}+1\right)$, and that $\Gamma(s+t)/\Gamma(s) \approx s^t$ for large s.[1] Taking all of these approximations together, we see that (3.33) may be rewritten as

$$g_1(E,\omega) = 2\omega^{-2}\left[\sum_{i=1}^{N}\left(\frac{k_BT}{2\pi m_i^3}\right)^{1/2}\int dS_i \int d\mathbf{X}_i^* \, \rho_T \left(\mathbf{F}_i \cdot \hat{\mathbf{n}}_i\right)^2 + \sum_{i=1}^{N}\sum_{j=i+1}^{N} R_{ij}^{d-1}\left(\frac{k_BT}{2\pi\mu_{ij}^3}\right)^{1/2}\int d\Omega_{ij}\int d\mathbf{X}_{ij}^* \, \rho_T \left(\mathbf{f}_{ij}\cdot\hat{\mathbf{r}}_{ij}\right)^2\right]. \tag{3.34}$$

Let us now pause and ask how this expression for g_1 scales with N. We can examine the quantities in (3.34) one by one, recalling that in the thermodynamic limit, we keep N/V and E/N fixed. We begin with the first line. The integrand will scale like $1/V^N$, since the force $\mathbf{F}_i$ should remain bounded in the thermodynamic limit, and since ρ_T must integrate to 1 when integrated over the N-particle configuration space. Therefore, the whole integral will scale like

[1] The asymptotic formula $\Gamma(s+t)/\Gamma(s) \approx s^t$ is a consequence of Stirling's approximation formula for the gamma function.

the billiard surface area S divided by the volume V, since we are integrating over the billiard surface and the configuration space of $N-1$ particles. The prefactor in front of the integral remains bounded with increasing N, since the temperature T is an intensive quantity. Finally, the sum over particles introduces an additional factor of $\sim N$, meaning that the first line will overall scale like $NS/V \sim S$. By an analogous argument, we can see that the second line will scale like $N \sim V$.

This result is intuitively reasonable: The first line of (3.34), which accounts for energy changes associated with the billiard surface, scales like the surface area S, while the second line, associated with sphere-sphere collisions which occur throughout the billiard, scales like the billiard volume V. Both of these contributions diverge in the thermodynamic limit, though since the volume of a billiard grows faster than its surface area, the sphere-sphere contribution will dominate for large enough N. Moreover, if we repeat this whole analysis of the thermodynamic limit for the diffusion coefficient g_2, we find that the contributions to g_2 scale in exactly the same way.

This scaling behavior leads us to the following simplification. Suppose we initialize our system with a definite energy E_0 at $t = 0$, corresponding to a distribution $\eta(E, 0) = \delta(E - E_0)$. After a short time Δt, the energy diffusion description tells us that the mean energy of the ensemble is given by $\langle \mathcal{E} \rangle \approx E_0 + g_1(E_0, \omega)\Delta t$, and that the ensemble acquires a width in energy space of order $\sqrt{\mathrm{Var}(\mathcal{E})} \approx \sqrt{g_2(E_0, \omega)\Delta t}$. Since g_1 and g_2 both diverge in the same way in the thermodynamic limit, for large enough N, the shift $g_1(E_0, \omega)\Delta t$ in the ensemble mean will be far larger than the energy spread $\sqrt{g_2(E_0, \omega)\Delta t}$. In other words, fluctuations in the system's energy become negligibly small relative to the systematic increase in the system's mean energy. For larger and larger N, these fluctuations will remain small for longer and longer times.

While the spread in the energy distribution remains small, we may approximate $\langle g_1(\mathcal{E},\omega)\rangle$ by $g_1(\langle\mathcal{E}\rangle,\omega)$. The expression (2.24) for the average rate of energy absorption then becomes a *closed* equation for $\langle\mathcal{E}\rangle$:

$$\frac{d\langle\mathcal{E}\rangle}{dt} = g_1\left(\langle\mathcal{E}\rangle,\omega\right). \tag{3.35}$$

This is a deterministic "equation of motion" for $\langle\mathcal{E}\rangle$, which can in principle be solved given an initial condition. Thus, in the thermodynamic limit, the full stochastic description furnished by the energy diffusion model effectively reduces to a deterministic evolution of $\langle\mathcal{E}\rangle$, which is fully characterized by the energy absorption rate g_1.

3.6.4 Energy absorption in a driven dilute gas of hard spheres

Assuming the validity of the deterministic equation (3.35), we now examine one special case: A dilute gas of hard spheres, which interact solely via their hard-core interactions. We set $U(\mathbf{X}) = 0$, and we assume that each particle is subject to the same driving force field, which addresses each particle independently (i.e., $\mathbf{F}_i = \mathbf{F}(\mathbf{x}_i)$ for some conservative force field $\mathbf{F}(\mathbf{x}) \equiv \mathbf{F}$). The undriven version of this system, with slight modifications, is the subject of the well-known *Boltzmann-Sinai* hypothesis [154]. This conjecture concerns the evolution of a collection of $N \geq 2$ hard spheres on a d-dimensional torus, moving inertially and interacting only via elastic collisions. The hypothesis states that for given values of the relevant conserved quantities (total energy E and total momentum $\mathbf{P}$), this system evolves chaotically and ergodically on the corresponding surface in phase space of constant E and $\mathbf{P}$. For a wide range of choices of the particle masses $m_1, m_2 \ldots m_N$, the Boltzmann-Sinai hypothesis has been rigorously proven

[154, 155].

Under these assumptions, our expression for g_1 simplifies significantly. Consider the integral in the second line of (3.34), corresponding to the sphere-sphere contributions. Since we are working in the dilute limit, interactions between the spheres will be relatively infrequent, and the statistical properties of the system will be well-approximated by those of an ideal gas of noninteracting point particles. Therefore, we incur only a small error if we replace the probability distribution $\rho_T = \rho_T(\mathbf{X})$ by the corresponding distribution for an ideal gas, which is simply $\rho_T(\mathbf{X}) = 1/V^N$. Then, we may integrate over all $N-2$ positions $\mathbf{x}_k$ for $k \neq i, j$, since $\mathbf{f}_{ij} = \mu_{ij}(\mathbf{F}_j/m_j - \mathbf{F}_i/m_i)$ is independent of these $\mathbf{x}_k$ (given our assumption that $\mathbf{F}_i = \mathbf{F}(\mathbf{x}_i)$). This gives a factor of V^{N-2}; the integral is now reduced to $V^{-2}\int d\Omega_{ij}\int d\mathbf{x}_i\ (\mathbf{f}_{ij}\cdot\hat{\mathbf{r}}_{ij})^2$. Finally, if we assume that $\mathbf{F}(\mathbf{x})$ is essentially constant on length scales comparable to the particle radii R_i, then $\mathbf{F}_j \approx \mathbf{F}_i = \mathbf{F}(\mathbf{x}_i)$, and we have $\mathbf{f}_{ij} = \mathbf{F}(\mathbf{x}_i)(m_i - m_j)/(m_i + m_j)$. Then, since $\mathbf{f}_{ij}$ is solely a function of $\mathbf{x}_i$, we may exactly integrate $(\mathbf{f}_{ij}\cdot\hat{\mathbf{r}}_{ij})^2$ over all solid angles Ω_{ij} (technically, for $\mathbf{x}_i$ very close to the wall, we can only integrate over angles where $\mathbf{x}_j = \mathbf{x}_i + \mathbf{r}_{ij}$ remains within the billiard; this constitutes a small "surface" correction that we ignore). This integration yields $B_d|\mathbf{f}_{ij}|^2$, our final expression for the integral in the second line of (3.34) is thus $B_d V^{-2}\left(\frac{m_i-m_j}{m_i+m_j}\right)^2\int d\mathbf{x}_i|\mathbf{F}(\mathbf{x}_i)|^2$. Note that $\mathbf{x}_i$ is now just a dummy variable here; $\int d\mathbf{x}_i|\mathbf{F}(\mathbf{x}_i)|^2$ is in fact independent of i.

Now, we could attempt to evaluate the first line of (3.34) in a similar way. However, including the surface correction we already neglected in the second line would generally yield extra terms which scale like the surface area of the billiard. Since we are ignoring these terms, for consistency we should neglect the first line of (3.34) entirely, which also scales like S. Thus in our final expression, the sphere-sphere contribution is all that remains:

$$g_1(E,\omega) = \frac{2\omega^{-2}B_d}{V}\overline{|\mathbf{F}|^2}\sum_{i=1}^{N}\sum_{j=i+1}^{N} R_{ij}^{d-1}\left(\frac{k_BT}{2\pi\mu_{ij}^3}\right)^{1/2}\left(\frac{m_i-m_j}{m_i+m_j}\right)^2. \tag{3.36}$$

Here, we have defined the average $\overline{|\mathbf{F}|^2} \equiv V^{-1}\int d\mathbf{x}|\mathbf{F}(\mathbf{x})|^2$.

We note two interesting properties of this expression. First, if the i^{th} and j^{th} spheres have equal masses, then the associated contribution to g_1 vanishes. This can be understood as follows. Note that when the spheres are at approximately the same position $\mathbf{x}_i \approx \mathbf{x}_j$, they both experience approximately the same force $\mathbf{F}(\mathbf{x}_i)\cos(\omega t)$. Since the spheres have equal masses, they will also experience the same acceleration. Therefore, during a period when these two spheres collide, we may move into an oscillating reference frame where this acceleration is approximately cancelled out, so that the spheres appear to move inertially. Relative to the original frame, the velocities of the spheres will be boosted by an amount $\approx -\mathbf{F}(\mathbf{x}_i)\sin(\omega t)/(m_i\omega)$. Now, on one hand, in this accelerated frame, the total kinetic energy of the two spheres will be unchanged during the period, since the spheres appear to collide without the influence of any forces (other than contact forces). On the other hand, at the beginning and end of the period, the velocity (and therefore the kinetic energy) of each sphere in the accelerated frame will coincide with its velocity in the original frame. It follows that the total kinetic energy of the spheres in the *original* frame is the same at the beginning and end of the period. That is, no net energy change occurs for these spheres during this period, and thus there are no energy changes associated with such collisions.

Second, the only dependence on the system's energy in (3.36) enters through the temperature T. Since $U(\mathbf{X}) = 0$, the energy of this system is entirely kinetic, and thus $E = \frac{d}{2}Nk_BT$. Therefore, combining (3.35) and (3.36), we see that $d\langle\mathcal{E}\rangle/dt = a\langle\mathcal{E}\rangle^{1/2}$, where a is a constant independent of $\langle\mathcal{E}\rangle$. If $\langle\mathcal{E}\rangle = E_0$ at $t = 0$, then the solution to this equation is

$$\langle \mathcal{E} \rangle(t) = \left(E_0^{1/2} + \frac{at}{2} \right)^2, \tag{3.37}$$

which grows proportional to t^2 for large t. This quadratic-in-time Fermi acceleration has also been observed in other billiard models [72, 156].

3.7 Comparison to existing results

We now briefly compare our work to previous results derived for driven billiard systems. A common feature of many driven billiards is a statistical tendency towards increasing particle speeds, known as Fermi acceleration. In this section, we provide some basic physical intuition for why this acceleration process may occur, and we demonstrate a correspondence between the billiards studied in our work and a different class of driven billiards, namely billiards with rapid, low-amplitude wall oscillations.

Our results are situated in a extensive literature on driven billiards, which have been proposed as models for phenomena ranging from electrical conduction [157, 158], to relativistic charged particle dynamics [159], to nuclear dissipation [146]. Billiard systems may either be driven via an external force applied between collisions, as in the present paper, or via time-dependence of the billiard walls. In the latter scenario, the billiard boundary is deformed and shifted as a function of time according to a pre-specified schedule, and changes in the particle's energy are induced by collisions with the moving wall. For a variety of models, it has been demonstrated that such systems are susceptible to *Fermi acceleration*: The particle exhibits a statistical bias towards energy-*increasing* collisions, leading to a systematic growth of the (average) energy [156, 160–165]. In particular, diffusive energy spreading via this mechanism

has been observed for certain models [72, 110, 121].

Let us briefly discuss the origins of Fermi acceleration. When and why does this statistical tendency towards increasing energy occur? Although the details of Fermi acceleration will differ from system to system, a toy model suffices to illustrate one way that this bias can emerge. Consider an ensemble of particles in one dimension, which move inertially apart from collisions with an oscillating wall. We specify the location of the wall by a function $x = f(t)$, which is periodic with period T, and define a corresponding wall velocity $u(t) \equiv f'(t)$. Without loss of generality, suppose that at the beginning of each period ($t = 0, T, 2T ...$), the wall is at the origin $x = 0$, so that $f(0) = 0$. Now, at $t = 0$, let us give the particles a common initial velocity $v > 0$, and uniformly distribute them in space for $x < 0$, to the left of the origin (this ensemble does not correspond to a normalized probability distribution, but this is unimportant for what follows). Over the course of a single period, a certain contingent of particles in the ensemble will collide with the wall, and each will gain or lose a certain amount of energy. We can then ask: On average, will the energy of the particles which collide increase or decrease?

To answer this question, consider specifically the collisions which occur in an infinitesimal interval of time from t to $t + dt$. The speed of a particle which collides during this time interval will change by an amount $\Delta v = -2u(t)$, which follows from the fact that in the *rest frame* of the wall, the velocity of the particle merely switches sign in an elastic collision. This speed change is positive when the wall is approaching the particles ($u(t) < 0$), and negative when it is receding from them ($u(t) > 0$). Now, as long as the speed of the wall is not too large, particles which collide during the time interval $(t, t + dt)$ originate from a range of initial positions of size $dx = (v - u(t))dt$ (see Figure 3.10 as a guide). This can be seen by switching to a reference frame co-moving with the particles, and asking how much distance the wall "sweeps out" during

the interval. Then, since the contingent of the ensemble which reaches the wall *anytime* during the period is all those particles initially between $x = -vT$ and $x = 0$, the relative fraction of colliding particles which collide specifically during the infinitesimal interval $(t, t + dt)$ is $dx/vT = (dt/T)(1 - u(t)/v)$. Thus, by integrating $\Delta v = -2u(t)$ over all such infinitesimal intervals from $t = 0$ to $t = T$, weighted by the factor $(1/T)(1 - u(t)/v)$, we obtain the average change in speed over all colliding particles:

$$\langle \Delta v \rangle = \frac{1}{T} \int_0^T dt \left(1 - \frac{u(t)}{v}\right) \Delta v = \frac{2}{v} \frac{1}{T} \int_0^T dt\, u(t)^2 > 0. \tag{3.38}$$

Here, we have used that fact that the displacement $\int_0^T dt\, u(t)$ over a single period vanishes, since the wall's motion is periodic.

Thus, over a single period, the ensemble exhibits on-average Fermi acceleration, as signalled by the increase in the particles' mean speed (note that via an analogous calculation, it is easy to show that the particles' average energy $\frac{1}{2}mv^2$ increases as well). Intuitively, this arises because when the wall is moving towards the particles, causing speed-increasing collisions, it can "sweep" over the particles at a faster rate than when it is receding. This bias is encoded in the factor $(1 - u(t)/v)$ in the average above, which gives more weight to times when speed-increasing collisions occur (when $u(t) < 0$) than to times when speed-decreasing collisions occur ($u(t) > 0$).

Naively extrapolating this model over many periods and to higher dimensions, we might then guess that in a chaotic billiard with oscillating walls, the same logic will ensure that on-average Fermi acceleration occurs. The reality is more complicated: Even in one dimension, after particles in an ensemble begin to collide with the wall, correlations are invariably established

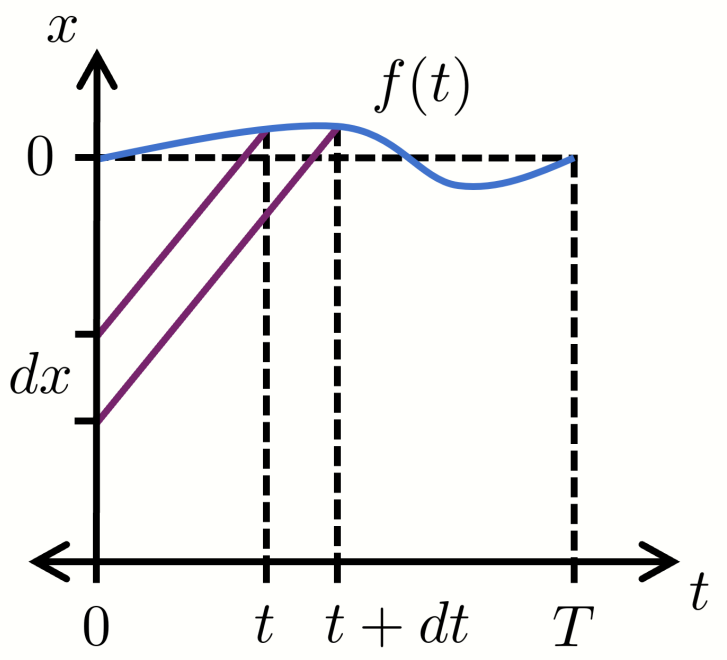

Figure 3.10: Position versus time diagram of collisions with an oscillating wall. The changing location of the wall over one period, given by $x = f(t)$, is specified by the solid blue curve. The purple diagonal lines trace the position versus time of two representative particles, which collide with the wall at t and $t + dt$. Particles which collide with the wall during this infinitesimal range of times originate from a range of initial positions of size $dx = (v - u(t))dt$. This figure is adapted from a similar diagram in [72].

between the positions and velocities of the particles, which influence the statistics associated with subsequent collisions. These statistics will not be fully captured by in the model just described, since we assumed an initial lack of correlations between particle positions and velocities. However, at a first level of approximation, this simple one-dimensional analysis is often a useful way to understand why a bias towards energy absorption arises in billiard systems.

Whether as a result of the mechanism described above or by other means, Fermi acceleration is thus a common feature of many driven billiard systems. Of course, in this section so far we have only discussed billiards with time-dependent boundaries. However, there is a natural correspondence these systems and the billiards studied in our work, which allows intuitions about Fermi acceleration to be applied to both types of billiards. In Section 3.3, we

noted that over a single period, the driving force perturbs the velocity of a billiard particle by an amount $\approx \mathbf{F}(\mathbf{x})\sin(\omega t)/(m\omega)$, and its position by $\approx -\mathbf{F}(\mathbf{x})\left[\cos(\omega t)-1\right]/(m\omega^2)$. Evidently, the particle's motion over a period is well-approximated as small, sinusoidal oscillations about a corresponding undriven trajectory of the particle. Therefore, we can imagine moving to an oscillating reference frame, wherein the particle exhibits approximately undriven motion, and the *walls* perform small, rapid oscillations. Accordingly, we hypothesize that for any rapidly driven billiard satisfying the assumptions of this paper, there is a particular billiard with oscillating boundaries which exhibits energy diffusion with the same drift and diffusion coefficients. For the special case of a standard billiard, $U(\mathbf{x}) = 0$, we can confirm this correspondence by comparing our results to those of [72], where energy diffusion is established for billiards in the "quivering limit," wherein the walls of a billiard undergo small, rapid periodic oscillations. Under this framework, it is straightforward to verify that if each point on the boundary of a quivering chaotic billiard oscillates about its mean position $\mathbf{x}$ with time-dependence $\mathbf{x}+\mathbf{F}(\mathbf{x})\cos(\omega t)/m\omega^2$, then the associated drift and diffusion coefficients are exactly those predicted in our model for a standard billiard subject to the force $\mathbf{F}(\mathbf{x})\cos(\omega t)$. It would be interesting to see whether a similar correspondence is valid in the general case, for $U(\mathbf{x}) \neq 0$.

Chapter 4: Energy diffusion in oscillator systems driven by weak correlated noise

4.1 Chapter summary

In this chapter, we discuss energy diffusion in two oscillator systems, each perturbed by weak, correlated noise. The first, studied in Section 4.2, is a particle in a one-dimensional potential well, subject to a small noisy force. The second, analyzed in Section 4.3, is a classical spin precessing about a magnetic field, perturbed by small fluctuations about the mean field. This work was done in conjunction with recent work by Antonis Kyprianidis and Chris Monroe, regarding how trapped ions can absorb energy from external noise (see Chapter 5 of [166] for more details). Both the particle system and the spin system can be described with an energy diffusion model, each with an associated Fokker-Planck equation. We find that both models may be understood as a formal infinite temperature limit of certain previously studied energy diffusion models, which govern the evolution of systems subject to *thermal* noise. Although these thermal noise models are well-studied in the literature, we nevertheless present these results as an example of the general utility of the energy diffusion description. Moreover, as we show, these two models are especially fruitful to analyze, since the Fokker-Planck equation for the particle may be solved approximately, and the Fokker-Planck equation for the spin admits an exact solution.

4.2 Particle in a potential well subject to weak, correlated noise

Consider a classical point particle constrained to one dimension, with position $x \equiv x(t)$ and velocity $v \equiv v(t)$. The particle is confined by a potential $U(x)$, and is driven by a random, time-dependent noise force $f(t)$. We refer to this as the "normal" noise model, to distinguish it from a model with *thermal* noise that we introduce shortly. The equations of motion are:

$$\frac{dx}{dt} = v, \quad m\frac{dv}{dt} = -U'(x) + f(t). \tag{4.1}$$

Due to the noise force $f(t)$, the particle's energy $E \equiv \frac{1}{2}mv^2 + U(x)$ varies with time, according to $dE/dt = f(t)v(t)$. We take $f(t)$ to be generated by a stationary stochastic process, characterized by a vanishing mean $\langle f(t) \rangle = 0$ and a correlation function $C_f(t) \equiv \langle f(0)f(t) \rangle$, which decays to zero over some correlation timescale τ_C. We also assume that the typical magnitude of $f(t)$ is small, so that significant energy changes only occur on timescales much longer than τ_C. Note that because of the finite correlation time of the noise, these dynamics are *not* equivalent to the standard Langevin description of a particle driven by noise, which assumes uncorrelated or "white" noise with $C_f(t) \propto \delta(t)$.

4.2.1 Energy diffusion description

Under these conditions, we anticipate that the system will undergo a random walk in energy space, which will manifest as a process of energy diffusion on timescales $\gg \tau_C$ (see Chapter 2, Section 2.7 for a discussion of the typical conditions under which energy diffusion occurs). Here, note that the decay of correlations necessary for diffusive evolution is induced by the *external*

noise. This is in contrast to the energy diffusion model developed in Chapter 2, wherein the *intrinsic* chaotic motion of the system generates the requisite decay of correlations. In any case, the process of energy diffusion is described by a Fokker-Planck equation

$$\frac{\partial \eta}{\partial t} = -\frac{\partial}{\partial E}\left(g_1 \eta\right) + \frac{1}{2}\frac{\partial^2}{\partial E^2}\left(g_2 \eta\right) \tag{4.2}$$

for the energy distribution $\eta(E,t)$. It just remains to obtain the energy drift and diffusion coefficients $g_1 \equiv g_1(E)$ and $g_2 \equiv g_2(E)$.

To do so, note that for weak noise, we may approximate $dE/dt = f(t)v(t)$ by $dE/dt \approx f(t)v(t;E_0)$ for short times, where $v(t;E_0)$ is the unperturbed velocity the particle would have in the *absence* of the noise. Because the particle is confined to a potential well, $v(t;E_0)$ will oscillate around zero with some energy-dependent period $T \equiv T(E_0)$. Upon decomposing $v(t;E_0)$ in a Fourier series $v(t;E_0) = \sum_{k\in\mathbb{Z}\setminus\{0\}} a_k e^{ik\omega t}$ with fundamental frequency $\omega \equiv \omega(E_0) = 2\pi/T(E_0)$, we have:[1]

$$\frac{dE}{dt} = f(t)v(t) \approx f(t)\sum_{k\in\mathbb{Z}\setminus\{0\}} a_k e^{ik\omega t}, \tag{4.3}$$

where

$$a_k \equiv a_k(E_0) = \frac{1}{T}\int_0^T dt\, v(t;E_0)e^{-ik\omega t}. \tag{4.4}$$

We can then use this expression to compute $\mathrm{Var}(E) \approx g_2(E_0)\Delta t$, the energy variance acquired by an ensemble of trajectories with initial energy E_0, over a short time Δt. This calculation

[1]The Fourier expansion for $v(t;E_0)$ has no $k=0$ term because the average velocity over a period must be zero. If this were not the case, then the particle would experience a nonzero displacement over the course of a period, which is inconsistent with the motion being periodic.

proceeds in the same way as the analogous calculation of $\mathrm{Var}(E)$ in Appendix A, starting from (A.2). The result is, for $\Delta t \gg T, \tau_C$:

$$g_2(E) \approx 2 \sum_{k=1}^{\infty} |a_k(E)|^2 S_f(k\omega), \tag{4.5}$$

where

$$S_f(\nu) \equiv \int_{-\infty}^{\infty} dt\, e^{-i\nu t} C_f(t) \tag{4.6}$$

is the power spectrum for the noise.

To obtain $g_1(E)$, we note that the arguments used to obtain the fluctuation-dissipation relation (2.22) in Chapter 2 apply equally well to the present system. So, since $\Sigma(E) = T(E)$ for a particle in a one-dimensional potential [167], we have:

$$g_1(E) = \frac{1}{2T} \frac{\partial}{\partial E} \Big(g_2 T \Big). \tag{4.7}$$

Substituting this expression into the Fokker-Planck equation (4.2), we obtain the analogue of (2.23) from Chapter 2:

$$\frac{\partial \eta}{\partial t} = \frac{1}{2} \frac{\partial}{\partial E} \left[g_2 T \frac{\partial}{\partial E} \left(\frac{\eta}{T} \right) \right]. \tag{4.8}$$

This equation, when combined with our expression (4.5) for g_2, fully characterizes the diffusive evolution of η.

4.2.2 Comparison with models of particles driven by thermal noise

This result can be compared to models of a particle interacting with a thermal bath, where the noise force associated with the bath has a finite correlation time [96, 99, 100, 106]. Such models were discussed earlier in Chapter 2, Section 2.7, where we gave a review of energy diffusion models studied by other researchers. These models begin with a generalized Langevin equation, which includes a memory kernel that encodes the non-Markovian influence of the bath. When written in the same notation as (4.1), this equation takes the form

$$\frac{dx}{dt} = v, \quad m\frac{dv}{dt} = -U'(x) - m\int_{-\infty}^{t} ds\, \gamma(t-s)v(s) + f(t). \tag{4.9}$$

Here, the second-to-last term on the right corresponds to the average frictional force exerted by the bath, and is characterized by a damping kernel $\gamma(t) = \gamma(-t)$. $f(t)$ then corresponds to fluctuations about this average force. From this equation, an energy diffusion description can be derived, given that the effect of the thermal bath is sufficiently weak.

Clearly, this equation coincides with (4.1) if $\gamma(t)$ is arbitrarily set to zero. However, the physical interpretation of this step is unclear, since the average effect of the forces exerted by the bath cannot be turned on and off independently of the fluctuations: Both are ultimately generated by the same physical mechanisms. In these thermal noise models, this connection is encoded by assuming a fluctuation-dissipation relation [96, 99, 100, 106]:

$$C_f(t) = mk_B T_b \gamma(t), \tag{4.10}$$

where T_b is the bath temperature. Substituting this into (4.9) yields

$$\frac{dx}{dt} = v, \quad m\frac{dv}{dt} = -U'(x) - \frac{1}{k_B T_b}\int_{-\infty}^{t} ds\, C_f(t-s)v(s) + f(t). \tag{4.11}$$

The Fokker-Planck equation corresponding to these equations of motion is (see, for example, Equation 151 in [106])

$$\frac{\partial \eta}{\partial t} = \frac{1}{2}\frac{\partial}{\partial E}\left[g_2 \frac{\eta}{k_B T_b} + g_2 T \frac{\partial}{\partial E}\left(\frac{\eta}{T}\right)\right], \tag{4.12}$$

where g_2 is again given by (4.5).

In the formal limit where T_b approaches infinity, with all other quantities like $U(x)$ and $C_f(t)$ held fixed, the generalized Langevin equation (4.11) and the Fokker-Planck equation (4.12) reduce to the corresponding equations (4.1) and (4.8) for the normal noise case. Of course, this is an unphysical limit: It is not clear how to hold $C_f(t)$ and other quantities constant while taking the limit $T_b \to \infty$, since the statistical properties of a heat bath will generally vary as its temperature changes. Nevertheless, we still anticipate that the normal noise model can serve as a good approximation of the thermal noise model, provided that the fluctuations in the bath forces (given by $f(t)$) dominate over the average force exerted by the bath (given by the term $-(k_B T_b)^{-1}\int_{-\infty}^{t} ds\, C_f(t-s)v(s)$).

4.2.3 The harmonic approximation

To conclude this section, we note that for the Fokker-Planck equation (4.8) for the normal noise model, an exact solution is available when the particle executes small oscillations in the potential well. This simplification has also been studied for the thermal noise Fokker-Planck equation (4.12); an exact solution can be obtained in this case as well [168]. We now describe

how the Fokker-Planck equation simplifies in this limit. We then present the solution, and discuss how this solution behaves asymptotically at long times.

In the small oscillation limit, the potential $U(x)$ may be approximated by a harmonic potential $U(x) \approx \frac{1}{2}m\omega_0^2(x-x_0)^2$ about some minimum point x_0, and the particle will oscillate sinusodially about this minimum at some energy-independent frequency ω_0. In this case, the unperturbed velocity $v(t;E)$ is simply $v(t;E) \approx \sqrt{2E/m}\cos(\omega_0 t)$ (up to an unimportant phase), and so the Fourier coefficients $a_k(E)$ are approximately zero for $k \neq \pm 1$. Therefore, our expression for the energy diffusion coefficient (4.5) reduces to

$$g_2(E) \approx \frac{E}{m} S_f(\omega), \tag{4.13}$$

and so the Fokker-Planck equation becomes (noting that the period $T = 2\pi/\omega_0$ is now independent of energy):

$$\frac{\partial \eta}{\partial t} = \frac{S_f(\omega_0)}{2m}\frac{\partial}{\partial E}\left[E\frac{\partial \eta}{\partial E}\right] \equiv \mathcal{L}\eta. \tag{4.14}$$

Here, we have introduced the differential operator $\mathcal{L} \equiv (S_f(\omega_0)/2m)\frac{\partial}{\partial E}\left(E\frac{\partial}{\partial E}\right)$. Since the minimum energy of the harmonic oscillator is $E = 0$, solutions to this equation are distributions $\eta(E,t)$ defined for $E \in [0,\infty)$.

We note that this Fokker-Planck equation predicts a constant average energy absorption rate of $d\langle E\rangle/dt = S_f(\omega_0)/2m$, as can be seen by multiplying the equation by E and then integrating over all energies. This same rate has been obtained elsewhere, for a *quantum* particle in a harmonic potential subject to noise [169, 170].

This equation may be solved by the same method as the Schrodinger equation in quantum

mechanics: By obtaining the eigenvalues $-\lambda$ and eigenfunctions $\phi_\lambda(E) \equiv \phi_\lambda$ of the operator $\mathcal{L}$. Because of the linearity of the Fokker-Planck equation, a general solution can then be expressed as a linear combination of the solutions $e^{-\lambda t}\phi_\lambda(E)$. To solve the eigenvalue equation $\mathcal{L}\phi_\lambda = -\lambda\phi_\lambda$, we note that upon making the change of variables $x = \sqrt{8m\lambda E/S_f(\omega_0)}$, this equation reduces to Bessel's equation for order $\alpha = 0$ [171]:

$$x^2\frac{\partial^2\phi_\lambda}{\partial x^2} + x\frac{\partial\phi_\lambda}{\partial x} + x^2\phi_\lambda = 0. \tag{4.15}$$

The solutions are therefore given by

$$\phi_\lambda(E) = \sqrt{\frac{2m}{S_f(\omega_0)}}J_0\left(\sqrt{\frac{8m\lambda}{S_f(\omega_0)}}E\right) = \sqrt{\frac{2m}{S_f(\omega_0)}}\sum_{k=0}^{\infty}\frac{1}{(k!)^2}\left(-\frac{2m\lambda}{S_f(\omega_0)}E\right)^k, \tag{4.16}$$

where $J_0(z)$ is a Bessel function of the first kind of order zero.[2] We have noted the power series expansion for the Bessel function, which will become important shortly. The prefactor $\sqrt{2m/S_f(\omega_0)}$ ensures that these eigenfunctions are orthogonal, in the sense that $\int_0^\infty dE\,\phi_\lambda(E)\phi_{\lambda'}(E) = \delta(\lambda - \lambda')$.[3] Note that we may restrict our attention to $\lambda > 0$ eigenfunctions, since $e^{-\lambda t}\phi_\lambda(E)$ diverges at long times for negative λ. A general solution to the Fokker-Planck equation may then be written as

$$\eta(E,t) = \int_0^\infty d\lambda\, a(\lambda)e^{-\lambda t}\phi_\lambda(E). \tag{4.17}$$

[2] An independent set of solutions is given in terms of Bessel functions of the second kind. However, these solutions diverge at $E = 0$, so we ignore them.

[3] This follows from the Bessel function closure equation $\int_0^\infty dx\, J_\alpha(ux)J_\alpha(vx)x = \delta(u-v)/u$ [171].

The weighting function $a(\lambda)$ is set by the initial condition $\eta(E,0)$. The orthogonality of the eigenfunctions implies that

$$a(\lambda) = \int_0^\infty dE\, \phi_\lambda(E)\eta(E,0). \tag{4.18}$$

To conclude this section, let us look at the behavior of such solutions at long times. For simplicity, suppose that the system begins with a definite energy E_0, so that $\eta(E,0) = \delta(E-E_0)$, which implies that $a(\lambda) = \phi_\lambda(E_0)$:

$$\eta(E,t) = \int_0^\infty d\lambda\, \phi_\lambda(E_0)e^{-\lambda t}\phi_\lambda(E). \tag{4.19}$$

At long times, the factor $e^{-\lambda t}$ implies that the integrand here will only be nonzero for $\lambda \approx 0$. We are then justified in replacing $\phi_\lambda(E_0)$ by its value at $\lambda = 0$, which is $\sqrt{2m/S_f(\omega_0)}$ according to the power series (4.16). Specifically, by looking at the size of the next term in the power series, we can see that this should be a good approximation provided that $S_f(\omega_0)t/mE_0 \gg 1$. Upon making this approximation, we can then substitute the power series expansion for $\phi_\lambda(E)$ into the integral, and evaluate the result:

$$
\begin{aligned}
\eta(E,t) &= \frac{2m}{S_f(\omega_0)} \int_0^\infty d\lambda\, e^{-\lambda t} \sum_{k=0}^{\infty} \frac{1}{(k!)^2} \left(-\frac{2m\lambda}{S_f(\omega_0)} E \right)^k \\
&= \frac{2m}{S_f(\omega_0)} \sum_{k=0}^{\infty} \frac{1}{(k!)^2} \left(-\frac{2m}{S_f(\omega_0)} E \right)^k \int_0^\infty d\lambda\, e^{-\lambda t} \lambda^k \\
&= \frac{2m}{S_f(\omega_0) t} \sum_{k=0}^{\infty} \frac{1}{(k!)^2} \left(-\frac{2m}{S_f(\omega_0) t} E \right)^k \int_0^\infty ds\, e^{-s} s^k \\
&= \frac{2m}{S_f(\omega_0) t} \sum_{k=0}^{\infty} \frac{1}{k!} \left(-\frac{2m}{S_f(\omega_0) t} E \right)^k \\
\eta(E,t) &= \frac{1}{k_B T_{\text{eff}}} \exp\left(-\frac{E}{k_B T_{\text{eff}}} \right).
\end{aligned}
\tag{4.20}
$$

In the final line, we have defined the effective temperature $k_B T_{\text{eff}} = S_f(\omega_0) t / 2m$. So, at long times such that $S_f(\omega_0) t / m E_0 \gg 1$ (as long as our initial harmonic approximation does not break down), the system's energy distribution approaches a Boltzmann distribution, with a temperature which grows linearly with time. Note that for this Boltzmann distribution, $\langle E \rangle = k_B T_{\text{eff}}$, so this linear growth of $k_B T_{\text{eff}}$ matches the result $d\langle E \rangle / dt = S_f(\omega_0)/2m$ noted previously.

4.3 Classical Heisenberg spin in a fluctuating magnetic field

Consider a classical magnetic moment or "spin," described by an evolving unit vector $\mathbf{S}(t) \equiv \mathbf{S}$. We assume that this spin precesses about a time-dependent magnetic field vector $\mathbf{B}(t) \equiv \mathbf{B}$ according to the equation

$$
\frac{d\mathbf{S}}{dt} = -\mathbf{B} \times \mathbf{S}. \tag{4.21}
$$

We work in units were magnetic fields have units of inverse time. This model is sometimes

referred to as a "Heisenberg spin" model [172, 173]; it is also the zero-damping limit of the Landau-Lifshitz or Landau–Lifshitz–Gilbert model [174, 175]. Note that the spin magnitude $|\mathbf{S}| = 1$ is preserved under these dynamics. With respect to some arbitrary (x, y, z) coordinate system, the vector $\mathbf{S}$ is specified uniquely by two variables: ϕ, the azimuthal angle, and S_z, the z-component of $\mathbf{S}$ (see Figure 4.1). Although it is not immediately apparent, the pair (ϕ, S_z) serves as a set of canonical coordinates for the system: For the Hamiltonian $H = -\mathbf{B} \cdot \mathbf{S}$ (expressed as a function of ϕ and S_z), it can be shown that the equation of motion (4.21) is entirely equivalent to the set of Hamilton's equations $d\phi/dt = \partial H/\partial S_z$ and $dS_z/dt = -\partial H/\partial \phi$ [172].

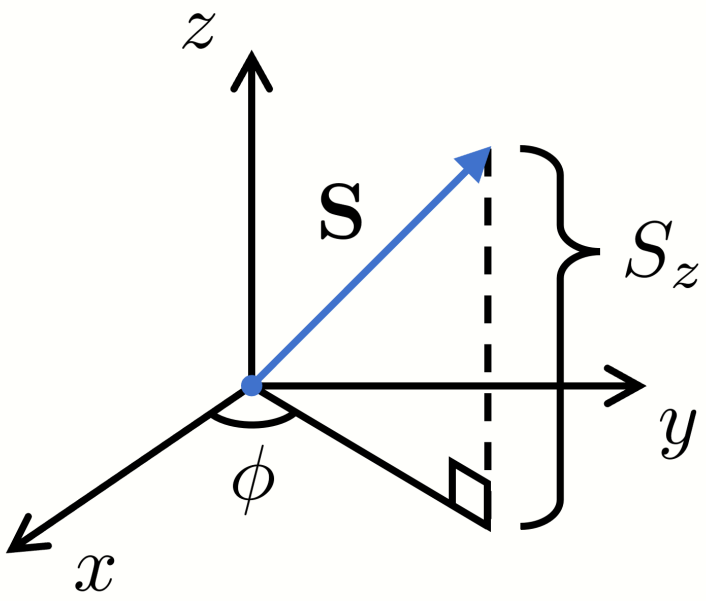

Figure 4.1: Diagram defining the coordinates ϕ and S_z, which specify the spin vector $\mathbf{S}$.

We assume that the magnetic field may be treated as a constant average field, plus some small random fluctuations or noise. If we orient the z-axis in the direction of the average field, we may write this as $\mathbf{B}(t) = \mathbf{B}_0 + \mathbf{b}(t)$, where $\mathbf{B}_0 = B_0\hat{\mathbf{z}}$ is a constant, and where $\mathbf{b}(t) = (b_x(t), b_y(t), b_z(t))$. We take $\mathbf{b}(t)$ to be generated by a stationary stochastic process, with vanishing averages $\langle b_i(t) \rangle = 0$ and with an associated correlation function $C_b(t) \equiv \langle b_i(0) b_i(t) \rangle$,

which decays over a timescale τ_C. The three components of $\mathbf{b}(t)$ are assumed to be statistically identical and independent.

4.3.1 Energy diffusion description

We define the energy of the system E as the Hamiltonian in the absence of the noise: $E \equiv -\mathbf{B}_0 \cdot \mathbf{S} = -B_0 S_z$. For $\mathbf{b}(t) = \mathbf{0}$, this energy is conserved under (4.21). For small, finite $\mathbf{b}(t)$, the noise causes the system to perform a random walk in energy space. Just as with the noise-driven particle in Section 4.2, we expect this to result in a process of energy diffusion on timescales $\gg \tau_C$. This process is described by a Fokker-Planck equation, with drift and diffusion coefficients $g_1(E)$ and $g_2(E)$. As before, g_1 and g_2 are related via the same fluctuation-dissipation relation as in Chapter 2, given by (2.22). Following (2.23), we may therefore express the Fokker-Planck equation as

$$\frac{\partial \eta}{\partial t} = \frac{1}{2}\frac{\partial}{\partial E}\left[g_2 \Sigma \frac{\partial}{\partial E}\left(\frac{\eta}{\Sigma}\right)\right]. \tag{4.22}$$

where $\Sigma \equiv \Sigma(E)$ is the density of states. Note that the process of energy diffusion is defined on the interval $[-B_0, B_0]$, between the maximum and minimum energies $E = \pm B_0$.

To obtain $g_2(E)$, we again use the relation $\mathrm{Var}(E) \approx g_2(E_0)\Delta t$. First, note that the equation of motion (4.21) implies that $dE/dt = \mathbf{B}_0 \cdot (\mathbf{b} \times \mathbf{S}) = B_0 \hat{\mathbf{z}} \cdot (\mathbf{b} \times \mathbf{S})$, so that the change in E from $t = 0$ to $t = \Delta t$ is given by

$$\Delta E = B_0 \int_0^{\Delta t} dt\, \hat{\mathbf{z}} \cdot (\mathbf{b}(t) \times \mathbf{S}(t)). \tag{4.23}$$

For weak noise, we may approximate the evolution of $\mathbf{S}(t)$ by its evolution in the absence of

noise. Without noise, the equation of motion (4.21) implies that $\mathbf{S}(t)$ simply precesses around the z-axis with angular frequency B_0. Assuming for simplicity that $\mathbf{S}_0(t)$ is in the (x,z)-plane at $t=0$, and recalling that $|\mathbf{S}|=1$, this means that we can approximate its evolution as $\mathbf{S}(t) \approx \sqrt{1-S_z^2}\cos(B_0 t)\hat{\mathbf{x}} - \sqrt{1-S_z^2}\sin(B_0 t)\hat{\mathbf{y}} + S_z\hat{\mathbf{z}}$. Here, S_z is constant. Upon substituting this into (4.23) above, we obtain

$$\Delta E \approx -B_0\sqrt{1-S_z^2}\int_0^{\Delta t} dt\ \left[b_x(t)\sin(B_0 t) + b_y(t)\cos(B_0 t)\right]. \tag{4.24}$$

This expression can then be substituted into $\mathrm{Var}(E) = \langle(\Delta E)^2\rangle - \langle\Delta E\rangle^2$. Since $\langle b_i(t)\rangle = 0$ and since the components $b_i(t)$ are statistically independent, the cross terms in the resulting expression vanish, and we are left with

$$\mathrm{Var}(E) = B_0^2(1-S_z^2)\int_0^{\Delta t} dt \int_0^{\Delta t} dt'\, C_b(t'-t)\left[\sin(B_0 t)\sin(B_0 t') + \cos(B_0 t)\cos(B_0 t')\right]. \tag{4.25}$$

This may be evaluated just like (2.16) in Chapter 2, Section 2.4, for $\Delta t \gg \tau_C, 1/B_0$. Noting that $E = -B_0 S_z$, the resulting expression for g_2 is then

$$g_2(E) = (B_0^2 - E^2)S_b(B_0), \tag{4.26}$$

where $S_b(\omega)$ is the power spectrum for the noise:

$$S_b(\omega) = \int_{-\infty}^{\infty} dt\, e^{-i\omega t} C_b(t). \tag{4.27}$$

To complete the characterization of the Fokker-Planck equation, we only need the density of states $\Sigma(E)$. $\Omega(E)$, the volume of phase space corresponding to energies $\leq E$, is found by integrating over all ϕ from 0 to 2π, and over S_z from -1 to E/B_0. The result is $\Omega(E) = 2\pi(1 + E/B_0)$; taking the derivative with respect to E yields $\Sigma(E) = 2\pi/B_0$. This is a constant density of states, so it cancels in the Fokker-Planck equation, which now becomes

$$\frac{\partial \eta}{\partial t} = \frac{S_b(B_0)}{2} \frac{\partial}{\partial E} \left[\left(B_0^2 - E^2 \right) \frac{\partial \eta}{\partial E} \right] \equiv \mathcal{L}\eta, \tag{4.28}$$

where we have defined the differential operator $\mathcal{L} \equiv \frac{S_b(B_0)}{2} \frac{\partial}{\partial E} \left[(B_0^2 - E^2) \frac{\partial}{\partial E} \right]$.

We have found two closely related results in the literature. First, Kubo and Hashitsume studied this same system, focusing on $f(\mathbf{S}, t)$, the probability distribution of $\mathbf{S}$ itself [176]. They obtained a Fokker-Planck equation for this distribution. We find that if $f(\mathbf{S}, t)$ is assumed to only depend on the spin energy $E = -B_0 S_z$, then the non-energy variables may be integrated out of their Fokker-Planck equation, and the result is (4.28). Second, Brown derived a Fokker-Planck equation in energy for a spin subject to *uncorrelated, thermal* noise [97]. This Fokker-Planck equation simplifies in the high-temperature limit, when the thermal energy $k_B T_b$ is much larger than the maximum spin energy $E = B_0$. This high temperature Fokker-Planck equation then coincides with our result (4.28), in the special case where we assume uncorrelated noise ($C_b(t) \propto \delta(t)$).

4.3.2 Exact solution to the Fokker-Planck equation

Just as for the noise-driven particle in Section 4.2.3, we may solve this equation by finding the eigenvalues $-\lambda$ and eigenfunctions $\phi_\lambda(E)$ of the differential operator $\mathcal{L}$. The following

solution is also given by Brown in [97], for the case of uncorrelated noise, but here we show that it applies equally well for correlated noise. Note that the eigenvalue equation $\mathcal{L}\phi_\lambda(E) = -\lambda\phi_\lambda(E)$ is simply the defining equation for the Legendre polynomials $P_n(x) = P_0(x), P_1(x), P_2(x)$ ..., up to constant factors [171]:

$$\frac{\partial}{\partial x}\left[\left(1-x^2\right)\frac{\partial P_n}{\partial x}\right] = -n(n+1)P_n. \tag{4.29}$$

It follows that there is a discrete set of eigenvalues $\lambda \equiv \lambda_n$ and eigenfunctions $\phi_\lambda(E) \equiv \phi_n(E)$ given by

$$\phi_n(E) = \sqrt{\frac{2n+1}{2B_0}}P_n\left(\frac{E}{B_0}\right), \quad \lambda_n = \frac{n(n+1)S_b(B_0)}{2}, \tag{4.30}$$

where the prefactor $\sqrt{(2n+1)/(2B_0)}$ guarantees the orthonormality of the eigenfunctions, expressed by $\int_{-B_0}^{B_0} dE\, \phi_m(E)\phi_n(E) = \delta_{mn}$.[4]

A general solution to the Fokker-Planck equation may then be expressed as a linear combination of these eigenfunctions, each multiplied by a factor $e^{-\lambda_n t}$:

$$\eta(E,t) = \sum_{n=0}^{\infty} a_n e^{-\lambda_n t}\phi_n(E), \tag{4.31}$$

where $a_n = \int_{-B_0}^{B_0} dE\, \phi_n(E)\eta(E,0)$ as a consequence of the orthogonality of the eigenfunctions. Note that at long times, all of the terms in this sum decay to zero except for the $n = 0$ term, since $\lambda_0 = 0$. Since $P_0(x) = 1$, we have $\phi_0(E) = \sqrt{1/(2B_0)}$ and $a_0 = \int_{-B_0}^{B_0} dE\, \sqrt{1/(2B_0)}\eta(E,0) = \sqrt{1/(2B_0)}$, and therefore:

[4] This follows from the orthogonality relation for Legendre polynomials, $\int_{-1}^{1} dx\, P_m(x)P_n(x) = 2\delta_{mn}/(2m+1)$.

$$\lim_{t\to\infty} \eta(E,t) = \frac{1}{2B_0}. \tag{4.32}$$

That is, the system approaches a completely uniform distribution in energy space in the long-time limit, independent of the initial distribution $\eta(E,0)$. This is the infinite temperature energy distribution $\eta_\infty(E) = \Sigma(E)/\int dE'\,\Sigma(E')$ (discussed previously in Chapter 2, Section 2.5), since the density of states $\Sigma(E)$ is a constant.

Chapter 5: Energy absorption and diffusion in quantum chaotic systems

5.1 Chapter summary

In this chapter, we investigate energy absorption and diffusion in driven quantum chaotic systems. Unlike Chapters 2 and 3, this chapter does not include any substantial new results. Rather, the goal here is to outline the conceptual frameworks and mathematical tools necessary for understanding energy absorption in quantum chaotic systems under rapid periodic driving. After an introduction in Section 5.2, we begin Section 5.3 with a review of Floquet theory, the standard formalism used to study periodically driven quantum systems. This leads to a discussion of the Floquet-Magnus expansion, a perturbative expansion in the driving period T, which furnishes an approximate description of the quantum evolution in the rapid driving regime. We describe the various connections between the Floquet-Magnus expansion, bounds on energy absorption, Floquet prethermalization, and the classical energy diffusion model developed in Chapter 2. In Section 5.4, we narrow our focus to quantum chaotic systems specifically, i.e., quantum systems with a classical chaotic counterpart. We provide a review of some key ideas in the study of quantum chaos, concentrating on random matrix theory and the Eigenstate Thermalization Hypothesis. Then, in Section 5.5, we demonstrate how such tools can be used to construct a random matrix model for a periodically driven quantum chaotic system. We conclude this chapter with a heuristic model of energy absorption in quantum chaotic systems under

periodic driving. This model, which is based on Fermi's golden rule, reduces to the classical energy diffusion description in the semiclassical limit.

5.2 Setup and introduction

The main subject of this chapter is quantum systems subject to a rapid periodic drive, with a focus on quantum chaotic systems (i.e., quantum systems with a classical chaotic counterpart). In this section, we define these systems and their dynamics. We then provide a brief discussion of the correspondence principle, to motivate our belief that these systems may be partially described by the classical energy diffusion model developed in Chapter 2.

5.2.1 Definition of the system(s) of interest

Our system of interest is a non-relativistic quantum system, isolated except for the influence of a time-periodic external drive. The time-dependent state of such a system is defined by the system's state vector $|\psi(t)\rangle \equiv |\psi\rangle$, an element in the system's Hilbert space $\mathcal{H}$. This Hilbert space is equipped with an inner product $\langle\psi_1|\psi_2\rangle = \langle\psi_2|\psi_1\rangle^*$ defined between any two vectors $|\psi_1\rangle$ and $|\psi_2\rangle$. The dynamics of $|\psi(t)\rangle$ are dictated by the system's Hamiltonian $\hat{H}(t) \equiv \hat{H}$, where the "hat" over $\hat{H}(t)$ denotes that $\hat{H}(t)$ is a linear operator which acts on vectors in the system's Hilbert space. As time elapses, $|\psi\rangle$ evolves within $\mathcal{H}$ in accordance with the Schrodinger equation

$$i\hbar\frac{d|\psi\rangle}{dt} = \hat{H}|\psi\rangle, \tag{5.1}$$

where $\hbar$ is the reduced Planck constant. We assume that $|\psi\rangle$ is normalized at $t = 0$ (i.e., $\langle\psi(0)|\psi(0)\rangle = 1$); evolution under the Schrodinger equation then preserves this normalization

for all time.

We assume that the quantum Hamiltonian $\hat{H}(t)$ may be obtained from the classical Hamiltonian $H(z,t) = H_0(z) + V(z,t/T)$ in Chapter (2) (see equation (2.1)) via an appropriate quantization procedure. The standard way to do this is to choose a particular set of canonical coordinates and momenta $\mathbf{q}$ and $\mathbf{p}$ for the classical system, define a corresponding set of operators $\hat{\mathbf{q}}$ and $\hat{\mathbf{p}}$ which satisfy canonical commutation relations, and replace $\mathbf{q}$ and $\mathbf{p}$ in $H(z,t)$ with $\hat{\mathbf{q}}$ and $\hat{\mathbf{p}}$ [177].[1] When constructed in such a procedure, $\hat{H}(t)$ inherits the time-periodicity of $H(z,t)$, and may be decomposed as

$$\hat{H}(t) = \hat{H}_0 + \hat{V}(t/T), \quad \hat{V}(s) = \hat{V}(s+1), \tag{5.2}$$

where T is the driving period, and where $\hat{H}_0$ and $\hat{V}(t/T)$ are the quantized versions of the classical observables $H_0(z)$ and $V(z,t/T)$. As in the classical case, we identify $\hat{H}_0$ as the "bare" or "undriven" Hamiltonian, and $\hat{V}(z,t/T)$ as the "drive."

Observable properties of this system are identified with Hermitian operators on $\mathcal{H}$, like $\hat{H}_0$ and $\hat{V}(t/T)$. In direct correspondence with the classical case, we identify the operator $\hat{H}_0$ (which is guaranteed to be Hermitian if constructed from an appropriate quantization procedure) with the energy of the system. The equation $\hat{H}_0|n\rangle = E_n|n\rangle$ defines the eigenvalues E_n and orthonormal eigenvectors $|n\rangle$ of $\hat{H}_0$, which are labelled by the integer index n. We have assumed that $\hat{H}_0$ has a discrete spectrum for notational convenience, but the discussion in this chapter does not hinge on this assumption. The Hermiticity of $\hat{H}_0$ implies that the state vector $|\psi(t)\rangle$ at any time

[1] If $H(z,t)$ is a sum of terms which each depend on $\mathbf{q}$ or $\mathbf{p}$ alone, as in a standard kinetic plus potential Hamiltonian, then the replacement of $\mathbf{q}$ and $\mathbf{p}$ in $H(z,t)$ with $\hat{\mathbf{q}}$ and $\hat{\mathbf{p}}$ is uniquely defined. Otherwise, this method is ambiguous due to the non-commutation of $\hat{\mathbf{q}}$ and $\hat{\mathbf{p}}$, and one must use operator-ordering conventions such as Weyl ordering [177, 178] to fully specify the replacement procedure.

may be expressed as a linear combination of the eigenvectors $|n\rangle$: $|\psi(t)\rangle = \sum_n c_n(t)|n\rangle$, where $c_n(t) = \langle n|\psi(t)\rangle$. In quantum mechanics, when the system is in the state $|\psi(t)\rangle$, $p_n(t) = |c_n(t)|^2$ gives the probability that if an energy measurement is made at time t, then the value E_n will be obtained. Therefore, the expectation value or average value of the system's energy at t is given by

$$\langle H_0\rangle_t = \sum_n |c_n(t)|^2 E_n = \langle\psi(t)|\hat{H}_0|\psi(t)\rangle. \tag{5.3}$$

More generally, the expectation value associated with an arbitrary operator $\hat{A}$ is given by $\langle A\rangle_t = \langle\psi(t)|\hat{A}|\psi(t)\rangle$.

Additionally, the relation $p_n(t) = |c_n(t)|^2$ tells us that the energy distribution for the system over a continuous range of energies E is given by:

$$\eta^Q(E,t) = \sum_n |c_n(t)|^2 \delta(E - E_n). \tag{5.4}$$

This is the quantum analogue of the classical energy distribution $\eta(E,t)$, defined by (2.5) in Chapter 2, Section 2.2. For $\hat{V}(t/T) = \hat{0}$, the Schrodinger equation (5.1) implies that $\eta^Q(E,t)$ is a constant, consistent with energy conservation. The main focus of this chapter is the time evolution of $\eta^Q(E,t)$ for nonzero $\hat{V}(t/T)$, in the rapid driving regime defined by sufficiently large $\omega = 2\pi/T$.

Later in this chapter, it will also be convenient to invoke the density operator formalism of quantum mechanics [179]. This framework is valid even if the state of the system of interest cannot be specified by a state vector $|\psi(t)\rangle$. This can occur if the system is described by a statistical ensemble of possible state vectors, or if the system is entangled with another system. In

these cases, the system's state is fully characterized by a density operator $\hat{\rho}(t) \equiv \hat{\rho}$, a nonnegative Hermitian operator with unit trace. $\hat{\rho}$ evolves in accordance with the von Neumann equation

$$i\hbar \frac{d\hat{\rho}}{dt} = [\hat{H}, \hat{\rho}], \tag{5.5}$$

where $[\hat{A}, \hat{B}]$ is the commutator between two operators $\hat{A}$ and $\hat{B}$. In the special case where the system can *also* be described by a state vector $|\psi(t)\rangle$, then the $\hat{\rho}(t)$ and $|\psi(t)\rangle$ representations are related via $\hat{\rho}(t) = |\psi(t)\rangle\langle\psi(t)|$, which denotes the outer product of $|\psi(t)\rangle$ with itself. In this case, the system is said to be in a pure state, and the von Neumann equation is fully equivalent to the Schrodinger equation (5.1).

In the density matrix description, the probability of measuring the energy value E_n is given by $p_n(t) = \rho_{nn}(t) \equiv \langle n|\hat{\rho}(t)|n\rangle$. The energy distribution in this case is then given by $\eta^Q(E,t) = \sum_n \rho_{nn}(t)\delta(E - E_n)$. In the pure state case, this reduces to (5.4), since $\rho_{nn}(t) = \langle n|\psi(t)\rangle\langle\psi(t)|n\rangle = |c_n(t)|^2$.

5.2.2 Energy diffusion and the correspondence principle

The systems studied with the energy diffusion model in Chapters 2 and 3 are all purely classical. However, recall from Chapter 1 that one of the original motivations for developing the energy diffusion description was to understand energy absorption in periodically driven *quantum* systems, such as Floquet prethermal systems and time crystal systems. The idea is that some of the quantum mechanical mechanisms which control energy evolution in such systems may alternatively be understood in terms of classical effects. This is in line with the *correspondence principle*, the notion that under appropriate conditions, the behavior of quantum systems may be

approximated in terms of classical physics [180, 181].

Since it was first formulated by Niels Bohr at the advent of quantum theory [182], the correspondence principle has served as a powerful guide for understanding quantum systems, motivated by the basic desideratum that our quantum mechanical theories of the world be consistent with the classical reality that appears in everyday life.[2] Although a reasonable consistency requirement, establishing the existence of this correspondence is nontrivial: At the microscopic quantum level, phenomena like superpositions and entanglement appear as fundamentally non-classical, and it is not *a priori* clear how such effects "wash out" to yield effectively classical evolution at the macroscopic or mesoscopic level. For an isolated quantum system, this emergence of classicality is usually understood to occur in the regime of high energies and large quantum numbers, while for quantum systems interacting with an environment, the phenomenon of *decoherence* also plays a key role in establishing classical-like properties. Mathematically, quantum-classical correspondence commonly appears as the result of some sort of limit: The semiclassical limit (taking Planck's constant $\hbar$ to zero) [180, 184, 185], the limit of large spin numbers for quantum spin systems [41, 186], or the limit of many environmental degrees of freedom in the context of decoherence [68, 187].

Motivated by the correspondence principle, we emphasize connections between quantum systems and their classical counterparts throughout this chapter. In the discussion of Floquet theory in Section 5.3, we see a tight parallel between Floquet theory as applied to classical and quantum systems, and we note how certain quantum bounds on energy absorption can be relevant in a classical context. Then, in Section 5.4, we describe how the dynamics of

[2] Technically, Bohr's original correspondence principle is more narrow than this general consistency requirement. For a discussion of the differences between Bohr's correspondence principle and its modern reinterpretation described here, see [183].

classical chaotic systems leave an "imprint" on the features of their quantum counterparts, and how quantum-classical correspondence manifests in models of slowly driven quantum chaotic systems. Finally, in Section 5.5, we show how the classical energy diffusion description can arise from a simplified model of a periodically driven quantum chaotic system, in the limit as $\hbar$ approaches zero. Ultimately, our hope is that these various connections can be placed in the context of a comprehensive account of energy absorption in periodically driven quantum chaotic systems, an account which the classical energy diffusion model may be one piece of.

5.3 Floquet theory, the Floquet-Magnus expansion, and energy diffusion

In the context of quantum mechanics, the tools of Floquet theory describe the evolution of quantum systems subject to a time-periodic Hamiltonian $\hat{H}(t) = \hat{H}(t+T)$. In this section, we provide an overview of Floquet analysis, and discuss the relationship between this theory and the energy diffusion framework established in Chapter 2. We first summarize the basic mathematics of Floquet theory, and introduce the idea of an effective Floquet Hamiltonian $\hat{H}_F$, which allows us to view the evolution under $\hat{H}(t)$ at the "stroboscopic" times $t = 0, T, 2T ...$ as evolution under the *time-independent* Hamiltonian $\hat{H}_F$. We then narrow our focus to the high-frequency driving regime specifically. In this limit, a useful approximation of a periodically driven system's dynamics is furnished by the Floquet-Magnus expansion. The Floquet-Magnus expansion is a perturbative expansion for the Floquet Hamiltonian $\hat{H}_F$, in powers of the driving period T. We describe this expansion, and then explain how the convergence of the Floquet-Magnus expansion places a limit on the amount of energy that can be absorbed by a system. We conclude this section by discussing some additional bounds on energy absorption in periodically driven quantum

systems, and by connecting these bounds to the classical energy diffusion description and to the phenomenon of Floquet prethermalization.

5.3.1 Introduction to Floquet theory

Floquet theory or Floquet analysis is the theory of linear differential equations (either finite or infinite dimensional) with coefficients which are periodic in the independent variable [188]. The essential components of this theory, including the central Floquet's theorem, were developed by researchers such as Floquet [189], Hill [190], and Lyapunov [191]. Since then, the tools they discovered have been used in a huge range of physical and mathematical settings, such as NMR systems [192–194], driven optical lattices [48, 49, 166, 195], ecological population models [196, 197], control theory [198, 199], correlated electron systems and optically-driven quantum materials [30, 31, 200], topological insulators [60], and laser-excited atoms and molecules [201, 202]. In quantum mechanics in particular, Floquet theory has proven especially useful in the study of two classes of systems: Systems with time-periodic Hamiltonians, and systems subject to potentials which are periodic in space (in this second class, Floquet's theorem is referred to as Bloch's theorem). We now introduce Floquet theory in the context of the first class of systems, systems with time-periodic Hamiltonians. In these systems, Floquet's theorem establishes a close analogy between periodically driven quantum systems on the one hand, and quantum systems with a time-*independent* Hamiltonian on the other. In particular, the theorem leads to the definition of the effective Floquet Hamiltonian $\hat{H}_F$, which may be used to obtain the evolution of the system at the stroboscopic times $t = 0, T, 2T$ .... In the following discussion, we give a proof of Floquet's theorem, flesh out the analogy between time-periodic and static quantum

systems, and finally describe how Floquet theory is equally applicable to classical Hamiltonian systems. The presentation of Floquet theory here closely follows treatments such as [195] and [12].

We begin by establishing some background needed to prove Floquet's theorem. We consider the systems described in Section 5.2: Quantum systems evolving under the Schrodinger equation (5.1), subject to the time-periodic Hamiltonian $\hat{H}(t) = \hat{H}(t+T)$, given by (5.2).[3] As with any system with a time-dependent Hamiltonian, periodic or otherwise, the evolution of such system is fully characterized by the associated unitary evolution operator $\hat{U}(t, t_0)$. By definition, $\hat{U}(t, t_0)$ maps the system from its state at a time t_0 to its new state at a later time t: If the state vector of the system at t_0 is given by $|\psi(t_0)\rangle$, then after evolution under the Schrodinger equation from t_0 to t, the new state vector is given by $|\psi(t)\rangle = \hat{U}(t, t_0)|\psi(t_0)\rangle$. An expression for $\hat{U}(t, t_0)$ can be obtained by formally solving the Schrodinger equation [179]:

$$\hat{U}(t, t_0) = \mathcal{T}\left[\exp\left\{-\frac{i}{\hbar}\int_{t_0}^{t} dt'\, \hat{H}(t')\right\}\right]. \tag{5.6}$$

Here, $\mathcal{T}[...]$ denotes that the exponential is appropriately time-ordered. However, this formal matrix exponential should be treated with care, since it is ultimately defined via an infinite series which may or may not converge.[4]

The evolution operator $\hat{U}(t, t_0)$ has two important properties which are especially relevant to our discussion. First, for any system with a time-dependent Hamiltonian, the following composition property [180] holds for any three times $t_1 \leq t_2 \leq t_3$:

[3] Note that Floquet analysis is equally applicable to a broader class of periodically driven quantum systems, including relativistic quantum systems [203, 204], quantum systems with no direct classical analogue, and open quantum systems described by a Lindblad equation [205–207].

[4] The same caveat holds for other exponentiated operators invoked in the following discussion, such as $e^{-i\hat{H}_0 T/\hbar}$.

$$\hat{U}(t_3, t_1) = \hat{U}(t_3, t_2)\hat{U}(t_2, t_1). \tag{5.7}$$

In words, this simply states that the evolution of the system from $t = t_1$ to $t = t_3$ can be divided into an evolution from $t = t_1$ to $t = t_2$, followed by an evolution from $t = t_2$ to $t = t_3$. Second, for periodically driven systems specifically, the evolution operator for the interval from t_0 to t is identical to the evolution operator for the interval exactly N periods before or after, for any $N \in \mathbb{Z}$:

$$\hat{U}(t + NT, t_0 + NT) = \hat{U}(t, t_0). \tag{5.8}$$

That is, because the Hamiltonian is time-periodic, the state obtained by evolving a given initial state vector $|\psi_0\rangle$ from t_0 to t must be identical to the state obtained by evolving $|\psi_0\rangle$ over a corresponding time interval N periods later, from $t_0 + NT$ to $t + NT$. This intuitively reasonable property can be easily established from (5.6), the time-ordered exponential form for $\hat{U}(t, t_0)$.

Now, consider the evolution of the system over M periods, from $t = 0$ to $t = MT$. By the composition property (5.7), the corresponding evolution operator $\hat{U}(MT, 0)$ is the ordered product of the evolution operators for each period, and by the time translation property (5.8), each of these one-period evolution operators is just equal to the evolution operator for the first period, $\hat{U}(T, 0)$. So to obtain the evolution of a state vector over M periods, it suffices to simply apply the so-called Floquet operator $\hat{U}_F \equiv \hat{U}(T, 0)$ M times. Defining the *time-independent* Floquet Hamiltonian $\hat{H}_F$ via $\hat{U}_F \equiv e^{-i\hat{H}_F T/\hbar}$, we therefore have:

$$\hat{U}(MT, 0) = \hat{U}_F^M = e^{-i\hat{H}_F MT/\hbar}. \tag{5.9}$$

Thus, provided we only view the evolution of the system at the discrete times $t = 0, T, 2T$ ... (at "strobosopic" times), the system appears as if it is evolving under the static Floquet Hamiltonian $\hat{H}_F$. In this sense, $\hat{H}_F$ is an effective Hamiltonian for the system. Note that although the relation $\hat{U}_F = e^{-i\hat{H}_F T/\hbar}$ does not uniquely define $\hat{H}_F$ (since the logarithm of a complex number or operator is multi-valued), the unitarity of $\hat{U}_F$ guarantees that at least *some* Hermitian operator $\hat{H}_F$ does satisfy $\hat{U}_F = e^{-i\hat{H}_F T/\hbar}$ [208].

As a unitary operator, $\hat{U}_F$ admits a complete set of orthonormal eigenvectors, which we index with a label α (these are also the eigenvectors of $\hat{H}_F$). Each Floquet eigenvector $|\alpha\rangle$ has a corresponding complex eigenvalue with unit modulus, which we write as $e^{-i\varepsilon_\alpha T/\hbar}$. Consistent with the non-uniqueness of $\hat{H}_F$, the "quasi-energies" ε_α are only defined modulo $2\pi\hbar/T = \hbar\omega$, so we may take them to lie within the interval $[0, \hbar\omega)$ if we like. The quasi-energies are the Floquet analogue of energy eigenvalues in a time-*independent* quantum system.

We now move to a proof of Floquet's theorem, which implies the result just obtained, but which also provides information about the system's evolution at other times $t \neq MT$. Suppose we now allow the system to evolve from $t = 0$ up to some arbitrary time t. This evolution will consist of an evolution over some M full periods, plus an extra evolution over a time $\tau \equiv t - MT = t \bmod T$ which is some fraction of a period (see Figure 5.1). The evolution over the M full periods has an associated evolution operator $\hat{U}(MT, 0) = e^{-i\hat{H}_F MT/\hbar}$, and the evolution operator for the final fraction of a period is $\hat{U}(t, t-\tau) = \hat{U}(MT+\tau, MT) = \hat{U}(\tau, 0)$. Therefore, the evolution operator for the full time interval $[0, t]$ may be expressed as

$$\begin{aligned}\hat{U}(t,0) &= \hat{U}(\tau,0)e^{-i\hat{H}_F MT/\hbar} = \hat{U}(\tau,0)e^{i\hat{H}_F\tau/\hbar}e^{-i\hat{H}_F\tau/\hbar}e^{-i\hat{H}_F MT/\hbar} \\ &= \hat{U}(\tau,0)e^{i\hat{H}_F\tau/\hbar}e^{-i\hat{H}_F t/\hbar} \equiv \hat{P}(t)e^{-i\hat{H}_F t/\hbar}.\end{aligned} \tag{5.10}$$

In the final expression here, we have introduced the operator $\hat{P}(t) \equiv \hat{U}(\tau,0)e^{i\hat{H}_F\tau/\hbar} = \hat{U}(t,0)e^{i\hat{H}_F t/\hbar}$,[5] which has been referred to as the fast-motion operator. As the product of two unitary operators, $\hat{P}(t)$ is itself unitary, and as a function of $\tau = t \bmod T$, $\hat{P}(t)$ is time-periodic with period T. Note also that $\hat{P}(t)$ reduces to the identity operator $\hat{I}$ at $t = 0, T, 2T ...$, since $\hat{U}(0,0) = \hat{I}$ and $e^{i\hat{H}_F \cdot 0/\hbar} = \hat{I}$. At these times, the above result reduces to (5.11).

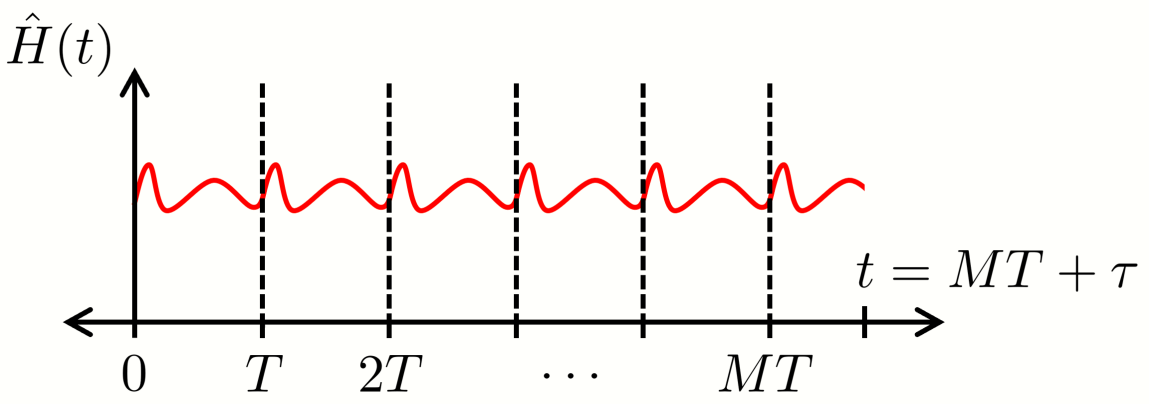

Figure 5.1: Evolution of $\hat{H}(t)$, represented by the solid red line, over M periods, plus a fraction of a period of duration τ.

This decomposition of $\hat{U}(t,0)$, into the periodic fast-motion operator $\hat{P}(t)$ and an evolution generated by the Floquet Hamiltonian $\hat{H}_F$, is known as Floquet's theorem [11, 12, 188, 209]. To see the consequences of this result, note that for an initial state vector $|\psi(0)\rangle$ at $t = 0$, the corresponding solution to the Schrodinger equation is given by $|\psi(t)\rangle = \hat{U}(t,0)|\psi(0)\rangle =$

[5] The second equality comes from $\hat{U}(\tau,0)e^{i\hat{H}_F\tau/\hbar} = \hat{U}(\tau,0)\hat{U}(MT,0)\hat{U}(0,MT)e^{i\hat{H}_F\tau/\hbar} = \hat{U}(\tau + MT, MT)\hat{U}(MT,0)e^{i\hat{H}_F MT/\hbar}e^{i\hat{H}_F\tau/\hbar} = \hat{U}(t,0)e^{i\hat{H}_F t/\hbar}$.

$\hat{P}(t)e^{-i\hat{H}_F t/\hbar}|\psi(0)\rangle$, by the definition of the evolution operator. In particular, if we select an eigenstate $|\alpha\rangle$ of $\hat{U}_F$ as our initial state, then the corresponding solution $|\psi_\alpha(t)\rangle$ takes the simple form

$$|\psi_\alpha(t)\rangle = e^{-i\varepsilon_\alpha t/\hbar}\hat{P}(t)|\alpha\rangle \equiv e^{-i\varepsilon_\alpha t/\hbar}|\alpha, t\rangle, \tag{5.11}$$

where we have defined the time-periodic *Floquet modes* $|\alpha, t\rangle \equiv \hat{P}(t)|\alpha\rangle$. The special solutions $|\psi_\alpha(t)\rangle$ are commonly referred to as *Floquet states*.

We can now see a clear analogy between time-independent systems and systems described by Floquet theory. On one hand, in a system with a time-independent Hamiltonian $\hat{H}_0$, the simplest solutions to the Schrodinger equation are given by multiplying an eigenstate $|n\rangle$ of $\hat{H}_0$ by the oscillating phase factor $e^{-iE_n t/\hbar}$, where E_n is the corresponding eigenenergy. Since the eigenstates $|n\rangle$ form a complete basis, a solution to the Schrodinger equation for a general initial condition may be constructed from a linear combination of these special solutions $e^{-iE_n t/\hbar}|n\rangle$. On the other hand, for a system governed by a time-periodic Hamiltonian $\hat{H}(t)$, we can obtain solutions to the Schrodinger equation (the Floquet states $|\psi_\alpha(t)\rangle$) by multiplying the Floquet modes $|\alpha, t\rangle = \hat{P}(t)|\alpha\rangle$ by the phase factor $e^{-iE_n t/\hbar}$. Because the Floquet modes are related to the complete set of Floquet eigenstates $|\alpha\rangle$ via the unitary transformation produced by $\hat{P}(t)$, the set of Floquet modes is complete as well (at each time t). Therefore a general solution may be constructed as a linear combination of the Floquet states $|\psi_\alpha(t)\rangle = e^{-i\varepsilon_\alpha t/\hbar}|\alpha, t\rangle$. In short, in moving from time-independent systems to time-periodic systems, time-independent energy eigenstates are replaced by time-periodic Floquet modes, and energy eigenvalues are replaced by quasi-energies. This analogy is compactly summarized in Table 5.2.

Time-independent Hamiltonian $\hat{H}_0$	Time-periodic Hamiltonian $\hat{H}(t)$
Eigenstates $\|n\rangle$	Floquet modes $\|\alpha, t\rangle \equiv \hat{P}(t)\|\alpha\rangle$
Energy levels E_n	Quasi-energies ε_α
Particular solutions $e^{-iE_nt/\hbar}\|n\rangle$	Floquet states $\|\psi_\alpha(t)\rangle \equiv e^{-i\varepsilon_\alpha t/\hbar}\|\alpha, t\rangle$
General solution $\sum_n a_n e^{-iE_nt/\hbar}\|n\rangle$	General solution $\sum_\alpha b_\alpha e^{-i\varepsilon_\alpha t/\hbar}\|\alpha, t\rangle$

Table 5.2: Comparison between evolution under a time-independent Hamiltonian and evolution under a time-periodic Hamiltonian.

Finally, although we have developed Floquet theory in the context of quantum systems, it is worth noting the same type of formalism may be constructed for periodically driven classical systems, both deterministic and stochastic [41, 210–212]. This may be surprising at first, since the development of Floquet theory given above is built on the linear structure of Schrodinger equation, whereas classical systems are generally governed by nonlinear evolution equations. However, this is not a problem, as long as we restrict our attention to the evolution of *probability distributions* over the states of such systems, instead of looking at individual trajectories. Because of the additive nature of probability, the evolution of these distributions is necessarily governed by linear equations: Rate equations for continuous-time discrete state Markov processes, Fokker-Planck equations for diffusive processes, the Liouville equation for Hamiltonian systems, and so on. Thus, Floquet theory can be applied to these types of systems just as in the quantum case. Let us look at how this works for periodically driven Hamiltonian systems.

The evolution of the phase space distribution $\rho \equiv \rho(z,t)$ for a periodically driven Hamiltonian system, like those discussed in Chapter 2, is governed by the Liouville equation $\partial\rho/\partial t = \{H, \rho\}$, where $H \equiv H(z,t)$ is the system's time-periodic Hamiltonian. As just

mentioned, this equation is linear, due to the linearity of the Poisson bracket $\{\cdot,\cdot\}$. If we define the Liouvillian operator $\hat{\mathcal{L}}(t) \equiv \hat{\mathcal{L}} \equiv i\{H,\cdot\}$ (a linear operator which acts on phase space distributions), we can rewrite the Liouville equation as

$$i\frac{\partial \rho}{\partial t} = \hat{\mathcal{L}}\rho, \tag{5.12}$$

in direct correspondence with the Schrodinger equation (5.1). Note that since $H(z,t)$ is time-periodic, $\hat{\mathcal{L}}(t)$ is as well. Moreover, if the inner product between two space distributions ρ and σ is defined as $(\rho,\sigma) \equiv \int dz\, \rho^*\sigma$, then it is straightforward to show that $\hat{\mathcal{L}}(t)$ is a Hermitian operator.

Comparing with the quantum case, we see that ρ and $\hat{\mathcal{L}}(t)$ have replaced $|\psi\rangle$ and $\hat{H}(t)$, respectively. We can now proceed exactly as before, beginning with the analogue of the evolution operator $\hat{U}(t,t_0)$. The classical version of $\hat{U}(t,t_0)$ evolves a distribution ρ from time t_0 to time t, and is formally given by a time-ordered exponential of $-i\int_{t_0}^{t} dt'\, \hat{\mathcal{L}}(t')$ (just as in (5.6)). Again, we define $\hat{U}_F$ as the evolution operator over one period, and we define a time-independent *Floquet Liouvillian* $\hat{\mathcal{L}}_F$ via $\hat{U}_F \equiv e^{-i\hat{\mathcal{L}}_F T}$. The Floquet Liouvillian, which is analogous to $\hat{H}_F$, is the non-unique Hermitian operator such that if ρ is evolved under the equation $i\partial\rho/\partial t = \hat{\mathcal{L}}_F\rho$ from $t=0$ to $t=T$, then the result will be the same as if ρ was propagated under the original time-periodic Liouville equation (5.12). Moreover, if $\hat{\mathcal{L}}_F$ can be expressed in the form $\hat{\mathcal{L}}_F \equiv i\{H_F,\cdot\}$, then this defines the *classical* Floquet Hamiltonian $H_F \equiv H_F(z)$. In this case, the evolution of a ensemble under the time-independent H_F is equivalent to evolution under the time-periodic Hamiltonian $H(z,t)$, provided that the system is observed at stroboscopic times. However, we have found no reason to believe that this classic H_F must exist in general.

5.3.2 The Floquet-Magnus expansion

The general framework of Floquet theory, while offering valuable conceptual insight, avoids the problem of any concrete calculations. Indeed, for most systems, quantities of interest like the Floquet operator $\hat{U}_F$ and the Floquet Hamiltonian $\hat{H}_F$ are difficult to evaluate exactly, and we have to make use of approximation schemes. In line with our interest in *rapid* periodic driving, we now turn to one such scheme: The Floquet-Magnus (FM) expansion. This is a perturbative expansion for $\hat{H}_F$ in powers of the driving period T, aimed at providing an approximate description of a system's dynamics in the limit of small T, or large driving frequencies $\omega = 2\pi/T$. In what follows, we provide an introduction to the FM expansion, in which we intuitively motivate why it can be a useful approximation, and present the first few terms in the expansion. We then discuss the convergence of the FM expansion, and how this relates to energy absorption and the energy diffusion description.

To motivate the FM expansion, recall that in the classical systems described in Chapter 2, the evolution of the system under a rapidly time-periodic Hamiltonian $H(z,t) = H_0(z) + V(z,t/T)$ is closely approximated by evolution under the time-averaged Hamiltonian $H_0(z)$, at least for short times. This can be demonstrated rigorously for systems with smooth $H(z,t)$, but it is also intuitively plausible that the effect of a time-periodic drive will nearly "average out" in the rapid driving regime. For a quantum system, these intuitions are equally reasonable, and the same mathematical theorems imply that over any finite time interval $t = 0$ to $t = \tau$, the evolution of $|\psi(t)\rangle$ under the time-periodic Hamiltonian $\hat{H}(t) = \hat{H}_0 + \hat{V}(t/T)$ approaches evolution under the time-averaged Hamiltonian $\hat{H}_0$ [32, 92]. In particular, this tells us that the evolution of the quantum system over a single period, as specified by the Floquet operator $\hat{U}_F = e^{-i\hat{H}_F T/\hbar}$, will

be very close to evolution under $\hat{H}_0$, given by $e^{-i\hat{H}_0 T/\hbar}$. This motivates us to expand the Floquet Hamiltonian $\hat{H}_F$ as a power series about $T = 0$, with the zeroth order term given by $\hat{H}_F^{(0)} = \hat{H}_0$, and the higher order terms providing successive corrections to $\hat{H}_0$ for finite T:

$$\hat{H}_F \stackrel{?}{=} \sum_{n=0}^{\infty} \hat{H}_F^{(n)} T^n. \tag{5.13}$$

This series is referred to as the Floquet-Magnus expansion.[6] Here, the operators $\hat{H}_F^{(n)}$ are independent of T, and the question mark over the equal sign denotes that such a series is not guaranteed to converge. The FM expansion can be understood as a special case of the Magnus expansion, which applies to systems with general time-dependent Hamiltonians, time-periodic or otherwise [209].

Many derivations of the terms in the FM expansion exist in the literature [12, 209]. The first three terms are given by [12]:

$$\hat{H}_F^{(0)} = \frac{1}{T}\int_0^T dt_1\, \hat{H}(t_1) = \hat{H}_0 \tag{5.14}$$

$$\hat{H}_F^{(1)} = \frac{1}{2i\hbar T^2}\int_0^T dt_1 \int_0^{t_1} dt_2\, [\hat{H}(t_1), \hat{H}(t_2)] \tag{5.15}$$

$$\begin{aligned}\hat{H}_F^{(2)} = \frac{1}{6(i\hbar)^2 T^3}\int_0^T dt_1 \int_0^{t_1} dt_2 \int_0^{t_2} dt_3 \Big(&\Big[\hat{H}(t_1), [\hat{H}(t_2), \hat{H}(t_3)]\Big] \\ &+ \Big[\hat{H}(t_3), [\hat{H}(t_2), \hat{H}(t_1)]\Big] \Big).\end{aligned} \tag{5.16}$$

Despite appearances, these expressions are independent of T, as can be seen by noting that $\hat{H}(t)$

[6] Note that some authors define the FM expansion in a slightly different way, as $\hat{H}_F = \sum_{n=0}^{\infty} \hat{\mathcal{H}}_F^{(n)}$. In this case, the term $\hat{\mathcal{H}}_F^{(n)}$ is proportional to T^n, and is related to the corresponding term in our expansion via $\hat{\mathcal{H}}_F^{(n)} = \hat{H}_F^{(n)} T^n$.

is a function of $s = t/T$ alone, and then changing the variables of integration to $s_1 = t_1/T$, $s_2 = t_2/T$, and so on. Higher order terms have a similar structure. The n^{th}-order term $\hat{H}_F^{(n)}$ consists of a prefactor $1/[n!(i\hbar)^n T^{n+1}]$, multiplied by an integral over times $t_1, t_2 \ldots t_n$ of a sum of nested commutators of $\hat{H}(t)$.

An important consequence of this structure is that each $\hat{H}_F^{(n)}$ is guaranteed to be a Hermitian operator, given the Hermiticity of $\hat{H}(t)$. This means that if the FM expansion truncated at any order M, denoted by $\hat{H}_{F,M} \equiv \sum_{n=0}^{M} \hat{H}_F^{(n)} T^n$, will be Hermitian as well. As a result, if we choose to approximate the exact Floquet Hamiltonian by $\hat{H}_{F,M}$, then the corresponding approximate Floquet operator $\hat{U}_{F,M} \equiv e^{-i\hat{H}_{F,M}T/\hbar}$ is unitary. Therefore, approximately evolving a state vector by repeated applications of $\hat{U}_{F,M}$ will exactly preserve the normalization of the state vector, and consequently conserve probability. This useful feature of the FM expansion is not present in certain other approximation schemes, such as standard time-dependent perturbation theory [209].

A similar expansion in powers of T applies to classical systems, governed by the time-periodic Hamiltonian $H(z,t) = H_0(z) + V(z, t/T)$. In this case, it is the Floquet Liouvillian which is being expanded as $\hat{\mathcal{L}}_F \stackrel{?}{=} \sum_{n=0}^{\infty} \hat{\mathcal{L}}_F^{(n)} T^n$. The terms in this expansion are identical in form to (5.14)–(5.16) above, but with $\hbar$ set to one, and with all $\hat{H}$ symbols replaced with $\hat{\mathcal{L}}$. Moreover, as described in [41] and [212], each term in this sum may be expressed as $\hat{\mathcal{L}}_F^{(n)} = \{H_F^{(n)}, \cdot\}$, for some phase space function $H_F^{(n)} \equiv H_F^{(n)}(z)$. Thus, we may equivalently think in terms of an expansion for the classical Floquet Hamiltonian, given by $H_F(z) \stackrel{?}{=} \sum_{n=0}^{\infty} H_F^{(n)}(z) T^n$, provided that such a Hamiltonian exists.

Our interest in the FM expansion lies in its relation to energy absorption in periodically driven quantum systems. To understand this connection, we need to consider the convergence properties of the expansion. First, suppose that for some range of possible periods T, from

$T = 0$ to $T = T^*$, the FM expansion converges to the exact Floquet Hamiltonian $\hat{H}_F$: That is, the sequence of partial sums $\hat{H}_{F,M} = \sum_{n=0}^{M} \hat{H}_F^{(n)} T^n$ approaches the limit $\hat{H}_F$ as M is taken to infinity.[7] In this case, the FM expansion is just the Taylor series expansion for $\hat{H}_F$ about $T = 0$, by the uniqueness property of power series representations [171]. The generalization of Taylor's theorem for operator-valued functions then places a bound on the difference between $\hat{H}_F$ and the truncated expansion $\hat{H}_{F,M}$, for any choice of M [213]. In particular, for $M = 0$, this theorem tell us that $\hat{H}_F$ differs from $\hat{H}_{F,0} = \hat{H}_0$ by an operator of size $o(T)$, which we denote $\hat{h} \equiv \hat{H}_F - \hat{H}_0$. Here, the size of an operator can be quantified by the operator norm $||\cdot||$ induced by the vector norm $|||\psi\rangle|| \equiv \sqrt{\langle\psi|\psi\rangle}$. For an operator $\hat{A}$, $||\hat{A}||$ is defined as the maximum of $||\hat{A}|\psi\rangle||$ over all possible normalized $|\psi\rangle$ [214].

By an appropriate choice of T, we can make $\hat{h}$ as small as we like. Then, $\hat{H}_F$ and $\hat{H}_0$ will be very close, and we expect that evolution under $\hat{H}_F$ should nearly conserve $\hat{H}_0$, since this evolution *exactly* conserves $\hat{H}_F$. We can make this intuition precise by deriving a simple bound on energy absorption. Suppose that we initialize our system in a state $|\psi(0)\rangle$ at $t = 0$, and then allow it to evolve for N periods under the time-periodic Hamiltonian $\hat{H}(t)$. Over this time period, what is the change in the expectation value of the energy, $\Delta\langle H_0\rangle \equiv \langle H_0\rangle_{NT} - \langle H_0\rangle_0$? Since the final state $|\psi(NT)\rangle$ can be alternatively obtained by evolving $|\psi(0)\rangle$ for a time NT under the time-independent $\hat{H}_F$, it follows that the expectation value of $\hat{H}_F = \hat{H}_0 + \hat{h}$ is conserved: $\langle H_0\rangle_{NT} + \langle h\rangle_{NT} = \langle H_0\rangle_0 + \langle h\rangle_0$, or $\Delta\langle H_0\rangle = -\langle h\rangle_{NT} + \langle h\rangle_0$. This last expression may then be bounded as follows:

[7] Technically, the statement $\lim_{M\to\infty} \hat{H}_{F,M} = \hat{H}_F$ is meaningless until we fix $\hat{H}_F$, which we mentioned previously is not uniquely defined. Really, what we mean by this limit is that there exists *some* operator $\hat{H}_F$ satisfying $\hat{U}_F = e^{-i\hat{H}_F T/\hbar}$ such that $\lim_{M\to\infty} \hat{H}_{F,M} = \hat{H}_F$.

$$
\begin{aligned}
|\Delta\langle H_0\rangle| &= |-\langle h\rangle_{NT} + \langle h\rangle_0| \\
&\leq |\langle h\rangle_{NT}| + |\langle h\rangle_0| = |\langle\psi(NT)|\hat{h}|\psi(NT)\rangle| + |\langle\psi(0)|\hat{h}|\psi(0)\rangle| \\
&\leq |||\psi(NT)\rangle|| \cdot ||\hat{h}|\psi(NT)\rangle|| + |||\psi(0)\rangle|| \cdot ||\hat{h}|\psi(0)\rangle|| \\
|\Delta\langle H_0\rangle| &\leq 2||\hat{h}|| = o(T).
\end{aligned}
\tag{5.17}
$$

Here, in moving from the second to the third line, we note that $\langle\psi(t)|\hat{h}|\psi(t)\rangle$ is the inner product of $|\psi(t)\rangle$ and $\hat{h}|\psi(t)\rangle$, which allows us to invoke the Cauchy-Schwarz inequality $|\langle\psi_1|\psi_2\rangle| \leq |||\psi_1\rangle|| \cdot |||\psi_2\rangle||$. Then, to obtain the final inequality, we recall that $|\psi(t)\rangle$ is normalized for all time ($|||\psi(t)\rangle|| = 1$), and that by the definition of the operator norm $||\cdot||$, $||\hat{h}|\psi\rangle||$ is less than or equal to $||\hat{h}||$ for any possible choice of normalized $|\psi\rangle$.

This bound tells us that the expectation value of the energy never strays away from its initial value by an amount greater than $2||\hat{h}||$, a quantity which can be made arbitrarily small for sufficiently small T. Thus, the convergence of the FM expansion to $\hat{H}_F$ implies that the energy absorbed by the system is bounded for all time, at least at the level of expectation values. In fact, analogous inequalities can easily be derived for the change in any moment $\langle H_0^k\rangle$, which tells us that change in the energy distribution overall is bounded as well. Moreover, since the Floquet formalism and the FM expansion are valid for classical Hamiltonian systems, all of these arguments apply equally well in the classical context.

When does the FM expansion converge to $\hat{H}_F$? One sufficient condition for the convergence of the FM expansion to $\hat{H}_F$ is given by

$$\frac{1}{\hbar}\int_0^T dt\,||\hat{H}(t)|| < \pi; \tag{5.18}$$

see [209]. Although a very general condition, the applicability of this criterion is limited for at least two reasons. First, it does not apply if $\hat{H}(t)$ is an unbounded operator ($||\hat{H}(t)|| = \infty$). This occurs generally in quantum particle systems with a kinetic energy term in the Hamiltonian, due to the unboundedness of the corresponding derivative operator $\partial^2/\partial x^2$. Similarly, for classical systems, where $\hat{H}(t)$ is replaced by the Liouvillian $\hat{\mathcal{L}}(t) = i\{H, \cdot\}$, the derivative operators which define the Poisson bracket mean that the spectrum of $\hat{\mathcal{L}}(t)$ generally has no upper bound. Second, even for systems like quantum spin systems, which have a finite dimensional Hilbert space that ensures that all operators are bounded, the above condition is generally difficult to satisfy for large systems. For a lattice of N spins with a physically reasonable Hamiltonian, the norm $||\hat{H}(t)||$ will generally scale with N. Thus, for a fixed period T, the inequality (5.18) will generally be violated for large enough N.

We have shown that the convergence of the FM expansion to $\hat{H}_F$ implies a bound on changes in a periodically driven system's energy. Conversely, if such a system is observed to absorb energy without bound for a given driving period T, this implies that the system's FM expansion cannot converge to $\hat{H}_F$ for that choice of T. This fact, which has been widely acknowledged in the literature on periodically driven quantum systems [12, 33, 42, 73], allows us to understand how the FM expansion is relevant to the energy diffusion framework developed in Chapter 2. For a classical system described by the energy diffusion model, energy absorption is slow, but ultimately builds up over long times. For systems with an unbounded phase space, diffusive growth of the system's (average) energy will generally continue without limit, while

for systems with a bounded phase space, changes in the system's energy are only bounded by the maximum and minimum values of the system's Hamiltonian. This is true regardless of how small T is, although the rate of energy absorption is greatly suppressed at high driving frequencies. Therefore, we are lead to the following conclusion: If the classical energy diffusion model offers a good approximate description of the energy dynamics of a quantum system for some choice of T, then the FM expansion does not converge to $\hat{H}_F$ for this T. Thus, investigating the convergence properties of the FM expansion for quantum chaotic systems is an essential prerequisite for understanding the potential extension of the energy diffusion model to the quantum regime.

5.3.3 Rigorous energy absorption bounds, Floquet prethermalization, and energy diffusion

Even if the FM expansion is does not converge to $\hat{H}_F$, the expansion can still be extremely useful for studying the dynamics of quantum and classical systems. As mentioned previously, one can attempt to approximately evolve the state vector of a periodically driven quantum system by repeated applications of the M^{th}-order approximate Floquet operator $\hat{U}_{F,M} \equiv e^{-i\hat{H}_{F,M}T/\hbar}$. A priori, it is not guaranteed that this will yield a good approximation of the evolving state vector, and even if it does, it is not clear how many driving periods such an approximation will remain good for. Fortunately, a large number of researchers have probed these questions, on the theoretical, numerical, and experimental fronts, especially in the past five to ten years. To conclude this section, we now review some of these developments. We first highlight some important rigorous bounds that have been established, which quantify the degree to which the evolution of a periodically driven system deviates from evolution under an approximate

effective Hamiltonian. We then explain how these bounds provide a generic explanation for the phenomenon of Floquet prethermalization, and briefly discuss some numerical and experimental studies of Floquet prethermal systems. Finally, we connect the results back to the energy diffusion description.

We begin with the rigorous bounds just mentioned. Suppose that the initial state vector $|\psi(0)\rangle$ of a quantum system is evolved under two different Hamiltonians: The exact time-periodic Hamiltonian $\hat{H}(t)$, and some effective time-independent Hamiltonian $\hat{H}^*$, which is meant to approximately capture the evolution under $\hat{H}(t)$. For quantum systems defined on a lattice, where each lattice site is associated with a Hilbert space of finite dimension, the error in such approximations may be precisely quantified. This includes spin systems, such as the quantum Ising model and its generalizations, fermionic systems (which may be mapped to spin systems [215]), and systems of hard-core bosons. Highly general results of this type were established around the same time by Kuwahara et al. and Abanin et al.: The results of Kuwahara et al. are obtained by bounding the terms of the FM expansion and invoking a special decomposition of the evolution operator [75, 76], and Abanin et al. derive their result by constructing a basis in which the system appears to be governed by a time-independent Hamiltonian plus a small correction [33, 216]. Despite these differing approaches, the bounds obtained by both groups are similar in essence. In both cases, an optimal effective Hamiltonian $\hat{H}^*$ is determined, which is approximately conserved under the exact dynamics, and which is close to the time-averaged Hamiltonian $\hat{H}_0$ (in Kuwahara et al., $\hat{H}^*$ is simply the FM expansion truncated at some optimal order). More specifically, if $\hat{H}^*(t)$ is the Hamiltonian $\hat{H}^*$ in the Heisenberg picture for the exact evolution, then the time-averaged rate of change of $\hat{H}^*(t)$ over a time interval of duration t satisfies a bound of the form

$$\frac{||\hat{H}^*(t) - \hat{H}^*(0)||}{t} \lesssim e^{-O(\omega)}, \tag{5.19}$$

for sufficiently large driving frequencies ω. In other words, $\hat{H}^*$ is approximately conserved up to a time which is exponentially[8] large in ω. Since $\hat{H}^*$ and $\hat{H}_0$ are close (precisely, they differ by an $O(T)$ quantity), this means that the energy of the system defined by $\hat{H}_0$ is approximately conserved as well. Moreover, $\hat{H}^*$ is not merely a quasi-conserved quantity: The actual dynamics generated under $\hat{H}^*$ are close to the exact dynamics generated by $\hat{H}(t)$, when considering the evolution of local quantities. For example, Abanin et al. show that for a local operator (an operator which only acts on a few lattice sites, or is a sum of such locally-acting operators), the difference between the operator's exact evolution and its evolution under $\hat{H}^*$ remains small up to a time which is exponentially large in ω.

As noted by their authors, these bounds (and generalizations thereof [39, 41, 47, 80]) offer a general picture of the process of Floquet prethermalization, which we previously discussed in Chapter 2, Section 2.5. Recall that in a prethermal system, the system reaches a quasi-steady state of thermal equilibrium with respect to an effective Hamiltonian. Now, in a system which obeys the bound (5.19), the evolution of the system is well-described by evolution under $\hat{H}^*$ up to some time $\tau^* \sim e^{O(\omega)}$. So, if the dynamics under $\hat{H}^*$ cause a relaxation to thermal equilibrium on some timescale τ_{th} (for example, if $\hat{H}^*$ satisfies the Eigenstate Thermalization Hypothesis [87, 88], see Section 5.4), then this relaxation will occur under periodic driving for large enough ω, when $\tau_{\text{th}} \ll \tau^*$. That is, sufficiently rapid driving leads to a separation of timescales between the timescale on which (pre)-thermalization occurs, and the timescale

[8]The word "exponentially" and the notation $e^{-O(\omega)}$ are both used slightly loosely in this discussion. More precisely, some bounds in the literature of the form (5.19) are only "quasi-exponential" in ω. For example, the bound of Abadal et al. scales like $\exp\left[-c\,\omega/(\log\omega)^3\right]$, for some constant c.

over which the system begins to deviate significantly from the effective evolution generated by $\hat{H}^*$. Hence the name *Floquet* prethermalization: The periodic drive facilitates the approximate stability of the prethermal steady state.

Floquet prethermalization has been observed in a range of models for periodically driving systems. In the quantum context, Floquet prethermal states with long lifetimes have been theoretically and numerically analyzed in models including spin chains with short- and long-range interactions [33, 39, 45, 47, 52, 71, 75, 76, 216–218], various versions of the Hubbard model [40, 43, 81, 219], and the quantum $O(N)$ model for interacting scalar fields [77]. Classically, Floquet prethermalization has been investigated in coupled kicked rotor systems [46, 78], as well as classical Heisenberg spin chains [44, 53, 55, 220]. In fact, the quantum energy absorption bound (5.19) has been extended to classical spin systems, by exploiting the classical limit of quantum spin systems (this limit consists of taking the spin number S to infinity) [41]. For quantum and classical models alike, researchers have probed both the simple prethermalization scenario described in the previous paragraph, but also more complicated dynamics. This includes prethermal time crystal systems [39, 45, 47, 53, 55, 220], in which the system oscillates between two or more thermal states (often related via a discrete symmetry), and systems which do not prethermalize to the standard canonical thermal state, but rather to a state described by a generalized Gibbs ensemble [46, 218]. Moreover, the studies listed in the present paragraph cover not just a range of systems, but also a range of driving protocols: This includes monochromatic driving, piecewise driving protocols which toggle instantaneously between one or more Hamiltonians, delta function kicks, and protocols which drive the system either locally or globally.

Within the past two years, these model systems have been complemented by experimental

realizations of Floquet prethermal states, on two types of physical platforms: Optical traps, and nuclear spin systems. In work by Rubio-Abadal et al., a prethermal state was established in a cloud of ultracold atoms in an optical lattice, driven via periodic modulation of the lattice's potential depth [48]. This state, judged to be thermal based on measurements of the hole density in the lattice, was found to persist for up to 10^4 drive cycles, with this prethermal lifetime increasing with increasing drive frequency. Kyprianidis et al. also used an optical trap platform, but towards a slightly different end: The realization of a prethermal discrete time crystal [166]. They engineered a system of trapped ions to simulate a periodically driven chain of spin-$1/2$ degrees of freedom. In this system, a long-lived prethermal state was established wherein the system oscillated between two states of opposite magnetization, at half the frequency of the drive. This subharmonic response is a defining feature of discrete time crystal systems. Meanwhile, Peng et al. engineered a Floquet prethermal state in a system of driven nuclear spins in a fluorapatite crystal, modelled by a spin-$1/2$ chain subject to a dipolar Hamiltonian and periodic kicks [49]. The prethermal state of this system, the lifetime of which was found to increase with drive frequency, was characterized by quasi-conservation of the time-averaged Hamiltonian and quick relaxation of the system's magnetization to the appropriate thermal value. Finally, a prethermal discrete time crystal was realized by Beatrez et al. in a system of carbon-13 nuclear spins, evolving according to dipolar interactions and electron-mediated site-specific fields [56]. Uniquely, in order to establish a prethermal state, these researchers drove the system simultaneously with two drives of different frequencies. Like in the trapped ion system of Kyprianidis et al., subharmonic oscillations of the system's magnetization were the key signature of time crystal behavior.

Hopefully, the present discussion has made it clear that Floquet prethermalization, and

related bounds on energy absorption, are presently a topic of much theoretical and experimental interest. How are these developments connected to the classical energy diffusion description, as outlined in Chapter 2? As discussed in Section 2.5 of that chapter, Floquet prethermalization also occurs in systems described by the energy diffusion model, when the chaotic mixing of trajectories in an ensemble establishes an effectively microcanonical distribution at some initial energy. Moreover, the rate of energy evolution in such systems is characterized by the power spectrum $S(\omega; E)$, which decays faster than any power of ω^{-1} for large ω (for smooth Hamiltonian systems). Thus the lifetime of the initial prethermal state grows rapidly with increasing ω. All of this is consistent with energy absorption bounds of the form (5.19). As mentioned previously, bounds of this type have been established for classical spin chains, which have been numerically observed to exhibit chaos [173, 221, 222]. Meanwhile, for systems of chaotic coupled rotors subject to periodic kicks, Floquet prethermalization and/or diffusion of energies has been observed in certain parameter regimes [78, 79, 223–226]. These potential points of agreement between previous studies and the energy diffusion description deserve further investigation. On the other hand, for quantum systems under rapid periodic driving, it is not clear if or when the classical energy diffusion description is able to serve as a good approximate model for energy absorption. However, at the very least, the prospects for such a quantum-classical correspondence are encouraged by the fact that the energy diffusion model and the bounds (5.19) do not conflict. In Section 5.5, we will continue to explore the possibility of quantum-classical correspondence, via an analysis of energy absorption in quantum systems based on Fermi's golden rule.

5.4 Quantum chaos and energy diffusion

Our analysis of energy diffusion in Chapter 2 relied crucially on the assumption of chaos and ergodicity of the undriven system's motion. These properties, and the phase space mixing implied by them, imbued the dynamics of the system with the effectively random character necessary to establish diffusive energy evolution. Consequently, in thinking about the potential relevance of the energy diffusion model to quantum mechanical systems, it is reasonable to first look to quantum systems with a classical chaotic counterpart, or "quantum chaotic" systems. In this section, we provide some relevant background necessary to investigate energy diffusion in such systems. First, we summarize how the tools of random matrix theory (RMT) have been used to understand the properties of quantum chaotic systems. Then, to get a sense of how the energy diffusion description may be applied to in a quantum setting, we present a literature review of energy diffusion models used to describe *slowly* driven quantum chaotic systems. Last, we describe two models of energy absorption in periodically driven quantum chaotic systems: A random matrix model, and a quasiclassical model of energy transitions based on Fermi's golden rule. As we will show, this second model reproduces the classical energy diffusion description in the semiclassical ($\hbar \to 0$) limit.

5.4.1 Quantum chaos and random matrix theory

We now give a brief introduction to quantum chaotic systems, with a focus on the role of random matrix theory in the modelling of these systems. Let us begin with a definition. Here, we take a "quantum chaotic" system to be a quantum mechanical system with a classical chaotic counterpart. Thus, for example, a quantum chaotic system can be obtained via the classical

Hamiltonian $H_0(z)$ from Chapter 2, by a quantization procedure like the one discussed in Section 5.2 in the present chapter. While this is a standard definition, other characterizations of quantum chaos have also been proposed, including definitions which attempt to avoid direct reference to classical analogues altogether (for example, definitions in terms of random matrix theory, a topic we will discuss shortly) [88, 227]. However, for our purposes, the standard definition is adequate. The study of quantum chaos is thus the study of the *imprint* of classical chaos on the properties and dynamics of quantum systems [13, 228, 229].

How can this imprint of classical chaos be described? Let us consider a quantum system with the Hamiltonian $\hat{H}_0$, obtained by quantizing $H_0(z)$, as discussed in Section 5.2 of this chapter. For such a time-independent Hamiltonian, the corresponding dynamics are fully characterized by the eigenvalues E_n and eigenvectors $|n\rangle$ of $\hat{H}_0$: Evolution of an initial state vector $|\psi(0)\rangle = \sum_n a_n|n\rangle$ under the Schrodinger equation yields the solution $|\psi(t)\rangle = \sum_n a_n e^{-iE_n t/\hbar}|n\rangle$. Therefore, we expect that any signatures of classical motion in the quantum dynamics should manifest in these eigenvalues and eigenvectors. Generally, such quantum-classical connections appear most prominently in the semiclassical limit, when the value of $\hbar$ is taken to zero.[9] For classically *integrable* systems, where the classical evolution is entirely non-chaotic, this limit can be comprehensively described by tools such as WKB (Wentzel–Kramers–Brillouin) theory. For example, time-independent WKB theory provides approximate semiclassical expressions for energy eigenstates and eigenvalues in terms of classical quantities [180]. However, for classically chaotic and ergodic systems, this method and other comparably simple approximations break down [230], and a different perspective is

[9] Of course, $\hbar$ is a fixed constant, and so such a limiting procedure is something of a mathematical abstraction. In reality, we should think of a semiclassical description as being valid at sufficiently high energies, much larger than any quantum energy scale associated with $\hbar$, or for sufficiently high quantum numbers.

needed. This perspective is provided by random matrix theory (RMT).

The central idea of RMT, as applied to quantum chaotic systems, is that although the *individual* eigenstates and eigenvalues of a quantum chaotic Hamiltonian may be difficult to characterize, large groups of eigenstates and eigenvalues have some surprisingly regular on-average or "statistical" properties [88]. Moreover, in the semiclassical limit, these statistical properties can be predicted in terms of properties of the system's classical counterpart. These regularities suggest an alternative approach to modelling quantum chaotic systems: Instead of attempting to exactly describe the system's Hamiltonian or other operators, simply replace the matrix corresponding to such an operator with a matrix which has the same statistics. This replacement matrix can be generated as a sample from a *random matrix ensemble*, tuned so that a typical matrix from the ensemble has the desired features. Then, assuming that these statistical properties are enough to capture the salient attributes of the system and its dynamics, the resulting model offers a valid coarse-grained description of the system.

To elucidate this modelling philosophy, we now discuss two different statistical features of quantum chaotic systems which can be reproduced with suitable random matrix models: The distribution of nearest-neighbor eigenvalue spacings, and the distribution of matrix elements of an operator in the eigenbasis of the Hamiltonian. These distributions are each related to an important conjecture in quantum chaos: The Bohigas-Giannoni-Schmit (BGS) conjecture, and the Eigenstate Thermalization Hypothesis (ETH), respectively. In both cases, we explain how these statistical properties are connected to the properties of the corresponding classical system. We begin by discussing the eigenvalue spacing distribution.

5.4.2 Level spacing distributions and the Bohigas-Giannoni-Schmit conjecture

Consider a quantum chaotic system with Hamiltonian $\hat{H}_0$, with associated energy levels E_n. Select a narrow interval of the energy axis from E to $E + \Delta E$, with ΔE chosen so that classical trajectories with energies in $[E, E + \Delta E]$ look similar to one another. Within this range, there will be a series of energy levels E_n, and a corresponding series of (normalized) nearest-neighbor level spacings $\varepsilon_n \equiv \rho(E)(E_{n+1} - E_n)$. Here, we have divided the level spacings by the mean level spacing $1/\rho(E)$, where $\rho(E)$ is the average density of states for the system; we now simply refer to these normalized spacings as level spacings. Even though the interval $[E, E + \Delta E]$ is classically small, the spectrum of $\hat{H}_0$ becomes very dense for small $\hbar$, and a large number of energy eigenvalues E_n will lie within it. Specifically, Weyl's law tells us that $\rho(E) \approx \Sigma(E)/h^d$ in the semiclassical regime [185]. So, in this limit, it becomes sensible to talk about an effectively continuous *distribution* $f(\varepsilon)$ of level spacings within this interval, where $f(\varepsilon)\, d\varepsilon$ gives the fraction of level spacings in the interval with sizes between ε and $\varepsilon + d\varepsilon$. As it turns out, the tools of RMT can provide an accurate characterization of this distribution, as we now describe.

To begin, we note two basic properties of the distribution $f(\varepsilon)$. First, this distribution is normalized by definition: $\int_0^\infty d\varepsilon f(\varepsilon) = 1$. Second, the first moment of $f(\varepsilon)$ is also equal to unity: $\langle \varepsilon \rangle = \int_0^\infty d\varepsilon f(\varepsilon)\varepsilon = 1$. This is because we have already normalized the level spacings by their mean size, so the average $\langle \varepsilon \rangle$ must be 1.

To characterize the remaining features of this distribution, we need to introduce the Gaussian Orthogonal Ensemble (GOE), an ensemble of real symmetric matrices which is one of the standard ensembles in RMT [231, 232]. Random matrix ensembles such as the GOE were

originally studied by Eugene Wigner, who used them to model the Hamiltonians of heavy atomic nuclei [88, 229, 233]. For $N \times N$ matrices, a sample matrix $\hat{M}$ from the GOE may be constructed in a simple way. First, sample each of the N diagonal matrix elements M_{ii} independently, from a Gaussian distribution with mean zero and a variance of 2. Then, sample the off-diagonal elements above the diagonal (M_{ij} with $j > i$) independently from a Gaussian with mean zero and unit variance (the remaining off-diagonal elements are then fixed by the symmetry condition $M_{ij} = M_{ij}$). Symbolically, we have:

$$M_{ij} = \begin{cases} \mathcal{N}(0,2) & \text{if } j = i \\ \mathcal{N}(0,1) & \text{if } j > i \\ M_{ji} & \text{if } j < i, \end{cases} \tag{5.20}$$

where $\mathcal{N}(\mu, \sigma^2)$ denotes a sample from a Gaussian distribution with mean μ and variance σ^2. Defined in this way, the GOE has the property of invariance under orthogonal transformations $\hat{M} \rightarrow \hat{O}^T \hat{M} \hat{O}$, where $\hat{O}$ is an arbitrary orthogonal matrix [231, 232]. That is, if the random matrix $\hat{M}$ (considered as a random variable, not an individual sample) has GOE statistics, then $\hat{O}^T \hat{M} \hat{O}$ does as well.

For any matrix sampled from the GOE, one may construct an eigenvalue spacing distribution over some small interval of eigenvalues $[x, x+\Delta x]$, just as we did for the Hamiltonian $\hat{H}_0$. The average of this distribution over all possible samples from the GOE is known as the Wigner-Dyson distribution $f_{WD}(\varepsilon)$. Although an analytical expression for this distribution is not available, for large N it can be closely approximated by the "Wigner surmise" [88, 232]

$$f_{WD}(\varepsilon) \approx \frac{\pi\varepsilon}{2} \exp\left(\frac{-\pi\varepsilon^2}{4}\right). \tag{5.21}$$

Among other things, one notable prediction of this distribution is the presence of level repulsion: The factor ε suppresses the probability of a near-overlap between eigenvalues. This feature is also present in many other random matrix ensembles.

Now, in general, the spacing distribution will vary from sample to sample, fluctuating around the mean distribution $f_{WD}(\varepsilon)$. However, for large N, these fluctuations are suppressed, and nearly all samples from the GOE will have spacing distributions which are quite close to $f_{WD}(\varepsilon)$. In other words, a single "typical" sample from the GOE is sufficient to reproduce the average spacing distribution for the ensemble. This property, somewhat analogous to the Law of Large Numbers, arises from the concentration of measure properties of random matrix ensembles [234]. Thus, if one does not want to invoke the Wigner surmise (5.21), $f_{WD}(\varepsilon)$ may also be approximated by sampling a *single* matrix from the GOE, assuming it is typical, and then computing its distribution.

What does this random matrix ensemble have to do with $f(\varepsilon)$, the distribution of spacings within $[E, E + \Delta E]$? Suppose that for some very large N, we sample a typical matrix from the GOE, and compute its spectrum within some narrow interval $[x, x + \Delta x]$. In a seminal paper [89], Bohigas, Giannoni, and Schmit proposed a conjecture: For a quantum chaotic system in the semiclassical limit with time-reversal symmetry, the energy levels in $[E, E + \Delta E]$ and the eigenvalues in $[x, x + \Delta x]$ have *the same* statistical properties (in particular, they share the same level spacing distribution $f_{WD}(\varepsilon)$).[10] These authors presented numerical evidence (see Figure

[10]For non-time reversal invariant systems, the random matrix should be selected from the Gaussian *Unitary* Ensemble, an ensemble of Hermitian matrices.

5.3) supporting their hypothesis for a desymmetrized version of the Sinai billiard, which has been proven to be classically chaotic. Since then, the BGS conjecture has been numerically corroborated for a range of systems, including models of the hydrogen atom in a magnetic field [235, 236], various billiards [237, 238], and a variety of lattice models [239–245]. For a discussion of this evidence, see [88]. For systems without a classical chaotic counterpart, the validity of the BGS conjecture for a given system is now frequently taken to *define* quantum chaos [88].

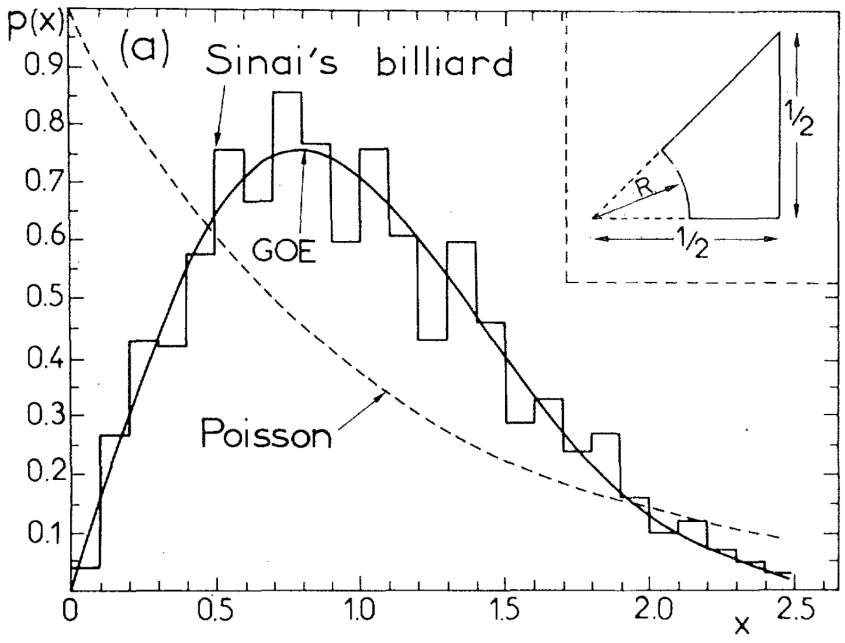

Figure 5.3: Plot from [89], displaying numerical evidence which corroborates the BGS conjecture. For the quantum desymmetrized Sinai billiard, the distribution of energy level spacings (blocky curve) is found to agree with the corresponding distribution for the GOE (smooth solid curve). As can be seen in the inset on the upper right, this billiard is defined as one eighth of the standard Sinai billiard (see Figure 3.3). The dashed curve corresponds to a Poissonian spacing distribution, the semiclassical level spacing distribution for classically *integrable* quantum systems [246].

Therefore, the success of the BGS conjecture suggests that, for modelling purposes, it may not be necessary to compute the exact spectrum of a quantum chaotic Hamiltonian. Instead, one

can artificially "mock up" a spectrum which (a) possesses the spacing distribution $f_{WD}(\varepsilon)$, and (b) reproduces certain properties of the original "true" Hamiltonian, like the average density of states $\rho(E)$. An example of this type of construction is given in Section 5.5. Alternatively, one may simply take a sample matrix from the GOE, and then investigate the properties of the system which has that matrix as a Hamiltonian. Variants on this approach are taken in many of the works mentioned in Section 5.4.4, where we discuss slowly driven quantum chaotic systems.

5.4.3 The Eigenstate Thermalization Hypothesis

Thus, it appears that the spectrum of a quantum chaotic Hamiltonian $\hat{H}_0$ can be accurately modelled with the tools of RMT, at least at a statistical level in the semiclassical limit. What about the eigenvectors of $\hat{H}_0$, denoted by $|n\rangle$? Specifically, let us look at the matrix elements $A_{mn} \equiv \langle m|\hat{A}|n\rangle$ of a Hermitian operator $\hat{A}$, defined by quantizing some function on phase space $A(z)$. As it turns out, the properties of these matrix elements can be characterized using semiclassical methods. We now review two important results in this context, and explain how they are connected to the Eigenstate Thermalization Hypothesis (ETH), a standard ansatz used to understand thermalization in isolated quantum systems.

First, consider the diagonal elements of $\hat{A}$, given by $A_{nn} \equiv \langle n|\hat{A}|n\rangle$. Each matrix element A_{nn} gives the expectation value of $\hat{A}$ when the system is in the energy eigenstate $|n\rangle$. How should we expect these expectation values to behave in the semiclassical limit? Recall that an eigenstate $|n\rangle$ is a stationary state of the quantum dynamics: Under the Schrodinger equation $i\hbar\, d|\psi\rangle/dt = \hat{H}_0|\psi\rangle$, this eigenstate just picks up a phase factor $e^{-iE_n t/\hbar}$, which leaves the expectation value of any operator unchanged. One possible classical analogue of this is a phase space distribution

ρ, confined to a surface of constant energy $E = E_n$, which is stationary under the Liouville equation $\partial\rho/\partial t = \{H_0, \rho\}$. For a system which is ergodic, the unique distribution meeting these requirements is the microcanonical distribution $\rho_E(z) = \delta(H_0(z) - E)/\Sigma(E)$ [83]. Thus, if signatures of classical chaos manifest in the eigenstates $|n\rangle$, it is reasonable to guess that the quantum expectation values A_{nn} are related to the classical averages $\langle A\rangle_E \equiv \int dz\, \rho_E(z) A(z)$.

In fact, such a connection has been established rigorously. Consider a classically narrow region of the energy axis $[E, E+\Delta E]$, as in our previous discussion of level spacing distributions. This interval has $N \approx \rho(E)\Delta E \approx \Sigma(E)\Delta/h^d$ energy levels, each with an associated expectation value A_{nn}. Now, let $\hbar$ approach zero, and let $\Delta E \propto \hbar$ go to zero at the same rate. This way, while the size of the interval $[E, E + \Delta E]$ will approach zero, $N \propto 1/h^{d-1}$ will approach infinity (provided that $d \geq 2$, which must be true for a chaotic system). In this limit, it has been proven that the averaged squared deviation between A_{nn} and $\langle A\rangle_E$ for eigenstates in this range approaches zero [185, 247]:

$$\lim_{\hbar \propto \Delta E \to 0} \frac{1}{N} \sum_{E_n \in [E, E+\Delta E]} |A_{nn} - \langle A\rangle_E|^2 = 0. \tag{5.22}$$

This theorem, first established for billiard systems by Shnirelman [248] and then later generalized, is valid for systems which are classically ergodic. It tells us that in the semiclassical limit, almost all matrix elements A_{nn} must approximately coincide with the classical average $\langle A\rangle_E$, with $E = E_n$.

Similarly, connections between a quantum chaotic system's classical counterpart and the off-diagonal matrix elements A_{mn} have also been established. One such connection arises when taking averages over "nearby" A_{mn}'s with similar values of E_m and E_n. Specifically, consider the

average of $|A_{mn}|^2$ over m and n such that $\frac{1}{2}(E_m + E_n) \approx \overline{E}$ and $E_n - E_m \approx \Delta$, for some choice of mean energy $\overline{E}$ and energy difference Δ. Wilkinson demonstrated that, in the semiclassical limit, such an average $\overline{|A_{mn}|^2}$ can be related to classical quantities [249, 250]:

$$\overline{|A_{mn}|^2} \approx h^{d-1} \frac{S_A(\Delta/\hbar; \overline{E})}{\Sigma(\overline{E})}, \tag{5.23}$$

Here, $S_A(\omega; E)$ is the microcanonical power spectrum for the observable $A(z)$, defined analogously to the power spectrum $S(\omega; E)$ in Chapter 2. That is, $S_A(\omega; E)$ is the Fourier transform of the autocorrelation function of $A(z)$:

$$C_A(t; E_0) \equiv \langle A(z_0^0) A(z_t^0) \rangle - \langle A(z_0^0) \rangle \langle A(z_t^0) \rangle, \tag{5.24}$$

$$S_A(\omega; E) = \int_{-\infty}^{\infty} dt\, e^{-i\omega t} C_A(t; E). \tag{5.25}$$

Thus, we see that while the diagonal elements A_{nn} are tied to the *equilibrium* classical quantity $\langle A \rangle_E$, off-diagonal elements A_{mn} are related to the *time evolution* of the counterpart classical system, as captured by the correlation function $C_A(t; E)$. This is sensible, since for an evolving state vector $|\psi(t)\rangle = \sum_n a_n e^{-iE_n t/\hbar}$, the time-dependence in the expectation value $\langle A \rangle_t = \sum_{m,n} a_m^* a_n e^{i(E_m - E_n)t/\hbar}$ appears in off-diagonal terms.

These two results, characterizing both the diagonal and off-diagonal matrix elements of $\hat{A}$, can be encapsulated together in the so-called Eigenstate Thermalization Hypothesis (ETH). This hypothesis, originally proposed in different forms by Deutsch [251] and Srednicki [252], has become central to the study of thermalization in isolated quantum systems [87, 88, 253]. The

standard modern form of the ETH is an ansatz for the matrix elements A_{mn}:

$$A_{mn} = A\left(\overline{E}\right)\delta_{mn} + \frac{1}{\sqrt{\rho\left(\overline{E}\right)}} f_A\left(\Delta/\hbar, \overline{E}\right) R_{mn}. \tag{5.26}$$

As noted by Srednicki, "All the factors in this formula need explanation" [87]. Here, $\overline{E} \equiv \frac{1}{2}(E_m + E_n)$ and $\Delta \equiv E_n - E_m$, and the functions $A(E)$ and $f_A(\omega, E)$ are real, smooth functions of their arguments. Without loss of generality, $f_A(\omega, E)$ may be taken to be a positive, even function of ω. Finally, the factor R_{mn} is a complex number satisfying $R_{nm} = R_{mn}^*$, which, when averaged in the manner of (5.23), yields $\overline{R_{mn}} = 0$ and $\overline{|R_{mn}|^2} = 1$. An operator $\hat{A}$ is said to satisfy the ETH if its matrix elements can be expressed in this form.

The generalization of Shnirelman's theorem (5.22) ensures that the ETH is valid for the diagonal elements A_{nn} if we choose $A(E) = \langle A \rangle_E$, since the second term in (5.26) goes to zero in the semiclassical limit (recall that $\rho(E) \approx \Sigma(E)/h^d$). This accounts for the term Eigenstate *Thermalization* Hypothesis: Every eigenstate expectation value A_{nn} encodes the microcanonical or thermal average $\langle A \rangle_E$. Meanwhile, for the off-diagonal elements, if we average the ETH ansatz over nearby m and n, Wilkinson's estimate (5.23) allows us to identify $f_A(\omega, E)^2 = S_A(\omega; E)/h$. In this sense, for quantum chaotic systems the ETH is not really a hypothesis at all, but rather an established result, as long as the operator $\hat{A}$ is obtained by quantizing a classical function $A(z)$. For many other systems, including systems without a direct classical analogue (like certain quantum lattice systems), the ETH has been numerically verified; for a summary see [88].

5.4.4 Energy diffusion in slowly driven quantum chaotic systems

To conclude this section, we now provide a review of theoretical and numerical work on energy diffusion in slowly driven quantum chaotic systems. This body of work includes analysis of both "real" quantum chaotic models and random matrix theory models. In these studies, researchers have explored the semiclassical limit, compared the results of different choices of RMT models, and investigated the difference between energy absorption in quantum chaotic and integrable systems. Particular attention has been paid to how these quantum chaotic systems correspond (or do not correspond) to their classical counterparts, adiabatically driven classical chaotic systems. As briefly discussed in Chapter 2, Section 2.7, these classical systems have also been studied with a energy diffusion description. Note that in this section, we restrict our attention to quantum systems which are chaotic even in the *absence* of driving, as opposed to systems like the kicked rotor [13, 139, 254], in which chaos is *induced* by an external drive.

By slowly driven quantum system, we mean a quantum system with a slowly time-dependent Hamiltonian $\hat{H}(t)$, with time-dependent eigenenergies $E_n(t)$ and eigenstates $|n,t\rangle$. In such systems, it is common to identify the system's energy with $\hat{H}(t)$, rather than with the time-averaged Hamiltonian.[11] If we write such a system's state vector as $\sum_n c_n(t)|n,t\rangle$, then the resulting expression $\langle H(t)\rangle_t = \sum |c_n(t)|^2 E_n(t)$ for the energy expectation value tells us that the system's energy can change in two ways: By changes in the populations $|c_n(t)|^2$ (i.e., energy level "transitions"), or changes in the energy levels $E_n(t)$. Here, the word "slowly" can refer to at least two things. On one hand, it could mean that the system is being driven at an adiabatic or approximately adiabatic rate, in the sense of the quantum adiabatic theorem. This theorem states

[11] Of course, these two definitions of energy may coincide at specific times. For example, for the time-periodic Hamiltonian $\hat{H}(t) = \hat{H}_0 + \hat{V}\cos(\omega t)$, $\hat{H}_0$ and $\hat{H}(t)$ are equal at $t = T/2, 3T/2, 5T/2\ldots$

that for sufficiently slow driving, if the system of interest is initialized in the state $|n, 0\rangle$ at $t = 0$, then it approximately remains in the state $|n, t\rangle$ throughout its evolution (up to a phase factor) [131]. Therefore, changes in the system's energy are dominated by changes in the $E_n(t)$'s, at least for short times. Let us refer to the range of driving speeds, where the adiabatic theorem is approximately applicable, as the "quantum adiabatic" regime. On the other hand, the drive may be faster than quantum adiabatic driving, but still slow relative to some classical timescale. In particular, suppose that the drive is slow enough that for the corresponding classical system, the *classical* adiabatic invariant is nearly conserved [98]. For these driving speeds, although the system's energy evolution is still slow in a classical sense, probability can flow quickly between the populations $|c_n(t)|^2$. We refer to this range of speeds, which is quantum mechanically fast but classically nearly adiabatic, as the "classically slow" regime. Both the quantum adiabatic and classically slow regimes are studied in the work that we now discuss.

For models of slowly driven quantum chaotic systems, diffusive evolution of energies has been observed in both of the regimes just mentioned. To understand this diffusion process, researchers have commonly taken two different routes: (a) Approximation of the system with a RMT model, followed by theoretical or numerical analysis of this model, and (b) numerical approximation of the exact dynamics under the Schrodinger equation. Under the umbrella of approach (a), a variety of Hamiltonians have been considered. These include: Hamiltonians constructed from matrices sampled from the GOE [255–257], Hamiltonians selected from a random matrix ensemble that depends on a parameter, the value of which determines the degree of chaoticity of the Hamiltonian [258, 259], and Hamiltonians with random terms sampled so as to match Wilkinson's semiclassical result (5.23) [117]. Meanwhile, in the vein of approach (b), a number of different models have been investigated, including chaotic billiard systems

[260, 261], the classically chaotic Pullen-Edmonds oscillator [262], and spin-$1/2$ chains that have been shown to have random matrix statistics [263, 264].

The results gathered from studying the models just listed, from both categories (a) and (b), are varied and impossible to fully summarize in just a few paragraphs. However, with respect to our aim of applying the classical energy diffusion description in Chapter 2 to quantum systems, a few salient lessons from these models stand out as especially relevant. First, the distinction between the quantum adiabatic regime and the classically slow regime manifests prominently at the level of the energy diffusion description. Both theoretical treatments and numerical experiments reveal that the rate of energy diffusion depends strongly on which regime is being considered [105, 114, 255, 265–267]. For example, Wilkinson demonstrated that for a class of random matrix models, the energy diffusion coefficient scales with a different power of the driving rate in these different regimes [265, 266]. Second, the semiclassical limit and the slow driving limit are often non-commuting [114, 267, 268]. On one hand, if the driving speed is reduced towards zero at fixed $\hbar$, one expects that the quantum adiabatic regime will be ultimately reached. On the other hand, for a fixed driving speed, taking $\hbar$ to zero generally results in the failure of the quantum adiabatic theorem. These two limits interact in various ways in different random matrix models. Third, slowly driven quantum chaotic systems can sometimes exhibit *dynamical localization*, meaning that the evolution of the system in energy space is ultimately bounded, in contrast to the indefinite energy absorption predicted by the energy diffusion description [258, 264]. This is similar in spirit to dynamical localization in systems like the quantum kicked rotor [254, 269], where this phenomenon has been investigated in detail. Finally, random matrix models can sometimes fail to describe certain important aspects of quantum chaotic systems, particularly those features which are related to the more

"regular" aspects of the corresponding classical motion. For example, numerical simulations of a quantum Bunomovich stadium billiard by Wisniacki and Vergini provide evidence that associated random matrix models do not account for the semiregular "bouncing ball" modes (see Figure 5.4) observed in the classical stadium [260]. Meanwhile, Elyutin and Rubtsov argue that certain non-diffusive elements of a quantum chaotic system's energy evolution may fail to be reproduced in a random matrix model which neglects correlations between matrix elements (for example, the model described in Section 5.5) [262].

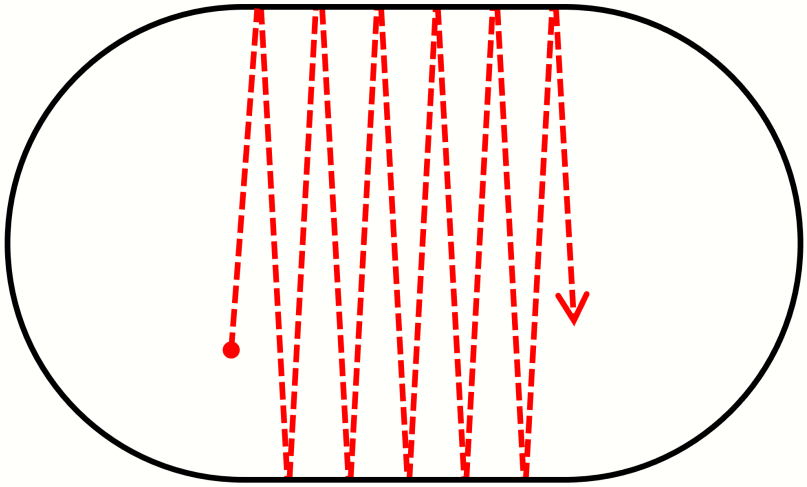

Figure 5.4: A bouncing ball mode in the Bunimovich stadium billiard. During this portion of a particle's trajectory, the particle's motion appears highly regular and non-chaotic.

All of these findings have potential implications for the study of quantum chaotic systems under *rapid* periodic driving. For example, the interaction between the slow driving limit and the semiclassical limit may be mirrored by a similar clash between the semiclassical and rapid driving limits. Alternatively, for some rapidly driven systems, dynamical localization may take place, especially if the Floquet-Magnus expansion for the system converges (see the discussion in Section 5.3). Because of these potential connections and others, the body of work discussed in this section is an ideal starting ground for thinking about quantum analogues to the classical

energy diffusion model described in Chapter 2.

5.5 Two models for energy absorption in periodically driven quantum chaotic systems

We conclude this chapter by describing two potential models for quantum chaotic systems under periodic driving, which may provide insight into energy absorption and diffusion in such systems. The first is a random matrix model, similar to some of the models for slowly driven quantum chaotic systems discussed in Section 5.4.4. This model is constructed so as to satisfy the BGS conjecture and the ETH. The second is a quasiclassical model, discussed elsewhere in the literature on energy diffusion [114, 117], which is based on two key assumptions: The validity of Fermi's golden rule for a time-dependent perturbation $\hat{V}\cos(\omega t)$, and the chaotic, ergodic nature of the quantum system's classical counterpart. Under these assumptions, the energy evolution of the system takes the form of a series of random energy jumps $E \to E \pm \hbar\omega$, which approaches a process of energy diffusion as the jump size becomes small in the semiclassical limit. The energy drift and diffusion coefficients in this model coincide with the classical results (2.22) and (2.20) as $\hbar$ approaches zero.

5.5.1 A periodically driven random matrix model

First, we describe a random matrix model, which is meant to serve as model for the quantum analogue of the classical systems discussed in Chapter 2. As discussed in Section 5.2, consider a quantum system with the Hamiltonian $\hat{H}(t) = \hat{H}_0 + \hat{V}\cos(\omega t)$, the quantized version of the monochromatic driving Hamiltonian in Chapter 2. If we substitute the form

$|\psi(t)\rangle = \sum c_n(t)e^{-iE_nt/\hbar}|n\rangle$ into the Schrodinger equation (5.1), and then take the inner product of the result with the eigenvector $|m\rangle$, we obtain

$$i\hbar\frac{dc_m}{dt} = \cos(\omega t)\sum_n V_{mn}e^{i(E_m-E_n)t/\hbar}c_n, \tag{5.27}$$

where $V_{mn} \equiv \langle m|\hat{V}|n\rangle$. This set of differential equations is mathematically equivalent to the Schrodinger equation.

Let us suppose that over a time interval of interest, the probability for the system to have an energy outside of some range $[E_{\min}, E_{\max}]$ is negligible, so that $c_n \approx 0$ for E_n outside of $[E_{\min}, E_{\max}]$. In this case, we can restrict our attention to c_n's such that $E_n \in [E_{\min}, E_{\max}]$, and our possibly infinite-dimensional system of differential equations becomes finite. Then, to solve these equations, we need two things: The energy levels $E_n \in [E_{\min}, E_{\max}]$, and the associated matrix elements V_{mn}. In principle, these could be obtained by diagonalizing $\hat{H}_0$, but we know that this is a nontrivial exercise for a quantum chaotic system. However, the previous discussion of RMT and the ETH suggests a natural way to model these quantities.

First, let us think about the energy eigenvalues E_n. Suppose that we have selected our interval $[E_{\min}, E_{\max}]$ such that $E_{\min}$ is an eigenvalue: Label this energy level E_0. What is the location of the next eigenvalue, E_1? Assuming for simplicity that the system possesses time-reversal symmetry, the BGS conjecture implies the distribution of normalized eigenvalue spacings of $\hat{H}_0$ should match the Wigner-Dyson distribution $f_{WD}(\varepsilon)$, the spacing distribution for a matrix sampled from the GOE. Therefore, instead of attempting to find the true value of E_1, we can model the eigenvalue spectrum by sampling a normalized spacing ε from $f_{WD}(\varepsilon)$, multiplying it by the local mean level spacing $1/\rho(E_0) \approx h^d/\Sigma(E_0)$ to get the corresponding

unnormalized spacing, and then setting the next energy level to be $E_1 = E_0 + \varepsilon/\rho(E_0)$. We can then sample the next level spacing in the same way, to obtain E_2, and we can continue generating energy levels in the same way until we surpass the energy $E_{\max}$. In this way, we will have constructed a model energy spectrum which both satisfies the BGS conjecture, and which has the proper semiclassical density of states $\rho(E) \approx \Sigma(E)/h^d$. This method of course assumes that the classical density of state $\Sigma(E)$ is known.

As for the required matrix elements V_{mn}, we can model these with the help of the ETH ansatz. If we replace A by V in the ETH ansatz (5.26), and make use of the relations $\rho(E) = \Sigma(E)/h^d$, $V(E) = \langle V \rangle_E$, and $f_V(\omega, E)^2 = S_V(\omega; E)/h$, we have

$$V_{mn} = \langle V \rangle_{\overline{E}} \, \delta_{mn} + \sqrt{h^{d-1} \frac{S_V\left(\Delta/\hbar, \overline{E}\right)}{\Sigma\left(\overline{E}\right)}} R_{mn}. \tag{5.28}$$

Given this expression, if the classical functions $\Sigma(E)$, $\langle V \rangle_E$, and $S_V(\omega; E)$ are known, then the only thing left to calculate is the quantities R_{mn}, which can be thought of as the elements of a matrix $\hat{R}$. Now, for a system with time-reversal symmetry, the basis of eigenvectors $|n\rangle$ can often be selected such that the V_{mn}'s are purely real [88]. In this case, a simple choice is to take $\hat{R}$ to be a matrix sampled from the GOE, as defined in (5.20) in Section 5.4.1. Note that a typical sample from the GOE is guaranteed to satisfy the previously mentioned conditions $\overline{R_{mn}} = 0$ and $\overline{|R_{mn}|^2} = \overline{R_{mn}^2} = 1$.

If the energy levels E_n and matrix elements V_{mn} are generated in this way, the system of equations (5.27) is then fully defined, and can in principle be integrated numerically. In principle, if the requisite classical quantities $\langle V \rangle_E$, $S_V(\omega; E)$, and $\Sigma(E)$ can be computed, this model could be used to probe the applicability of the classical energy diffusion description in Chapter 2 to

quantum chaotic systems under rapid periodic driving. Presently, we are attempting to implement this model for a periodically driven particle in a two-dimensional clover billiard, which was numerically simulated in a classical context in Chapter 3, Section 3.5 (this is a driven standard billiard in the language of Chapter 3). The classical Hamiltonian for this system is $H(z,t) = p_x^2/2m + p_y^2/2m - Fx\cos(\omega t)$, where (x,y) and (p_x,p_y) are position and momentum coordinates, and where F is a constant. This system has several simplifying properties which make the random matrix model relatively easy to construct. First, $\Sigma(E)$ is independent of energy and equal to $\Sigma(E) = 2\pi mA$, where A is the billiard area. Second, the reflection symmetry of the billiard implies that $\langle V\rangle_E = -F\langle x\rangle_E = 0$. Finally, the inertial nature of motion in an undriven standard billiard implies that for every classical trajectory at a given energy, there is another trajectory with unit energy which traces out the same path in space, but at a different speed. As a consequence of this time-scaling symmetry, it can be shown that the power spectrum $S_V(\omega;E) = F^2 S_x(\omega;E)$ satisfies the relation $S_x(\omega;E) = S\left(\omega/\sqrt{E};1\right)/\sqrt{E}$. Therefore, to obtain $S_x(\omega;E)$ for any energy, it suffices to compute it for the single energy $E = 1$.

Now, this random matrix model may not capture all of the relevant features of a given quantum chaotic system. In this case, one can attempt to add nuance to the model in various ways. For example, statistical correlations can be introduced, either between successive energy level spacings, or between the elements of the matrix $\hat{V}$. Of course, in the end, even if such features are included, the ultimate test of a random matrix model is still comparison with the original quantum chaotic system.

5.5.2 The Fermi's golden rule model of energy diffusion

We now review a quasiclassical model of energy absorption in quantum chaotic systems, based on Fermi's golden rule, which yields the classical energy diffusion description in the semiclassical ($\hbar \to 0$) limit. As with the random matrix model just discussed, we take the system's Hamiltonian to be $\hat{H}(t) = \hat{H}_0 + \hat{V}\cos(\omega t)$, where $\hat{H}_0$ and $\hat{V}$ are obtained by quantizing the corresponding observables in Chapter 2. We would like to understand the evolution of this system's energy distribution, where we identify $\hat{H}_0$ as the system's energy operator, with associated eigenvalues E_n and eigenstates $|n\rangle$. If the drive $\hat{V}\cos(\omega t)$ can be treated as weak, then a common way to model this evolution is via Fermi's golden rule, which can be derived in the context of first-order time-dependent perturbation theory. Using rough quasiclassical language, Fermi's golden rule tells us that transitions between energy eigenstates of $\hat{H}_0$ proceed in discrete jumps of $\pm\hbar\omega$, with transition rates expressible in terms of the matrix elements of $\hat{V}$ in the eigenbasis of $\hat{H}_0$.

Motivated by this picture of energy transitions, let us divide the energy axis into a series of intervals of equal size $\hbar\omega$. We label each interval by an integer index $k = 0, 1, 2 ...$, and let $E^k \equiv k\hbar\omega$ define the center of the k^{th} interval. Each of these intervals corresponds to a coarse-grained energy state of the system. We now model the system's energy evolution in terms of classical-like stochastic transitions between these states (see Figure 5.5). More precisely, we define a continuous-time Markov jump process [93, 94] on the set of energy states k, with the transition rate $\Gamma_{k,k\pm1}$ between neighboring states k and $k \pm 1$ provided by Fermi's golden rule [131, 179]:

$$\Gamma_{k,k\pm1} = \frac{\pi}{2\hbar}\overline{|V_{mn}|^2}\rho\left(E^{k\pm1}\right). \tag{5.29}$$

As in the random matrix model just discussed in Section 5.5.1, $\rho(E)$ is the average density of states of the undriven system, and $V_{mn} \equiv \langle m|\hat{V}|n\rangle$ is a matrix element connecting the eigenstates $|m\rangle$ and $|n\rangle$. Here, the average $\overline{|V_{mn}|^2}$ is similar to the average (5.23) in Section 5.4, except we are averaging over a narrow range of states n with $E_n \approx E_m \pm \hbar\omega$, and then averaging over all m in the k^{th} interval. $\Gamma_{k,k\pm1}$ is the probability per unit time that the system will transition to the state $k \pm 1$, given that it is in the state k. Assuming that the evolution of the system on this set of states is Markovian (i.e., the probability of a transition only depends on the current state of the system, and not previous states), these transition rates fully specify the stochastic dynamics of the system.

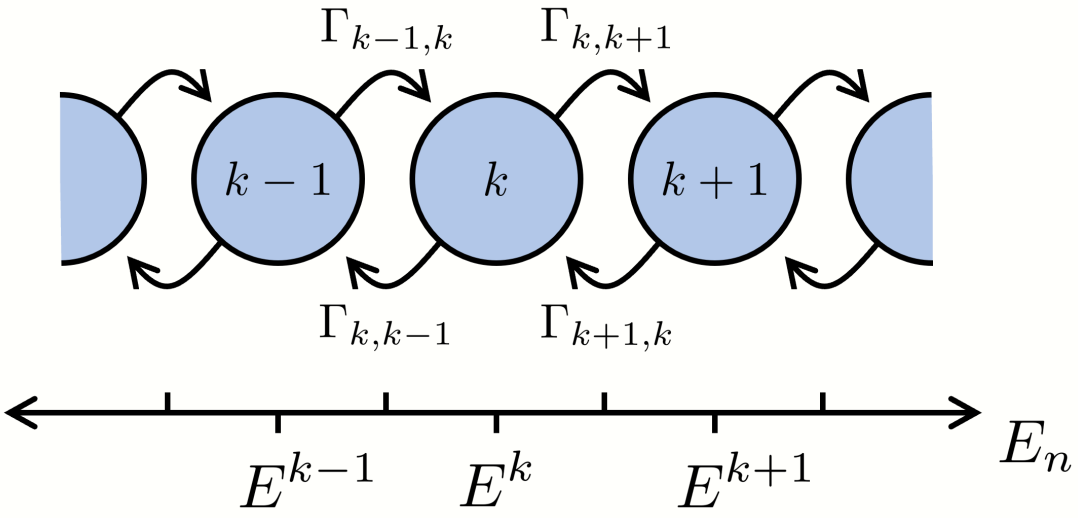

Figure 5.5: Diagram of the Markov jump model for the quantum evolution of the system. Each coarse-grained energy state k, represented by a blue circle, corresponds to a range of the energy axis of size $\hbar\omega$, centered at $E^k = k\hbar\omega$. The rate of stochastic jumping between these states is specified by the transition rates $\Gamma_{k,k\pm1}$, given by (5.29).

We pause to note that, as with any quantum jump model of this type, we are *not* claiming

that the system actually moves through a series of energy states k which are localized in energy space. Underneath this quasiclassical model, the evolution is still fundamentally quantum mechanical, and the quantum state may be spread out in a coherent superposition of many energy eigenstates at any given moment. Rather, the assumption is that despite the quantum character of the underlying dynamics, the *energy distribution* $\eta^Q(E,t)$ (coarse-grained over the energy spacing $\hbar\omega$) nevertheless evolves in the same way as the energy distribution for an ensemble of classical-like systems, which evolve in the discrete space of states k in accordance with the transition rates (5.29). An individual realization of this random process, given by a particular progression through the states k, has no direct physical meaning, since the system does not really evolve through such states. However, thinking about the quantum evolution of the system in terms of this counterpart stochastic process will be useful for understanding how diffusive energy evolution emerges in the quantum context.

What is the classical limit of this Markov jump model, as $\hbar$ approaches zero? Well, assuming that the undriven system's classical counterpart is chaotic and ergodic, we may use Wilkinson's semiclassical result (5.23) in Section 5.4 to approximate the average $\overline{|V_{mn}|^2}$ as $\overline{|V_{mn}|^2} \approx h^{N-1} S_V\left(\omega; E^k\right) / \Sigma(E^k)$.[12] $S_V(\omega; E)$ is the classical microcanonical power spectrum for the phase space function $V(z)$; note that this may be related to $S(\omega; E)$ (the power spectrum for $\dot{V}(z)$) via $S(\omega; E) = \omega^2 S_V(\omega; E)$.[13] Upon substituting this estimate for $\overline{|V_{mn}|^2}$ into the Fermi's golden rule rates (5.29), and invoking Weyl's law $\rho(E) \approx \Sigma(E)/h^d$, we obtain

[12] Wilkinson's formula actually gives the slightly more accurate estimate $\overline{|V_{mn}|^2} \approx h^{N-1} S_V\left(\omega; E^k + \hbar\omega/2\right) / \Sigma\left(E^k + \hbar\omega/2\right)$. However, when we ultimately take the classical limit of the energy diffusion coefficient in this model ((5.31)), the corrections included by using this better approximation vanish, so here we neglect them from the start for simplicity.

[13] The relation $S(\omega; E) = \omega^2 S_V(\omega; E)$ follows from the fact that the autocorrelation function of $\dot{V}(z)$ is minus the second time derivative of the autocorrelation function of $V(z)$. In Fourier space, this derivative corresponds to multiplication by $(i\omega)^2 = -\omega^2$.

$$\Gamma_{k,k\pm1} = \frac{S(\omega; E^k)}{4(\hbar\omega)^2}. \tag{5.30}$$

Given these semiclassical Fermi's golden rule rates, we can now think about how a diffusive evolution of energies arises from the random walk model. For small enough $\hbar$, each energy jump of size $\hbar\omega$ will be very small relative to any classical energy scale. In particular, $\hbar\omega$ will be small relative to the scale over which $S(\omega; E)$ changes significantly as a function of E. It follows that for sufficiently small $\hbar$, the transition rates (5.30) will be almost constant over a large number of successive energy states k. As a result, whenever the system jumps from a state k to $k' = k \pm 1$, the subsequent jump will be essentially uncorrelated with it, since the transition rate in the new state is almost the same regardless of whether the new state is $k' = k + 1$ or $k' = k - 1$. Moreover, the near-constancy of the transition rates means that these jumps will have nearly identical statistics. Thus, as in the classical case, we see that the energy evolution of the system over an appropriate time interval appears as a sequence of many independent, statistically identical energy changes, resulting in a process of diffusion in energy space. This diffusive description, which is continuous both in time and in energy space, is valid on a coarse-grained timescale much longer than the typical time between quantum jumps, and on a coarse-grained energy scale much larger than $\hbar\omega$.

As a result, the evolution of the coarse-grained energy distribution is governed by a Fokker-Planck equation, just like (2.11) in Chapter 2. It now remains to determine the drift and diffusion coefficients associated with this equation. We proceed just as we did in the classical case. The quantum diffusion coefficient $g_2^Q(E, \omega)$ is given by $\mathrm{Var}(E)/\Delta t$, where $\mathrm{Var}(E)$ is the variance acquired by the energy distribution after a short time Δt, given that the system was initialized with the energy $E = E^k$. To calculate this, divide the time interval

from $t = 0$ to $t = \Delta t$ into $N \gg 1$ subintervals of equal duration $\delta t = \Delta t/N$. Then, given that the system is initialized in the state k, consider the energy change ΔE over this interval as a sum of N changes $\delta E_1, \delta E_2 \ldots \delta E_N$ associated with each subinterval. For small δt, each of these subinterval changes is either $+\hbar\omega$ or $-\hbar\omega$, with approximately equal probability $\Gamma_{k,k+1}dt \approx \Gamma_{k,k-1}dt$, or zero with approximate probability $1-\Gamma_{k,k+1}dt-\Gamma_{k,k-1}dt$. It follows that the variance of each subinterval change is $(\Gamma_{k,k+1} + \Gamma_{k,k-1})(\hbar\omega)^2 dt \approx 2\Gamma_{k,k+1}(\hbar\omega)^2 dt$. Since these subinterval changes are statistically independent, the variance of $\Delta E = \sum_{i=1}^{N} \delta E_i$ is simply $\mathrm{Var}(\Delta E) = \sum_{i=1}^{N} \mathrm{Var}(\delta E_i) = 2\Gamma_{k,k+1}(\hbar\omega)^2 \Delta t$. Since $\mathrm{Var}(\Delta E) = \mathrm{Var}(E)$, substituting (5.30) into this expression yields

$$g_2^Q(E,\omega) = \frac{1}{2} S(\omega; E) = g_2(E,\omega), \tag{5.31}$$

in agreement with the classical result.

In principle, we can calculate the quantum drift coefficient $g_1^Q(E,\omega)$ via a similar computation, though we would need to be careful to account for the small difference in probability between the transitions $k \to k+1$ and $k \to k-1$ (this difference is neglected in (5.30)).[14] Instead, we now obtain $g_1^Q(E,\omega)$ by relating it to $g_2^Q(E,\omega)$ via a fluctuation dissipation relation, as in the classical case. We do so by returning to the exact quantum dynamics; i.e., evolution of the density operator $\hat{\rho}$ under the von Neumann equation (5.5). Note that the identity operator $\hat{I}$ is an unnormalized stationary solution to the von Neumann equation, since the identity operator commutes with all other operators. It follows that the corresponding unnormalized energy distribution should be a stationary solution to the Fokker-Planck equation

[14] This calculation requires the more accurate approximation for $\overline{|V_{mn}|^2}$ given in footnote 12.

(after the appropriate coarse-graining in energy space). Recall from Section 5.2 that for a density operator $\hat{\rho}$, the corresponding energy distribution is $\eta^Q(E) = \sum_n \rho_{nn}\delta(E - E_n)$, where $\rho_{nn} = \langle n|\hat{\rho}|n\rangle$. Thus, for $\hat{\rho} = \hat{I}$, we have the unnormalized energy distribution $\sum_n \delta(E - E_n)$: This is just the undriven system's fine-grained density of states, which after coarse-graining yields $\rho(E)$. Thus, the average density of states $\rho(E) \propto \Sigma(E)$ is a stationary solution to the Fokker-Planck equation. Then, by the same arguments as in Chapter 2, Section 2.4, it follows that the same fluctuation-dissipation relation (2.22) is also valid for the quantum energy diffusion process. Since $g_2^Q(E, \omega) = g_2(E, \omega)$, the fluctuation-dissipation relation implies that $g_1^Q(E, \omega) = g_1(E, \omega)$ as well. The quantum and classical energy diffusion processes are thus mathematically identical.

Of course, the analysis just described has some clear problems. For instance, coherences between different energy eigenstates of the system are effectively ignored (as is often done implicitly in many applications of Fermi's golden rule). Moreover, it is not obvious that the validity of Fermi's golden rule is consistent with the semiclassical limit. This is because Fermi's golden rule is derived in the context of perturbation theory, which naturally assumes small rates of transition between energy states, while by (5.30), the rates predicted by Fermi's golden rule itself diverge as $\hbar$ approaches zero. Other authors have discussed such issues in more detail; see for example [114] and [117]. Despite these limitations, this model is valuable insofar as it highlights an important connection between periodically driven quantum systems and the classical energy diffusion picture.

Chapter 6: Outlook and future work

In this thesis, we have examined energy absorption in periodically driven chaotic systems, both classical and quantum. Although we found the energy diffusion framework extremely useful for characterizing the energy evolution of such systems, many questions concerning the accuracy and range of validity of this model were left unanswered. This is particularly true in the context of periodically driven *quantum* chaotic systems, where our trust in the energy diffusion description is ultimately based on heuristic models like the model described in Chapter 5, Section 5.5.2, and on previous work on slowly driven systems (discussed in Chapter 5, Section 5.4.4). In this chapter, we discuss some possible avenues for future work, which might help to close these gaps in our understanding.

6.1 Further tests of the classical energy diffusion model

In the realm of classical systems, one clear direction for future work is to test the energy diffusion description in additional model systems. In Chapter 3, Section 3.5, we corroborated the energy diffusion model with numerical simulations of a driven particle in a clover-shaped billiard. In some ways, this system is an ideal testing ground for studying energy diffusion. For one, an undriven particle in the clover billiard is mathematically guaranteed to exhibit chaotic and ergodic motion [110]. Moreover, the Fokker-Planck equation for this system is exactly solvable

(see the solution (E.4) and the surrounding discussion in Appendix E). However, the disadvantage of the clover billiard as a model system is that it is decidedly "non-generic" in certain respects, suggesting that it is a significant "inductive leap" to take the numerical simulations of the clover billiard as a validation of the energy diffusion description more generally. Most noticeably, the collisions with the wall correspond to a discontinuous evolution in phase space. This manifests as the characteristic ω^{-2} scaling of the energy drift and diffusion coefficients g_1 and g_2 for billiard systems (see (3.19) and (3.18) in Chapter 3), in contrast to the more rapid decay of these coefficients for smooth systems. In addition, the clover billiard is not a many-body system, in contrast to many of the systems commonly studied in statistical physics and condensed matter.

Beyond single-particle billiards like the clover billiard, several classes of systems suggest themselves as additional test cases for the energy diffusion model. First, one can consider periodically driven many-particle billiards or systems of hard spheres, as described in Chapter 3, Section 3.6. These systems have the advantage that in certain special cases, the associated Fokker-Planck equation admits an exact solution. For example, in the dilute gas of hard spheres analyzed in Section 3.6.4, the coefficients $g_1 \propto E^{1/2}$ and $g_2 \propto E^{3/2}$ scale with energy in the same way as in the clover billiard (since the temperature T in (3.36) is proportional to E). This implies that the solution (E.4) to the clover billiard's Fokker-Planck equation is equally applicable to the dilute hard sphere gas.

Second, certain many-body generalizations of the kicked rotor model [13, 139] may be a viable testing ground for the energy diffusion description. These systems are defined by a chain of N pendula or "rotors" with angular coordinates $\phi_1, \phi_2 \ldots \phi_N$ and corresponding momenta $p_1, p_2 \ldots p_N$, which are coupled together via a Hamiltonian such as:

$$H = \sum_{i=1}^{N} \left[\frac{p_i^2}{2m} - \kappa \cos\left(\phi_{i+1} - \phi_i\right) \sum_{n \in \mathbb{Z}} \delta\left(t - nT\right) \right]. \tag{6.1}$$

The effect of this Hamiltonian is to make adjacent rotors instantaneously "kick" each other at evenly spaced times $t = 0, T, 2T \ldots$. In certain parameter regimes, Floquet prethermalization and diffusion of energy has been observed in such models, and in their quantum mechanical analogues [78, 79, 223–226]. It would be useful to compare these results to the predictions of the energy diffusion model studied in Chapter 2. Note that technically, a system with the Hamiltonian (6.1) cannot satisfy the assumption of ergodicity invoked in this thesis, since the dynamics under the corresponding time-averaged Hamiltonian have a conserved quantity: the total momentum $P = \sum_{i=1}^{N} p_i$. However, this not an essential problem, since if we consider a particular surface of constant P in phase space, and divide this surface into sub-surfaces of constant energy, then it is still possible for the system to evolve ergodically on each of these sub-surfaces.

Finally, one may consider chains of interacting classical spin degrees of freedom, or "Heisenberg spin chains," as a potential testbed for the energy diffusion model. In these models, each of the N spins is described by a unit vector $\mathbf{S}_1, \mathbf{S}_2 \ldots \mathbf{S}_N$, which evolves under the influence of both external magnetic fields and the fields of neighboring spins (this is a noiseless, many-spin version of the model described in Chapter 4, Section 4.3) [172, 173]. Periodic driving in Heisenberg chains may take the form of, for example, periodic modulation of an external magnetic field. Since chaos has been numerically observed in certain spin chains [173, 221, 222], we expect that the energy diffusion model may be relevant to understanding energy absorption in these systems. If so, this would offer another explanation for Floquet prethermalization in these models, which has been both numerically observed and theoretically predicted [41, 44].

6.2 Generalization of the energy diffusion model to systems with a nontrivial high-frequency driving limit

While more work can be done to validate the energy diffusion model as described in Chapter 2, we also anticipate that this model may be generalized in some respects. One important possible generalization would be to systems with a nontrivial high-frequency driving limit, as described in works such as [12]. In the systems studied in the present thesis, the limit of high-frequency driving is taken at fixed driving amplitude. In this limit, the driven evolution of the system approaches the undriven motion, which is governed by the time-averaged Hamiltonian: We refer to this as a "trivial" high-frequency limit. However, more interesting limiting procedures are possible. For example, one may consider a situation where as the drive frequency ω approaches infinity, the amplitude of the driving term in the Hamiltonian is made to scale like some power of ω. One famous example where this scaling occurs is in the Kapitza pendulum model [2]. In this system, the fulcrum of a pendulum bob of mass m and fixed length l under the influence of gravity is made to rapidly oscillate in the vertical direction like $A\cos(\omega t)$ (see Figure 6.1). If we take the amplitude A to be proportional to ω^{-1}, it can be shown that this system is described by a Hamiltonian of the form [12]:

$$H = \frac{p^2}{2m} - m\cos\theta\left(\omega_0^2 + \lambda\omega\cos\left(\omega t\right)\right). \tag{6.2}$$

Here, θ is the position coordinate of the pendulum, giving the angular displacement of the pendulum away from the vertical, and p is the corresponding momentum. We take $\theta = 0$ to correspond to the pendulum hanging straight down. ω_0 and λ are constants.

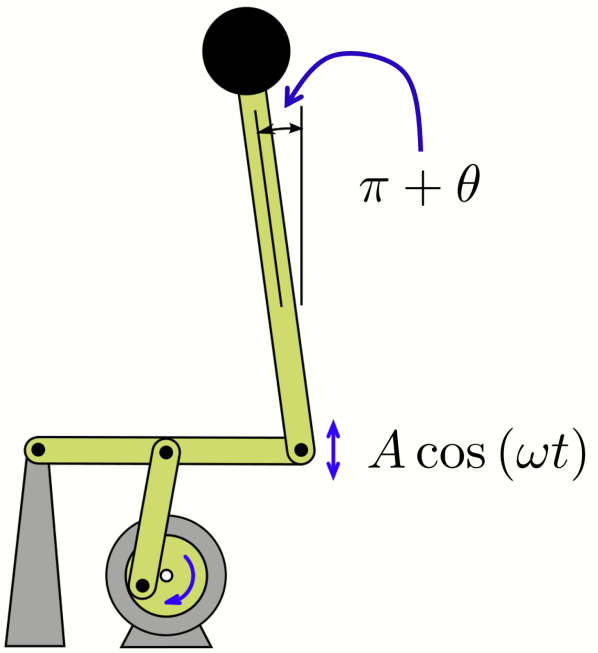

Figure 6.1: Diagram of one mechanism which can realize the Kapitza pendulum. Here, a rotating motor causes a lever arm to oscillate up and down. At the end of this lever is the fulcrum of the pendulum, which oscillates vertically as $A\cos(\omega t)$. This diagram was drawn by Chris Burks, and was taken from Wikipedia.

In this Hamiltonian, the drive term $\propto \omega\cos(\omega t)$ scales linearly with the drive frequency. As a result, as ω approaches infinity, the dynamics of the system do *not* approach the dynamics associated with the time-averaged Hamiltonian $H_0 \equiv p^2/2m - m\omega_0^2\cos\theta$. Rather, in this limit, it can be shown that the system's dynamics are governed by an effective infinite-frequency Hamiltonian [12]:

$$H_{\text{eff}} \equiv \frac{p^2}{2m} - m\omega_0^2\cos\theta + \frac{m\lambda^2}{4}\sin^2\theta \neq H_0. \tag{6.3}$$

Crucially, provided that $\lambda^2 > 2\omega_0^2$, the effective potential $U_{\text{eff}}(\theta) \equiv -m\omega_0^2\cos\theta + m\lambda^2\sin^2\theta/4$ has a local minimum at $\theta = \pi$ (see Figure 6.2), which corresponds to the pendulum being perfectly inverted. This means that in the high-frequency driving limit, this inverted position of

the pendulum becomes stable; this counterintuitive behavior of the Kapitza pendulum is known as dynamical stabilization.

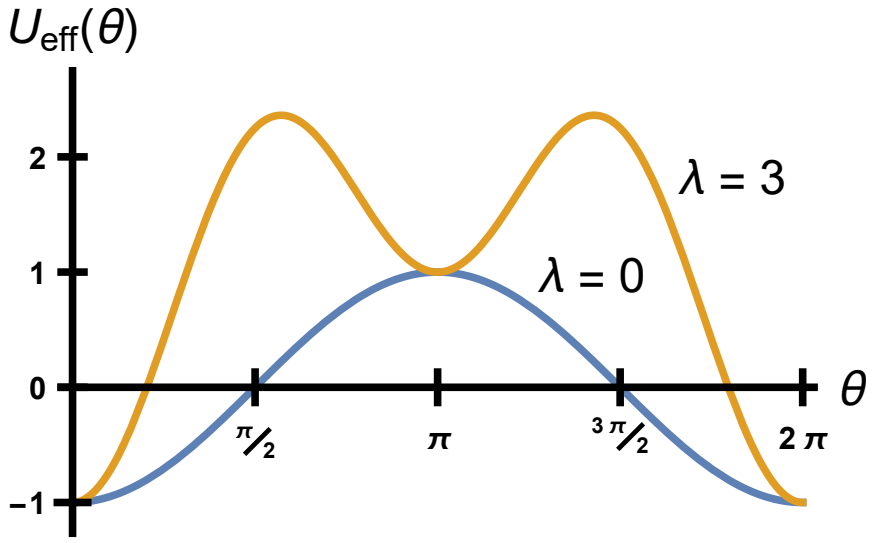

Figure 6.2: Plot of the effective potential $U_{\text{eff}}(\theta)$ for the Kapitza pendulum, for $m = \omega_0 = 1$. For $\lambda = 0$ (blue curve), this is just the time-averaged potential, which has a local maximum at $\theta = \pi$. This value of θ corresponds to the pendulum being inverted, which is an unstable equilibrium. In contrast, for $\lambda = 3 > \sqrt{2}\omega_0 = \sqrt{2}$ (orange curve), $U_{\text{eff}}(\theta)$ has a local *minimum* at $\theta = \pi$, so this equilibrium point is now stable.

How is this connected to the energy diffusion description? Well, under the infinite frequency Hamiltonian (6.3), the dynamics of the pendulum will *not* be chaotic, since the pendulum only has a single degree of freedom. However, one can imagine an analogous periodic driving protocol for a system with ≥ 2 degrees of freedom, wherein the driving amplitude is made to scale proportional to some power of ω; for examples, see [12, 218, 270]. Suppose that for such a system, an infinite-frequency effective Hamiltonian H_{eff} can be obtained, and that the dynamics under this Hamiltonian are chaotic and ergodic. For large but finite driving frequencies, we anticipate that the dynamics of the system will be closely approximated by evolution under H_{eff}, plus a small perturbation. This suggests that the dynamics of the system might be described by a process of energy diffusion, where the energy of the system is now associated with the

infinite-frequency Hamiltonian H_{eff}, rather than the time-averaged Hamiltonian. Here, it is the chaotic, ergodic nature of motion under H_{eff} which induces the decay of correlations necessary for diffusive evolution.

One interesting feature of this version of the energy diffusion model is that prethermalization occurs with respect to the Hamiltonian H_{eff}. This is consistent with certain Floquet prethermal model systems, where prethermalization has been observed to occur with respect to a Hamiltonian other than the time-averaged Hamiltonian [218, 270]. Of course, this potential generalization of the energy diffusion model has only been roughly sketched here. More work needs to be done to understand whether such a generalization is valid, and if so, to determine the associated energy drift and diffusion coefficients.

6.3 Testing the energy diffusion description in quantum chaotic systems

Finally, we reemphasize that more work needs to be done to understand the applicability of the classical energy diffusion description to periodically driven quantum chaotic systems. A full account of this potential quantum-classical correspondence would describe both the range of validity of the energy diffusion model in quantum systems, and the quantum corrections to this classical description. Probing these connections can be done with both theoretical and numerical methods.

First, a number of theoretical semiclassical methods could be employed to explore the relationship between periodically driven quantum systems and the energy diffusion description. In Chapter 5, Section 5.4 we already discussed the use of random matrix theory to this end. If the validity of the BGS conjecture is assumed, then the tools of random matrix theory can be

employed to model the properties of the system's Hamiltonian. However, even without random matrix theory, semiclassical techniques can be used to approximately describe the evolution of quantum systems in terms of classical dynamics. For example, the van Vleck formula provides a semiclassical expression for the quantum evolution operator, which should remain valid for short times at least [271]. Regardless of the specific approach taken, one important object to study in an analysis of energy diffusion in quantum systems is the Floquet Hamiltonian $\hat{H}_F$, and its associated Floquet-Magnus expansion. As discussed previously in Chapter 5, Section 5.3, the convergence properties of the Floquet-Magnus expansion are closely tied to the system's ability to absorb energy from the drive.

Second, numerical simulations can offer another perspective on the possibility of quantum-classical correspondence. One numerical approach is to simulate a random matrix model of a periodically driven quantum chaotic system, like the one constructed in Chapter 5, Section 5.5.1. Alternatively, for a given "real" quantum chaotic system, one can attempt to compute the actual energy levels and matrix elements needed to approximately solve the Schrodinger equation. In either approach, solutions to the Schrodinger equation (and the resulting energy distribution) could be compared to the predictions of the energy diffusion description. Also, the Floquet Hamiltonian $\hat{H}_F$ (or equivalently, the Floquet operator $\hat{U}_F$) could in principle be calculated; diagonalizing this operator would provide important information about the system's evolution. Of course, regardless of the numerical method pursued, difficulties arise in the semiclassical limit, where the density of states $\rho(E) \approx \Sigma(E)/h^d \propto h^{-d}$ becomes very large. In this regime, many energy levels of the system need to be simulated, leading to extremely large matrix computations.

Appendix A: Generalization to non-monochromatic drives

Here, we generalize the calculation of the diffusion coefficient g_2 in Chapter 2 for non-monochromatic periodic drives $V(z, t/T)$.

A general periodic driving term may always be decomposed as a Fourier series with fundamental frequency ω:

$$V(z, t/T) = \sum_{k \in \mathbb{Z} \setminus \{0\}} V_k(z) e^{ik\omega t}. \tag{A.1}$$

Here, since $V(z, t/T)$ is a real-valued function, the phase space functions $V_k(z) \equiv V_k$ must satisfy the relation $V_{-k} = V_k^*$. The sum runs over the set of all integers excluding zero, since $V(z, t/T)$ has zero time average over a period by definition.

The instantaneous rate of change of the system's energy is given by (2.4). Substituting the decomposition (A.1) into this expression yields

$$\frac{dE}{dt} = -\sum_{k \in \mathbb{Z} \setminus \{0\}} \dot{V}_k(z) e^{ik\omega t}, \tag{A.2}$$

where we have defined $\dot{V}_k(z) \equiv \dot{V}_k \equiv \{V_k, H_0\}$.[1] If we integrate this expression over a time Δt, we can use it to compute $\mathrm{Var}(E) = \langle (\Delta E)^2 \rangle - \langle \Delta E \rangle^2$, the energy variance acquired by an ensemble of trajectories over this time (this is analogous to (2.16)):

[1] Note that $\dot{V}_k$ is generally *not* equal to the time derivative of V_k, but they do coincide for the undriven system.

$$\mathrm{Var}(E) = \sum_{k,l\in\mathbb{Z}\setminus\{0\}} \int_0^{\Delta t} dt \int_0^{\Delta t} dt'\, e^{-ik\omega t + il\omega t'} C_{neq}^{(kl)}(t,t';E_0). \tag{A.3}$$

Here, $C_{neq}^{(kl)}(t,t';E_0) \equiv \langle \dot{V}_k^*(z_t)\dot{V}_l(z_{t'})\rangle - \langle \dot{V}_k^*(z_t)\rangle\langle \dot{V}_l(z_{t'})\rangle$ is a nonequilibrium correlation function, and $\langle ...\rangle$ denotes an average over a microcanonical distribution of initial conditions with energy E_0.

Just like in the monochromatic case, we now approximate these correlation functions $C_{neq}^{(kl)}(t,t';E_0)$ by their equilibrium counterparts, defined in terms of the undriven trajectories z_t^0:

$$C^{(kl)}(s;E_0) \equiv \langle \dot{V}_k^*(z_0^0)\dot{V}_l(z_s^0)\rangle - \langle \dot{V}_k^*(z_0^0)\rangle\langle \dot{V}_l(z_s^0)\rangle. \tag{A.4}$$

If we make this substitution in (A.3), and use the variable of integration $s \equiv t' - t$ instead of t', we have

$$\mathrm{Var}(E) = \sum_{k,l\in\mathbb{Z}\setminus\{0\}} \int_0^{\Delta t} dt \int_{-t}^{\Delta t - t} ds\, e^{i(l-k)\omega t + il\omega s} C^{(kl)}(s;E_0). \tag{A.5}$$

Now, consider the (k,l) term in this sum, which we denote by I_{kl}. If we reverse the order of integration, the outer integral over s will run from $-\Delta t$ to Δt, and the inner integral over t will run over some subset of the range $[0,\Delta t]$, determined by the value of s. The inner integral is a simple integral of $e^{i(l-k)\omega t}$, which for $l \neq k$ is bounded in magnitude by $2/(|l-k|\omega)$. The magnitude of I_{kl} is thus bounded by

$$|I_{kl}| \leq \frac{2}{|l-k|\omega} \int_{-\Delta t}^{\Delta t} ds\, |C^{(kl)}(s;E_0)|, \tag{A.6}$$

where we have invoked the triangle inequality $|\int_a^b dx\, f(x)| \leq \int_a^b dx\, |f(x)|$ for integrals.

As in the monochromatic case, we are interested in $\Delta t \gg \tau_C$, since the system will only exhibit energy diffusion on timescales much longer than τ_C, the intrinsic correlation time for the system. For $s \gg \tau_C$, the correlation function $C^{(kl)}(s; E_0)$ will be approximately zero. Thus for $\Delta t \gg \tau_C$, we incur little error by setting the range of s in (A.6) to $(-\infty, +\infty)$. (A.6) then becomes a Δt-independent bound on $|I_{kl}|$. Since we are ultimately interested in calculating $g_2(E_0, \omega) = \mathrm{Var}(E)/\Delta t$, this bound tells us that the $l \neq k$ contributions to g_2 can be neglected, since $I_{kl}/\Delta t$ will be very small for large Δt.

Meanwhile, the $l = k$ terms in (A.5) are generally not negligible. For these terms, the integral over t and s can be approximated using the same techniques as was used to evaluate (2.16) in the monochromatic case; details may be found in references such as [124]. If we make these approximations, and relabel E_0 as E, our final expression for $g_2(E_0, \omega) = \mathrm{Var}(E)/\Delta t$ becomes

$$g_2(E, \omega) = 2 \sum_{k=1}^{\infty} S^{(k)}(k\omega; E). \tag{A.7}$$

where

$$S^{(k)}(\nu; E) = \int_{-\infty}^{\infty} dt\, e^{-i\nu t} C^{(kk)}(t; E) \tag{A.8}$$

is the power spectrum of $\dot{V}_k(z_t^0)$, which is equal to the Fourier transform of the the autocorrelation function $C^{(kk)}(t; E) = \langle \dot{V}_k^*(z_0^0) \dot{V}_k(z_t^0) \rangle - \langle \dot{V}_k^*(z_0^0) \rangle \langle \dot{V}_k(z_t^0) \rangle$ by the Wiener-Khinchin theorem [125]. Note that the sum over k now only runs over positive integers. This is because the k term $S^{(k)}(k\omega; E)$ and the $-k$ term $S^{(-k)}(-k\omega; E)$ can be shown to be equal, by invoking the relation

$V_{-k} = V_k^*$. Therefore we have just included the positive k terms, and then doubled the result.

Finally, we can quickly confirm that this reduces to the result (2.20) for the monochromatic case, when $V(z, t/T) = V(z)\cos(\omega t)$. In this case, we have $V_{\pm 1}(z) = V(z)/2$, and $V_k(z) = 0$ for $k \neq \pm 1$. For this choice of the functions V_k, (A.7) simplifies to (2.20).

Appendix B: Details in the derivation of the fluctuation-dissipation relation

Here, we argue that the quantity in square brackets in (2.21) is zero, which allows us to establish the fluctuation-dissipation relation (2.22) (see Chapter 2, Section 2.4). We do so by identifying this quantity with an unnormalized probability current, which we then show must vanish.

To begin, let us define a probability current J for systems described by the energy diffusion model. For a given solution η, we define:

$$J[\eta](E,t) \equiv -\frac{d}{dt}\int_{E_{\min}}^{E} dE'\,\eta(E',t). \tag{B.1}$$

Here, $E_{\min}$ denotes the minimum possible energy of the system, which may be $-\infty$. By definition, $J[\eta](E,t) \equiv J$ gives the instantaneous rate of flow of probability across the point E in energy space at the time t. Put differently, over a short time interval $[t, t+dt]$, $J[\eta](E)dt$ is the fraction of trajectories in the ensemble which increase from an energy $< E$ to an energy $> E$, minus the fraction which go the other way.

If we move the time derivative in (B.1) under the integral sign, and use the expression for $\partial\eta/\partial t$ furnished by the Fokker-Planck equation (2.11), then we may integrate with respect to E' to obtain

$$J[\eta](E,t) = K[\eta](E,t) - K[\eta](E_{\min},t), \tag{B.2}$$

where we have defined $K[\eta](E,t) \equiv g_1\eta - \frac{1}{2}\partial(g_2\eta)/\partial E$.

In fact, the boundary term $K[\eta](E_{\min},t)$ can be shown to vanish, by way of the construction in Figure B.1. At any given time t, consider a solution η' to the Fokker-Planck equation which is identical to η for E near $E_{\min}$, but which vanishes along with its derivatives near $E = E_{\max}$ (the maximum possible energy of the system, which may be infinite). By construction, we have $K[\eta'](E_{\min},t) = K[\eta](E_{\min},t)$ and $K[\eta'](E_{\max},t) = 0$. Moreover, by conservation of the total probability, we know that $J[\eta'](E_{\max},t)$ must vanish, which implies that $K[\eta'](E_{\max},t) = K[\eta'](E_{\min},t)$ by (B.2). Combining these equalities, we see that the boundary term $K[\eta](E_{\min},t)$ must be zero, and so (B.2) takes the form:

$$J[\eta](E,t) = g_1\eta - \frac{1}{2}\frac{\partial}{\partial E}\left(g_2\eta\right). \tag{B.3}$$

This vanishing of the boundary term is physically plausible, since the instantaneous flow of probability at an energy E should only depend on the behavior of η near E. If this term was nonzero, it would suggest a "nonlocal" probability current from $E_{\min}$ to E (or vice versa), which is inconsistent with the small energy changes predicted by the energy diffusion description.

With the expression (B.3) identified as the probability current, we can return to (2.21) in Chapter 2, Section 2.4. (2.21) now simply tells us that the unnormalized current $J[\Sigma](E)$ is constant as a function of E:

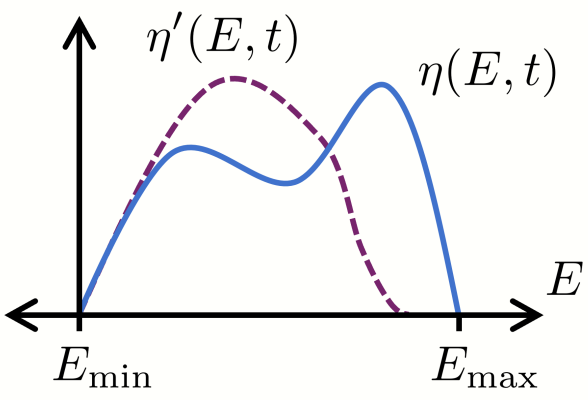

Figure B.1: Construction used to establish the expression (B.3) for the probability current, for a system with a finite range of possible energies. The distribution $\eta'(E,t)$ (dashed purple line) is defined so that it is equal to the distribution $\eta(E,t)$ (solid blue line) around $E = E_{\min}$, and so that it vanishes along with its derivatives near $E = E_{\max}$.

$$0 = -\frac{\partial}{\partial E}\left[g_1\Sigma - \frac{1}{2}\frac{\partial}{\partial E}\left(g_2\Sigma\right)\right] = -\frac{\partial J[\Sigma](E)}{\partial E}. \tag{B.4}$$

We may determine this constant via a construction similar to the one pictured in Figure B.1. Consider a normalized solution to the Fokker-Planck equation $\Sigma'(E,t) \equiv \Sigma'$ which is equal to Σ for energies near $E_{\min}$ at some time t. Such a solution exists as long as the volume of phase space $\Omega(E)$ (see (2.8)) is finite, which we previously assumed. By (B.3), the currents $J[\Sigma](E_{\min})$ and $J[\Sigma'](E_{\min},t)$ are equal. But by the definition of the probability current (B.1), $J[\Sigma'](E_{\min},t)$ must vanish, and so $J[\Sigma](E_{\min})$ is zero as well. Since $J[\Sigma](E)$ is a constant, this means that it must vanish for *all* E: $J[\Sigma](E) = g_1\Sigma - \frac{1}{2}\partial(g_2\Sigma)/\partial E = 0$. Solving this equation for g_1 yields the fluctuation-dissipation relation (2.22).

Appendix C: Details in the calculation of g_2 for billiard systems

In this appendix, we fill in certain technical details of the calculations in Chapter 3, where we derived the expression (3.18) for the energy diffusion coefficient for billiard systems. We start from (3.13) in Chapter 3 (labelled as (C.1) in this appendix), which expresses the energy variance $\mathrm{Var}(\mathcal{E})$ in terms of a sum over collisions with the billiard wall. We argue that correlations between different terms in this sum may be effectively ignored for large ω, allowing us to obtain the simplified expression (3.14) ((C.8) in this appendix). We then further evaluate this quantity in terms of an integral over the billiard boundary, leading to the result (3.15).

First, we reproduce (3.13) here:

$$\begin{aligned}\mathrm{Var}(\mathcal{E}) = 4\omega^{-2}&\left\langle \left[\sum_{k=1}^{N} (\mathbf{F}_k \cdot \hat{\mathbf{n}}_k)\,(\mathbf{v}_k \cdot \hat{\mathbf{n}}_k)\sin(\omega t_k)\right]^2 \right\rangle \\ - 4\omega^{-2}&\left\langle \sum_{k=1}^{N} (\mathbf{F}_k \cdot \hat{\mathbf{n}}_k)\,(\mathbf{v}_k \cdot \hat{\mathbf{n}}_k)\sin(\omega t_k)\right\rangle^2 + O(\omega^{-3}).\end{aligned} \tag{C.1}$$

Let us start at the second term, corresponding to the square of $\langle \Delta\mathcal{E}\rangle$. Defining the shorthand $a_k \equiv (\mathbf{F}_k \cdot \hat{\mathbf{n}}_k)\,(\mathbf{v}_k \cdot \hat{\mathbf{n}}_k)$, we have:

$$\langle \Delta\mathcal{E}\rangle = 2\omega^{-1}\left\langle \sum_{k=1}^{N} a_k \sin(\omega t_k)\right\rangle + O(\omega^{-2}). \tag{C.2}$$

The k^{th} term in this sum depends on a_k and t_k, which are ultimately determined by the initial conditions $(\mathbf{x}_0, \mathbf{v}_0)$ for each particle in the ensemble. Since $(\mathbf{x}_0, \mathbf{v}_0)$ is randomly sampled according to the microcanonical distribution (3.8), a_k, t_k, and N are all random variables. Therefore, we may express the average of each term as an average with respect to $P_k(a_k, t_k, N)$, the joint probability distribution for a_k, t_k, and N. By the rules of conditional probability, $P_k(a_k, t_k, N)$ may be decomposed as

$$P_k(a_k, t_k, N) = P_k(a_k, N) P_k(t_k | a_k, N), \tag{C.3}$$

where $P_k(a_k, N)$ is the joint probability distribution for a_k and N, and $P_k(t_k|a_k, N)$ is the probability distribution for t_k, conditioned on particular values of a_k and N. For the k^{th} term in (C.2), we then compute the average by summing over all possible values of N, and integrating over all values of a_k and t_k:

$$\langle \Delta \mathcal{E} \rangle = 2\omega^{-1} \sum_{N=0}^{\infty} \sum_{k=1}^{N} \int da_k \, P_k(a_k, N) \, a_k \int dt_k \, P_k(t_k | a_k, N) \sin(\omega t_k) + O(\omega^{-2}). \tag{C.4}$$

Recall that the quantities being averaged over are associated with trajectories in an ensemble of *driven* particles. However, for large values of ω, each driven trajectory is only weakly perturbed from its undriven counterpart: The trajectory evolved from the same initial condition $(\mathbf{x}_0, \mathbf{v}_0)$, but with $\mathbf{F}(\mathbf{x}) = \mathbf{0}$. So, to leading order in ω^{-1}, we may replace $P_k(a_k, N)$ with $P_k^0(a_k, N)$, the joint distribution for a_k and N in the absence of driving. Similarly, we replace $P_k(t_k|a_k, N)$ with $P_k^0(t_k|a_k, N)$, the conditional distribution for t_k in the absence of

driving. Importantly, these new undriven distributions are entirely independent of ω, since they are completely determined by the dynamics of the undriven trajectories. Assuming that these undriven distributions differ from their driven counterparts by an amount of order $O(\omega^{-1})$, we obtain:

$$\langle \Delta \mathcal{E} \rangle = 2\omega^{-1} \sum_{N=0}^{\infty} \sum_{k=1}^{N} \int da_k \, P_k^0(a_k, N) \, a_k \int dt_k \, P_k^0(t_k | a_k, N) \sin(\omega t_k) + O(\omega^{-2}). \tag{C.5}$$

Finally, consider the inner integral over t_k. The integrand is the product of $P_k^0(t_k|a_k, N)$, which is independent of ω, and $\sin(\omega t_k)$, an oscillatory function with zero time average. It is straightforward to show that integrals of this form approach zero like ω^{-1} or faster for large ω. Therefore, this integral is of order $O(\omega^{-1})$ for each k, and we are left with

$$\langle \Delta \mathcal{E} \rangle = O(\omega^{-2}). \tag{C.6}$$

This implies that $\mathrm{Var}(\mathcal{E}) = \langle (\Delta \mathcal{E})^2 \rangle + O(\omega^{-4})$. We may now express (3.13) as:

$$\mathrm{Var}(\mathcal{E}) = 4\omega^{-2} \left\langle \sum_{k=1}^{N} \sum_{l=1}^{N} a_k a_l \sin(\omega t_k) \sin(\omega t_l) \right\rangle + O(\omega^{-3}). \tag{C.7}$$

We evaluate this average similarly to how we computed $\langle \Delta \mathcal{E} \rangle$. The logic is the same: To leading order, the average may be calculated with respect to the ensemble of *undriven* trajectories. Then, for $l \neq k$, the integrals over t_k and t_l in the average are of order $O(\omega^{-1})$, because of the oscillating factor $\sin(\omega t_k) \sin(\omega t_l)$ in the integrand. The contribution of the $l \neq k$ terms to $\mathrm{Var}(\mathcal{E})$ is therefore of order $O(\omega^{-3})$, because of the factor ω^{-2} outside the sum. For the $l = k$ terms, we

note that $\sin(\omega t_k)\sin(\omega t_l) = \sin^2(\omega t_k) = \frac{1}{2} - \frac{1}{2}\cos(2\omega t_k)$, the sum of a constant term and an oscillatory term. The contributions to $\mathrm{Var}(\mathcal{E})$ corresponding to the oscillatory term $-\frac{1}{2}\cos(2\omega t_k)$ are also of order $O(\omega^{-3})$. Thus, the only remaining contribution to $\mathrm{Var}(\mathcal{E})$ is given by

$$\mathrm{Var}(\mathcal{E}) = 2\omega^{-2}\left\langle \sum_{k=1}^{N} a_k^2 \right\rangle_0 + O(\omega^{-3}), \tag{C.8}$$

where we have added the subscript 0 to emphasize that the average is over the ensemble of undriven particles. Recalling that $a_k = (\mathbf{F}_k \cdot \hat{\mathbf{n}}_k)(\mathbf{v}_k \cdot \hat{\mathbf{n}}_k)$, we see that this is (3.14) in Chapter 3.

We briefly pause to interpret this result. In evaluating $\langle(\Delta\mathcal{E})^2\rangle$ and $\langle\Delta\mathcal{E}\rangle$, we have seen that for large ω, the oscillatory factors $\sin(\omega t_k)$ average to zero. These factors become effectively uncorrelated with one another, and with the quantities a_k. Intuitively, this lack of correlation arises because otherwise similar trajectories in the ensemble may have totally different values of $\sin(\omega t_k)$: Two nearby trajectories with even a small difference between their associated collision times t_k will have a huge $O(\omega)$ difference in the corresponding values of ωt_k. As a result, the phases $\omega t_k \bmod 2\pi$ effectively become independent random variables, uniformly distributed on $[0, 2\pi)$.

To reiterate, the average (C.8) is taken over a microcanonical ensemble of initial conditions with energy E_0, evolved for a time Δt according to the *undriven* equations of motion. The sum $\sum_{k=1}^{N} a_k^2$ is over all collisions which occur from $t = 0$ to $t = \Delta t$. Our strategy will be to decompose this sum into many small contributions, evaluate the average of each contribution, and then add up all these results.

Specifically, let us divide up the boundary of the billiard into infinitesimal patches, indexed

by a variable l: Each patch is centered on a point $\mathbf{x}^{(l)}$ on the boundary, and has a $(d-1)$-dimensional hyper-area dS. Moreover, we partition velocity space into infinitesimal hypercubes of hyper-volume $d^d\mathbf{v}$ labeled by m, each centered on a velocity point $\mathbf{v}^{(m)}$. Finally, we divide up the time interval from $t = 0$ to $t = \Delta t$ into infinitesimal segments of duration dt, beginning at successive times $t^{(n)} = n\,dt = 0,\ dt,\ 2\,dt\,...$. Let us now sum a_k^2, *only* counting collisions associated with a particular choice of the indices l, m, and n: Those collisions which occurred on the patch containing $\mathbf{x}^{(l)}$, with incoming velocity in the velocity cell corresponding to $\mathbf{v}^{(m)}$, between the times $t^{(n)}$ and $t^{(n)} + dt$. If we denote an average over such a restricted sum with $\langle ... \rangle_{0,l,m,n}$, then $\mathrm{Var}(\mathcal{E})$ is just a sum over such averages:

$$\mathrm{Var}(\mathcal{E}) = 2\omega^{-2} \sum_{l,m,n} \left\langle \sum_{k=1}^{N} a_k^2 \right\rangle_{0,l,m,n} + O(\omega^{-3}). \tag{C.9}$$

For a given choice of l, m, and n, what is this average? Well, for all collisions associated with a particular l and m, we have that $a_k^2 \approx \left[\mathbf{F}(\mathbf{x}^{(l)}) \cdot \hat{\mathbf{n}}(\mathbf{x}^{(l)})\right]^2 \left[\mathbf{v}^{(m)} \cdot \hat{\mathbf{n}}(\mathbf{x}^{(l)})\right]^2 \equiv (\mathbf{F} \cdot \hat{\mathbf{n}})^2 (\mathbf{v} \cdot \hat{\mathbf{n}})^2$, so this factor can be brought outside the average. Then, we are simply averaging over the number of collisions corresponding to l, m, and n. This is only nonzero for a small fraction of the ensemble with associated phase space volume $\mathbf{v}^{(m)} \cdot \hat{\mathbf{n}}(\mathbf{x}^{(l)})\, dt\, dS\, d^d\mathbf{v} \equiv \mathbf{v} \cdot \hat{\mathbf{n}}\, dt\, dS\, d^d\mathbf{v}$ (see Figure C.1); the corresponding average is therefore $\rho_{E_0}(\mathbf{x}^{(l)}, \mathbf{v}^{(m)}) \equiv \rho_{E_0}$ times this volume elment. Thus, we can convert the sum of over l, m, and n into an integral over $\mathbf{x}$, $\mathbf{v}$, and t, obtaining:

$$\mathrm{Var}(\mathcal{E}) = 2\omega^{-2}\Delta t \int dS \int_{\mathbf{v}\cdot\hat{\mathbf{n}}>0} d^d\mathbf{v}\, \rho_{E_0} (\mathbf{F} \cdot \hat{\mathbf{n}})^2 (\mathbf{v} \cdot \hat{\mathbf{n}})^3 + O(\omega^{-3}). \tag{C.10}$$

Note the restriction to $\mathbf{v} \cdot \hat{\mathbf{n}}(\mathbf{x}) > 0$, since a collision can only occur if the incoming

velocity $\mathbf{v}$ is directed towards the wall. We can interpret the quantity $\rho_{E_0}(\mathbf{x}, \mathbf{v})\, \mathbf{v} \cdot \hat{\mathbf{n}}(\mathbf{x})$ as the differential average collision rate in the microcanonical ensemble, for collisions at the point $\mathbf{x}$ on the boundary with incoming velocity $\mathbf{v}$. $\mathrm{Var}(\mathcal{E})$ is then obtained by integrating $[\mathbf{F}(\mathbf{x}) \cdot \hat{\mathbf{n}}(\mathbf{x})]^2\, [\mathbf{v} \cdot \hat{\mathbf{n}}(\mathbf{x})]^2$ over all possible collisions, weighted by the rate at which each type of collision occurs.

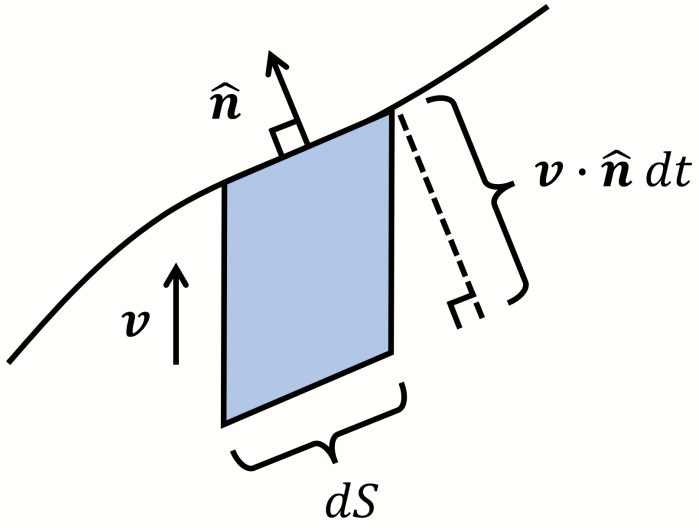

Figure C.1: Diagram of collisions associated with a given choice of l, m, and n, for the case of $d = 2$ dimensions. The curved line represents the billiard boundary, and $\hat{\mathbf{n}}(\mathbf{x}^{(l)}) \equiv \hat{\mathbf{n}}$ is the outward-facing normal near such collisions. Over the infinitesimal time interval from $t^{(n)}$ to $t^{(n)} + dt$, any particle in the shaded parallelogram with velocity $\mathbf{v}^{(m)} \equiv \mathbf{v}$ will collide with the boundary sometime during this interval. The area of this parallelogram is $\mathbf{v} \cdot \hat{\mathbf{n}}\, dt\, dS$, and so collisions associated with l, m, and n correspond to a phase space volume of $\mathbf{v} \cdot \hat{\mathbf{n}}\, dt\, dS\, d^d\mathbf{v}$. Analogous arguments apply to higher-dimensional billiards.

With the definition of $\rho_{E_0}(\mathbf{x}, \mathbf{v})$ (see (2.6)), we may perform the integral over $\mathbf{v}$ using d-dimensional spherical coordinates. The result is

$$\mathrm{Var}(\mathcal{E}) = \frac{4B_{d-1}\omega^{-2}\Delta t}{(d+1)m\Sigma(E_0)} \int dS\, v_{E_0}^{d+1}\, (\mathbf{F} \cdot \hat{\mathbf{n}})^2 + O(\omega^{-3}). \tag{C.11}$$

Here, B_{d-1} is the hyper-volume of the unit ball in $(d-1)$-dimensional space, and $v_{E_0}(\mathbf{x}) \equiv v_{E_0}$

is defined as in (3.16).

We can rewrite this expression in terms of $\gamma_{E_0}(\mathbf{x})$, the differential average collision rate for collisions at the location $\mathbf{x}$. $\gamma_{E_0}(\mathbf{x})$ is obtained by integrating $\rho_{E_0}(\mathbf{x}, \mathbf{v})\, \mathbf{v} \cdot \hat{\mathbf{n}}(\mathbf{x})$ over all $\mathbf{v}$ such that $\mathbf{v} \cdot \hat{\mathbf{n}}(\mathbf{x}) > 0$. This is another spherical integral; the result is given by (3.17). Comparing (3.17) and (C.11), we obtain (3.15) in Chapter 3.

Appendix D: Alternative calculation of g_2 for billiards

In this appendix, we provide an alternative derivation of the energy diffusion coefficient in a billiard system. We show that the billiard-specific expression for g_2, given by (3.18), may be obtained directly from the more general result $g_2(E,\omega) = \frac{1}{2}S(\omega;E)$. This establishes consistency between the general approach of Chapter 2, applicable to an arbitrary chaotic Hamiltonian system subject to a a rapid periodic drive, and the billiard calculations in Chapter 3.

The result $g_2(E,\omega) = \frac{1}{2}S(\omega;E)$, first given in (2.20), is valid under the general assumptions for energy diffusion laid out in Chapter 2, plus the assumption of a monochromatic driving Hamiltonian $V(z)\cos(\omega t)$. The power spectrum $S(\omega;E) = \int_{-\infty}^{\infty} dt\, e^{-i\omega t}C(t;E)$ is the Fourier transform of the autocorrelation function $C(t;E)$ for the observable $\dot{V}(z_t^0)$. Since $C(t;E) \equiv \langle \dot{V}(z_0^0)\dot{V}(z_t^0)\rangle - \langle \dot{V}(z_0^0)\rangle\langle \dot{V}(z_t^0)\rangle$ is a real-valued, even function of t, we may ignore the imaginary part of the factor $e^{-i\omega t}$ in its Fourier transform, and express g_2 as

$$g_2(E,\omega) = \int_0^{\infty} dt\, \cos(\omega t)C(t;E). \tag{D.1}$$

Note the new range of integration $(0,\infty)$.

To begin deriving the billiard-specific expression for g_2, given by (3.18), let us now integrate by parts twice in the above expression. Upon doing so, we find that the boundary terms at $t=\infty$ vanish, since $C(t;E)$ and its time derivatives approach zero for large t (this is the

decay of correlations induced by the chaotic dynamics). We are then left with

$$g_2(E,\omega) = -\omega^{-2}C'(0^+;E) - \omega^{-2}\int_0^\infty dt\ \cos(\omega t)C''(t;E), \tag{D.2}$$

where primes $'$ denote partial derivatives with respect to time, and where $C'(0^+;E)$ is the limit of $C'(t;E)$ as t approaches zero from the right. Now, the integral on the right hand side will decay to zero as ω approaches infinity: This integral is simply the real part of a Fourier transform, and the Fourier transform of any well-behaved (e.g., square-integrable) function will approach zero at large arguments. Therefore, for large ω, the leading order contribution to g_2 is simply given by

$$g_2(E,\omega) = -\omega^{-2}C'(0^+;E). \tag{D.3}$$

For Hamiltonian systems with smooth dynamics in phase space, this expression simply provides the unhelpful approximation $g_2(E,\omega) = 0$: For such systems, $C(t;E)$ is a smooth, even function of t, and therefore $C'(t;E)$ is odd and must vanish at $t = 0$. This is reflective of the fact that the Fourier transform of a smooth function decays faster than any power of ω^{-1} for large ω [126]. However, for a billiard, the discontinuous evolution of the system during collisions produces a cusp at $t = 0$ in the autocorrelation function $C(t;E)$, allowing the slope $C'(0^+;E)$ at the cusp to be nonzero (see Figure D.1). We now turn to the calculation of this slope.

By definition, we can compute $C'(0^+;E)$ by considering the correlation function $C(t;E)$ for small $t > 0$, and then taking the limit of $[C(t;E) - C(0;E)]/t$ as t approaches zero. For a billiard, $V(z)$ corresponds to the potential function $V(\mathbf{x})$, and therefore $\dot{V}(z_t)$ is given by $dV(\mathbf{x}_t)/dt = -\mathbf{F}(\mathbf{x}_t)\cdot\mathbf{v}_t \equiv -\mathbf{F}_t\cdot\mathbf{v}_t$. The correlation function $C(t;E)$ is then

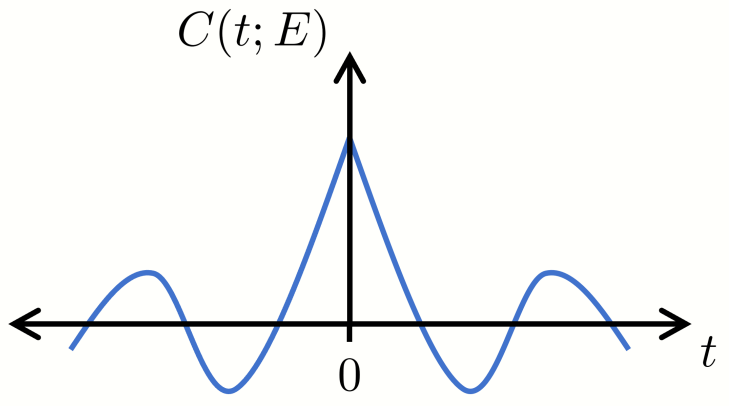

Figure D.1: The autocorrelation function $C(t;E) = \langle (\mathbf{F}_0 \cdot \mathbf{v}_0)\,(\mathbf{F}_t \cdot \mathbf{v}_t)\rangle$ for a typical billiard system. $C'(0^+;E)$ is the slope of $C(t;E)$ to the right of the cusp at $t = 0$.

$$C(t;E) = \langle (\mathbf{F}_0 \cdot \mathbf{v}_0)\,(\mathbf{F}_t \cdot \mathbf{v}_t)\rangle, \tag{D.4}$$

where we have noted that $\langle \mathbf{F}_t \cdot \mathbf{v}_t \rangle = 0$, since $-\mathbf{F}_t \cdot \mathbf{v}_t$ is the time derivative of $V(\mathbf{x}_t)$, and the equilibrium average of the time derivative of any phase space function must vanish.

Now, the ensemble average defining $C(t;E)$ is an integral over microcanonically distributed initial conditions $(\mathbf{x}_0, \mathbf{v}_0)$. For small (infinitesimal) $t > 0$, we may divide these initial conditions and the corresponding trajectories into two groups: Trajectories which evolve smoothly according to Newton's law (3.1) during the interval $[0,t]$, and trajectories which include a single collision with the billiard boundary during this time interval. Working to first order in t, for the first class of trajectories we may approximate $\mathbf{F}_t \cdot \mathbf{v}_t$ by $\mathbf{F}_0 \cdot \mathbf{v}_0 + t\,\left[d\,(\mathbf{F}_t \cdot \mathbf{v}_t)\,/dt\right]_{t=0}$. For the trajectories with a collision, by the reflection law (3.2) we have $\mathbf{F}_t \cdot \mathbf{v}_t \approx \mathbf{F}_0 \cdot \mathbf{v}_0 - 2(\mathbf{F}_0 \cdot \hat{\mathbf{n}})(\mathbf{v}_0 \cdot \hat{\mathbf{n}})$, where $\hat{\mathbf{n}}$ is the unit normal to the wall at the point of collision (there is also a term of order t here, but the fraction of trajectories with a collision is itself of order t, so we can neglect this). So, if we use $\langle ... \rangle_C$ and $\langle ... \rangle_{NC}$ to denote modified averages where we only integrate over trajectories which collide (C) or do not collide (NC) with the wall, then we have

$\langle ... \rangle = \langle ... \rangle_C + \langle ... \rangle_{NC}$, and our approximations for the two cases yield:

$$\begin{aligned} C(t;E) = &\langle (\mathbf{F}_0 \cdot \mathbf{v}_0)^2 \rangle_C - 2\langle (\mathbf{F}_0 \cdot \mathbf{v}_0)(\mathbf{F}_0 \cdot \hat{\mathbf{n}})(\mathbf{v}_0 \cdot \hat{\mathbf{n}}) \rangle_C \\ &+ \langle (\mathbf{F}_0 \cdot \mathbf{v}_0)^2 \rangle_{NC} + t \left\langle (\mathbf{F}_0 \cdot \mathbf{v}_0) \left. \frac{d(\mathbf{F}_0 \cdot \mathbf{v}_0)}{dt} \right|_{t=0} \right\rangle_{NC} + O(t^2). \end{aligned} \tag{D.5}$$

In this expression, the first and third terms sum to yield $\langle (\mathbf{F}_0 \cdot \mathbf{v}_0)^2 \rangle = C(0;E)$. Since the fraction of trajectories which collide with the wall is of order t, the fourth term is just the unmodified average $t \langle (\mathbf{F}_0 \cdot \mathbf{v}_0) [d(\mathbf{F}_t \cdot \mathbf{v}_t)/dt]_{t=0} \rangle$, up to $O(t^2)$ corrections. But this average vanishes, since $(\mathbf{F}_0 \cdot \mathbf{v}_0)[d(\mathbf{F}_t \cdot \mathbf{v}_t)/dt]_{t=0}$ is just the time derivative of $(\mathbf{F}_t \cdot \mathbf{v}_t)^2/2$ at $t = 0$ (recall that equilibrium averages of time derivatives vanish). We are left with

$$C(t;E) = C(0;E) - 2\langle (\mathbf{F}_0 \cdot \mathbf{v}_0)(\mathbf{F}_0 \cdot \hat{\mathbf{n}})(\mathbf{v}_0 \cdot \hat{\mathbf{n}}) \rangle_C + O(t^2). \tag{D.6}$$

This modified average over colliding trajectories may then be computed similarly to the average (C.9) in Appendix C, using Figure C.1 as a guide. For a given $\mathbf{v}_0$, and a given infinitesimal patch of the billiard wall (with hyper-area dS), a set of trajectories in a region of volume $(\mathbf{v}_0 \cdot \hat{\mathbf{n}})\, t\, dS$ will collide with the patch. Integrating over all such patches, and over all velocities $\mathbf{v}_0$ with $\mathbf{v}_0 \cdot \hat{\mathbf{n}} > 0$, we obtain

$$C(t;E) = C(0;E) - 2t \int dS \int_{\mathbf{v}_0 \cdot \hat{\mathbf{n}} > 0} d\mathbf{v}_0\, \rho_E\, (\mathbf{F}_0 \cdot \mathbf{v}_0)(\mathbf{F}_0 \cdot \hat{\mathbf{n}})(\mathbf{v}_0 \cdot \hat{\mathbf{n}})^2 + O(t^2), \tag{D.7}$$

where $\rho_E \equiv \rho_E(\mathbf{x}_0, \mathbf{v}_0)$ is the microcanonical distribution.

Finally, consider the integral over $\mathbf{v}_0$ in the above expression. We can decompose any $\mathbf{v}_0$ as $\mathbf{v}_0 = v_\parallel \hat{\mathbf{n}} + \mathbf{v}_\perp$, where $v_\parallel \equiv \mathbf{v}_0 \cdot \hat{\mathbf{n}}$ is the component of $\mathbf{v}_0$ parallel to $\hat{\mathbf{n}}$, and $\mathbf{v}_\perp \equiv \mathbf{v}_0 - v_\parallel \hat{\mathbf{n}}$ is the projection of $\mathbf{v}_0$ parallel to the billiard boundary. The integral over $\mathbf{v}_0$ may be considered as an integral with respect to $v_\parallel$ and $\mathbf{v}_\perp$ separately, where the integral over $v_\parallel$ runs from 0 to ∞, and the integral over $\mathbf{v}_\perp$ runs over all $\mathbf{v}_\perp \in \mathbb{R}^{d-1}$. This decomposition becomes useful when we consider the factor $(\mathbf{F}_0 \cdot \mathbf{v}_0) = v_\parallel (\mathbf{F}_0 \cdot \hat{\mathbf{n}}_0) + \mathbf{F}_0 \cdot \mathbf{v}_\perp$ in the integral. When we integrate over $\mathbf{v}_\perp$, the integral over the second term $\mathbf{F}_0 \cdot \mathbf{v}_\perp$ vanishes, since we are integrating uniformly over all possible orientations of $\mathbf{v}_\perp$ (this follows from the fact that $\rho_E \propto \delta(\mathcal{E}(\mathbf{x}_0, \mathbf{v}_0) - E) = \delta\left(\frac{1}{2}mv_\parallel^2 + \frac{1}{2}m|\mathbf{v}_\perp|^2 + U(\mathbf{x}_0) - E\right)$ is a spherically symmetric function of $\mathbf{v}_\perp$). Thus, upon dropping this term, we obtain the result

$$C(t; E) = C(0; E) - 2\,t \int dS \int_{\mathbf{v}_0 \cdot \hat{\mathbf{n}} > 0} d\mathbf{v}_0\, \rho_E\, (\mathbf{F}_0 \cdot \hat{\mathbf{n}})^2\, (\mathbf{v}_0 \cdot \hat{\mathbf{n}})^3 + O(t^2). \tag{D.8}$$

Taking the limit as t goes to zero, and substituting the result into (D.3), then yields our desired expression for g_2:

$$g_2(E, \omega) = 2\omega^{-2} \int dS \int_{\mathbf{v}_0 \cdot \hat{\mathbf{n}} > 0} d\mathbf{v}_0\, \rho_E\, (\mathbf{F}_0 \cdot \hat{\mathbf{n}})^2\, (\mathbf{v}_0 \cdot \hat{\mathbf{n}})^3\,. \tag{D.9}$$

This is (C.10) in Appendix C, up to a factor of Δt and $O(\omega^{-3})$ corrections. The subsequent calculations in Appendix C show that this expression is equal to (3.18), the billiard-specific expression for g_2 obtained in Chapter 3.

Appendix E: Description of numerical calculations for the clover billiard

Here, we describe the details of the numerical simulations presented in Chapter 3, Section 3.5. For a particle in the clover billiard subject to a force $\mathbf{F}\cos(\omega t)$, we discuss how to evolve the particle according to the equations of motion, and how to solve the corresponding Fokker-Planck equation.

First, let us describe the evolution of the trajectory ensemble. We consider an ensemble of particles with initial energy E_0 at $t = 0$, with a microcanonical distribution of initial conditions. For a standard billiard ($U(\mathbf{x}) = 0$), the microcanonical distribution (2.6) corresponds to sampling the initial positions $\mathbf{x}_0$ from a uniform distribution over the billiard's area, and the initial velocities $\mathbf{v}_0$ from an isotropic distribution with fixed speed $v_0 \equiv \sqrt{2E_0/m}$. We generate $N \gg 1$ independent samples in this way, and then evolve each sample in time by alternately integrating the equations of motion (3.1), and updating the velocity according to the reflection law (3.2) whenever the particle collides with the wall. In between the k^{th} and $(k+1)^{\text{th}}$ collisions, we may integrate (3.1) explicitly to obtain $\mathbf{x}_t$ and $\mathbf{v}_t$. Using the same notation as in Section 2.4, we find:

$$\mathbf{x}_t = \mathbf{x}_k + \left[\mathbf{v}_k^+ - \frac{\mathbf{F}}{m\omega}\sin(\omega t_k)\right](t - t_k) - \frac{\mathbf{F}}{m\omega^2}\Big[\cos(\omega t) - \cos(\omega t_k)\Big], \tag{E.1}$$

$$\mathbf{v}_t = \mathbf{v}_k^+ + \frac{\mathbf{F}}{m\omega}\Big[\sin(\omega t) - \sin(\omega t_k)\Big]. \tag{E.2}$$

We see that the particle rapidly oscillates within a small envelope about a straight-line average trajectory. Given the above expressions, finding the next position and velocity at the $(k+1)^{\text{th}}$ collision is simply a matter of solving numerically for where and when this trajectory next intersects with the billiard wall.

In this way, we determine the trajectory of each particle in the ensemble between $t = 0$ and some $t = \Delta t$. Then, for any time $t \in [0, \Delta t]$, we compute the energy $\mathcal{E} = \frac{1}{2}m|\mathbf{v}_t|^2$ of each particle, and collect all of these energy values into a histogram. This histogram gives an excellent approximation of the energy distribution $\eta(E,t)$; it only deviates from $\eta(E,t)$ due to the finite number of samples and the small machine error accrued when computing each trajectory.

To compare these results with the energy diffusion description, we then solve the Fokker-Planck equation (2.11). For a standard billiard, the Fokker-Planck equation admits an analytical solution which has been studied previously. To show this, we note that by (3.21) and (3.22), we have $g_1 = CE^{1/2}$ and $g_2 = 4CE^{3/2}/(d+1)$, where C is a constant independent of energy. If we substitute these expressions into (2.11), and define the rescaled time variable $s \equiv Ct$, then after some manipulations we obtain:

$$\frac{\partial \eta}{\partial s} = \frac{2}{d+1}\frac{\partial}{\partial E}\left[E^{(1+d)/2}\frac{\partial}{\partial E}\left(E^{(2-d)/2}\eta\right)\right]. \tag{E.3}$$

This equation is identical to Equation (60) in [72]. This reference also provides the solution to this equation for the initial condition $\eta(E,0) = \delta(E - E_0)$, which we reproduce here:

$$\eta(E,t) = \eta(E, s/C) = \frac{d+1}{sE_0^{1/2}} \left(\frac{E}{E_0}\right)^{(d-3)/4} I_{d-1}\left[\frac{4(d+1)}{s} E_0^{1/4} E^{1/4}\right] \cdot \exp\left[-\frac{2(d+1)}{s}\left(E_0^{1/2} + E^{1/2}\right)\right]. \tag{E.4}$$

Here, $I_{d-1}(x)$ is the modified Bessel function of the first kind, of order $d-1$.

It only remains to compute the constant C for the special case of the clover billiard:

$$C = \left(\frac{2}{m}\right)^{3/2} \frac{\omega^{-2}}{\lambda} \frac{1}{S} \int dS \, (\mathbf{F} \cdot \hat{\mathbf{n}})^2 \,. \tag{E.5}$$

In $d = 2$ dimensions, S is the perimeter of the billiard, and the integral over dS is a line integral over the billiard boundary. For a constant $\mathbf{F}(\mathbf{x}) = \mathbf{F}$, upon performing the appropriate line integrals we find that $S^{-1} \int dS \, [\mathbf{F}(\mathbf{x}) \cdot \hat{\mathbf{n}}(\mathbf{x})]^2 = F^2/2$, where $F \equiv |\mathbf{F}|$. Then, we can use the relation $\lambda \equiv d \dfrac{B_d}{B_{d-1}} \dfrac{V}{S}$ with $d = 2$ to obtain $\lambda = \pi V/S$. In two dimensions, V is the area of the billiard. V and S are geometric quantities which may be computed in terms of the radii R_1 and R_2. For the specific case of $R_1 = 1$ and $R_2 = 2$, we find that $\lambda \approx 2.610$. Upon combining these results, and setting $m = 1$, we obtain:

$$C \approx 0.5419 \, \omega^{-2} F^2. \tag{E.6}$$

With this result, we may now determine the distribution $\eta(E,t)$ at any time t, given the parameter choices $m = 1$, $R_1 = 1$, $R_2 = 2$, and $\mathbf{F} = F(\hat{\mathbf{x}} + \hat{\mathbf{y}})/\sqrt{2}$. We simply select values for F and ω, and then substitute the resulting value of C into (E.4) (recalling that $s = Ct$, and that $d = 2$).

Bibliography

[1] B. Van der Pol and J. Van der Mark. Frequency demultiplication. *Nature*, 120:363, 1927.

[2] P. L. Kapitza. Dynamical stability of a pendulum when its point of suspension vibrates, and pendulum with a vibrating suspension. *Collected papers of P. L. Kapitza*, 2:714–737, 1965.

[3] T. Dittrich, F. Großmann, P. Jung, B. Oelschlägel, and P. Hänggi. Localization and tunneling in periodically driven bistable systems. *Physica A*, 194(1):173, 1993.

[4] R. Chacón. Inhibition of chaos in Hamiltonian systems by periodic pulses. *Phys. Rev. E*, 50:750, 1994.

[5] S. Yoshida, C. O. Reinhold, P. Kristöfel, J. Burgdörfer, S. Watanabe, and F. B. Dunning. Floquet analysis of the dynamical stabilization of the kicked hydrogen atom. *Phys. Rev. A*, 59(6):R4121, 1999.

[6] T. M. Antonsen, R. T. Faghih, M. Girvan, E. Ott, and J. Platig. External periodic driving of large systems of globally coupled phase oscillators. *Chaos*, 18(3):037112, 2008.

[7] T. Nag, S. Roy, A. Dutta, and D. Sen. Dynamical localization in a chain of hard core bosons under periodic driving. *Phys. Rev. B*, 89:165425, Apr 2014.

[8] E. Bairey, G. Refael, and N. H. Lindner. Driving induced many-body localization. *Phys. Rev. B*, 96:020201(R), Jul 2017.

[9] A. Haldar and A. Das. Dynamical many-body localization and delocalization in periodically driven closed quantum systems. *Ann. Phys.*, 529(7):1600333, 2017.

[10] R. Khasseh, R. Fazio, S. Ruffo, and A. Russomanno. Many-body synchronization in a classical Hamiltonian system. *Phys. Rev. Lett.*, 123:184301, 2019.

[11] L. D'Alessio and M. Rigol. Long-time behavior of isolated periodically driven interacting lattice systems. *Phys. Rev. X*, 4:041048, 2014.

[12] M. Bukov, L. D'Alessio, and A. Polkovnikov. Universal high-frequency behavior of periodically driven systems: from dynamical stabilization to Floquet engineering. *Adv. Phys.*, 64(2):139, 2015.

[13] E. Ott. *Chaos in dynamical systems*. Cambridge University Press, Cambridge, 2002.

[14] W. Paul. Electromagnetic traps for charged and neutral particles. *Rev. Mod. Phys.*, 62(3):531, 1990.

[15] R. E. March. An introduction to quadrupole ion trap mass spectrometry. *J. Mass Spectrom.*, 32(4):351–369, 1997.

[16] D. J. Wineland, W. M. Itano, and R. S. Van Dyck Jr. High-resolution spectroscopy of stored ions. *Adv. At. Mol. Opt. Phys.*, 19:135–186, 1983.

[17] D. A. R. Dalvit, R. L. de Matos Filho, and F. Toscano. Quantum metrology at the Heisenberg limit with ion trap motional compass states. *New J. Phys.*, 8(11):276, 2006.

[18] J. P. Home. Quantum science and metrology with mixed-species ion chains. *Adv. At. Mol. Opt. Phys.*, 62:231–277, 2013.

[19] C. R. Monroe and D. J. Wineland. Quantum computing with ions. *Scientific American*, 299(2):64–71, 2008.

[20] E. R. Andrew. Magic angle spinning. *Int. Rev. Phys. Chem.*, 1(2):195–224, 1981.

[21] J. W. Hennel and J. Klinowski. Magic-angle spinning: a historical perspective. In *New techniques in solid-state NMR*, pages 1–14. Springer, 2005.

[22] W. D. Phillips. Nobel lecture: Laser cooling and trapping of neutral atoms. *Rev. Mod. Phys.*, 70(3):721, 1998.

[23] H. J. Metcalf and P. Van der Straten. Laser cooling and trapping of neutral atoms. *The Optics Encyclopedia: Basic Foundations and Practical Applications*, 2007.

[24] R. H. Webb. Confocal optical microscopy. *Rep. Prog. Phys.*, 59(3):427, 1996.

[25] D. W. Lupo and M. Quack. IR-laser photochemistry. *Chem. Rev.*, 87(1):181–216, 1987.

[26] W. Demtröder. *Laser spectroscopy: basic concepts and instrumentation*. Springer Science & Business Media, 2013.

[27] J. P. Dowling and G. J. Milburn. Quantum technology: the second quantum revolution. *Philos. Trans. Royal Soc. A*, 361(1809):1655–1674, 2003.

[28] M. Atzori and R. Sessoli. The second quantum revolution: role and challenges of molecular chemistry. *J. Am. Chem. Soc.*, 141(29):11339–11352, 2019.

[29] I. H. Deutsch. Harnessing the power of the second quantum revolution. *PRX Quantum*, 1(2):020101, 2020.

[30] T. Oka and S. Kitamura. Floquet engineering of quantum materials. *Annu. Rev. Condens. Matter Phys.*, 10:387–408, 2019.

[31] M. Rodriguez-Vega, M. Vogl, and G. A. Fiete. Low-frequency and Moiré–Floquet engineering: a review. *Ann. Phys.*, 435:168434, 2021.

[32] S. Rahav, I. Gilary, and S. Fishman. Effective Hamiltonians for periodically driven systems. *Phys. Rev. A*, 68:013820, Jul 2003.

[33] D. A. Abanin, W. De Roeck, W. W. Ho, and F. Huveneers. Effective Hamiltonians, prethermalization, and slow energy absorption in periodically driven many-body systems. *Phys. Rev. B*, 95:014112, Jan 2017.

[34] K. Fang, Z. Yu, and S. Fan. Realizing effective magnetic field for photons by controlling the phase of dynamic modulation. *Nat. Photonics*, 6(11):782–787, 2012.

[35] S. Zamani, R. Jafari, and A. Langari. Floquet dynamical quantum phase transition in the extended XY model: nonadiabatic to adiabatic topological transition. *Phys. Rev. B*, 102(14):144306, 2020.

[36] J. H. Mentink, K. Balzer, and M. Eckstein. Ultrafast and reversible control of the exchange interaction in Mott insulators. *Nat. Commun.*, 6(1):1–8, 2015.

[37] M. Sameti and M. J. Hartmann. Floquet engineering in superconducting circuits: From arbitrary spin-spin interactions to the Kitaev honeycomb model. *Phys. Rev. A*, 99(1):012333, 2019.

[38] S. Chaudhary, D. Hsieh, and G. Refael. Orbital Floquet engineering of exchange interactions in magnetic materials. *Phys. Rev. B*, 100(22):220403, 2019.

[39] D. V. Else, B. Bauer, and C. Nayak. Prethermal phases of matter protected by time-translation symmetry. *Phys. Rev. X*, 7:011026, Mar 2017.

[40] A. Herrmann, Y. Murakami, M. Eckstein, and P. Werner. Floquet prethermalization in the resonantly driven Hubbard model. *EPL*, 120(5):57001, Dec 2017.

[41] T. Mori. Floquet prethermalization in periodically driven classical spin systems. *Phys. Rev. B*, 98(10):104303, 2018.

[42] T. Mori, T. N. Ikeda, E. Kaminishi, and M. Ueda. Thermalization and prethermalization in isolated quantum systems: a theoretical overview. *J. Phys. B*, 51(11):112001, 2018.

[43] K. Mallayya, M. Rigol, and W. De Roeck. Prethermalization and thermalization in isolated quantum systems. *Phys. Rev. X*, 9:021027, 2019.

[44] O. Howell, P. Weinberg, D. Sels, A. Polkovnikov, and M. Bukov. Asymptotic prethermalization in periodically driven classical spin chains. *Phys. Rev. Lett.*, 122:010602, 2019.

[45] F. Machado, G. D. Kahanamoku-Meyer, D. V. Else, C. Nayak, and N. Y. Yao. Exponentially slow heating in short and long-range interacting Floquet systems. *Phys. Rev. Res.*, 1:033202, Dec 2019.

[46] A. Rajak, I. Dana, and E. G. Dalla Torre. Characterizations of prethermal states in periodically driven many-body systems with unbounded chaotic diffusion. *Phys. Rev. B*, 100(10):100302(R), 2019.

[47] F. Machado, D. V. Else, G. D. Kahanamoku-Meyer, C. Nayak, and N. Y. Yao. Long-range prethermal phases of nonequilibrium matter. *Phys. Rev. X*, 10:011043, 2020.

[48] A. Rubio-Abadal, M. Ippoliti, S. Hollerith, D. Wei, J. Rui, S. L. Sondhi, V. Khemani, C. Gross, and I. Bloch. Floquet prethermalization in a Bose-Hubbard system. *Phys. Rev. X*, 10:021044, 2020.

[49] P. Peng, C. Yin, X. Huang, C. Ramanathan, and P. Cappellaro. Floquet prethermalization in dipolar spin chains. *Nat. Phys.*, page 1, 2021.

[50] J. Zhang, P. W. Hess, A. Kyprianidis, P. Becker, A. Lee, J. Smith, G. Pagano, I.-D. Potirniche, A. C. Potter, and A. Vishwanath. Observation of a discrete time crystal. *Nature*, 543(7644):217, 2017.

[51] N. Y. Yao, A. C. Potter, I.-D. Potirniche, and A. Vishwanath. Discrete time crystals: Rigidity, criticality, and realizations. *Phys. Rev. Lett.*, 118:030401, 2017.

[52] A. Russomanno, F. Iemini, M. Dalmonte, and R. Fazio. Floquet time crystal in the Lipkin-Meshkov-Glick model. *Phys. Rev. B*, 95(21):214307, Jun 2017.

[53] N. Y. Yao, C. Nayak, L. Balents, and M. P. Zaletel. Classical discrete time crystals. *Nat. Phys.*, 16(4):438, Feb 2020.

[54] A. Kyprianidis, F. Machado, W. Morong, P. Becker, K. S. Collins, D. V. Else, L. Feng, P. W. Hess, C. Nayak, G. Pagano, N. Y. Yao, and C. Monroe. Observation of a prethermal discrete time crystal. 2021.

[55] A. Pizzi, A. Nunnenkamp, and J. Knolle. Classical approaches to prethermal discrete time crystals in one, two, and three dimensions. *Phys. Rev. B*, 104(9):094308, 2021.

[56] W. Beatrez, C. Fleckenstein, A. Pillai, E. Sanchez, A. Akkiraju, J. Alcala, S. Conti, P. Reshetikhin, E. Druga, M. Bukov, et al. Observation of a long-lived prethermal discrete time crystal created by two-frequency driving. *arXiv preprint arXiv:2201.02162*, 2022.

[57] R. Citro, E. G. Dalla Torre, L. D'Alessio, A. Polkovnikov, M. Babadi, T. Oka, and E. Demler. Dynamical stability of a many-body Kapitza pendulum. *Ann. Phys.*, 360:694–710, 2015.

[58] C. Ying, Q. Guo, S. Li, M. Gong, X.-H. Deng, F. Chen, C. Zha, Y. Ye, C. Wang, Q. Zhu, et al. Floquet prethermal phase protected by U(1) symmetry on a superconducting quantum processor. *Phys. Rev. A*, 105(1):012418, 2022.

[59] N. H. Lindner, G. Refael, and V. Galitski. Floquet topological insulator in semiconductor quantum wells. *Nat. Phys.*, 7(6):490–495, 2011.

[60] J. Cayssol, B. Dóra, F. Simon, and R. Moessner. Floquet topological insulators. *Phys. Status Solidi (RRL)–Rapid Research Letters*, 7(1-2):101–108, 2013.

[61] G. Usaj, P. M. Perez-Piskunow, L. E. F. Foa Torres, and C. A. Balseiro. Irradiated graphene as a tunable Floquet topological insulator. *Phys. Rev. B*, 90(11):115423, 2014.

[62] J. Roßnagel, S. T. Dawkins, K. N. Tolazzi, O. Abah, E. Lutz, F. Schmidt-Kaler, and K. Singer. A single-atom heat engine. *Science*, 352(6283):325–329, 2016.

[63] J. Klatzow, J. N. Becker, P. M. Ledingham, C. Weinzetl, K. T. Kaczmarek, D. J. Saunders, J. Nunn, I. A. Walmsley, R. Uzdin, and E. Poem. Experimental demonstration of quantum effects in the operation of microscopic heat engines. *Phys. Rev. Lett.*, 122(11):110601, 2019.

[64] N. Van Horne, D. Yum, T. Dutta, P. Hänggi, J. Gong, D. Poletti, and M. Mukherjee. Single-atom energy-conversion device with a quantum load. *npj Quantum Inf.*, 6(1):1–9, 2020.

[65] O. Kyriienko and A. S. Sørensen. Floquet quantum simulation with superconducting qubits. *Phys. Rev. Appl.*, 9(6):064029, 2018.

[66] E. Boyers, M. Pandey, D. K. Campbell, A. Polkovnikov, D. Sels, and A. O. Sushkov. Floquet-engineered quantum state manipulation in a noisy qubit. *Phys. Rev. A*, 100(1):012341, 2019.

[67] H. Qiao, Y. P. Kandel, J. S. Van Dyke, S. Fallahi, G. C. Gardner, M. J. Manfra, E. Barnes, and J. M. Nichol. Floquet-enhanced spin swaps. *Nat. Commun.*, 12(1):1–9, 2021.

[68] M. A. Schlosshauer. *Decoherence and the quantum-to-classical transition*. Springer Science & Business Media, 2007.

[69] K. Ann and G. Jaeger. Finite-time destruction of entanglement and non-locality by environmental influences. *Found. Phys.*, 39(7):790–828, 2009.

[70] A. Lazarides, A. Das, and R. Moessner. Equilibrium states of generic quantum systems subject to periodic driving. *Phys. Rev. E*, 90:012110, 2014.

[71] D. A. Abanin, W. De Roeck, and F. Huveneers. Exponentially slow heating in periodically driven many-body systems. *Phys. Rev. Lett.*, 115(25):256803, Dec 2015.

[72] J. Demers and C. Jarzynski. Universal energy diffusion in a quivering billiard. *Phys. Rev. E*, 92:042911, 2015.

[73] P. Ponte, A. Chandran, Z. Papić, and D. A. Abanin. Periodically driven ergodic and many-body localized quantum systems. *Ann. Phys.*, 353:196, 2015.

[74] J. Rehn, A. Lazarides, F. Pollmann, and R. Moessner. How periodic driving heats a disordered quantum spin chain. *Phys. Rev. B*, 94:020201(R), 2016.

[75] T. Mori, T. Kuwahara, and K. Saito. Rigorous bound on energy absorption and generic relaxation in periodically driven quantum systems. *Phys. Rev. Lett.*, 116:120401, 2016.

[76] T. Kuwahara, T. Mori, and K. Saito. Floquet-Magnus theory and generic transient dynamics in periodically driven many-body quantum systems. *Ann. Phys.*, 367:96, Apr 2016.

[77] S. A. Weidinger and M. Knap. Floquet prethermalization and regimes of heating in a periodically driven, interacting quantum system. *Sci. Rep.*, 7(1):1–10, 2017.

[78] A. Rajak, R. Citro, and E. G. Dalla Torre. Stability and pre-thermalization in chains of classical kicked rotors. *J. Phys. A*, 51(46):465001, 2018.

[79] S. Notarnicola, F. Iemini, D. Rossini, R. Fazio, A. Silva, and A. Russomanno. From localization to anomalous diffusion in the dynamics of coupled kicked rotors. *Phys. Rev. E*, 97:022202, Feb 2018.

[80] M. C. Tran, A. Ehrenberg, A. Y. Guo, P. Titum, D. A. Abanin, and A. V. Gorshkov. Locality and heating in periodically driven, power-law-interacting systems. *Phys. Rev. A*, 100:052103, Nov 2019.

[81] E. Dalla Torre and David Dentelski. Statistical Floquet prethermalization of the Bose-Hubbard model. *SciPost Phys.*, 11(2):040, 2021.

[82] J. L. Lebowitz and O. Penrose. Modern ergodic theory. *Phys. Today*, 26(2):23–29, 1973.

[83] L. E. Reichl. *A modern course in statistical physics*. Arnold, London, 1980.

[84] J. R. Dorfman. *An introduction to chaos in nonequilibrium statistical mechanics*. Cambridge Lecture Notes in Physics. Cambridge University Press, Cambridge, 1999.

[85] M. Wojtkowski. Principles for the design of billiards with nonvanishing Lyapunov exponents. *Comm. Math. Phys.*, 105(3):391, 1986.

[86] V. J. Donnay. Using integrability to produce chaos: billiards with positive entropy. *Comm. Math. Phys.*, 141(2):225, 1991.

[87] M. Srednicki. The approach to thermal equilibrium in quantized chaotic systems. *J. Phys. A*, 32(7):1163–1175, Jan 1999.

[88] L. D'Alessio, Y. Kafri, A. Polkovnikov, and M. Rigol. From quantum chaos and eigenstate thermalization to statistical mechanics and thermodynamics. *Adv. Phys.*, 65(3):239–362, 2016.

[89] O. Bohigas, M.-J. Giannoni, and C. Schmit. Characterization of chaotic quantum spectra and universality of level fluctuation laws. *Phys. Rev. Lett.*, 52(1):1, 1984.

[90] W. Hodson and C. Jarzynski. Energy diffusion and absorption in chaotic systems with rapid periodic driving. *Phys. Rev. Res.*, 3:013219, Mar 2021.

[91] H. Goldstein. *Classical mechanics*. Addison-Wesley, Reading, Massachusetts, 2nd edition, 1980.

[92] J. A. Murdock. *Perturbations: Theory and methods*. Society for Industrial and Applied Mathematics, Philadelphia, 1999.

[93] N. G. Van Kampen. *Stochastic processes in physics and chemistry*, volume 1. Elsevier, 1992.

[94] C. W. Gardiner. *Handbook of stochastic methods for physics, chemistry, and the natural sciences*. Springer Series in Synergetics. Springer-Verlag, Berlin, 1985.

[95] H. A. Kramers. Brownian motion in a field of force and the diffusion model of chemical reactions. *Physica*, 7(4):284–304, 1940.

[96] R. W. Zwanzig. Contribution to the theory of Brownian motion. *Phys. Fluids*, 2(1):12–19, 1959.

[97] W. F. Brown. Thermal fluctuations of a single-domain particle. *Phys. Rev.*, 130(5):1677, 1963.

[98] E. Ott. Goodness of ergodic adiabatic invariants. *Phys. Rev. Lett.*, 42:1628, 1979.

[99] R. F. Grote and J. T. Hynes. Energy diffusion-controlled reactions in solution. *J. Chem Phys.*, 77(7):3736–3743, 1982.

[100] B. Carmeli and A. Nitzan. Non-Markovian theory of activated rate processes. I. Formalism. *J. Chem. Phys.*, 79(1):393–404, 1983.

[101] N. B. Delone, B. P. Kraĭnov, and Shepelyanskiĭ. Highly-excited atoms in the electromagnetic field.

[102] G. Casati, B. V. Chirikov, D. L. Shepelyansky, and I. Guarneri. Relevance of classical chaos in quantum mechanics: The hydrogen atom in a monochromatic field. *Phys. Rep.*, 154(2):77–123, 1987.

[103] R. Brown, E. Ott, and C. Grebogi. The goodness of ergodic adiabatic invariants. *J. Stat. Phys.*, 49(3-4):511, 1987.

[104] R. Brown, E. Ott, and C. Grebogi. Ergodic adiabatic invariants of chaotic systems. *Phys. Rev. Lett.*, 59:1173, 1987.

[105] M. Wilkinson. Dissipation by identical oscillators. *J. Phys. A*, 23(15):3603, 1990.

[106] S. Linkwitz and H. Grabert. Energy diffusion of a weakly damped and periodically driven particle in an anharmonic potential well. *Phys. Rev. B*, 44:11888–11900, Dec 1991.

[107] S. Linkwitz and H. Grabert. Enhancement of the decay rate of a metastable state by an external driving force. *Physical Review B*, 44(21):11901, 1991.

[108] C. Jarzynski. Diffusion equation for energy in ergodic adiabatic ensembles. *Phys. Rev. A*, 46:7498, 1992.

[109] T. Hesselroth. Application of the non-Markovian Fokker-Planck equation to the resonant activation of a Josephson junction. *Phys. Rev. E*, 48(1):46, 1993.

[110] C. Jarzynski. Energy diffusion in a chaotic adiabatic billiard gas. *Phys. Rev. E*, 48:4340, 1993.

[111] C Jarzynski. Multiple-time-scale approach to ergodic adiabatic systems: Another look. *Physical review letters*, 71(6):839, 1993.

[112] C. Jarzynski. Thermalization of a Brownian particle via coupling to low-dimensional chaos. *Phys. Rev. Lett.*, 74(15):2937, 1995.

[113] D. Cohen. Quantum dissipation due to the interaction with chaotic degrees of freedom and the correspondence principle. *Phys. Rev. Lett.*, 82:4951, 1999.

[114] D. Cohen. Chaos and energy spreading for time-dependent Hamiltonians, and the various regimes in the theory of quantum dissipation. *Ann. Phys.*, 283(2):175, 2000.

[115] D. Cohen and T. Kottos. Quantum-mechanical nonperturbative response of driven chaotic mesoscopic systems. *Phys. Rev. Lett.*, 85:4839, 2000.

[116] P. V. Elyutin. Gibbs attractor: A chaotic nearly hamiltonian system, driven by external harmonic force. *Phys. Rev. E*, 69:036207, 2004.

[117] P. V. Elyutin. Energy diffusion in strongly driven quantum chaotic systems. *J. Exp. Theor. Phys.*, 102(1):182, 2006.

[118] A. Verso and J. Ankerhold. Semiclassical theory of energy diffusive escape in a duffing oscillator. *Phys. Rev. E*, 82(5):051116, 2010.

[119] G. Bunin, L. D'Alessio, Y. Kafri, and A Polkovnikov. Universal energy fluctuations in thermally isolated driven systems. *Nat. Phys.*, 7:913, 2011.

[120] S. De Bièvre and P. E. Parris. Equilibration, generalized equipartition, and diffusion in dynamical Lorentz gases. *J. Stat. Phys.*, 142(2):356, 2011.

[121] C. P. Dettmann and E. D. Leonel. Periodic compression of an adiabatic gas: Intermittency-enhanced Fermi acceleration. *EPL*, 103(4):40003, 2013.

[122] I. Tikhonenkov, A. Vardi, J. R. Anglin, and D. Cohen. Minimal Fokker-Planck theory for the thermalization of mesoscopic subsystems. *Phys. Rev. Lett.*, 110(5):050401, 2013.

[123] S. De Bièvre, C. Mejía-Monasterio, and P. E. Parris. Dynamical mechanisms leading to equilibration in two-component gases. *Phys. Rev. E*, 93:050103(R), May 2016.

[124] F. Reif. *Fundamentals of statistical and thermal physics*. McGraw-Hill, Tokyo, 1965.

[125] R. Kubo, M. Toda, and N. Hashitsume. *Statistical physics II: Nonequilibrium statistical mechanics*. Springer Series in Solid-State Sciences. Springer, Berlin Heidelberg, 2012.

[126] R. N. Bracewell. *The Fourier transform and its applications*. McGraw-Hill Kogakusha, Ltd., Tokyo, second edition, 1978.

[127] W. R. Gilks, S. Richardson, and D. Spiegelhalter. *Markov chain Monte Carlo in practice*. Chapman & Hall/CRC Interdisciplinary Statistics. Taylor & Francis, New York, 1995.

[128] R. G. Gallager. *Stochastic processes: Theory for applications*. Cambridge University Press, Cambridge, 2013.

[129] S. Kullback and R. Leibler. On information and sufficiency. *Ann. Math. Stat*, 22(1):79–86, 1951.

[130] T. M. Cover. *Elements of information theory*. John Wiley & Sons, 1999.

[131] J. J. Sakurai and E. D. Commins. Modern quantum mechanics, revised edition, 1995.

[132] G. E. Crooks. Entropy production fluctuation theorem and the nonequilibrium work relation for free energy differences. *Phys. Rev. E.*, 60(3):2721, 1999.

[133] U. Seifert. Entropy production along a stochastic trajectory and an integral fluctuation theorem. *Phys. Rev. Lett.*, 95(4):040602, 2005.

[134] E. M. Sevick, R. Prabhakar, S. R. Williams, and D. J. Searles. Fluctuation theorems. *Annu. Rev. Phys. Chem.*, 59:603–633, 2008.

[135] U. Seifert. Stochastic thermodynamics, fluctuation theorems and molecular machines. *Rep. Prog. Phys.*, 75(12):126001, 2012.

[136] G. E. Crooks. Nonequilibrium measurements of free energy differences for microscopically reversible Markovian systems. *J. Stat. Phys.*, 90(5):1481–1487, 1998.

[137] V. Y. Chernyak, M. Chertkov, and C. Jarzynski. Path-integral analysis of fluctuation theorems for general Langevin processes. *J. Stat. Mech.: Theory Exp.*, 2006(08):P08001, 2006.

[138] B. V. Chirikov. Research concerning the theory of non-linear resonance and stochasticity. Technical report, CM-P00100691, 1971.

[139] B. V. Chirikov. A universal instability of many-dimensional oscillator systems. *Phys. Rep.*, 52(5):263, 1979.

[140] W. Hodson and C. Jarzynski. Energy diffusion and prethermalization in chaotic billiards under rapid periodic driving. *Phys. Rev. E*, 104(6):064210, 2021.

[141] Y. G. Sinai. Dynamical systems with elastic reflections. *Russ. Math. Surv.*, 25(2):137, 1970.

[142] L. A. Bunimovich. On the ergodic properties of nowhere dispersing billiards. *Comm. Math. Phys.*, 65(3):295, 1979.

[143] N. I. Chernov. Sinai billiards under small external forces. In *Ann. Henri Poincaré*, volume 2, page 197. Springer, 2001.

[144] V. V. Beletsky, E. I. Kugushev, and E. L. Starostin. Free manifolds of dynamical billiards. In *Dynamics of Vibro-Impact Systems*, page 29. Springer, 1999.

[145] N. Chernov. Entropy, Lyapunov exponents, and mean free path for billiards. *J. Stat. Phys.*, 88(1):1, 1997.

[146] J. Blocki, Y. Boneh, J. R. Nix, J. Randrup, M. Robel, A. J. Sierk, and W. J. Swiatecki. One-body dissipation and the super-viscidity of nuclei. *Ann. Phys.*, 113(2):330, 1978.

[147] M. E. Fisher. The free energy of a macroscopic system. *Arch. Ration. Mech. Anal.*, 17(5):377–410, 1964.

[148] R. B. Griffiths. A proof that the free energy of a spin system is extensive. *J. Math. Phys.*, 5(9):1215–1222, 1964.

[149] J. L. Lebowitz and E. H. Lieb. Existence of thermodynamics for real matter with Coulomb forces. *Phys. Rev. Lett.*, 22(13):631, 1969.

[150] E. H. Lieb and J. L. Lebowitz. The constitution of matter: Existence of thermodynamics for systems composed of electrons and nuclei. *Adv. Math.*, 9(3):316–398, 1972.

[151] H. Touchette. The large deviation approach to statistical mechanics. *Phys. Rep.*, 478(1-3):1–69, 2009.

[152] H.-O. Georgii. The equivalence of ensembles for classical systems of particles. *J. Stat. Phys.*, 80(5):1341–1378, 1995.

[153] H. Touchette. Equivalence and nonequivalence of ensembles: thermodynamic, macrostate, and measure levels. *J. Stat. Phys.*, 159(5):987–1016, 2015.

[154] Nándor Simányi. Further developments of Sinai's ideas: the Boltzmann–Sinai hypothesis. In *The Abel Prize 2013-2017*, pages 287–298. Springer, 2019.

[155] Nándor Simányi. The Boltzmann-Sinai ergodic hypothesis in full generality (without exceptional models). *ArXiv Mathematics e-prints*, 2005.

[156] V. Gelfreich and D. Turaev. Fermi acceleration in non-autonomous billiards. *J. Phys. A*, 41(21):212003, 2008.

[157] N. I. Chernov, G. L. Eyink, J. L. Lebowitz, and Y. G. Sinai. Steady-state electrical conduction in the periodic Lorentz gas. *Comm. in Math. Phys.*, 154(3):569–601, 1993.

[158] N. Chernov, H.-K. Zhang, and P. Zhang. Electrical current in Sinai billiards under general small forces. *J. Stat. Phys.*, 153(6):1065–1083, Oct 2013.

[159] A. Veltri and V. Carbone. Radiative intermittent events during Fermi's stochastic acceleration. *Phys. Rev. Lett.*, 92(14):143901, 2004.

[160] E. Fermi. On the origin of the cosmic radiation. *Phys. Rev.*, 75:1169, Apr 1949.

[161] S. M. Ulam. On Some Statistical Properties of Dynamical Systems. In *Fourth Berkeley Symposium on Mathematical Statistics and Probability*, page 315, January 1961.

[162] A. Barnett, D. Cohen, and E. J. Heller. Rate of energy absorption for a driven chaotic cavity. *J. Phys. A*, 34(3):413, 2001.

[163] A. K. Karlis, P. K. Papachristou, F. K. Diakonos, V. Constantoudis, and P. Schmelcher. Hyperacceleration in a stochastic Fermi-Ulam model. *Phys. Rev. Lett.*, 97(19):194102, 2006.

[164] A. K. Karlis, F. K. Diakonos, and V. Constantoudis. A consistent approach for the treatment of Fermi acceleration in time-dependent billiards. *Chaos*, 22(2):026120, 2012.

[165] B. Batistić. Exponential fermi acceleration in general time-dependent billiards. *Phys. Rev. E*, 90:032909, 2014.

[166] A. Kyprianidis. *Simulating many-body quantum spin models with trapped ions*. PhD thesis, University of Maryland, College Park, 2021.

[167] L. D. Landau and E. M. Lifshitz. Mechanics third edition: Volume 1 of course of theoretical physics. *Elsevier Science*, 1976.

[168] S. Okuyama and D. W. Oxtoby. A simple analytical eigenvalue calculation for barrier crossing rates in the weak coupling limit. *J. Chem. Phys.*, 87(6):3611–3617, 1987.

[169] R. Zwanzig. Theory of vibrational relaxation in liquids. *J .Chem. Phys.*, 34(6):1931–1935, 1961.

[170] Q. A. Turchette, B. E. King, D. Leibfried, D. M. Meekhof, C. J. Myatt, M. A. Rowe, C. A. Sackett, C. S. Wood, W. M. Itano, C. Monroe, et al. Heating of trapped ions from the quantum ground state. *Phys. Rev. A*, 61(6):063418, 2000.

[171] G. Arfken. *Mathematical Methods for Physicists*. Academic Press, Inc., San Diego, third edition, 1985.

[172] N. D. Mermin. Time-dependent correlations in a solvable ferromagnetic model. *Phys. Rev.*, 134:A112, 1964.

[173] J. A. G. Roberts and C. J. Tompson. Dynamics of the classical Heisenberg spin chain. *J. Phys. A*, 21(8):1769, 1988.

[174] L. Landau and E. Lifshitz. On the theory of the dispersion of magnetic permeability in ferromagnetic bodies. In *Perspectives in Theoretical Physics*, pages 51–65. Elsevier, 1992.

[175] T. L. Gilbert. A phenomenological theory of damping in ferromagnetic materials. *IEEE Trans. Magn.*, 40(6):3443–3449, 2004.

[176] R. Kubo and N. Hashitsume. Brownian motion of spins. *Prog. Theor. Phys. Supplement*, 46:210–220, 1970.

[177] B. Hatfield. *Quantum field theory of point particles and strings*. CRC Press, 2018.

[178] M. Srednicki. *Quantum field theory*. Cambridge University Press, 2007.

[179] F. Schwabl. *Quantum mechanics*. Springer Science & Business Media, 2007.

[180] E. Merzbacher. *Quantum mechanics*. Jones & Bartlett Publishers, 1961.

[181] D. Bohm. *Quantum theory*. Courier Corporation, 2012.

[182] J. R. Nielsen. *The correspondence principle (1918-1923)*. Elsevier, 2013.

[183] A. Bokulich and P. Bokulich. Bohr's Correspondence Principle. In Edward N. Zalta, editor, *The Stanford Encyclopedia of Philosophy*. Metaphysics Research Lab, Stanford University, Fall 2020 edition, 2020.

[184] A. Voros. Semi-classical approximations. In *Annales de l'IHP Physique théorique*, volume 24, pages 31–90, 1976.

[185] M. Zworski. *Semiclassical analysis*, volume 138. American Mathematical Soc., 2012.

[186] E. H. Lieb. The classical limit of quantum spin systems. *Commun. Math. Phys.*, 31(4):327–340, 1973.

[187] W. H. Zurek. Environment-induced superselection rules. *Phys. Rev. D*, 26(8):1862, 1982.

[188] C. Chicone. Ordinary differential equations with applications, 2000.

[189] G. Floquet. Sur les équations différentielles linéaires à coefficients périodiques. In *Annales scientifiques de l'École normale supérieure*, volume 12, pages 47–88, 1883.

[190] G. W. Hill. On the part of the motion of the lunar perigee which is a function of the mean motions of the sun and moon. *Acta Math.*, 8(1):1–36, 1886.

[191] A. M. Lyapunov. The general problem of the stability of motion. *Int. J. Control*, 55(3):531–534, 1992.

[192] I. Scholz, J. D. van Beek, and M. Ernst. Operator-based Floquet theory in solid-state nmr. *Solid State Nucl. Magn. Reson.*, 37(3-4):39–59, 2010.

[193] E. S. Mananga and T. Charpentier. On the Floquet–Magnus expansion: applications in solid-state nuclear magnetic resonance and physics. *Phys. Rep.*, 609:1–49, 2016.

[194] K. L. Ivanov, K. R. Mote, M. Ernst, A. Equbal, and P. K. Madhu. Floquet theory in magnetic resonance: Formalism and applications. *Prog. Nucl. Magn. Reson. Spectrosc.*, 126:17–58, 2021.

[195] M. Holthaus. Floquet engineering with quasienergy bands of periodically driven optical lattices. *J. Phys. B*, 49(1):013001, 2015.

[196] C. A. Klausmeier. Floquet theory: a useful tool for understanding nonequilibrium dynamics. *Theor. Ecol.*, 1(3):153–161, 2008.

[197] J. P. Tian and J. Wang. Some results in Floquet theory, with application to periodic epidemic models. *Appl. Anal.*, 94(6):1128–1152, 2015.

[198] R. A. Calico and W. E. Wiesel. Control of time-periodic systems. *J. Guid. Control Dyn.*, 7(6):671–676, 1984.

[199] S. C. Sinha and P. Joseph. Control of general dynamic systems with periodically varying parameters via Liapunov-Floquet transformation. 1994.

[200] I. A. Assi, J. P. F. LeBlanc, M. Rodriguez-Vega, H. Bahlouli, and M. Vogl. Floquet engineering and nonequilibrium topological maps in twisted trilayer graphene. *Phys. Rev. B*, 104(19):195429, 2021.

[201] K. Drese and M. Holthaus. Floquet theory for short laser pulses. *Eur. Phys. J. D*, 5(1):119–134, 1999.

[202] S.-I. Chu and D. A. Telnov. Beyond the Floquet theorem: generalized Floquet formalisms and quasienergy methods for atomic and molecular multiphoton processes in intense laser fields. *Phys. Rep.*, 390(1-2):1–131, 2004.

[203] F. H. M. Faisal and T. Radożycki. Three-dimensional relativistic model of a bound particle in an intense laser field. *Phys. Rev. A*, 47(5):4464, 1993.

[204] T. Saue and H. J. Aa. Jensen. Linear response at the 4-component relativistic level: Application to the frequency-dependent dipole polarizabilities of the coinage metal dimers. *J. Chem. Phys.*, 118(2):522–536, 2003.

[205] C. M. Dai, Z. C. Shi, and X. X. Yi. Floquet theorem with open systems and its applications. *Phy. Rev. A*, 93(3):032121, 2016.

[206] C. M. Dai, H. Li, W. Wang, and X. X. Yi. Generalized Floquet theory for open quantum systems. *arXiv preprint arXiv:1707.05030*, 2017.

[207] A. Schnell, A. Eckardt, and S. Denisov. Is there a Floquet lindbladian? *Phys. Rev. B*, 101(10):100301, 2020.

[208] J. D. Jackson. *Mathematics for quantum mechanics: an introductory survey of operators, eigenvalues, and linear vector spaces*. Courier Corporation, 2012.

[209] S. Blanes, F. Casas, J.-A. Oteo, and J. Ros. The Magnus expansion and some of its applications. *Phys. Rep.*, 470(5-6):151–238, 2009.

[210] L. E. Reichl. Transition in the Floquet rates of a driven stochastic system. *J. Stat. Phys.*, 53(1):41–48, 1988.

[211] P. Jung and P. Hänggi. Stochastic nonlinear dynamics modulated by external periodic forces. *EPL*, 8(6):505, 1989.

[212] S. Higashikawa, H. Fujita, and M. Sato. Floquet engineering of classical systems. 2018.

[213] R. Mathias. Approximation of matrix-valued functions. *SIAM J. Matrix Anal. Appl.*, 14(4):1061–1063, 1993.

[214] E. Kreyszig. *Introductory functional analysis with applications*, volume 17. John Wiley & Sons, 1991.

[215] F. Verstraete and J. I. Cirac. Mapping local Hamiltonians of fermions to local Hamiltonians of spins. *J. Stat. Mech.: Theory Exp.*, 2005(09):P09012, 2005.

[216] D. Abanin, W. De Roeck, W. W. Ho, and F. Huveneers. A rigorous theory of many-body prethermalization for periodically driven and closed quantum systems. *Commun. Math. Phys.*, 354(3):809–827, 2017.

[217] K. Mallayya and M. Rigol. Heating rates in periodically driven strongly interacting quantum many-body systems, 2019.

[218] A. Lerose, J. Marino, A. Gambassi, and A. Silva. Prethermal quantum many-body Kapitza phases of periodically driven spin systems. *Phys. Rev. B*, 100(10):104306, 2019.

[219] A. Russomanno, M. Fava, and R. Fazio. Chaos and subdiffusion in infinite-range coupled quantum kicked rotors. *Phys. Rev. B*, 103(22):224301, 2021.

[220] A. Pizzi, A. Nunnenkamp, and J. Knolle. Classical prethermal phases of matter. *Phys. Rev. Lett.*, 127(14):140602, 2021.

[221] P. I. Belobrov, V. V. Beloshapkin, G. M. Zaslavskii, and A. G. Tret'yakov. Order and chaos in classical models of spin chains. *Zh. Eksp. Teor. Fiz.*, 87:310–322, 1984.

[222] F. Borgonovi, G. L. Celardo, M. Maianti, and E. Pedersoli. Broken ergodicity in classically chaotic spin systems. *J. Stat. Phys.*, 116(5):1435–1447, 2004.

[223] K. Kaneko and T. Konishi. Diffusion in Hamiltonian dynamical systems with many degrees of freedom. *Phys. Rev. A*, 40(10):6130, 1989.

[224] M. Falcioni, U. M. B. Marconi, and A. Vulpiani. Ergodic properties of high-dimensional symplectic maps. *Phys. Rev. A*, 44(4):2263, 1991.

[225] M. Mulansky, K. Ahnert, A. Pikovsky, and D. L. Shepelyansky. Strong and weak chaos in weakly nonintegrable many-body Hamiltonian systems. *J. Stat. Phys.*, 145(5):1256–1274, 2011.

[226] Y. Sadia, E. G. D. Torre, and A. Rajak. From prethermalization to chaos in periodically driven coupled rotors. *arXiv preprint arXiv:2108.11421*, 2021.

[227] P. Kos, M. Ljubotina, and T. Prosen. Many-body quantum chaos: Analytic connection to random matrix theory. *Phys. Rev. X*, 8(2):021062, 2018.

[228] M. Berry. Quantum chaology, not quantum chaos. *Phys. Scr.*, 40(3):335, 1989.

[229] J. M. G. Gómez, K. Kar, V. K. B. Kota, R. A. Molina, A. Relano, and J. Retamosa. Many-body quantum chaos: Recent developments and applications to nuclei. *Phys. Rep.*, 499(4-5):103–226, 2011.

[230] A. Voros and P. Leboeuf. Multiplicative formulation of quantum mechanics. Technical report, CEA Centre d'Etudes de Saclay, 1991.

[231] F. J. Dyson. Statistical theory of the energy levels of complex systems. i. *J. Math. Phys.*, 3(1):140–156, 1962.

[232] M. L. Mehta. *Random matrices*. Elsevier, 2004.

[233] E. P. Wigner. Distribution of neutron resonance level spacing. *Columbia University Report CU175*, 1957.

[234] G. W. Anderson, A. Guionnet, and O. Zeitouni. *An introduction to random matrices*. Number 118. Cambridge University Press, 2010.

[235] D. Wintgen and H. Friedrich. Regularity and irregularity in spectra of the magnetized hydrogen atom. *Phys. Rev. Lett.*, 57(5):571, 1986.

[236] D. Delande and J. C. Gay. Quantum chaos and statistical properties of energy levels: Numerical study of the hydrogen atom in a magnetic field. *Phys. Rev. Lett.*, 57(16):2006, 1986.

[237] O. Bohigas, M.-J. Giannoni, and C. Schmit. Spectral properties of the Laplacian and random matrix theories. *J. Phys. (Paris), Lett.*, 45(21):1015–1022, 1984.

[238] M. Sieber and F. Steiner. Quantum chaos in the hyperbola billiard. *Phys. Lett. A*, 148(8-9):415–420, 1990.

[239] C. Kollath, G. Roux, G. Biroli, and A. M. Läuchli. Statistical properties of the spectrum of the extended Bose–Hubbard model. *J. Stat. Mech.: Theory Exp.*, 2010(08):P08011, 2010.

[240] L. F. Santos and M. Rigol. Onset of quantum chaos in one-dimensional bosonic and fermionic systems and its relation to thermalization. *Phys. Rev. E*, 81(3):036206, 2010.

[241] L. F. Santos and M. Rigol. Localization and the effects of symmetries in the thermalization properties of one-dimensional quantum systems. *Phys. Rev. E*, 82(3):031130, 2010.

[242] M. Rigol and L. F. Santos. Quantum chaos and thermalization in gapped systems. *Phys. Rev. A*, 82(1):011604, 2010.

[243] L. F. Santos, F. Borgonovi, and F. M. Izrailev. Onset of chaos and relaxation in isolated systems of interacting spins: Energy shell approach. *Phys. Rev. E*, 85(3):036209, 2012.

[244] Y. Y. Atas, E. Bogomolny, O. Giraud, and G. Roux. Distribution of the ratio of consecutive level spacings in random matrix ensembles. *Phys. Rev. Lett.*, 110(8):084101, 2013.

[245] Y. Y. Atas, E. Bogomolny, O. Giraud, P. Vivo, and E. Vivo. Joint probability densities of level spacing ratios in random matrices. *J. Phys. A*, 46(35):355204, 2013.

[246] M. V. Berry and M. Tabor. Level clustering in the regular spectrum. *Proc. R. Soc. A*, 356(1686):375–394, 1977.

[247] B. Helffer, A. Martinez, and D. Robert. Ergodicité et limite semi-classique. *Commun. Math. Phys.*, 109(2):313–326, 1987.

[248] A. I. Shnirel'man. Ergodic properties of eigenfunctions. *Uspekhi Matematicheskikh Nauk*, 29(6):181–182, 1974.

[249] M. Feingold and A. Peres. Distribution of matrix elements of chaotic systems. *Phys. Rev. A*, 34:591, Jul 1986.

[250] M. Wilkinson. A semiclassical sum rule for matrix elements of classically chaotic systems. *J. Phys. A*, 20(9):2415, jun 1987.

[251] J. M. Deutsch. Quantum statistical mechanics in a closed system. *Phys. Rev. A*, 43(4):2046, 1991.

[252] M. Srednicki. Chaos and quantum thermalization. *Phys. Rev. E*, 50(2):888, 1994.

[253] J. M. Deutsch. Eigenstate thermalization hypothesis. *Rep. Prog. Phys.*, 81(8):082001, 2018.

[254] D. R. Grempel, R. E. Prange, and S. Fishman. Quantum dynamics of a nonintegrable system. *Physical Review A*, 29(4):1639, 1984.

[255] M. Wilkinson and E. J. Austin. Dynamics of a generic quantum system under a periodic perturbation. *Phys. Rev. A*, 46(1):64, 1992.

[256] O. M. Auslaender and S. Fishman. Correlations in the adiabatic response of chaotic systems. *Phys. Rev. Lett.*, 84(9):1886, 2000.

[257] O. M. Auslaender and S. Fishman. The quantum-classical crossover in the adiabatic response of chaotic systems. *J. Phys. A*, 33(10):1957, 2000.

[258] S. Mizutori and S. Åberg. Quantum mechanical diffusion in complex surroundings. *Phys. Rev. E*, 56(6):6311, 1997.

[259] S. Radionov and S. Åberg. Nuclear friction and quantum mechanical diffusion. *Phys. Rev. C*, 71(6):064304, 2005.

[260] D. A. Wisniacki and E. Vergini. Influence of phase-space localization on the energy diffusion in a quantum chaotic billiard. *Phys. Rev. E*, 59(6):6579, 1999.

[261] D. Cohen and D. A. Wisniacki. Stadium billiard with moving walls. *Phys. Rev. E*, 67(2):026206, 2003.

[262] P. V. Elyutin and A. N. Rubtsov. Energy diffusion in strongly driven quantum chaotic systems: the role of correlations of the matrix elements. *J. Phys. A*, 41(5):055103, 2008.

[263] K. Kudo and K. Nakamura. Energy diffusion in frustrated quantum spin chains exhibiting Gaussian orthogonal ensemble level statistics. *Phys. Rev. B*, 71(14):144427, 2005.

[264] K. Kudo and K. Nakamura. Dynamical stability for finite quantum spin chains against a time-periodic inhomogeneous perturbation. *Chaos, Solitons & Fractals*, 40(1):166–171, 2009.

[265] M. Wilkinson. Statistical aspects of dissipation by Landau-Zener transitions. *J. Phys. A*, 21(21):4021, 1988.

[266] M. Wilkinson. Diffusion and dissipation in complex quantum systems. *Phys. Rev. A*, 41(9):4645, 1990.

[267] M. Wilkinson and E. J. Austin. A random matrix model for the non-perturbative response of a complex quantum system. *J. Phys. A*, 28(8):2277, 1995.

[268] M. V. Berry and J. M. Robbins. Chaotic classical and half-classical adiabatic reactions: geometric magnetism and deterministic friction. *Proc. R. Soc. A*, 442(1916):659–672, 1993.

[269] B. V. Chirikov, F. M. Izrailev, and D. L. Shepelyansky. Quantum chaos: localization vs. ergodicity. *Physica D*, 33(1-3):77–88, 1988.

[270] M. Bukov, S. Gopalakrishnan, M. Knap, and E. Demler. Prethermal Floquet steady states and instabilities in the periodically driven, weakly interacting Bose-Hubbard model. *Phys. Rev. Lett.*, 115(20):205301, 2015.

[271] R. G. Littlejohn. The Van Vleck formula, Maslov theory, and phase space geometry. *J. Stat. Phys.*, 68(1):7–50, 1992.